THE ASSESSMENT OF ULTRASONIC INSTRUMENTS IN DENTISTRY

by

SIMON CHRISTIAN LEA

B.Sc. (Hon's) M.Sc. CSci CPhys MInstP

A thesis submitted to the
Faculty of Medicine and Dentistry
of
The University of Birmingham
for the degree of
DOCTOR OF PHILOSOPHY

Faculty of Medicine and Dentistry
School of Dentistry
St. Chad's Queensway
Birmingham B4 6NN

February 2004

UNIVERSITY OF
BIRMINGHAM

University of Birmingham Research Archive

e-theses repository

This unpublished thesis/dissertation is copyright of the author and/or third parties. The intellectual property rights of the author or third parties in respect of this work are as defined by The Copyright Designs and Patents Act 1988 or as modified by any successor legislation.

Any use made of information contained in this thesis/dissertation must be in accordance with that legislation and must be properly acknowledged. Further distribution or reproduction in any format is prohibited without the permission of the copyright holder.

Abstract

Introduction: Ultrasonic scalers are an accepted alternative to hand instruments for the removal of plaque, calculus and stains from teeth. Although the use of these instruments is widespread, the vibrational motion of scalers is not fully understood. Their high frequency, low displacement amplitude oscillations have previously been difficult to analyse. Laser vibrometry is a non-invasive technique for measuring the vibration characteristics of oscillating objects.

Aim: The aim of this research thesis was to utilise scanning laser vibrometry to assess a range of dental ultrasonic systems under various operating conditions similar to those employed clinically.

Materials and Methods: Scaler tip vibrations were measured whilst operating under different working parameters including water flow rate, generator power setting, load and wear. Other parameters such as the amount of cavitation that occurs around the instrument and the heat generated at the tooth surface were also investigated. The vibration characteristics of endosonic K-files and powered toothbrushes were assessed and a study into the presence or absence of cavitation around powered toothbrushes was also performed.

Results: Working parameters such as water flow rate, generator power setting, load and wear were shown to significantly affect the magnitude of scaler tip vibrations. Cavitation was found to occur around some designs of ultrasonic scaler, whereas no cavitation was observed around any of the powered toothbrushes tested.

Discussion: Larger, heavier scaler inserts tended to produce a more linear increase in tip displacement amplitude with increasing generator power setting than smaller lighter tips. Wear of the metallic probe, increases in water flow rate and load were generally shown to cause a decrease in scaler tip displacement amplitude. However, scaler tips did not often respond to a

change in operating conditions in exactly the same way, demonstrating the high variability between these instruments. This high degree of variability was also noticeable between tips of the same design. This vibration displacement amplitude variability was also suggested as the reason for the observed differences in the amount of cavitation produced around scaler tips of the same design.

Conclusions: The use of scanning laser vibrometry revealed differences in the operation characteristics of different ultrasonic scalers. Clinicians and researchers should be aware of the variability in the performance of ultrasonic scalers since this may affect both clinical procedures and future research. Further research into the design and operation of ultrasonic scaler tips is needed.

CONTENTS

List of Figures x

List of Tables xiv

List of Symbols xv

List of Equations xix

List of Units xx

Acronyms xxi

Preface xxiii

1. Introduction 1

1.1 Introduction 1

1.2 Infrasound 1

1.3 Ultrasound 2

1.3.1 Ultrasound in Industry 3

1.3.2 Ultrasound in Medicine 4

1.3.3 Ultrasound in Dentistry 5

1.3.3.1 Ultrasonic Scalers 5

1.4 Problems of Instrument Standardisation 6

1.5 Aims 7

1.6 Objectives 8

2. Fundamental Physics 9

2.1 Introduction 9

2.2 Methods of Ultrasound Generation 9

2.2.1 Piezoelectricity 10

2.2.2 Magnetostriction 12

2.3 Pressure Fields Generated by Ultrasonic Sound Waves 15

2.4 Biophysical Phenomena 17

2.4.1 Cavitation 17

2.4.2 Production of Cavitation 18

2.4.3 Acoustic Streaming 20

2.5 Lasers 22

2.5.1 Bohr Model of the Atom 22

2.5.2 Metastable States 24

2.5.3 Application to Lasers – Reference to Helium-Neon Lasers 26

2.5.4 Properties of Lasers 30

2.6 The Doppler Effect and Laser Vibrometry 32

2.6.1 Doppler Frequency Shift due to Moving Source 33

2.6.2 Doppler Frequency Shift due to Moving Observer 35

2.6.3 Doppler Frequency Shift - Reflection from Vibrating Target 37

2.7 Heat and Friction 38

2.7.1 Fundamental Laws of Friction 38

3. Literature Review 41

3.1 Periodontology 41

3.1.1 Dental Anatomy 41

3.1.2 Plaque and Calculus 41
3.1.3 Periodontal Disease 42
3.1.4 Prevention and Treatment 43
3.2 The Ultrasonic Scaler 44
3.2.1 Origins of Ultrasound in Dentistry 44
3.2.2 Introduction of the Ultrasonic Scaler 46
3.2.3 Present Knowledge 49
3.3 Other Dental Ultrasonic Instruments 51
3.3.1 Endosonic Instruments 51
3.3.2 Retrograde Instruments 52
3.4 Non-Ultrasonic Instruments in Dentistry 53
3.4.1 Sonic Instruments 53
3.4.2 Powered Toothbrushes 54
3.5 Lasers in Dentistry 55
3.6 Development of the Laser Vibrometer 56
3.7 Laser Vibrometry 57
3.7.1 General Applications 57
3.7.2 Applications in Industry 59
3.7.3 Applications in Biology, Medicine and Dentistry 59
3.8 Infrared Thermography (Thermal Imaging) 61
3.9 Cavitation 62
3.9.1 The Discovery of Cavitation 62
3.9.2 Cavitation in Nature 63
3.9.3 Cavitation in Dentistry 63

4. Measurement Techniques 65

Assessment of Vibration

4.1 Introduction 65

4.2 Scanning Laser Vibrometer Optics 66

4.3 Measurement of Vibration Velocity 69

4.4 The Bragg Cell 72

Assessment of Heat Generation

4.5 Introduction 75

4.6 Temperature Measurement 75

4.7 Principles of Infrared Thermography (Thermal Imaging) 76

4.8 Imaging Systems 77

4.9 Selection of Scaler Systems 78

Assessment of Cavitation Production

4.10 Introduction 79

4.11 Cavitation Quantification used in Dentistry 80

4.11.1 Sonoluminescence 80

4.11.2 Weissler Reaction 80

4.11.3 Fricke's Dosimeter 81

4.12 The Terephthalate Dosimeter 82

5. Materials and Methods 85

The Scanning Laser Vibrometer

5.1 Introduction 85

5.2 Laser Vibrometer Instrumentation 86

5.2.1 Scanning Laser Vibrometer Specification 86

5.2.2 Defining a Scan Area – The Measurement Grid 86
5.2.3 Removing Parallax Error 89
5.2.4 The Reference Signal 90
5.2.4.1 Electromagnetic Induction 90
5.2.4.2 Acoustic Reference 91
5.2.5 Acquisition Settings 91
5.3 The Target Object 92
5.3.1 Identification of Vibration Orientation 92
5.3.2 Scaler Tip Water Flow Rate 92
5.3.3 Ultrasound Generator Power Dial Re-Calibration 93
5.3.4 *In Vitro* Tooth Model 94
5.4 SLV Calibration 97
5.5 Scaler Tip Vibration Characterisation 97
5.6 Water Flow Rate and Scaler Tip Vibration 97
5.7 Displacement Amplitude of Unloaded Ultrasonic Scaler Inserts 98
5.8 Load and Ultrasonic Scaler Tip Displacement Amplitude 102
5.9 Wear and Scaler Tip Displacement Amplitude 106
5.9.1 Unadjusted Scalers 106
5.9.2 Scaler Tip Grinding 109
5.10 Single-Scan Multi-Axial Assessment of Scaler Tip Vibrations 114
5.10.1 Theory 114
5.10.2 Method 117
5.11 The Vibration Patterns of Powered Toothbrushes 119
5.11.1 Microphone / Inductance Coil Comparisons 119
5.11.2 Toothbrush Area Scans 122

5.12 The Vibration Patterns of Endosonic K-Files 122

Thermal Imaging

5.13 Heat Generated during *In Vitro* Ultrasonic Instrumentation 125

The Terephthalate Dosimeter

5.14 Cavitation around Ultrasonic Scalers 129

5.15 Cavitation around Powered Toothbrushes 132

6. Results 135

The Scanning Laser Vibrometer

6.1 SLV Presentation Mode 135

6.1.1 Colour Map 135

6.1.2 Colour Dots 135

6.1.3 Isolines 138

6.1.4 Profile Mode 138

6.1.5 3D-Mesh 138

6.1.6 Summary 141

6.2 SLV Calibration 141

6.3 Scaler Tip Vibration Characterisation 141

6.4 Water Flow Rate and Scaler Tip Vibration 143

6.4.1 Oscillation of the Scaling Tip 143

6.5 Displacement Amplitude of Unloaded Ultrasonic Scaler Inserts 146

6.5.1 Piezoelectric Generators 146

6.5.2 Magnetostrictive Generators 149

6.6 Load and Ultrasonic Scaler Tip Displacement Amplitude 151

6.6.1 Statistical Analysis 154

6.6.1.1 Piezoelectric Generators 154

6.6.1.2 Magnetostrictive Generators 155

6.7 Wear and Scaler Tip Displacement Amplitude 156

6.7.1 Statistical Analysis 167

6.7.1.1 FSI-100 Tips 167

6.7.1.2 FSI-1000 Tips 168

6.7.1.3 FSI-SLI-10S Tips 169

6.8 Single-Scan Multi-Axial Assessment of Scaler Tip Vibrations 170

6.9 The Vibration Patterns of Powered Toothbrushes 173

6.9.1 Microphone / Inductance Coil Comparison 173

6.9.2 Toothbrush Area Scans 173

6.10 The Vibration Patterns of Endosonic K-Files 178

6.10.1 Statistical Analysis 178

Thermal Imaging

6.11 Heat Generated during *In Vitro* Ultrasonic Instrumentation 186

The Terephthalate Dosimeter

6.12 Cavitation around Ultrasonic Scalers 195

6.13 Cavitation around Powered Toothbrushes 195

7. Discussion 198

7.1 Introduction 198

The Scanning Laser Vibrometer

7.2 Water Flow Rate and Scaler Tip Vibration 200

7.3 Displacement Amplitude of Unloaded Ultrasonic Scaler Inserts 205

7.4 Scaler Tip Performance under Various Load Conditions 207

7.5 The Effect of Wear on Scaler Tip Displacement Amplitude 210

7.6 Single-Scan Multi-Axial Assessment of Scaler Tip Vibrations 211

7.7 The Vibration Patterns of Powered Toothbrushes 212

7.7.1 Interpretation of Data 214

7.8 The Vibration Patterns of Endosonic K-Files 217

Thermal Imaging

7.9 Heat Generated during *In Vitro* Ultrasonic Instrumentation 223

7.9.1 Risk of Tooth Damage 224

The Terephthalate Dosimeter

7.10 Cavitation around Ultrasonic Scalers 226

7.11 Cavitation around Powered Toothbrushes 229

7.12 Impact of the Current Work on Previous Research 229

8. Conclusions 237

8.1 The Scanning laser Vibrometer 237

8.1.1 Specific Conclusions 237

8.1.2 General Conclusions 238

8.2 Thermal Imaging 239

8.3 The Terephthalate Dosimeter 240

9. Further Work 238

Scanning Laser Vibrometer

9.1 Design of New Scaler Instruments for Clinical Use 238

9.2 Further Evaluation of Endosonic K-Files using SLV 239

9.3 SLV to Correlate Tip Vibration with Cavitation Production 239

Thermal Imaging

9.4 Thermal Imaging of Scaling Procedures *In Vivo* 240

The Terephthalate Dosimeter

9.5 Terephthalate Dosimeter to Assess Cavitation around Loaded Scalers 241

9.6 Does Cavitation Occur in the Flowing Water Supply? 241

9.7 Was Tip Surface Wear Due to Cavitation? 242

10. References 243

11. Appendices

Appendix 1. Published Papers

Appendix 2. Published Abstracts

Appendix 3. EPSRC Individual Grant Review

List of Figures

Chapter 2

Figure 2.1	Mechanical distortion of a metallic conductor due to piezoelectricity.	11
Figure 2.2	Magnetostrictive transducer – a ferromagnetic stack within a solenoid.	14
Figure 2.3	Ultrasound wave propagation through a medium.	16
Figure 2.4	The ultrasound field may cause the bubble to oscillate.	19
Figure 2.5	Ultrasonic waves can generate acoustic streaming.	21
Figure 2.6	Bohr's model of the Hydrogen atom.	23
Figure 2.7	Energy level diagrams used to represent complex atoms.	25
Figure 2.8	Energy level diagram for He-Ne laser.	28
Figure 2.9	Stimulated emission.	29
Figure 2.10	Doppler frequency shift - stationary observer / moving source.	34
Figure 2.11	Doppler frequency shift - moving observer / stationary source.	36

Chapter 3

Figure 3.1.	Structure of the tooth.	40

Chapter 4

Figure 4.1	Optical configuration of a typical scanning laser vibrometer.	67
Figure 4.2	Beam splitter splits laser beam into a reference and object beam.	68
Figure 4.3	Action of λ/4-plate on polarisation of light.	70
Figure 4.4	A Bragg cell or Acousto Optic Modulator (AOM).	73

Chapter 5

Figure 5.1	The scanning laser vibrometer system.	87
Figure 5.2	Measurement grid superimposed over video image of target scaler tip.	88
Figure 5.3	Ultrasound generators used throughout this research.	95
Figure 5.4	Extracted teeth were partially embedded in resin.	96
Figure 5.5	Scaler tips used to investigate effect of load on tip displacement.	101
Figure 5.6	A scaler tip brought into contact with a tooth and the load cell.	103
Figure 5.7	A measurement point guides the laser to a point on the scaler tip.	105
Figure 5.8	Tips utilised in wear investigation.	107
Figure 5.9	Relative orientation of unloaded scaler tip and SLV camera head.	108
Figure 5.10	‘Slimline’ scaler insert contacted against a resin embedded tooth.	110
Figure 5.11	Removal of tip length using a grinding stone.	112
Figure 5.12	Ground tip characteristic of tips worn down through normal usage.	113
Figure 5.13	Schematic of multi-axis vibration assessment experimental set-up.	116
Figure 5.14	Mirror enables vibration data acquisition from multiple orientations.	118
Figure 5.15	Orientation of Sonicare powered toothbrush and SLV camera head.	120
Figure 5.16	Laser directed to bristle tips furthest from the toothbrush handle.	121
Figure 5.17	Orientation of endosonic files, relative to the SLV camera head.	124
Figure 5.18	Scaler tips used for thermal imaging investigation including.	126
Figure 5.19	Orientation of thermal imaging system and piezoelectric scaler tip.	127
Figure 5.20	Scaler tips used during cavitation investigation.	130

Figure 5.21 Scaler tip arrangement during cavitation investigation. 131

Figure 5.22 Powered toothbrushes used throughout the cavitation investigation. 134

Chapter 6

Figure 6.1 Colour map representation of a TFI-3 scaler tips vibration. 136

Figure 6.2 Vibration analysis - data superimposition. 137

Figure 6.3 Stills from 3D-mesh animation of vibration data. 139

Figure 6.4 Orientation of 3D-mesh relative to scaler tip probe. 140

Figure 6.5 Colour map images of various scaler tips. 142

Figure 6.6 Frequency spectrum obtained during a laser vibrometer scan. 144

Figure 6.7 Effect of water flow on tip displacement at various generator powers. 147

Figure 6.8 Displacement data for FSI-100 inserts (all load conditions). 163

Figure 6.9 Displacement data for FSI-1000 inserts (all load conditions). 164

Figure 6.10 Displacement data for FSI-SLI-10S inserts (all load conditions). 165

Figure 6.11 Combined displacement data for all inserts. 166

Figure 6.12 2-D graphical representation of longitudinal / lateral tip vibrations. 171

Figure 6.13 3-D scaler tip vibration pattern depicting elliptical motion. 172

Figure 6.14 Colour map images of powered toothbrushs. 174

Figure 6.15 Stills from Braun 3D vibration data animated as a 3D-mesh. 175

Figure 6.16 Stills from Sonicare vibration data animated as a 3D-mesh. 176

Figure 6.17 Colour map images of vibration data for endosonic K-files. 179

Figure 6.18 Vibration data displayed as a 3D-mesh for endosonic K-files. 180

Figure 6.19 Displacement amplitude along the file length for endosonic K-files. 183

Figure 6.20 File displacement amplitude vs generator power for #15 / #35 K-file. 185

Figure 6.21 Thermal images obtained using magnetostrictive scaler. 187/188

Figure 6.22 Thermal images obtained using piezoelectric scaler. 189

Figure 6.23 Measurement points positioned along scaler length. 190

Figure 6.24 Temperature variation with time (MP) – 0.25N and 1.00N. 192

Figure 6.25 Temperature variation with time (SPS) – low, medium and high power. 193

Figure 6.26 Temperature variation with time (MP / SPS) – 10, 20 and 40ml/min. 194

Figure 6.27 [$^{\bullet}$OH] concentrations vs sonication time for TFI-10 / TFI-3 inserts. 197

Chapter 7

Figure 7.1 Water flow over a scaler tip – quarter flow. 202

Figure 7.2 Water flow over a scaler tip – half flow. 203

Figure 7.3 Water flow over a scaler tip – full flow. 204

Figure 7.4 Vibration analysis of counter-rotary powered toothbrush. 216

Figure 7.5 Frequency spectra for unloaded endosonic K-files. 220

Figure 7.6 3D mesh representations of unloaded endosonic K-files. 221

Figure 7.7 Potential effects of cavitation on scaler tip surface. 229

List of Tables

Chapter 5

Table 5.1	Geometric data of tips in displacement amplitude/loading study.	100

Chapter 6

Table 6.1	Displacement amplitude of scaler tips – various power/water settings.	145
Table 6.2	Displacement amplitude of unloaded scaler tips – all power settings.	148
Table 6.3	Significance values for tip comparisons.	150
Table 6.4	Displacement amplitude (piezoelectric tips) - all powers / each load.	152
Table 6.5	Displacement amplitude (magnetostrictive tips) - all powers / each load.	153
Table 6.6	Displacement amplitude - unadjusted scaler tips (loaded/unloaded).	157
Table 6.7	Displacement amplitude - scaler tips - 1mm removed (loaded/unloaded).	158
Table 6.8	Displacement amplitude - scaler tips - 2mm removed (loaded/unloaded).	159
Table 6.9	Percentage tip displacement decrease - 1mm/2mm removal - unloaded.	160
Table 6.10	Percentage tip displacement decrease - 1mm/2mm removal - (0.50N).	161
Table 6.11	Percentage tip displacement decrease - 1mm/2mm removal - (1.00N).	162
Table 6.12	Vibration frequency/displacement amplitude for powered toothbrushes.	177
Table 6.13	Displacement amplitude along #15 k-file / various power settings.	181
Table 6.14	Displacement amplitude along #35 k-file / various power settings.	182
Table 6.15	Displacement amplitude of #15/#35 k-file - power settings 1 to 5.	184
Table 6.16	[$^{\bullet}$OH] concentrations after sonication of TA solution with scaler tips.	196

List of Symbols

General

μ	micro – usually denotes 10^{-6} of some value, i.e. $\mu m = 10^{-6}m$
°	degrees – may denote the size of an angle / measurement of temperature
v	velocity, particularly of a wave (measured in metres per second)
f	frequency of a wave (measured in Hz)
ν	frequency of a wave (measured in Hz)
λ	wavelength of a wave (measured in metres)
T	time period of a wave (measured in seconds); $T = 1/f$
θ	angle (measured in degrees)
ρ	density (measured in kg / m^3)
$\pm$	plus or minus; usually used in relation to expression of an error associated with a reading, i.e. the displacement was $30 \pm 0.5\mu m$
<	less than
>	more than
=	is equal to
~	approximates to
$\approx$	approximately equal to
%	percentage, number of times in 100 something occurs
#	abbreviation for ‘number’

Lasers

$\delta\lambda$	a small change in wavelength
h	Planck constant; 6.626×10^{-34}Js
π	Pi; 3.142
$\hbar$	$h / 2\pi$; 1.055×10^{-34}Js
E_T	total energy (measured in Joule)
E_P	potential energy (measured in Joule)
E_K	kinetic energy (measured in Joule)
E_i	initial energy (measured in Joule)
E_f	final energy (measured in Joule)
L_{COH}	coherence length (measured in meters)
Z	atomic number

Doppler Shift Analysis

t_0	denotes initial wave at time zero
t_T	wave emitted after time T has elapsed
λ'	denotes a reduction in wavelength
λ''	denotes an increase in wavelength
u	observer constant velocity
v	wavefront constant velocity toward observer
v'	increase in relative velocity of wavefront by (v + u)
v''	reduction in relative velocity of wavefront by (v – u)
f_0	fundamental frequency (measured in Hz)
f_1	an increase in frequency from the fundamental f_0

f_2	a second increase in frequency from $f_0 + f_1$
f_D	frequency $f_1 + f_2$, represents Doppler frequency shift from vibrating object
f_R	centre frequency

Heat and Friction

F	frictional force, measured in Newton
N	normal force, the force at 90° to a plain surface
μ	coefficient of friction

The Scanning Laser Vibrometer

I_{output}	current output at vibrometer photodiode, proportional to f_D (measured in milli-amps)
$\lvert f_D \rvert$	vertical bars denote the magnitude of the internal value, i.e. magnitude of f_D
λ_A	acoustic wavelength (measured in meters)
$\lambda/4$ – plate	quarter wave plate; used for changing the polarisation of light

Terephthalate Dosimeter

I_2	iodine
KI	potassium iodide
CCl_4	carbon tetrachloride
$K^{\bullet}$	potassium radical
$I^{\bullet}$	iodine radical
$^{\bullet}OH$	hydroxyl radical
$[^{\bullet}OH]$	hydroxyl radical concentration

Fe^{2+}	ferrous ion
Fe^{3+}	ferric ion
OH^-	hydroxyl ion

Endosonics

V_s	streaming velocity
ω	angular frequency; 2π times the oscillation frequency
ε_0	displacement amplitude of file
a	file radius
τ	hydrodynamic shear stress
η	kinematic viscosity of the fluid
δ	boundary layer thickness

List of Equations

[2.1]	$v = f\lambda$	12/32
[2.2]	$r = (1/\omega) \cdot \sqrt{(3\gamma P_o / \rho)}$	18
[2.3]	$E_i - E_f = h\nu$	24
[2.4]	$L_{COH} = \frac{\lambda^2}{\delta\lambda}$	30
[2.5]	$T = \frac{1}{f}$	33
[2.6]	$F = \mu N$	38
[4.1]	$f_D = \frac{2u(t)}{\lambda}$	69
[4.2]	$u(t) = f_D\lambda / 2$	69
[4.3]	$I_{output} \propto \lvert f_0 - (f_0 \pm f_D) \rvert$	71
[4.4]	$I_{output} \propto \lvert f_D \rvert$	71
[4.5]	$2d \sin\theta = n\lambda$	72
[4.6]	$2\lambda_A \sin\theta = \lambda$	72
[4.7]	$I_{output} \propto \lvert (f_0 + f_R) - (f_0 \pm f_D) \rvert$	74
[4.8]	$I_{output} \propto \lvert f_R \pm f_D \rvert$	74
[5.1]	$\text{time} = \frac{\text{distance}}{\text{velocity}}$	114
[5.2]	$OM^2 = OT^2 + MT^2$	115
[7.1]	$V_s = \frac{\omega\varepsilon_0^2}{a}$	219
[7.2]	$\tau = \frac{\eta\omega\varepsilon_0^2}{a\delta}$	222

List of Units

Hz	Hertz – unit of frequency, SI unit is (1 / second) or s^{-1}
KHz; MHz	kHz = kilo Hertz or 10^3Hertz; MHz = mega Hertz or 10^6Hertz
m	meter – unit of distance
μm; nm	μm = (1/1,000,000) × 1m or 10^{-6}m; nm = 10^{-9}m
atm	atmospheres – unit of pressure
s	second – unit of time
K	Kelvin – unit of absolute temperature
°C	degrees Celsius – unit of temperature relative to freezing point of water
ms^{-1}	metres per second – unit of velocity (or speed)
kg	kilogram – unit of mass
W	Watt – unit of power

Acronyms

SLV	scanning laser vibrometer
a.c.	alternating current
d.c.	direct current
SONAR	SOund NAvigation and Ranging
NDT	non-destructive testing
CO_2	carbon dioxide
HIFU	high intensity focussed ultrasound
TA	terephthalic acid
He-Ne	Helium-Neon
PZT	lead zirconate titanate
PVDF	polyvinyladine difluoride
YAG	yttrium-aluminium-garnet
LASER	Light Amplification by Stimulated Emission of Radiation
Nd: YAG	Neodymium: Yttrium Aluminium Garnet
Er:YAG	Erbium: Yttrium Aluminium Garnet
GaAlAs	Gallium Aluminium Arsenide
LDF	Laser Doppler Flowmetry
LDV	laser Doppler velocimetry
BS	beam splitter
λ/4-plate	quarter wave plate
RF	radio frequency
AOM	acousto-optic modulator
KE	kinetic energy

EM	electromagnetic
EPSRC	Engineering and Physical Sciences Research Council
FFT	fast Fourier transform
EMS	Electro Medical Systems
SPS	sustained performance system
SPSS	Statistical Package for the Social Sciences
TFI	through flow insert
FSI	focussed spray insert
FSI-SLI-10S	focussed spray insert – slimline – 10 straight
LDF	laser Doppler flowmetry

Preface

The work in this thesis has been undertaken over a period of 4 years at The University of Birmingham, School of Dentistry. Some of the material contained within this thesis has been published in scientific and professional journals and presented at scientific conferences and meetings.

Published Papers

- Lea SC, Landini G & Walmsley AD. Vibration Characteristics of Ultrasonic Scalers assessed with Scanning Laser Vibrometry. Journal of Dentistry, 2002; **30**: 147-151.

- Lea SC & Walmsley AD. Technology, Ultrasonics and Dentistry. Dental Update, 2002; **29**: 390-395.

- Lea SC, Landini G & Walmsley AD. The Displacement Amplitude of Ultrasonic Scaler Inserts. Journal of Clinical Periodontology, 2003; **30**: 505-510.

- Lea SC, Landini G & Walmsley AD. Ultrasonic Scaler Tip Performance under Various Load Conditions. Journal of Clinical Periodontology, 2003; **30**: 876-881.

- Lea SC, Price GJ & Walmsley AD. Does Cavitation Occur around Powered Toothbrushes? Journal of Clinical Periodontology, 2004; **31**: 77-78.

- Lea SC, Landini G & Walmsley AD. Assessing the Vibrations of Dental Ultrasonic Scalers. Journal of Sound and Vibration, 2004; **271**: 1113-1120.

- Lea SC, Landini G & Walmsley AD. Thermal Imaging of Ultrasonic Scaler Tips during Tooth Instrumentation. Journal of Clinical Periodontology, 2004; **31**: 370-375.

- Lea SC, Walmsley AD, Lumley PJ & Landini G. A New Insight into the Oscillation Characteristics of Endosonic Files used in Dentistry. Physics in Medicine and Biology, 2004; **49**: 2095-2102.

- Lea SC, Landini G & Walmsley AD. A Novel Method for the Evaluation of Powered Toothbrush Oscillation Characteristics. American Journal of Dentistry, 2004; **17**: 307-309.

- Lea SC, Price GJ & Walmsley AD. A Study to Determine whether Cavitation Occurs around Dental Ultrasonic Scaling Instruments. Ultrasonics Sonochemistry, 2005; **12**: 233-236.

Published Abstracts

- Walmsley AD, Landini G & Lea S. Vibration Characteristics of Ultrasonic Scalers with Scanning Laser Vibrometry. Journal of Dental Research, 2000; **79**: 1173.

- Lea SC, Landini G & Walmsley AD. Acoustic Output of Ultrasonic Generators using Scanning Laser Vibrometry. Journal of Dental Research, 2001; **80**: 1170.

- Lea SC, Landini G & Walmsley AD. Scanning Laser Vibrometry to Assess Output of Powered Toothbrushes. Journal of Dental Research, 2001; **80**: 1171.

- Lea SC, Price GJ & Walmsley AD. A Study to Determine whether Cavitation Occurs Around Ultrasonic Instruments. Journal of Dental Research, 2003; **82** (Special Issue B): B-90.

- Lea SC, Landini G & Walmsley AD. Heat Generation during Ultrasonic Instrumentation of Tooth Surfaces. Journal of Dental Research, 2003; **82** (Special Issue C): C-493.

- Lea SC, Landini G & Walmsley AD. Effect of Loading on Generator Output and Tip Displacement Amplitude. Journal of Dental Research, 2003; **82** (Special Issue C): C-493.

Work Presented

- Walmsley AD, Landini G & Lea S. Scanning Laser Vibrometry Applied to Ultrasonic Scalers. British Society for Dental Research, 2000 (Lancaster University, England).

- Lea SC, Landini G & Walmsley AD. Principles of Scanning Laser Vibrometry as Applied to Ultrasonic Scalers. Birmingham, Bristol and Cardiff Section Meeting, British Society for Dental Research, September 2000 (Ross-on-Wye, Wales).

- Lea SC, Landini G & Walmsley AD. Acoustic Output of Ultrasonic Generators using Scanning Laser Vibrometry. British and Irish Division, British Society for Dental Research, 2001 (Queens University, Belfast, N. Ireland).

- Lea SC, Landini G & Walmsley AD. Scanning Laser Vibrometry to Assess the Vibration of Powered Toothbrushes. British and Irish Division, British Society for Dental Research, 2001 (Queens University, Belfast, N. Ireland).

- Lea SC. Comparing Magneto and Piezon Ultrasonic Scalers. Periodontal Opinion Leader Meeting, September 2001 (Weybridge, Surrey, England).

- Walmsley AD & Lea SC. Ultrasonic Dental Descaling of Teeth. Polytec Vibrometer Users Meeting, September 2001 (Loughborough University, England).

- Walmsley AD, Landini G & Lea SC. Assessment of Ultrasonic Instruments used in Dentistry. Engineering and Physical Sciences Research Council Laser Users Meeting, May 2002 (Manchester, England).

- Lea SC, Landini G & Walmsley AD. Heat Generation during Ultrasonic Instrumentation of Tooth Surfaces. Pan European Festival of Oral Science, International Association for Dental Research, September 2002 (Cardiff, Wales).

- Lea SC, Landini G & Walmsley AD. Effect of Loading on Generator Output and Tip Displacement Amplitude. Pan European Festival of Oral Science, International Association for Dental Research, September 2002 (Cardiff, Wales).

- Lea SC, Price GJ & Walmsley AD. A study to determine whether cavitation occurs around ultrasonic instruments. International Association for Dental Research, June 2003 (Gothenburg, Sweden).

- Lea SC, Price GJ & Walmsley AD. Sonochemical Monitoring of Radical Production in Dental Ultrasound. 9th Meeting of the European Sonochemistry Society, April 2004 (Badajoz, Spain).

Miscellaneous

Some of this work has also been featured as the cover picture for the professional dental journal, Dental Update.

- Cover Picture: An ultrasonic scaler whose vibration is being measured by the use of a scanning laser vibrometer. Dental Update, 2000; Vol. 27(5).

- Cover Picture: A colour mapped image of the vibration of an ultrasonic scaler superimposed onto a video of the instrument. Dental Update, 2001; Vol. 28(2).

CHAPTER 1

INTRODUCTION

1.1 Introduction

Energy may be propagated from one point to another through solids, liquids and gases in the form of acoustic waves. Acoustic waves are mechanical, requiring a material medium for their propagation. They are also longitudinal waves, where the displacement of the disturbance at the source is parallel to the direction in which the waves travel, the energy of the wave being carried as a succession of compressions and rarefactions. Acoustic waves cover a wide frequency spectrum, within which exists the human audible range, extending from approximately 50Hz up to a maximum frequency of approximately 20kHz (20,000Hz). Outside this range of frequencies sound is inaudible to man. Acoustic waves with frequencies below the audible range are termed infrasound and those with frequencies greater than the audible range are known as ultrasound.

1.2 Infrasound

Acoustic waves with frequency below 50Hz, known as infrasound, are encountered in many situations, both of man made and naturally occurring origins. Audible sound is relatively short lived, since the energy it carries is rapidly absorbed due to the viscosity of the air. Elephants emit infrasonic calls of between 15 and 40Hz, which other elephants may hear and use to determine the origin of the call (McComb *et al*. 2003). In 1883, the eruption of Krakatoa in Indonesia generated infrasonic waves that propagated around the world several times (Monroe 2002).

The large distances infrasound waves are able to travel make them ideal for detecting illegal nuclear bomb tests (Monroe 2002). A bomb test performed in China during 1980 was detected 6 hours later in Alaska and then re-registered as the waves completed a second lap of the earth (Rozell 1999). On September 11th 2001, an infrasound station in the central Canadian province of Manitoba detected the collapse of the World Trade Centre towers (Monroe 2003).

1.3 Ultrasound

Ultrasound is usually defined as sound with frequency above the bandwidth of human hearing (Webb 1988). This is frequency in excess of approximately 20kHz. In nature, many animals rely on ultrasound for communication, navigation and food location. Bat ultrasound is highly sensitive and enables them to differentiate between a falling leaf and a moth whilst flying at full speed in total darkness. A lesser-known use of animal ultrasound is by some species, such as moths, which have developed a technique of avoiding capture by bats by exploiting the bats ability to differentiate between themselves and falling leaves. Upon detecting the ultrasound of approaching bats the moths simply stop flying and fall to the ground (Hutson *et al*. 2001). Dolphins, whales and porpoises also use ultrasound and echolocation to communicate with each other and to navigate (Wade 2000).

The generation of ultrasound by humans goes as far back as Lord Rayleigh's book 'The Theory of Sound', first published in 1877 and the Curies' discovery of the piezoelectric effect in 1880 (Duck *et al*. 1998). However, the earliest ultrasonic transducer was the development of a whistle in 1883 by Francis Galton (1822-1911) who was investigating the threshold frequencies of animal and human hearing (Mason 1990). The first commercial application of

ultrasonics was the development of the 'echo-sounder', by Paul Langévin (1872-1946), during World War 1 (Duck *et al*. 1998). This eventually became underwater SONAR (SOund NAvigation and Ranging) and was used during World War 2 for submarine detection. Since this time, the technology of ultrasound has advanced and its applications have become increasingly diverse, finding use in industry, medicine and dentistry.

1.3.1 Ultrasound in Industry

Industrial uses of ultrasound are highly varied. In the field of non-destructive testing (NDT) ultrasound is used for assessing the integrity of many engineering structures such as bridges, aircraft and even nuclear reactors (Scruby & Drain 1990). This technique is particularly popular for defect detection since images may be formed of the interiors of the material under test.

Ultrasound is also used in the field of sonochemistry as a catalyst to accelerate inefficient chemical reactions (Mason 1990) as well as being used as an ultrasonic cleaner and for the welding metals and plastics (Mason 1990; Raichel 2000). More recently ultrasound has found application in the brewing industry and may be used to speed up the beer production process (Jamieson 2001). Currently, it may take between five and seven days to produce a pint of beer from start to finish and, for most of this time, the beer is stored in large vessels whilst the carbon dioxide (CO_2) produced during fermentation is removed. The use of an ultrasonic 'whistle' could enable beer manufacturers to de-gas their beers almost instantly by causing the CO_2, dissolved in the water, to diffuse into microscopic CO_2 bubbles that expand and float to the surface of the liquid.

1.3.2 Ultrasound in Medicine

Although commonly used in medicine for imaging of the foetus in the womb, ultrasound may also be used to image many other organs and finds application in the fields of gynaecology, opthalmics and can even be used for the echographic visualisation of infant brain anatomy (Webb 1988). An acoustic window (the anterior fontanel) enables brain scans to be performed, allowing the diagnosis of cerebral haemorrhage in premature babies as well as the detection of congenital malformations (Webb 1988). Ultrasound has been utilised in medicine for many years in physiotherapy to aid massage, to help treat strained muscles and speed up the repair of damaged tissues (Webb 1988). Doppler ultrasound can also be used to map the flow of blood through the blood vessels and the heart (Webb 1988). More recently, high intensity focussed ultrasound (HIFU) has been shown in animal studies to occlude blood vessels, stop bleeding from hepatic and splenic injuries and arrest haemorrhage from capillary beds and major blood vessels (Vaezy *et al*. 1999 & 2001). This could soon lead to high-intensity ultrasound waves being used to treat internal bleeding at accident scenes (Vaezy *et al*. 1999 & 2001).

1.3.3 Ultrasound in Dentistry

There are many instruments available to dental clinicians that enable them to improve and maintain oral health. Tools such as curettes require the operator to manually manoeuvre the instrument over the tooth surface. Advances in technology, however, have led to many of these instruments becoming ultrasonic (Lea *et al*. 2002a) in an attempt to reduce treatment time and operator fatigue whilst at the same time improving the overall standard of oral health. The introduction of ultrasonic instruments has enabled many dental routines to be improved.

Ultrasound is a useful and widely used technology in dentistry and ultrasonic units are present in many dental practices in the United Kingdom. First used to drill cavities in teeth, the principle use of ultrasound has changed to that of a scaling instrument to remove plaque and calculus from tooth surfaces. The basic method of ultrasound generation has altered little over the last 50 years. The main changes that have occurred within dental ultrasonics are in relation to the insert design and the type and shape of the probe. These probes can be used for a variety of tasks including scaling of teeth, endodontics and apical surgery.

1.3.3.1 Ultrasonic Scalers

Ultrasonic scalers were first introduced into the field of periodontics in the 1950's and are accepted as an alternative to the use of hand instruments in the removal of plaque, calculus and stains from teeth. The generators, which drive the scaler tips, operate using magnetostriction or piezoelectricity and produce ultrasound in the lower kilohertz range (usually 20-30kHz).

Ultrasonic instruments remove deposits from tooth surfaces via the mechanical chipping action of the scaler tip. As water flows over the surface of the tip, to minimise the heat generated at the tip / tooth treatment site, streaming patterns close to the tip surface may be observed (Khambay & Walmsley 1999). This is known as acoustic streaming and this assists in the removal of deposits from the treatment site.

Another phenomenon of the ultrasonic scaler, which occurs within the cooling water supply, is the production of cavitation. Cavitation may generally be categorised as stable or inertial (un-stable) bubble activity within a liquid. It is the energy generated in the destructive inertial

cavitation that results in large shockwaves, which may disrupt plaque and calculus during ultrasonic scaling (Laird & Walmsley 1991). The water flowing over the tip, therefore, not only cools but may also bring about additional cleaning effects.

The main advance in ultrasonic scaling instrument technology has been the introduction of slimmer probe tips, which are designed to improve access to the tooth and root surfaces during scaling procedures. These tips usually include an internal borehole that allows the water to reach the working tip and it is this that limits the minimum tip size that may be used clinically without breakage occurring.

1.4 Problems of Instrument Standardisation

Although the use of these instruments is widespread in dentistry the vibrational motion of scaler insert probes is not fully understood. The vibrations of probes driven at ultrasonic frequencies are difficult to visualise due to their high frequency oscillations and small associated displacement amplitudes. Therefore it is not simple to determine whether they are working correctly. Previous assessment of the oscillation of these instruments was performed by directing a beam of light onto the tip of a scaler probe which, when reflected off a scratch on the surface, resulted in a pinpoint of light (Walmsley *et al*. 1986a & b). This pinpoint of light became elongated into a thin bright line when the apparatus was operated, the length of the line indicating the excursion of the probe tip. This technique gave an indication that there were potential problems with instrument standardisation. However, this procedure was time-consuming and did not allow detailed visualisation of the probe movement or accurate measurement of its displacement amplitude.

The technique of scanning laser vibrometry has made it possible to study the vibration patterns of ultrasonic dental equipment (Lea *et al*. 2002b & 2003a&b, 2004a&b; Trenter *et al*. 2002 & 2003). Laser vibrometry is a non-invasive technique for measuring the vibration velocity of oscillating objects. Laser light, scattered from the vibrating target object, is Doppler frequency shifted, the magnitude of the shift being proportional to the velocity of the target. From this, the associated computer software can be used to calculate the vibration frequency and displacement amplitude of the oscillating target. This allows the user to observe the tip motion easily and therefore assess the currently available ultrasonic systems.

1.5 Aims

The aims of this study are to gain a better understanding of the vibration characteristics of ultrasonic scalers using a scanning laser vibrometer (SLV). The effects of water flow rate, generator power setting, load and wear on the magnitude of scaler tip vibrations were investigated. Further investigations were performed using a thermal imaging system to determine the heat generated at the tip/tooth contact site during ultrasonic instrumentation and, using a terephthalate dosimeter, the occurrence of cavitation around ultrasonic scalers was evaluated.

Further aims to this study include gaining an understanding of endosonic K-file and powered toothbrush vibration characteristics using the SLV. Using the terephthalate dosimeter the occurrence of cavitation around powered toothbrushes was also investigated.

1.6 Objectives

- Characterise the motion of various designs of dental ultrasonic scalers
- Measure the displacement amplitude of scaler tips, at various generator power settings, to determine the effect of water flow rate on the vibrations
- Measure the variation in displacement amplitude of unloaded ultrasonic scaler inserts at increasing generator power settings
- Assess ultrasonic scaler tip performance under various load conditions by measuring tip displacement amplitude at various generator power settings
- Assess the effect of tip wear on ultrasonic scaler tip performance under various load conditions
- Perform single-scan multi-axial assessment of scaler tip vibrations
- Assess the vibration patterns of powered tooth brushes by using a different triggering mechanism to enable data acquisition
- Assess the vibration patterns of unloaded endosonic K-files
- Measure the heat generated at the tip/tooth contact site during ultrasonic instrumentation using various operating conditions
- Assess the occurrence of cavitation around ultrasonic scalers and determine which designs maximise its production
- Determine whether cavitation occurs around powered tooth brushes

CHAPTER 2

FUNDAMENTAL PHYSICS

2.1 Introduction

Throughout this research, techniques have been utilised that derive from fundamental physical phenomena. Ultrasonic instruments such as scalers, endosonic files and retrograde tips are driven to vibrate at ultrasonic frequencies by piezoelectric and magnetostrictive methods and so these methods of ultrasound generation are described. The biophysical phenomena associated with ultrasound, including the conditions that lead to the onset of cavitation in its varying forms and acoustic streaming are also described. The scanning laser vibrometer, used here to assess the vibrations of the ultrasonic instruments, comprises a highly sophisticated optical system utilised in conjunction with a Helium-Neon laser. The laser is an important component of the vibrometer system and so the physics of laser generation and the properties that make lasers essential for vibrometry are discussed. This also includes an introduction to the Doppler effect, the phenomenon upon which all laser vibrometry is based. Furthermore, the fundamental laws of friction and heat generation are described.

2.2 Methods of Ultrasound Generation

Solid materials are generally composed of symmetrical molecules. However, some materials are made of asymmetrical molecules and these can be made to undergo physical changes in their shape through the application of an external force, which causes a re-orientation of their molecules. The two most regularly encountered physical systems for generating ultrasound make use of this phenomenon. Some materials change shape when the externally applied force is electrical and others when an electromagnetic signal is used. These phenomena are

known as the piezoelectric effect and magnetostriction respectively. Both systems employ rapid changing of the physical dimensions of a solid generator, with one of the generator's surfaces coupled to the medium where the ultrasound is required. The following sections discuss the methods of ultrasound generation in further detail, along with some medical applications in which each system has found particular use.

2.2.1 Piezoelectricity

This effect was first discovered by the Curies' in 1880 (Duck *et al*. 1998) who found that when they mechanically compressed certain crystals an electric charge was generated on the crystal surface. Piezoelectricity is observed in materials with an asymmetrical distribution of electrical charge. If two surfaces of a disc of piezoelectric material are coated with a thin film of a metallic conductor, a voltage may be obtained when the disc is mechanically strained. Conversely, the disc may be mechanically distorted when a potential difference is applied across the same two conducting surfaces (Williams 1986). The distortion effect of a piezoelectric element when an alternating voltage is applied across it is shown (Figure 2.1).

Many naturally occurring crystals such as quartz, tourmaline and zinc oxide are piezoelectric. Early man-made ultrasound transducers were fabricated from synthetic ceramic known as lead zirconate titanate (PZT) or barium titanate. More recently polyvinyladine difluoride (PVDF) has become commonly used. Man-made transducers are extremely stiff and capable of exerting/sustaining large forces. However, the magnitudes of the crystal face oscillations are very small. To achieve the maximum amplitude ultrasound wave for the minimum input of energy, the frequency of the applied electronic signal is made the same as the natural or resonant frequency of the crystal and is known as the fundamental resonant frequency.

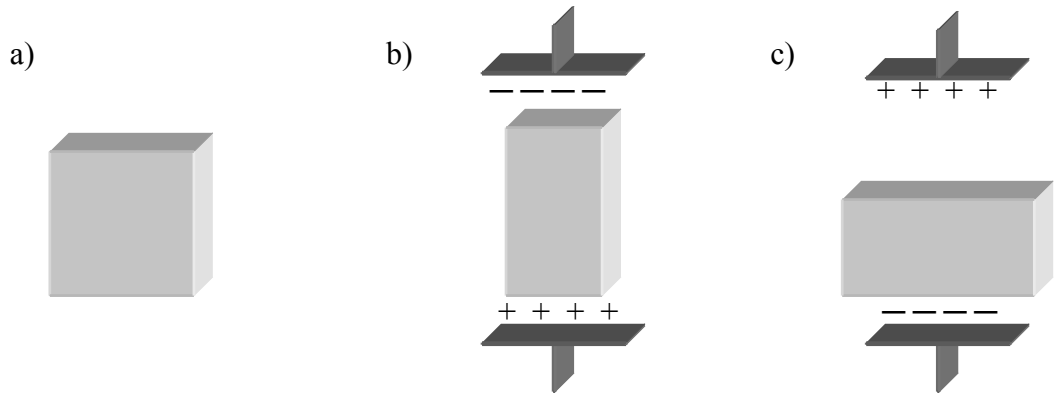


Figure 2.1 Piezoelectricity is observed in materials with an asymmetrical distribution of electrical charge. A piezoelectric material coated with a thin film of a metallic conductor, may be mechanically distorted when a potential difference is applied across the conducting surfaces. The undeformed material (a) may be stretched (b) and compressed (c) by a sinusoidal voltage.

Ultrasound produced using piezoelectricity is usually of quite high frequency (greater than 30kHz) and this makes it very popular in the field of medical imaging. Sound waves (or any other waves) travel through a material with velocity, v, related to the frequency and wavelength as given by;

$$v = f\lambda \qquad [2.1]$$

where f is the frequency of the wave and λ the wavelength. For a given medium (constant velocity of sound), greater acoustic frequency leads to a shorter wavelength, which improves resolution. However, the magnitude of the frequency used is also dependent upon the body part to be imaged. Though near-surface scans (mammography, thyroid etc) use high frequencies (7-10 MHz) the beam is greatly attenuated. Imaging of deeper tissues requires the use of lower frequencies, usually of the order of 3.5 MHz or 5 MHz. In the field of dentistry, piezoelectric transducers are driven at a frequency of approximately 30 kHz. At these frequencies, ultrasound is commonly produced by magnetostriction.

2.1.2 Magnetostriction

Ferromagnetic materials are composed of molecules which themselves have both north and south poles. These materials are magnetic when the individual north poles are predominantly aligned in the same direction (Williams 1986).

If this bar magnet is now placed within a solenoid, through which an alternating electrical current is passed, the magnet will change its shape at twice the frequency of that current. Superimposed upon this alternating current is a direct current, passed through the same coil, which provides a constant magnetic field and prevents the magnet from becoming

demagnetised. This changing magnetic field induces eddy currents within the core. To reduce this, the core is constructed from many strips or lamellae.

Changes in the length of the core material are very small (microns). As with piezoelectricity, maximum efficiency is therefore obtained by driving the stack at its resonant frequency, which is made possible by using a core size carefully chosen to be of resonant length.

A diagrammatic representation of a typical magnetostrictive transducer assembly is shown (Figure 2.2). With current (a.c. and d.c.) flowing through the coil the stack vibrates predominantly in the direction indicated by the arrow. Ultrasonic waves therefore travel both towards and away from the velocity transformer or probe. When the resonance condition is met, waves reflected from the air-backed face interfere constructively with the next new wave generated and maximum displacement amplitude is obtained. The waves are then conducted to the dental scaling tip or probe.

For ultrasonic frequencies of greater than 500kHz, much smaller transducer elements are required which are very difficult to produce. Therefore, magnetostrictive devices are mainly used for the production of ultrasound in the range 20-100 kHz, making them of particular use in the field of dentistry, where frequencies of between 20 and 30 kHz are generally utilised.

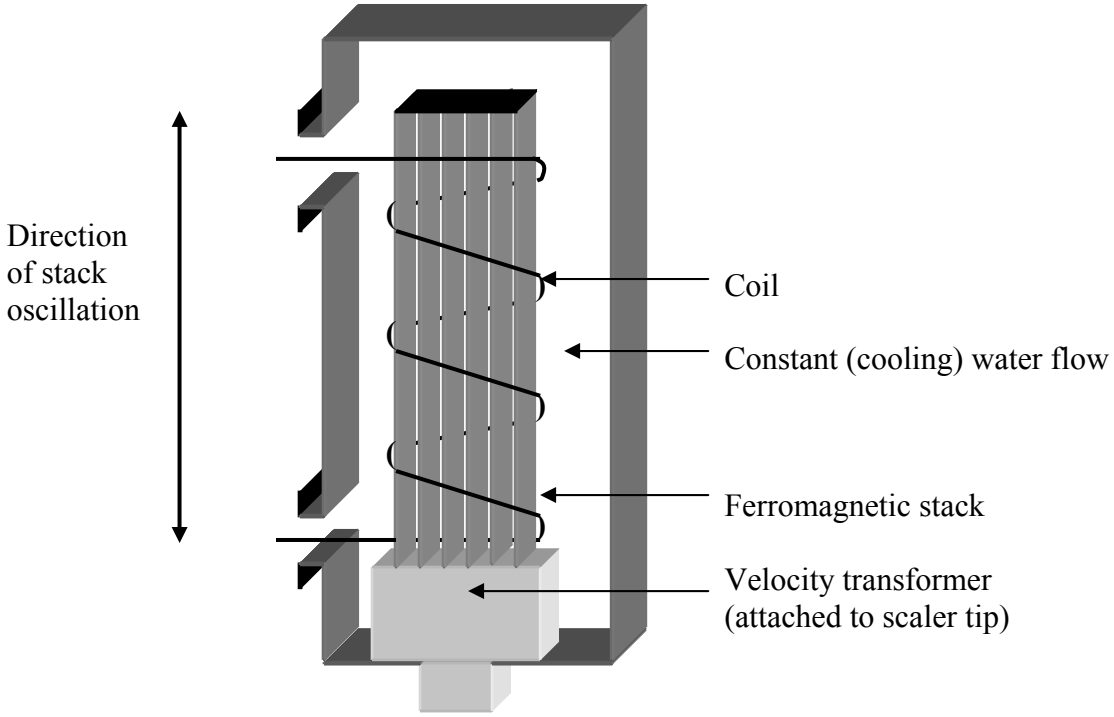


Figure 2.2 A ferromagnetic stack is placed within a solenoid, through which an alternating electric current is passed. The stack changes its shape at twice the frequency of the current. Superimposed upon the alternating current is a direct current, passed through the same coil, which provides a constant magnetic field preventing demagnetisation of the magnet. The core is constructed from lamellae to reduce the effects of eddy currents.

2.3 Pressure Fields Generated by Ultrasonic Sound Waves

Ultrasound waves are longitudinal (compressional) waves, which means that the direction of particle vibration is in the same direction as that of the propagating wave. To simplify the motion when ultrasound waves propagate as plane progressive waves, it is useful to consider the propagating medium as being composed of an infinite number of thin layers, parallel to the advancing wave front (Figure 2.3a). At any given time some of these parallel layers may be displaced from their original position either in, or away from, the direction of wave motion or may even be at their original position (Figure 2.3b). The sound field therefore produces a series of compressions and rarefactions within the fluid. Compressions are regions where the layers in the fluid are moving towards a common point, resulting in a region of increased pressure. Conversely, rarefactions are regions where the layers are moving away from that point resulting in regions of reduced pressure. Pressure variation at various points in a medium may be described by a sine wave (Figure 2.3c), where the positive y-axis denotes increased pressure (compression) and the negative y-axis denotes reduced pressure (rarefaction).

If we consider ultrasound waves propagating in a liquid medium, each ‘layer’ of the medium oscillates with simple harmonic motion about its central, undisturbed position. There is no net motion of any of the layers, energy is transferred between layers and it is this that leads to the overall transfer of energy from one point to another.

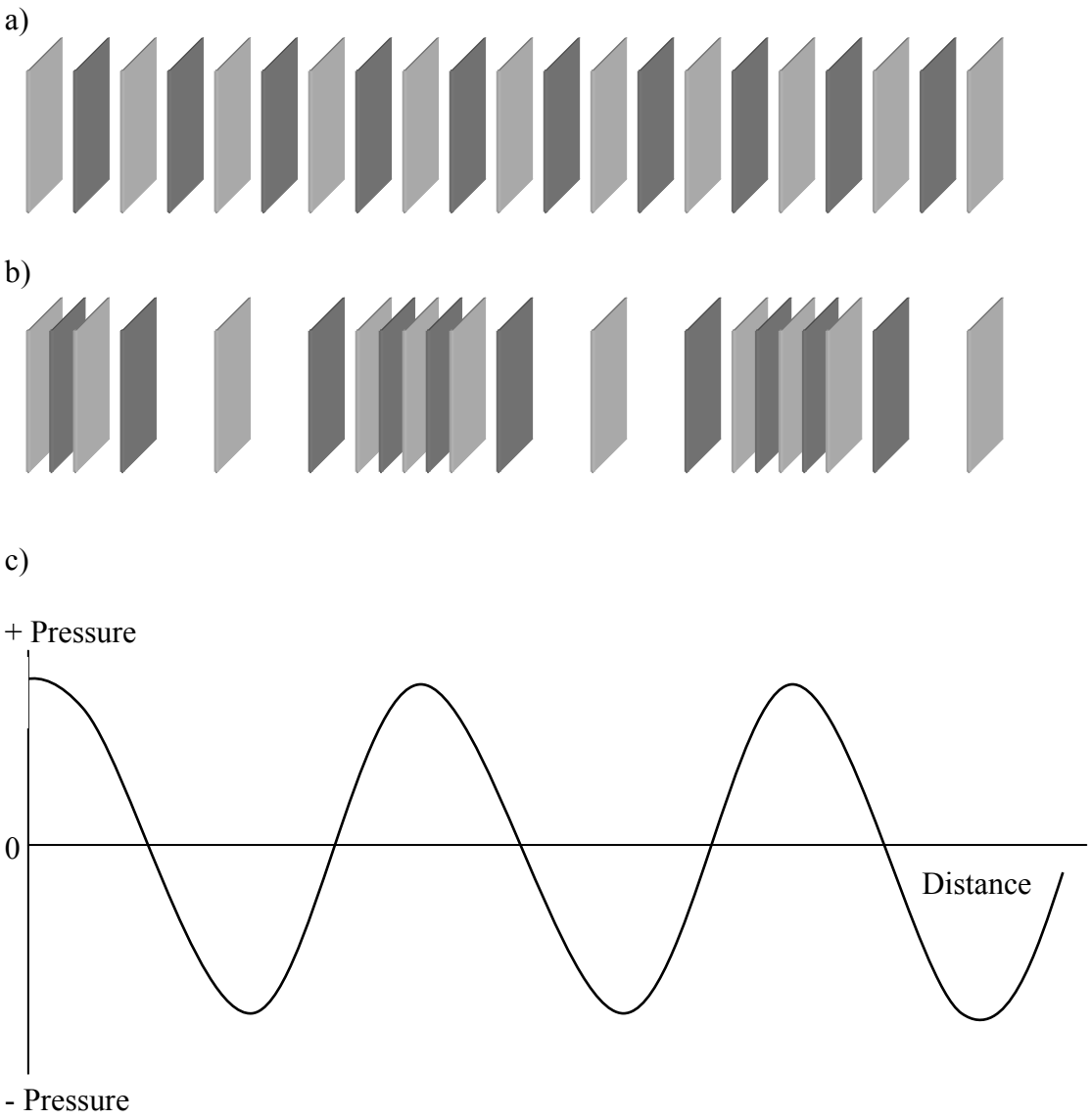


Figure 2.3 a) Ultrasound waves propagate as plane progressive waves and may be thought of as being composed of an infinite number of thin layers (shown in two grey tones simply to aid viewing). b) At arbitrary time some of these parallel layers may be displaced from their original position or may be at their original position. c) Pressure variation in a medium may be described by a sine wave, where the positive y-axis denotes increased pressure (compression) and the negative y-axis denotes reduced pressure (rarefaction).

2.4 Biophysical Phenomena

2.4.1 Cavitation

There are numerous definitions of cavitation to be found within the literature. Neppiras (from Leighton 1994) defines cavitation as occurring, "whenever a new surface, or cavity, is created within the body of a liquid, a cavity being defined as any bounded volume, whether empty or containing a gas or vapour, with at least part of the boundary being liquid". However, cavitation is not necessarily 'formed' from the medium but may be seeded by the presence of gaseous bubbles within the medium known as 'cavitation nuclei'. This leads to a more general definition of cavitation by Apfel (Daniels *et al*. 1995), which refers to cavitation as, "the formation of pockets of gas in the liquid arising either as a result of the creation of a new cavity or through the expansion of a pre-existing gaseous nucleus". Generally, cavitation refers to the production and growth of bubbles by negative pressure excursions and to their subsequent behaviour (Duck *et al.* 1998).

Cavitation may be subdivided into two main types, known as stable cavitation and inertial or collapse cavitation (previously known as transient cavitation) (Barnett *et al*. 1997). As the name suggests, stable cavitation bubbles are relatively permanent and may oscillate for many acoustic cycles (Neppiras 1980). Conversely, inertial cavitation bubbles oscillate violently and may expand to many times their original size before they rapidly collapse. During the final phase of collapse, internal bubble temperatures in excess of 5,000K may be reached (Suslick 1989; Leighton 1994; Debus *et al*. 1999) and pressures may reach 500 bars (Suslick 1989).

2.4.2 Production of Cavitation

The formation and growth of bubbles in an ultrasound field depends upon many complex independent and interdependent variables. These include the number of seeding nuclei and the quantity and solubility of each dissolved gas in the medium. Smaller bubbles in the ultrasound field may grow in size through a process known as rectified diffusion. The ultrasound field is comprised of a series of compressions and rarefactions, which correspond to regions of high and low pressure (Figure 2.4). This alternating pressure field causes the bubble to oscillate between extreme conditions where it is compressed to its smallest radius and then allowed to grow to its largest radius (Figure 2.4). When the bubble is compressed the pressure of the gas inside is greater than that of the surrounding medium and so gas diffuses out of the bubble, over its entire surface (Figure 2.4). In the rarefaction phase of the ultrasound field the bubble is at its largest and gas diffuses into the bubble, again over its entire surface (Figure 2.4). The surface area of the fully expanded bubble is larger than that of the compressed bubble and so, throughout the compression and expansion cycle there is a net flux of previously dissolved gas out of solution and into the bubble, leading to growth of the bubble (Figure 2.4). This is a fairly simplified view, since the normal tendency of a small gas bubble is to shrink and so a fairly high power acoustic field is required just for the bubble to maintain its size and an even higher power field to enable the bubble to grow (Williams 1986). Whether or not a bubble collapses (for a field of given intensity) also depends on its size relative to the resonant size for that particular frequency. This is given by equation 2.2, where r is the bubble radius, ω is 2π times the applied frequency, ρ is the surrounding liquid density, γ the ratio of the specific heats of the gases within the bubble and P_o is the pressure amplitude (Williams 1986).

$$r = (1/\omega) \times \sqrt{(3\gamma P_o / \rho)} \qquad [2.2]$$

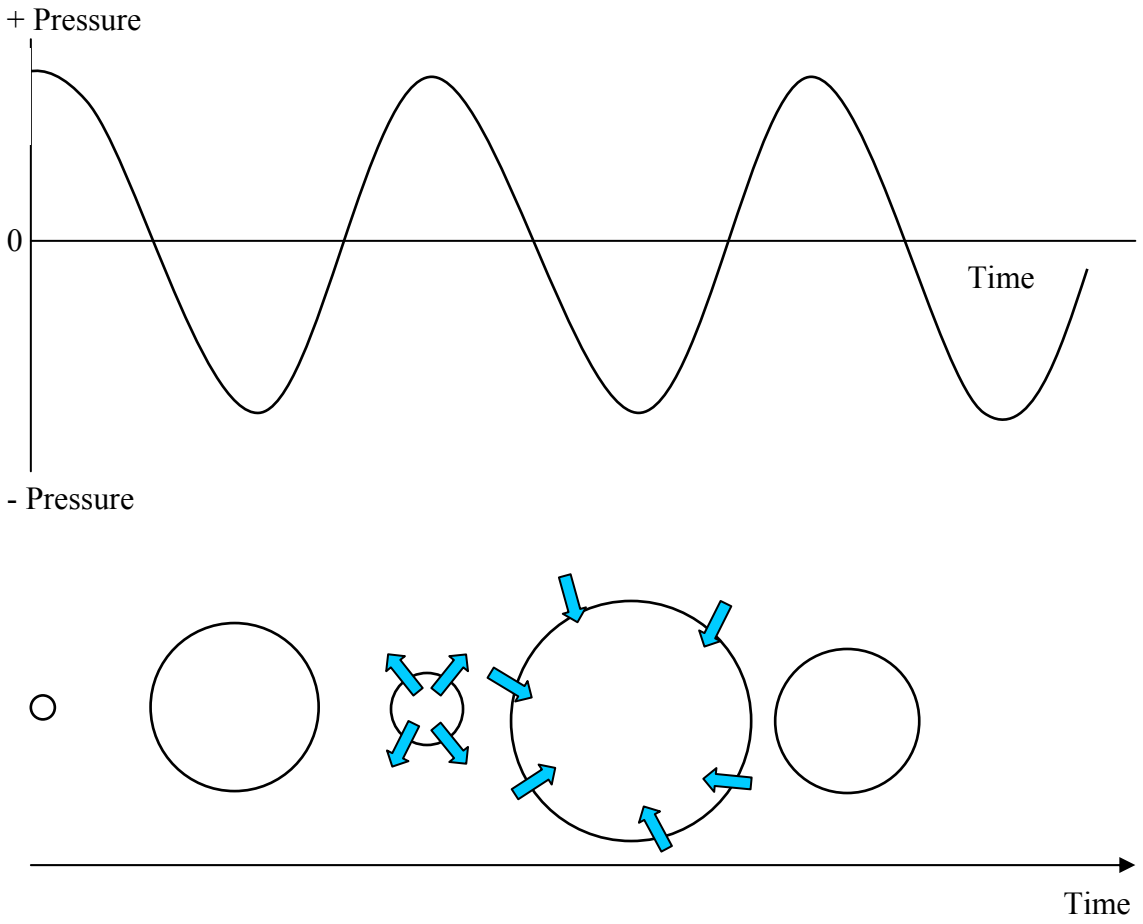


Figure 2.4 The ultrasound field is comprised of a series of compressions and rarefactions. These correspond to regions of high and low pressure, which cause the bubble to oscillate between extreme conditions of compression (smallest radius) and expansion (largest radius). During the compression phase, the pressure inside the bubble is greater than that of the surrounding medium and gas diffuses out of the bubble, over its entire surface. In the rarefaction phase, the bubble is at its largest and gas diffuses into the bubble, again over its entire surface. The surface area of the fully expanded bubble is larger than that of the compressed bubble and so there is a net flux of previously dissolved gas out of solution and into the bubble, leading to growth of the bubble.

If the bubble is far from the resonant size (larger or smaller) the bubble may undergo small amplitude oscillations and shrink. If a bubble fragments, resulting in lots of smaller bubbles that are too small to nucleate inertial cavitation, rectified diffusion can cause these bubbles to grow, making inertial cavitation a self-nucleating process.

2.4.3 Acoustic Streaming

It has been demonstrated that ultrasonic waves are capable of generating pressure gradients within the medium supporting the wave (Section 2.3). If the medium is a fluid, as in the circumstances surrounding ultrasonic scalers, then the fluid can move. This results in the bulk flow of the fluid, known as acoustic streaming (Figure 2.5). Streaming velocities are quite low and are generally of the order of a few centimetres per second (Duck *et al*. 1998; Khambay & Walmsley 1999). However, rapid rates of change of streaming velocity occur producing velocity gradients, which result in substantial hydrodynamic shear stresses (Williams 1986). The forces generated are large enough to disrupt biological cells and tissues and may therefore aid in the removal of biofilms such as dental plaque (Khambay & Walmsley 1999).

As discussed in Section 2.4.2, bubble growth occurs via a process of rectified diffusion in which gas is taken from the liquid near the bubble. This can result in a local depletion of dissolved gas, which may reduce the rate of further bubble growth. However, streaming fields continuously refresh the liquid at the bubble wall with water from further away that still has gas dissolved within it. The converse of this situation also applies in that if a gas bubble is dissolving the streaming has the effect of removing the excess gas, thereby enhancing the rate of dissolution (Duck *et al*. 1998).

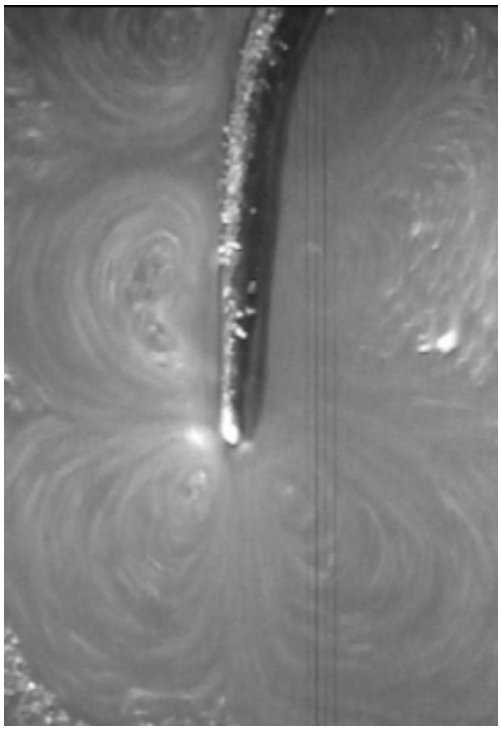




Figure 2.5 Ultrasonic waves can generate pressure gradients within the medium supporting the wave. If the medium is a fluid, as surrounds ultrasonic scalers, then a resulting bulk flow of the fluid occurs, known as acoustic streaming. (Pictures courtesy of Professor A.D. Walmsley, Birmingham School of Dentistry).

2.5 Lasers

2.5.1 Bohr Model of the Atom

The theory of laser physics requires an appreciation of basic atomic structure. Bohr's model of the Hydrogen atom (Figure 2.6) comprises a single electron of mass, m and charge –e circularly orbiting a positively charged nucleus of mass, M and charge +Ze, where Z is the atomic number (in the case of Hydrogen, Z = 1). From the classical laws of electrodynamics, Bohr stated his four postulates for electron motion, "An electron in an atom moves in a circular orbit about the nucleus under the influence of the Coulomb attraction between the electron and the nucleus, obeying the laws of classical mechanics" (Eisberg & Resnick 1985).

Bohr's second postulate states that electrons may only move in definite, quantized orbits, that is, "Instead of the infinity of orbits which would be possible in classical mechanics, it is only possible for an electron to move in an orbit for which its orbital angular momentum L is an integral multiple of ħ, Planck's constant divided by 2π" (Eisberg & Resnick 1985).

Bohr's final postulates were, "Despite the fact that it is constantly accelerating, an electron moving in such an allowed orbit does not radiate electromagnetic energy. Thus, its total energy E_T remains constant" (Eisberg & Resnick 1985). "Electromagnetic radiation is emitted if an electron, initially moving in an orbit of total energy E_i, discontinuously changes its motion so that it moves in an orbit of total energy E_f. The frequency of the emitted radiation ν is equal to the quantity ($E_i - E_f$) divided by Planck's constant h" (Eisberg & Resnick 1985). This last statement may alternatively be expressed as:

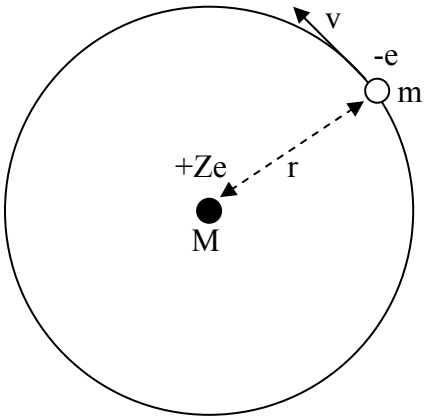


Figure 2.6 Bohr's model of the Hydrogen atom comprises a single electron of mass, m and charge –e circularly orbiting a positively charged nucleus of mass, M and charge +Ze, where Z is the atomic number.

$$E_i - E_f = h\nu \qquad [2.3]$$

where E_i is the initial orbit's total energy and E_f that of the final orbit. The total energy, E_T, of an electron in a Bohr orbit may be obtained by adding the potential energy, E_P and kinetic energy, E_K, of the electron.

Since atoms are generally much more complex than the Hydrogen atom, orbital diagrams can get large and confusing. Therefore, energy level diagrams are used, which are simply horizontal lines drawn to an energy scale (Figure 2.7). Electron orbit jumps may then be represented by vertical arrows between these levels, with the direction of the arrow representing the direction of the jump.

2.5.2 Metastable States

Most atoms in a gas exist in a low energy state, known as the ground state. On the application of energy to these atoms, through collision with another atom / particle, heating etc, a valence electron may be promoted to a higher energy orbital and the atom is now said to be in an excited state. The valence electron remains in this excited state for approximately 1.6×10^{-8} seconds before jumping to a lower energy level (preferably returning to the ground state). This jump is accompanied by the emission of a photon, with frequency ν, determined by the initial and final energy levels of the transition.

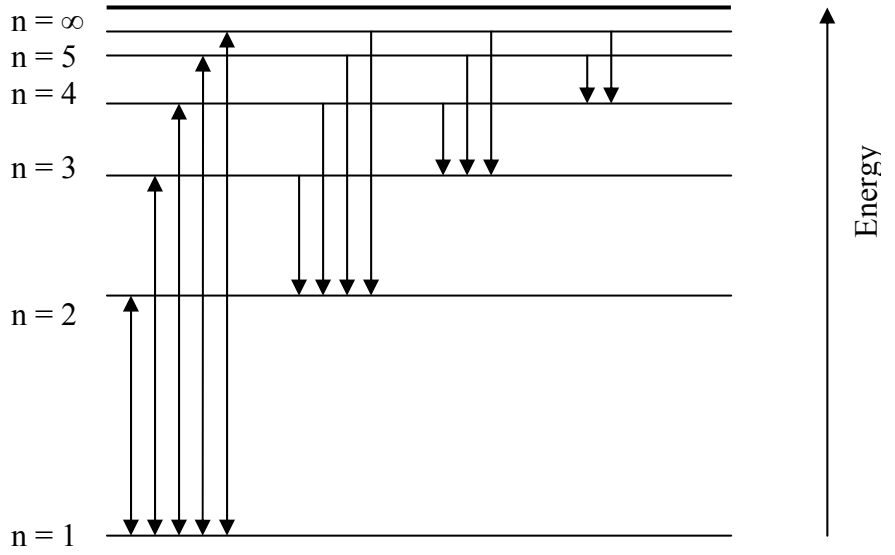


Figure 2.7 Atoms are generally more complex than the Hydrogen atom. To avoid large and confusing orbital diagrams energy level diagrams are used, which are horizontal lines drawn to an energy scale (scale not shown). Electron orbit jumps are represented by vertical arrows between levels. The direction of the arrow represents the direction of the jump.

Sometimes, however, it is not possible for the excited atom to return to the ground state in a single electron jump. The electron jumps to an energy level of greater energy than the ground state (but lower than that from which it came) and becomes trapped. From here, selection rules will not allow the electron to return to the ground state with the emission of a photon and indeed the atom may only return to the ground state by imparting its energy to another colliding atom. Both the existence of metastable states and the energy transfer, through collisions, between an atom in a metastable state and another atom, are important concepts in understanding laser physics.

2.5.3 Application to Lasers - Reference to Helium-Neon Lasers

A laser is a device that amplifies the intensity of light through a quantum process known as stimulated emission and, in fact, the name laser is itself an acronym for this process (Light Amplification by Stimulated Emission of Radiation). The principles of the laser were first put forward by CH Townes and AL Schawlow in a paper published in 1958 (Jenkins & White 1981). There are several types of laser currently available today. These include gas lasers such as Helium-Neon, Carbon Dioxide and Argon lasers, solid lasers such as the Ruby laser or Neodynium YAG (yttrium-aluminium-garnet) laser and molecular lasers such as the Eximer laser. Of these, Helium-Neon (He-Ne) lasers are among the most widely used in optical investigations because they are highly stable, may be operated in a continuous mode (rather than pulsed) and are relatively inexpensive.

He-Ne lasers are composed of a glass tube filled with a mixture of Helium and Neon atoms with between 5 and 7 times as many Helium atoms in the mixture as Neon atoms. When connected to a high voltage power supply, electrodes sealed into the ends of this tube produce

a current of electrons, which flow through the tube. When these free electrons collide with the Helium atoms, the Helium atoms are promoted to an excited state (Figure 2.8). When these excited Helium atoms collide with Neon atoms in their ground state there is a strong likelihood that the excitation energy of the Helium atom will be transferred to the Neon atom due to the near equality of the two excitation energy levels in the two atoms (Figure 2.8). This raises an electron in the Neon atom into an excited orbit and leads to the Helium atom returning to its ground state. This process of using electron-atom collisions to raise the Helium and Neon atoms to excited states is known as pumping.

This energy level of the Neon atom is metastable and, after a period of time, the Neon atom de-excites through the emission of a photon of wavelength 632.8nm (Figure 2.8). It is the emission of light at this wavelength, by Neon atoms, which leads to lasing action. To achieve laser action it is necessary to pump a large number of atoms into excited states and establish what is known as a population inversion. That is, there are more atoms in metastable states than there are in the ground state. If a population inversion is attained, an emitted photon, on passing another Neon atom in a metastable state, may stimulate that atom to emit a photon of the exact same frequency and return the atom to its ground state (Figure 2.9a). This stimulated photon has exactly the same frequency, direction and polarisation (spatial coherence) and the exact same speed and phase (temporal coherence) as the primary photon. Both of these photons may now be considered as primary sources and can stimulate emissions from other metastable Neon atoms in the same manner (Figure 2.9b). A chain reaction may now be developed leading to highly coherent, highly intense, monochromatic radiation.

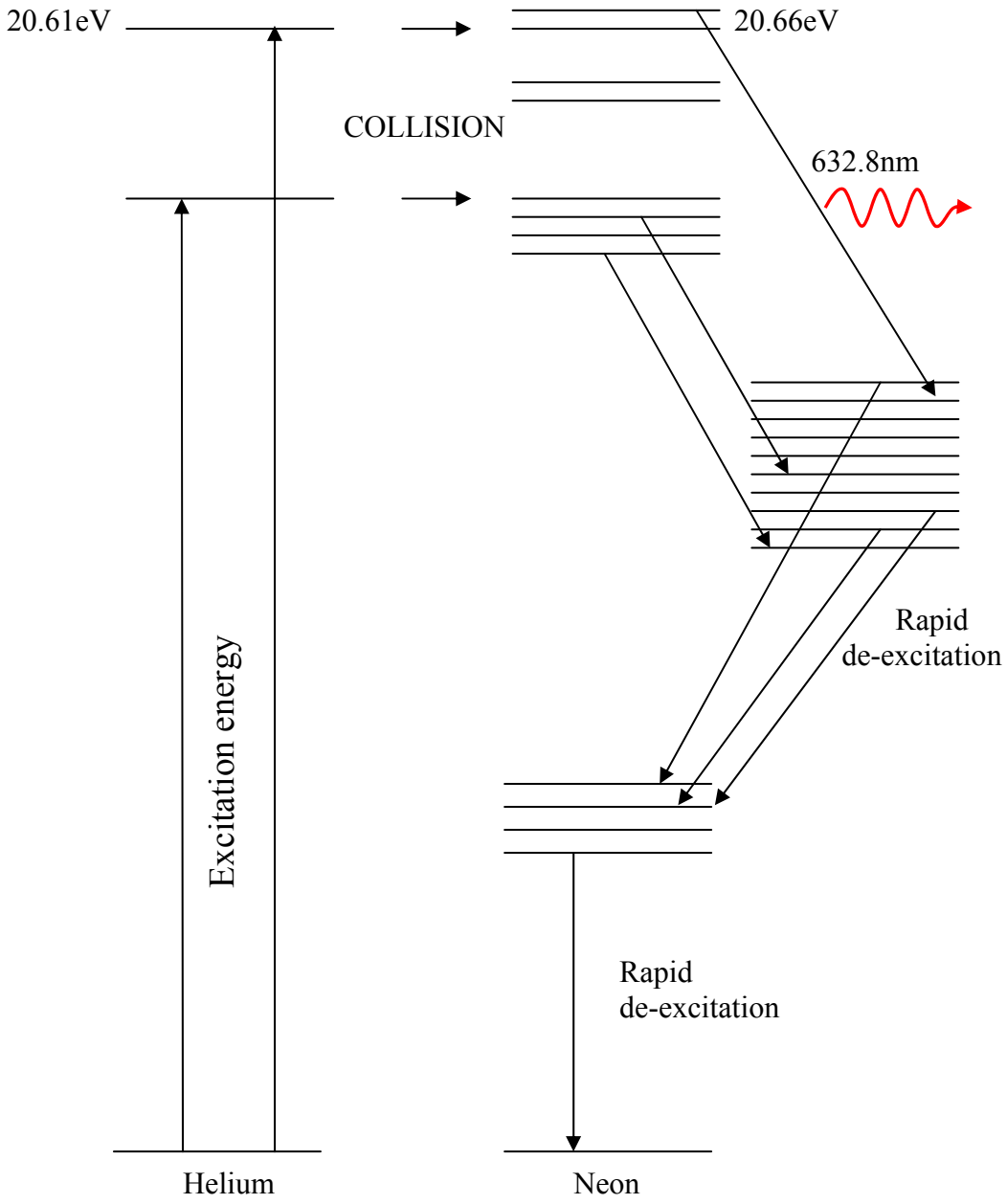
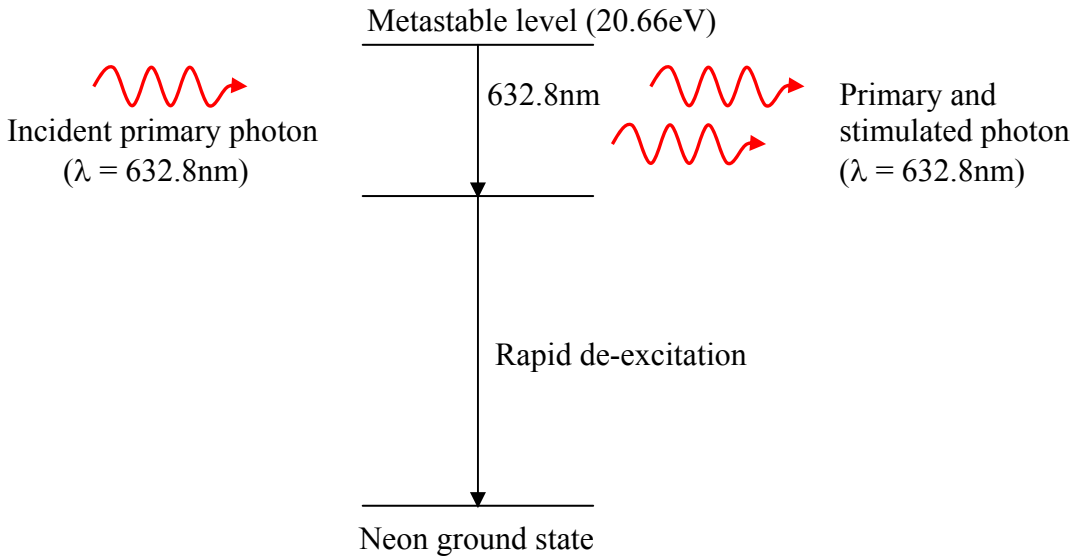


Figure 2.8 He-Ne lasers comprise a glass tube filled with Helium and Neon atoms. A high voltage power supply produces a current of electrons, which flow through the tube. These collide with the Helium atoms, which are promoted to an excited state. The excited Helium atoms collide with Neon atoms in their ground state and the excitation energy of the Helium atoms is transferred to the Neon atoms. This excites the Neon atom to a metastable state from which it de-excites through the emission of a photon of wavelength 632.8nm.

a.



b.

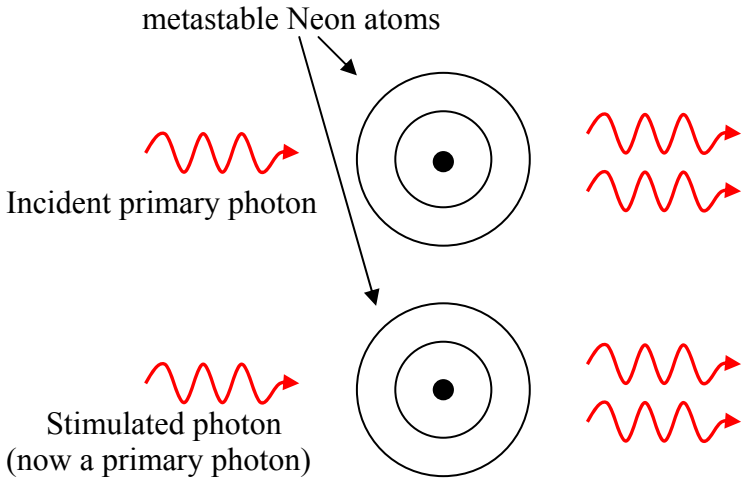


Figure 2.9 a) Laser action requires a larger number of atoms in metastable states than in the ground state. If this population inversion is attained, an emitted photon may stimulate an excited Neon atom to emit a photon with the exact same frequency and spatial and temporal coherence. b) Both photons are now considered primary sources and can stimulate emissions from other metastable Neon atoms in the same manner. A chain reaction may now be developed leading to highly coherent, highly intense, monochromatic radiation.

2.5.4 Properties of Lasers

There are four major optical properties of lasers that make them virtually essential for the laser vibrometer measurement technique (Scruby and Drain 1990), including monochromaticity, coherence, directionality and high intensity.

Light from sources other than lasers may cover a range of frequencies. Laser light is monochromatic since it typically comes from a single atomic transition with a single, precise wavelength. Although the He-Ne laser has several transitions that may lead to light wave emission, some of which are indicated in Figure 2.8, the most intense amplified wavelength is that with wavelength 632.8nm and, through careful design and construction of the laser, it is possible to obtain true single-frequency operation. Monochromaticity enables high coherence to be obtained. The word coherence is used to describe how well a wave disturbance at a point in space or time correlates with a disturbance at another point (Scruby & Drain 1990). Ordinary light is not coherent since it comes from independent atoms that emit on relatively long time scales. For lasers, a common stimulus initiates the emissions and so the emitted photons have a definite phase relation to each other. Coherence is determined by how well the wavefronts remain in step with each other and this is related to the spread of wavelengths within the light. The distance a light ray travels before losing its coherence is known as the coherence length and this may be given (approximately) by the expression:

$$L_{COH} = \frac{\lambda^2}{\delta\lambda} \qquad [2.4]$$

where λ is the wavelength and $\delta\lambda$ is the spread in wavelength. Therefore, in the case where $\delta\lambda \rightarrow \lambda$, as is the case for a filament lamp, the coherence length is very small. However, for a single-wavelength laser, the coherence length is of the order of 10^{10} wavelengths (approximately 6km).

In laser vibrometry, good coherence between the scattered object beam and the reference beam (Section 3.5) is essential since this means the two light disturbances can be made to interfere and produce a predictable interference pattern. The long coherence length also means that an object beam longer than the internally reflected reference beam may be used. That is, the distance to the vibrating target object is not critical and will not affect the sensitivity of the system.

The high coherence of laser beams results in very low beam divergence, enabling the beam to be focussed to very small spot sizes. Similar beam divergence with conventional light sources may only be attained through extreme collimation of the beam, resulting in very low light intensities. The small beam spot size, achievable with lasers, enables both high spatial resolution and increased sensitivity through the collection of a larger proportion of the light scattered from rough surfaces. Low beam divergence also means that the scanner head may be placed at fairly large distances from the target object without appreciable beam spreading allowing for remote measurements if required.

The He-Ne laser used in this laser vibrometer system has an optical power output of approximately 1mW (1 milli Watt). However, the small spot sizes the beam may be focussed down to produce large power densities leading to an increase in system sensitivity.

2.6 The Doppler Effect and Laser Vibrometry

Wave motion is generated by a vibrating source. Wavefronts are emitted from the source with a frequency, f, equal to that of the source and travel with a velocity, v, given by equation 2.1;

$$v = f\lambda \qquad [2.1]$$

where λ is the wavelength of the wave in a given medium. An observer at an arbitrary distance, x, away from the source will hear a particular note (for sound waves) or view a certain colour (electromagnetic waves), determined by the frequency of the waves. Provided both the source and observer remain stationary, the frequency of the waves observed will remain constant. For sound waves there will be no audible change in the note heard and for visible light waves there will be no colour change.

If a relative motion between the source of the waves and the observer is now introduced (due to motion by one or both) the above condition no longer holds true and there is an apparent change in the wave frequency. This effect is known as the Doppler shift and is named after the Austrian physicist, Christian Johann Doppler (1803-1853), who first observed the effect in 1842 (Jenkins & White 1981). The Doppler shift, most commonly encountered in sound as a change in acoustic pitch, is the physical principle upon which all scanning laser vibrometers operate. The cause of the apparent frequency change depends upon whether it is the source, or the observer that is in motion. The following sections are intended to demonstrate how a relative motion between a source of waves and an observer can lead to a change in the perceived frequency of the waves.

2.6.1 Doppler Frequency Shift due to Moving Source

First consider the case of a stationary observer with a source of waves (sound or light waves) moving towards them. Before any motion, the observer experiences waves with a frequency, f, as shown in Figure 2.10a. The time period, T, between wavefronts, for any wave motion is given by;

$$T = \frac{1}{f} \qquad [2.5]$$

Now consider the case where the source of the wavefronts (with frequency, f, velocity, v and time between wavefronts, T) is in motion and moves towards the observer with a constant velocity, u (Figure 2.10b). The source emits an initial wave at time zero (t_0) and then a second wave after a time T has elapsed (t_T). However, in the time period, T, the source of waves has moved towards the observer and reduced the distance between itself and the initial wavefront. A reduction in the spacing between wavefronts is effectively a reduction in wavelength, λ'. Since there is no change in the velocity of the waves, it may be seen from Equation 2.1 that a decrease in wavelength must lead to an apparent increase in perceived frequency. i.e. a source of waves moving towards a stationary observer appears to emit wavefronts with greater frequency than the same source at rest. If the same source of waves is moving away from the observer with a constant velocity, u (Figure 2.10c), then in time period, T, the source of waves has moved away from the observer and increased the distance between itself and the initial wavefront (Figure 2.10c). This is effectively an increase in wavelength, λ''. Again, since there is no change in the velocity of the waves, it may be seen from Equation 2.1 that an increase in wavelength leads to a decrease in frequency. i.e. a source of waves moving away from a stationary observer appears to emit wavefronts with a reduced frequency than the same source at rest.

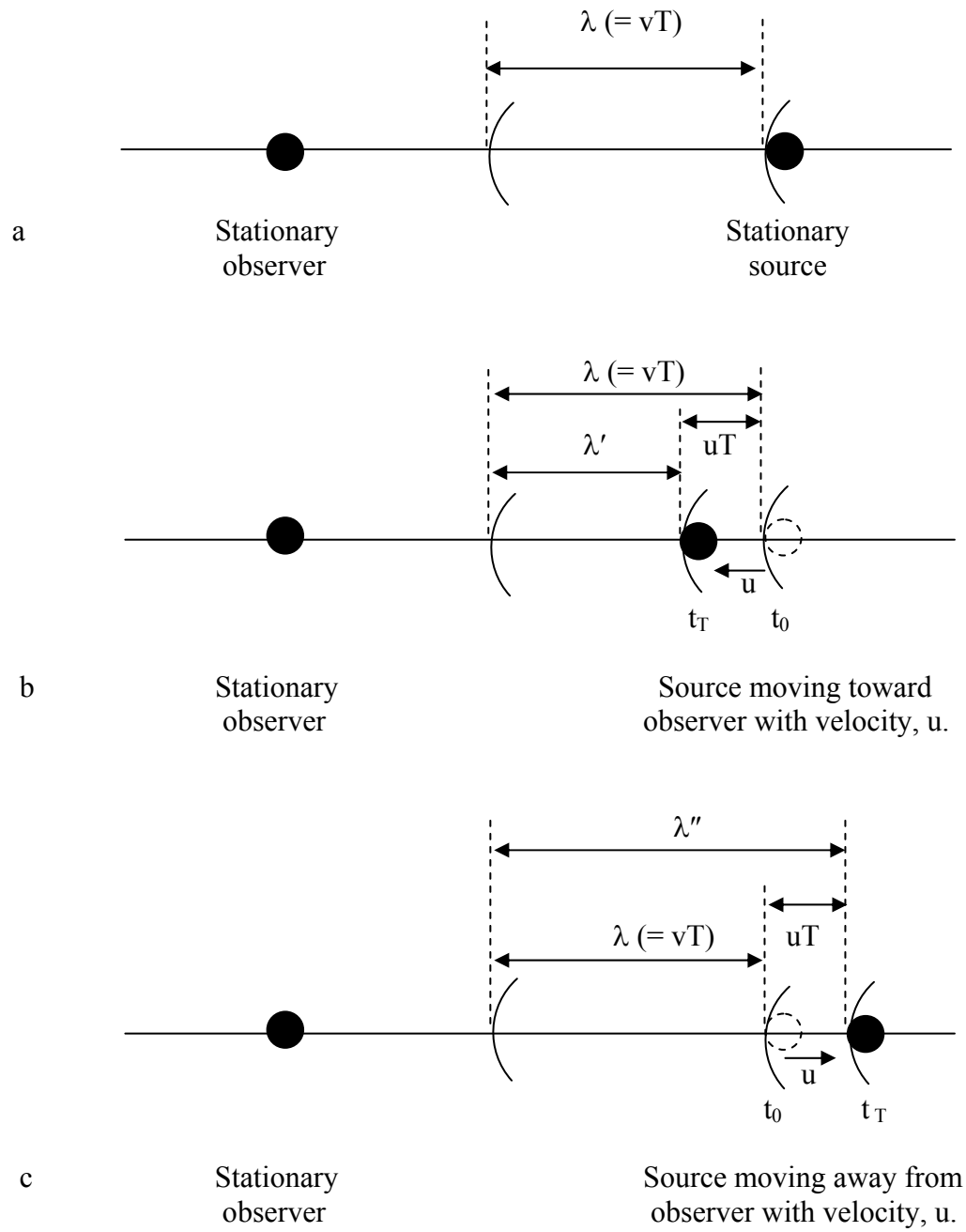


Figure 2.10 a) With a stationary source, a stationary observer experiences wavefronts with a frequency, f, separated by a distance, λ. b) Source moving toward the observer with constant velocity, u, shortens the apparent wavelength to λ′. c) Source moving away from the observer with constant velocity, u, increases the apparent wavelength to λ″.

2.6.2 Doppler Frequency Shift due to Moving Observer

Consider the case where the source of the wavefronts (with frequency, f, period, T and wavefront velocity, v) is stationary and the observer moves towards the source of the waves with a constant velocity, u (Figure 2.11b). The source emits a wave at time zero (t_0) and then a second wave after a time T has elapsed (t_T). In the time period, T, the observer has moved towards the wavefront with constant velocity, u and the wavefront has approached the observer with constant velocity, v. There is therefore an increase in the relative velocity of the wavefront by an amount (v + u) i.e. v′. The source continues to emit wavefronts at the same wavelength but they appear to be approaching the observer much faster. Since there is no change in the wavelength of the waves, it may be seen from Equation 2.1 that an increase in wave velocity at constant wavelength must lead to an apparent increase in the perceived frequency. i.e. an observer moving towards a stationary source of waves encounters wavefronts with greater frequency than when at rest.

If the observer now moves away from the same source of waves with a constant velocity, u (Figure 2.11c) then in the time period, T, the observer reduces the relative velocity of the wavefront by an amount (v – u) i.e. v″. The source continues to emit wavefronts at the same wavelength but they appear to be slower in reaching the observer. Since there is no change in the wavelength of the waves, it may be seen from Equation 2.1 that this decrease in wave velocity at constant wavelength must lead to an apparent reduction in the perceived frequency. i.e. an observer moving away from a stationary source of waves encounters wavefronts with less frequency than when at rest.

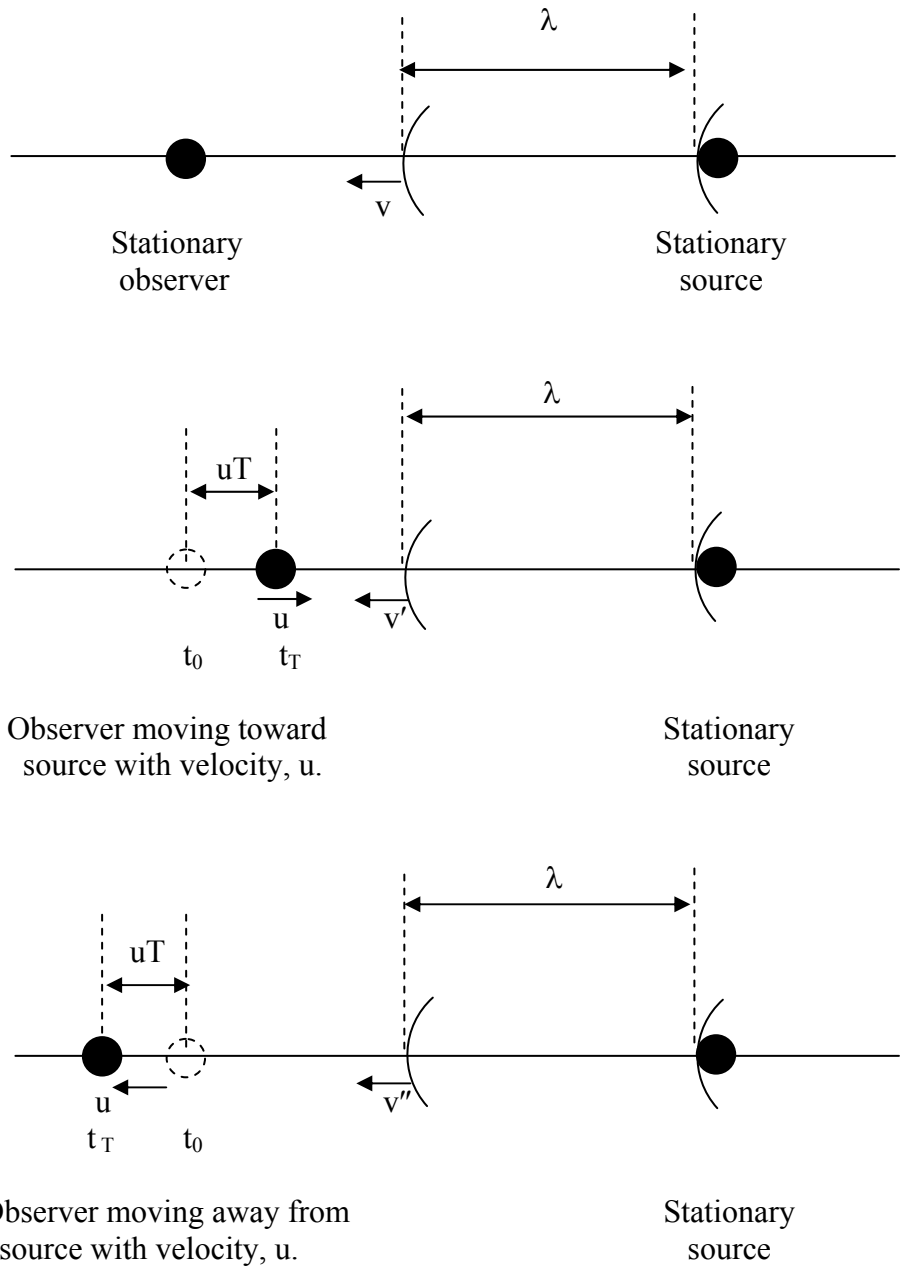


Figure 2.11 a) With a stationary source, a stationary observer experiences wavefronts with a frequency, f, travelling with a velocity, v. b) Observer moving toward the source with constant velocity, u, increases the relative velocity to v′. c) Observer moving away from the source with constant velocity, u, decreases the relative velocity to v″.

2.6.3 Doppler Frequency Shift on Reflection from a Vibrating Target

The laser vibrometer emits a stable source of laser light of constant frequency, which is then scattered from a vibrating target object. The scanner head of the laser vibrometer detects this scattered light, the frequency of which is Doppler shifted from the original laser beam. Since both the emitter and the observer of the light waves are stationary (i.e. the scanner head of the laser vibrometer) the Doppler frequency shift of the scattered laser beam is due to the vibrating target object, from which the laser light is scattered.

Initially, consider a stationary source (the scanner head) which emits light with frequency, f_0 and an object moving toward that source (the vibrating target object in the forward moving phase of its cycle). This is equivalent to the stationary source / moving observer scenario previously discussed (Section 2.6.2). As the object moves towards the source, it encounters more wavefronts per unit time than if it was stationary. Therefore, the observed light frequency is higher than that initially emitted from the source (i.e. blue shifted). This increased frequency is designated $f_0 + f_1$. The vibrating body scatters this light at the same frequency as it received (i.e. $f_0 + f_1$).

For the scattered beam, we now consider the case of a stationary observer (the scanner head) and a source moving towards the observer (discussed in Section 2.6.1). Since the distance between successive wavefronts (i.e. the wavelength) is being reduced (due to the motion of the source towards the camera), the frequency of the light observed at the scanner head is increased by an amount f_2, i.e. $f_0 + f_1 + f_2$. The frequency of this double Doppler shifted signal is designated $f_0 \pm f_D$ (where $f_D = f_1 + f_2$) and the inclusion of the $\pm$ allows for both the forward and backward motion of the target object.

2.7 Heat and Friction

Ultrasonic scaler systems are commonly used for the debridement of tooth and root surfaces. The primary cleaning mechanism of these devices is the mechanical chipping action of the scaler tip when it traverses the tooth surface. During dental ultrasonic scaling procedures, heat is generated due to friction between the tooth and the oscillating tip.

2.7.1 Fundamental Laws of Friction

The fundamental laws of solid friction were first formulated by Leonardo da Vinci (1452-1519) and were subsequently formalised by Coulomb (1736-1806) (Dhinojwala *et al*. 1996). Frictional force, F, is given by the product of a material parameter (coefficient of friction, μ) and the normal force, N.

$$\text{i.e.} \quad F = \mu N \qquad [2.6]$$

Frictional force is independent of the relative sliding speed between the two surfaces (McMillan 1997), though deviations can occur at very large velocities (Elmer 1997). Although dental scaler tips operate at high frequencies (25 to 30 kHz), the speeds of the tips are small (generally less than 10 ms^{-1}) and will not affect the frictional force. Frictional force is also independent (at given load) of the macroscopic contact area (McMillan 1997). Therefore, when the scaler tip is pressed against the tooth surface (for given load), the area of tip in contact with the tooth will not affect the frictional force or the heat generated.

CHAPTER 3

LITERATURE REVIEW

3.1 Periodontology

3.1.1 Dental Anatomy

Teeth are used for mastication and assist in speech. They are also important for a person's appearance in society. In humans there are two sets of teeth - the deciduous and permanent dentitions (Scott & Symons 1974). The deciduous dentition, which precedes the permanent dentition, is normally shed as the permanent teeth erupt.

Teeth may be anatomically divided into two main regions: the crown and the root. The crown is the part of the tooth that is normally visible in the oral cavity, above the gingival line or margin (Figure 3.1). The crown is covered by a hard, acellular, inert tissue called enamel (Figure 3.1). Enamel is the most highly mineralised tissue in the body (Ten Cate 1989). This high mineral content means that enamel is very brittle, unable to withstand the forces generated during mastication without fracture (Ten Cate 1989). Enamel is therefore supported by dentine, a specialised connective tissue, which is encased within the enamel (Figure 3.1) and both supports and compensates for its brittleness (Ten Cate 1989). Enclosed within the dentine is the central pulp chamber (Figure 3.1) that contains a soft connective tissue called pulp (Scott & Symons 1974). The pulp produces and nourishes the dentine that surrounds it and carries the nerves that make dentine sensitive (Ten Cate 1989). The tissues of the tooth crown are what give teeth their hardness and resilience and also provide teeth with a unique permanence that may be used to trace human evolution as well as being a means of identification in forensic science.

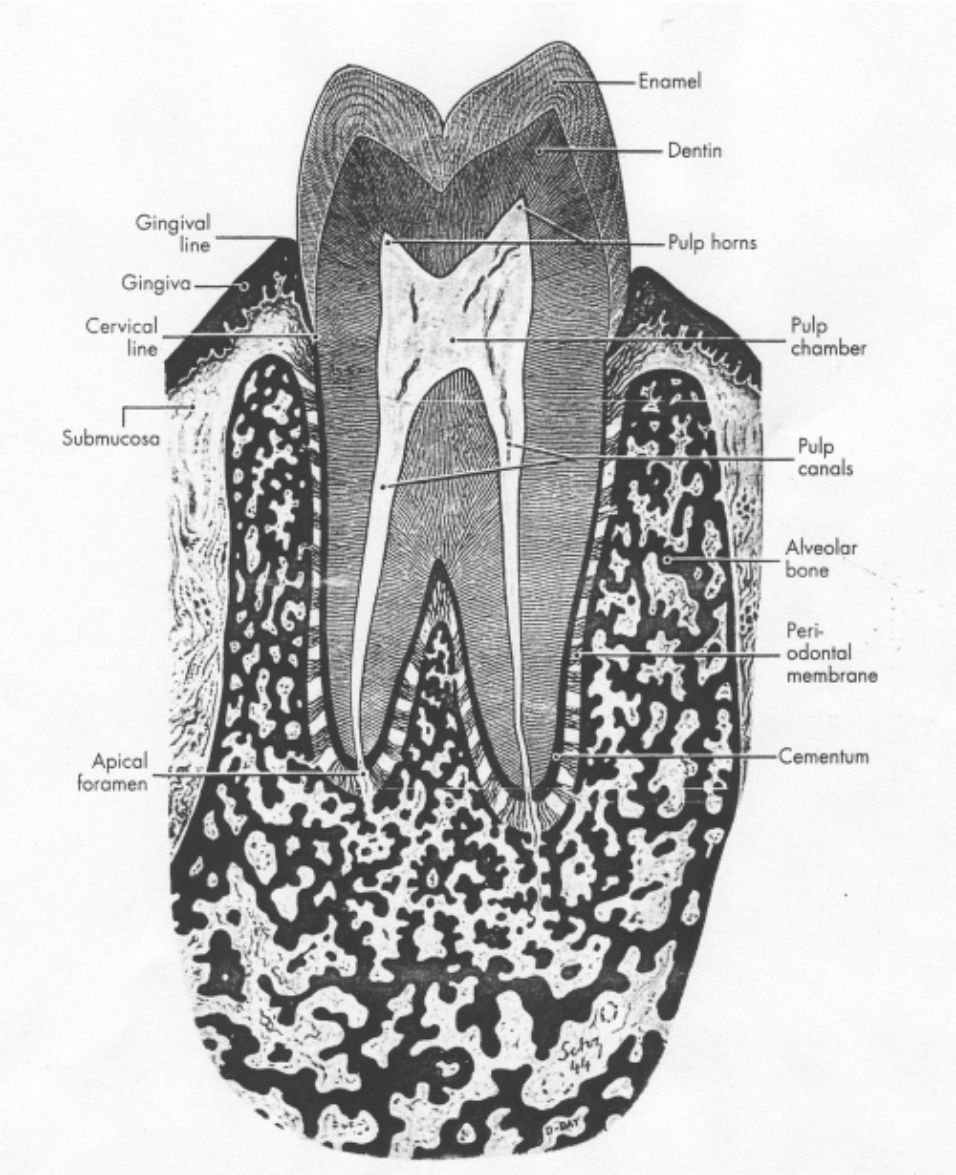


Figure 3.1. The structure of the tooth and its supporting structures (Brand & Isselhard, Anatomy of Orofacial Structures, 1998).

Teeth are connected to the jaw, via the root, by a specialised supporting apparatus that consists of alveolar bone, periodontal ligament (also termed periodontal membrane) and cementum (Scott & Symons 1974; Ten Cate 1989) protected by the gingiva (Figure 3.1). Cementum is a hard, bonelike substance that covers the root of teeth (Scott & Symons 1974; Ten Cate 1989). Between this and the alveolar bone is the periodontal ligament or membrane. This connects the tooth to the jaw in such a way as to allow the tooth to withstand the forces of mastication. Periodontal ligament also has a sensory function, enabling us to determine, for example, when our teeth come into contact with each other.

3.1.2 Plaque and Calculus

Once a tooth has erupted, materials gather on its surfaces. The first of these is a thin (approximately 0.1μm) organic layer known as salivary pellicle, which forms rapidly on teeth after cleaning (Collins *et al*. 2000). This soon becomes colonised by plaque-forming bacteria and usually precedes the formation of plaque.

Dental plaque is always present on teeth, particularly in anatomical areas protected from host defences, such as occlusal fissures and around the gingival crevice (Samaranayake 1998). Plaque may be defined as a tenacious microbial deposit, which forms on the hard tissue surfaces of the mouth, comprising living, dead and dying bacteria and their products, together with host compounds mainly derived from saliva (Samaranayake 1998). The composition of plaque may vary dramatically between different sites on the same tooth, the same site on different teeth and even at different times on the same tooth site (Samaranayake 1998). Plaque is described in relation to its site of origin and may be supragingival, subgingival or appliance associated (Collins *et al*. 2000). Though it may be removed easily through regular oral

hygiene practices such as brushing, plaque is a major factor in the initiation of inflammatory periodontal disease (Collins *et al*. 2000) and provides the organic matrix for calculus formation.

If plaque is allowed to grow undisturbed the degenerating bacteria within may act as seeding agents of mineralisation (Samaranayake 1998). The mineralised bacterial plaque deposit is known as calculus. This is a much harder substance than plaque and requires a more vigorous method of removal to prevent or control inflammatory periodontal disease. Calculus is usually classified according to its location relative to the gingival margin. Supragingival calculus is light in colour and exists on the visible portion of teeth above the gingival margin whereas subgingival calculus, which is usually colonised by anaerobic bacteria, occurs below the crest of the gingival margin and is darker in colour and denser than supragingival calculus.

Calculus may attach itself to the tooth or root surface by several methods and though it may cause little damage to periodontal tissues itself, its presence is associated with periodontal disease (Collins *et al*. 2000). Calculus may also contain toxins derived from plaque that may result in irritation to the gingival tissues. The presence of subgingival calculus is significant since this indicates that the periodontal disease has progressed from gingivitis to periodontitis (Collins *et al*. 2000).

3.1.3 Periodontal Disease

Inflammatory periodontal disease progresses through a series of continuous steps. Gingivitis and chronic periodontitis are often considered to be two stages of the same disease process (Collins *et al*. 2000).

Gingivitis may be characterised by superficial inflammation of the gingival tissues. This is observed as redness, swelling and loss of stippling. Any increase in pocket depth is due to gingival swelling and not loss of attachment. The severity of chronic gingivitis may range between a slight colour / texture change to a severe erythema with possible spontaneous bleeding. Chronic gingivitis is largely symptomless and people suffering from this condition may only become aware of it when their gums bleed slightly during tooth brushing. This condition may be completely reversed in its early stages by an improvement in oral care.

Periodontitis affects all periodontal tissues, particularly the periodontal ligament. Periodontitis is characterised by a loss of attachment, which results in true pocket formation and / or recession and bone loss (Collins *et al*. 2000; Chapple & Gilbert 2002). The periodontal damage caused by loss of attachment is irreversible though it may be possible to stabilise the condition (Chapple & Gilbert 2002).

3.1.4 Prevention and Treatment

The treatment of gingivitis and periodontitis depends upon the severity and the cause of the condition. Early gingivitis may be reversed by an improvement in the general standard of oral care of the patient at home. Löe *et al*. (1965) demonstrated that after gingivitis had been induced in patients with previously healthy gingiva (through the withdrawal of all active oral cleanliness), reinstitution of oral hygiene resulted in healthy gingival conditions.

Prevention and treatment of periodontal disease is normally achieved through the thorough removal of plaque and calculus, which is important for adjacent tissue health to be achieved (Garrett 1977). Although calculus is inert it has a rough texture that promotes plaque

accumulation (Chapple & Gilbert 2002). Tools available to the clinician for treating and cleaning the tooth surface include root planing using hand curettes and the use of anti-microbials and mouthrinses. Another instrument available to the clinician for the debridement of teeth is the ultrasonic scaler.

3.2 The Ultrasonic Scaler

3.2.1 Origins of Ultrasound in Dentistry

The first use of ultrasound in dentistry (Catuna 1953) as a cavity preparation technique generated great interest in the application of ultrasound to dental procedures. Pitt Roche (1954) demonstrated the cutting action of a 50-Watt drill adapted to enable dental cavity preparation and pre-clinical trials found that accurate cutting of hard dental structures could be accomplished rapidly (Nielsen *et al*. 1955) with only slight application pressures being required for operation. Clinically, Oman and Applebaum (1954) reported the successful utilisation of an ultrasonic device to prepare cavities in the teeth of patients. It was further reported that the technique produced accurate, smooth cuts on enamel and dentine whilst patients experienced little or no discomfort (Oman & Applebaum 1955). The first ultrasonic instruments were used in conjunction with an abrasive slurry at the cutting tip (Nielsen *et al*. 1955), which was usually a thick mix of aluminium oxide and water, applied intermittently. Though these instruments were found to give excellent control, this abrasive slurry obstructed observation of the cutting (Nielsen *et al*. 1955).

The use of ultrasound for cavity preparation was thought to offer many advantages (Postle 1958). Pulp reaction to ultrasonic cavity preparation was similar to conventional methods of preparation (Zander 1958) and operating times for ultrasonic and rotary instruments were

found to compare favourably (Tylman 1958). Ultrasonic cavity preparation was also found to have no deleterious effect upon the tissues of forming teeth or upon the partially formed developing permanent successor when ultrasonic energy was applied to a deciduous tooth (Zach 1958).

Ultrasound used for dental cutting causes vibrations of the teeth. Research to determine whether or not transmission of these vibrations had an adverse effect on the periodontal membrane, alveolar bone or gingivae showed that no injury was caused to any of these structures (Mallernee 1958). However, some research was less favourable toward the ultrasonic cutting device. A biologic evaluation of the cutting process reported "severe pulp changes and alterations in dentine formation, which were not present in teeth prepared by rotary methods, were found in teeth cut by the ultrasonic handpiece." and "more severe and more frequent disturbances in amelogenesis were found to be associated with the ultrasonic vibratory cutting process than with conventional methods" (Hansen & Nielsen 1956).

The concept of using ultrasound for cutting / drilling hard tissues was never completely discarded (Knapp & Bernier 1959; Waplington *et al*. 1995; Khambay & Walmsley 2000a&b). However, the high-speed rotary drill eventually became the tool of choice for cavity preparation when work by Street (1959) stated "the ultrasonic method of cutting carious or sound enamel, carious or sound dentine and certain types of restorative materials does not approach the effectiveness that can be demonstrated with the ultra high-speed rotational instruments."

3.2.2 Introduction of the Ultrasonic Scaler

Whilst much time and effort was spent evaluating ultrasonic instruments as cutting tools, it was Zinner (1955) who first reported the application of ultrasound for the removal of calculus from tooth surfaces using an instrument operated with water rather than abrasive slurry. The application of ultrasonic instruments to scaling procedures was investigated *in vitro* and *in vivo* to demonstrate the technique's effectiveness and to compare the ultrasonic technique to routine hand scaling methods (Johnson & Wilson 1957). The conclusions of this early work were very favourable for the ultrasonic instrument, stating that stains were effectively removed and cementum under calculus was virtually unharmed. The technique was more rapid than with conventional hand instruments and patients registered a preference for ultrasonic instruments (Johnson & Wilson 1957). Patient preference for the ultrasonic scaling method was also observed in a study utilising a newly designed Cavitron ultrasonic unit (Wilson 1958). This new unit was designed specifically for use in scaling procedures and had a built in water temperature regulator, a newly designed handpiece and utilised tips that were a permanent part of the insert (Wilson 1958).

Other researchers concluded that the ultrasonic method was no improvement over hand instrumentation and that there was reduced tactile sensitivity, no saving of time and poor field of vision (Burman *et al*. 1958). However, they agreed with Johnson & Wilson (1957) that patient reception of the device was good and that they expressed no more initial discomfort than experienced with hand instruments. McCall & Szmyd (1960) observed that most of their subjects actually expressed a preference for the ultrasonic method and that there was no statistical difference in root sensitivity or in tissue trauma. However, they did suggest that the Cavitron instrument could be further improved (McCall & Szmyd 1960).

Towards the end of the 1960's the ultrasonic dental unit was recognised as an effective tool in accomplishing the healing of diseased periodontal tissues (Clark 1969). Although problems such as clinical burn or coagulation had initially occurred with ultrasonic instrumentation (Ewen 1961), it was now generally regarded as being "safe, convenient, acceptable to the patient and very effective" (Clark 1969).

The ultrasonic technique was shown to satisfactorily remove plaque and calculus (Ewen 1960) and healing following ultrasonic curettage was more satisfactory than that following hand curettage (Goldman 1961; Sanderson 1966). However, the ultrasonic method was only considered to be suitable as an adjunct to hand planing (Stende & Schaffer 1961; Suppipat 1974). Clinical opinion was that the ultrasonic instrument did not plane the root surface as was thought necessary for successful periodontal therapy and was, therefore, to be followed by routine root planing with hand instruments to obtain a smooth hard root (Stende & Schaffer 1961). This view was disputed by Moskow & Bressman (1964) who stated "successful root smoothing and partial cementum removal can be carried out efficiently by use of ultrasonic instruments." Suppipat (1974) noted that calculus and stain removal was quicker with ultrasonic instruments and that patients preferred this method of treatment. However, he too expressed concern over the final root surface roughness caused by excessive application pressure caused by poor tactile sense (Suppipat 1974). The spread of oral micro-organisms, via the 'cavitation spray' or aerosol, into the surrounding air was also a drawback, even if the system was operated by a well-trained person.

The varying views regarding the final tooth and root surface finish generated much interest. Scanning electron microscope studies were performed (Jones *et al*. 1972; Pameijer *et al*.

1972; Wilkinson & Maybury 1973; D'Silva *et al*. 1979) to compare the root surface of teeth following instrumentation using hand and ultrasonic instrumentation and resulted in conflicting views. D'Silva *et al*. (1979) felt that ultrasonic instruments were superior when used in the treatment of incisor teeth but had no advantage when used for treating molars. Similarly, Pameijer *et al*. (1972) observed that although the topography of roots following ultrasonic instrumentation was less flat than produced during hand scaling, the surface textures at high magnifications were not significantly different for the two techniques. In contrast to the findings of Pameijer *et al*. (1972), Wilkinson and Maybury (1973) found ultrasonic instruments produced irregular root surfaces characterised by depressions and irregular ridges that may facilitate the accumulation of plaque. The differences in the two reports were discussed in an editorial comment, which followed the report by Wilkinson and Maybury (1973). The editors noted that the different results could be due to differences in the surfaces under investigation, differences in specimen preparation or, most importantly from the viewpoint of this present work, 'differences in the ultrasonic instruments, the tips and the vibratory settings in the two studies.'

Towards the end of the 1970's and the start of the 1980's research was performed that would lead to dental ultrasonic scaler units being employed in the majority of dental surgeries in the UK. A study comparing the clinical improvement of gingival conditions following hand and ultrasonic instrumentation of periodontal pockets, using four individual operators, demonstrated no significant differences between the two techniques (Torfason *et al*. 1979). This study was conducted over a period of two months. Soon after the publication of the results of this investigation a second study was performed to accumulate even more data regarding the healing events following non-surgical periodontal therapy (Badersten *et al*.

1981). This study was performed using an observation period of thirteen months and, once again, no difference was observed in the results obtained using the hand and ultrasound method of treatment.

3.2.3 Present Knowledge

Since the 1980's there has been an increase in the amount of research into the clinical performance and operational characteristics of dental scalers. The operational characteristics of ultrasonic scalers are usually investigated *in vitro* and generally assess the effects of load, tip angulation and generator power setting on scaler tip oscillation characteristics (Walmsley *et al*. 1986a&b; Williams & Walmsley 1988; Lumley *et al*. 1993; Chapple *et al*. 1995). Many studies have been performed and reports written that compare hand and ultrasonic instruments (Smart *et al*. 1990; Chiew *et al*. 1991; Cross-Poline *et al*. 1995; Schlageter *et al*. 1996; Drisko 1998; Schmidlin *et al*. 2001).

Flemmig *et al*. (1997 & 1998a&b) performed a series of *in vitro* investigations to assess the performance of sonic instruments and both piezoelectric and magnetostrictive ultrasonic instruments under various conditions of load, tip angulation and instrumentation duration. This combination of working parameters was found to affect the defect depth and volume produced using both sonic and ultrasonic scalers (Flemmig *et al*. 1997 & 1998a&b). A study by Busslinger (2001) compared magnetostrictive and piezoelectric ultrasonic instruments directly. This investigation suggested that piezoelectric instruments were more efficient than magnetostrictive instruments but also left the instrument tooth surface rougher. There was also an increase in the amount of understanding of the biophysical effects associated with the ultrasonic scalers, such as cavitation and streaming (Walmsley *et al*. 1988; Laird & Walmsley

1991; Walmsley *et al*. 1992; Khambay & Walmsley 1999) and the role these effects could play in the cleaning of tooth and root surfaces (Walmsley *et al*. 1988).

Potential hazards of ultrasonic scalers were also investigated to determine whether there were any deleterious effects associated with the instruments (Walmsley *et al*. 1986c, 1987 & 1997). A review of the literature has indicated that ultrasonic scalers are generally safe to use providing sensible precautions are made regarding the duration of use of the instrument, that the water flow rate is adequate (not less than 20ml/min) and that the use of magnetostrictive instruments should be avoided when either the clinician or patient has a pacemaker (Trenter & Walmsley 2003).

The Research, Science and Therapy Committee of the American Academy of Periodontology performed a detailed review of the current literature to produce a position paper concerning sonic and ultrasonic scalers in periodontics (Drisko *et al*. 2000). The conclusions of this paper included:

- Sonic and ultrasonic instruments attain similar results to hand instruments in terms of plaque, calculus and endotoxin removal.
- Instrument width may mean manual scalers provide less access to furcations than ultrasonic instruments.
- It is unclear whether powered or hand instruments produce the greatest degree of root surface roughness.
- It is unclear whether root surface roughness affects long-term wound healing.
- A disadvantage of powered scalers is the production of contaminated aerosols.

3.3 Other Dental Ultrasonic Instruments

3.3.3 Endosonic Instruments

The pulp of a tooth may become infected following dental decay. If such a situation arises, the pulp is extirpated and the pulp chamber cleaned and shaped for filling. This cleaning has traditionally been undertaken using hand instruments. However, since Martin (1976) introduced the first commercial machine designed specifically for ultrasonic root canal instrumentation, the technique of endosonics has become an established part of root canal therapy (Lumley *et al*. 1991).

Endosonic files are driven to oscillate at ultrasonic frequencies of 25 to 30kHz, by generators that convert electrical energy into ultrasonic waves via a process of either magnetostriction or piezoelectricity. When operated, the files vibrate in a transverse manner, setting up a characteristic pattern of nodes and anti-nodes along the length of the file (Walmsley 1987; Walmsley & Williams 1989). When the file is moved vertically within the root canal, it is this transverse vibration that produces the filing of dentine.

Like ultrasonic scalers, endosonic files are utilised in conjunction with an irrigating solution, which acts to regulate heating and assist in the removal of debris from the treatment site. An advantage of endosonic systems over hand instruments is the generation of biophysical effects, within the irrigant, around the oscillating file. It is unlikely that inertial (also known as transient or collapse) cavitation, commonly associated with dental ultrasonic scalers, occurs during clinical instrumentation (Ahmad *et al*. 1987a, 1988) due to the generated sound field producing pressure differences insufficient to cause bubble implosion (Lumley *et al*. 1991). A more likely biophysical effect is the generation of complex, steady-state streaming fields,

known as acoustic streaming (Ahmad *et al*. 1987a, 1990). These streaming fields produce large hydrodynamic shear stresses (Laird & Walmsley 1991), which are capable of dislodging or de-aggregating clumps of bacteria and assist in moving the irrigant around the root canal.

3.3.4 Retrograde Instruments

The first application of ultrasound in apical surgery was described by Richman (1957), where an ultrasonic chisel was used to cut bone and resect tooth tissue (Waplington *et al*. 1995). The use of ultrasonic instruments, for the preparation of root end cavities during endodontic surgery, is becoming more widespread. Ultrasonic tips enable easier access by cutting at 90 degrees to the root surface and provide cleaner surfaces than those created by burs (Walmsley *et al*. 1996). A variety of tip designs are available, varying in complexity from simple curves to multi-angled bending. Ultrasonic tips are smaller in size than rotary instruments, allowing better access to the resected root end, minimising the loss of bone/root length. Research has shown that these tips operate most efficiently at medium to high power settings (Waplington *et al*. 1995). However, these tips are prone to breakage, with the incidence of breakage increasing with excessive angulation of the tip (Walmsley *et al*. 1996). To minimise the risk of breakage, the instrument should be switched on with the probe contacting the tooth surface and minimal pressure applied during clinical use. Like ultrasonic scalers and endosonic instruments, retrograde tips should be accompanied by irrigation for removing debris and reduction of heat at the tip/tooth interface. Care should also be taken to avoid contact of the heated tip with bone or soft tissues.

3.4 Non-Ultrasonic Instruments in Dentistry

3.4.3 Sonic Instruments

Sonic scalers, or air turbine scalers, were introduced into the dental market in the 1970's as less expensive alternatives to ultrasonic scalers for scaling and root planing procedures (Laurell 1990). Unlike ultrasonic scaling instruments, which operate at frequencies of between 20 and 30kHz, sonic scaling tips are usually driven to oscillate at frequencies in the range 2 to 6kHz. As well as being cheaper than ultrasonic instruments, sonic scalers are air driven and so may be connected directly to the air turbine outlet of a dental unit (Laurell & Pettersson 1988). Sonic scaler tips generally oscillate in an elliptical manner (Gankerseer & Walmsley 1987) although the mode of oscillation depends upon the material from which the instrument is made, the insert design and the air pressure input (Gankerseer & Walmsley 1987; Kocher & Plagmann 1997a&b). Sonic scaler tip performance is affected by the application of load, with an increase in load resulting in a progressive decrease in the scaler tip displacement amplitude (Gankerseer & Walmsley 1987). The manner in which the tips oscillate affects the efficacy of the instruments in the removal of tooth substances and also has a bearing on any possible damage relating to dental tissues (Gankerseer & Walmsley 1987).

Initial investigations into the clinical effectiveness of sonic instruments found that sonic scalers used in conjunction with hand instruments were more effective for the removal of subgingival calculus than either method used alone (Gellin *et al*. 1986). More recently, studies comparing sonic and ultrasonic scaling techniques have concluded that sonic scalers produce no difference in clinical response to ultrasonic scalers (Loos *et al*. 1987) and that the sonic scaler provides an effective alternative to hand instruments for basic periodontal treatment (Laurell & Pettersson 1988).

Compared to ultrasonic scalers relatively little has been published on sonic scalers (Gankerseer & Walmsley 1987). Research has included substance loss and root surface texture alteration following sonic scaler instrumentation (Kocher *et al*. 2001, Kocher & Plagmann 1997a&b) and heat propagation in dentine during instrumentation with different sonic scaler tips (Kocher & Plagmann 1996). There are many differences between ultrasonic and sonic scalers including cost, the method by which the vibrations of the instruments are generated and, indeed, the frequencies at which the vibrations occur. A further difference is in the production of biophysical forces, such as cavitation, commonly detected with ultrasonic scaling instruments (Lea *et al*. 2005). Cavitation is thought to aid the removal of substances on tooth surfaces. Shock waves generated during bubble collapse disrupt colonies of plaque and provide a 'scrubbing' action (Walmsley *et al*. 1988). It is unlikely that cavitational activity occurs around sonic scaler tips since the generated acoustic pressure field does not oscillate with high enough frequency to cause the rapid bubble growth and subsequent collapse within the lifetime of the bubble.

3.4.4 Powered Toothbrushes

There has been much research into the cleaning efficacy of powered toothbrushes and whether or not they are as effective as manual toothbrushes (Johnson & McInnes 1994; Grossman *et al*. 1996; Heasman & McCracken 1999; Danser *et al*. 2000; Mantokoudis *et al*. 2001). *In vitro* investigations have been performed to assess the effect of toothbrush head action, contact load and duration of use on the removal of deposits from tooth surfaces (Khambay & Walmsley 1995; Schemehorn & Henry 1996). These studies were complimented by clinical trials to evaluate their efficacy *in vivo* (Johnson & McInnes 1994; Van der Weijden *et al*. 1996).

When investigating the performance of powered toothbrushes it is important to consider the mechanical oscillations of the toothbrush head and bristles. It is possible that head/bristle oscillation frequency and displacement amplitude may affect the amount of plaque removal (Grossman *et al*. 1996). Assessment of these vibration characteristics, and how they alter with the application of different loads, may aid the understanding of plaque removal from tooth surfaces and allow the targeting of specific designs to improve toothbrush efficacy.

3.5 Lasers in Dentistry

Among the first to investigate the potential application of lasers to dentistry were Stern and Sognnaes (1964), who evaluated the effects of two types of laser exposure on dental hard tissue. Since this time, lasers have become more widely used in the field of dentistry. Carbon Dioxide (CO_2) lasers can be used as surgical instruments (Tuffin & Carruth 1980), in procedures such as gingivectomies (Pick *et al*. 1985; Roed-Petersen 1993) and can also be used to excise benign, pre-malignant and malignant lesions in the mouth (Frame 1985). Following laser treatment oedema, swelling and post-operative pain are reduced although the laser does not cure these conditions any better than a scalpel (Frame 1985) and healing times are comparable. The Er:YAG (Erbium: Yttrium Aluminium Garnet) laser is most commonly used for hard tissue removal and can be used to produce cavities in enamel and dentine. Benefits of lasers, over conventional drilling instruments, for such procedures include their non-contacting nature, which reduces the amount of vibration produced. Lasers are also quieter and can sterilise as they cut. However, there are also several undesirable side effects that occur when lasers are used on hard dental tissues, of which thermal effects are a main concern. Severe cracking and dentine carbonisation can occur and there is the possibility that

the temperatures generated could cause severe damage of a cellular nature to the dental pulp (Jeffrey *et al*. 1990).

Dental applications of lasers can be more than just 'invasive' procedures. The use of the Doppler shift of laser light, to measure flow velocity, is the basis of a technique known as Laser Doppler Flowmetry (LDF). This method is used in dentistry to assess the vitality of the dental pulp of teeth (Gazelius *et al*. 1988; Watson *et al*. 1992; Mesaros & Trope 1997; Evans *et al*. 1999). Laser light is transmitted to the dental pulp via a fibre-optic probe placed against the tooth surface. Light reflected from moving red blood cells is Doppler frequency shifted, whilst that reflected from stationary objects is not. The proportion of shifted to unshifted light within the reflected beam gives a semi-quantitative measurement of blood flow through the tissue (Evans *et al*. 1999; Roebuck *et al*. 2000).

3.6 Development of the Laser Vibrometer

The history of the laser vibrometer has been discussed extensively elsewhere (Drain 1980). The development of the laser led to many optical measurement techniques, previously thought impracticable, to become possible. Flow patterns in fluids were studied by the introduction of dyes into the flow stream and observing the resulting streamlines. However, this technique became inaccurate for flow velocities of 0.05 cms^{-1} or less due to diffusion of the dye molecules through the medium. Yeh and Cummins (1964) demonstrated that the Doppler shift of laser light, scattered from particulate matter seeded in a flow of water, could be used to determine flow velocity. Using this technique, they were able to perform flow measurements to a minimum detectable flow velocity of 0.004 cms^{-1}.

Today, the use of laser vibrometry has, in many situations, replaced the use of accelerometers or other forms of surface contacting sensors due to its non-intrusive nature. The technique is particularly useful where surfaces may be very hot or easily damped. Laser Doppler vibrometry is now an established technique for the non-contacting measurement of vibration, at a single point, on solid surfaces. However, there are some situations, such as ultrasonic scaler tips, where the vibration pattern of the whole surface of the tip is required and not just a single point on the surface. Moving the target in front of the stationary laser beam would be both inaccurate and would also introduce noise into the system due to vibrations caused by the mechanisms guiding and moving the target. Since the target must therefore remain fixed, the laser beam instead should be scanned over the target object. It was this need that led to the introduction of the scanning laser vibrometer (SLV).

3.7 Laser Vibrometry

Despite being a relatively new technology, the range of applications to which laser vibrometry has already been applied is vast and it would be impossible for all its uses to be covered in this work. However, it is hoped that the following will give a guide as to the broad spectrum of fields and specialities that make use of the technique of laser vibrometry and will demonstrate how laser vibrometry is becoming an invaluable tool for non-contacting vibration analysis.

3.7.1 General Applications

A problem encountered in art conservation is that associated with the detachment of plaster, of historical murals and fresco paintings, from the wall. The traditional technique for performing structural diagnostics on these works of art is the percussion method (Fricke-

Begemann *et al*. 2000), where the restorer knocks on the painting surface and senses the surface vibrations with his fingertips and listens to the sound induced (Castellini *et al*. 2000). This can be a slow and cumbersome technique that also depends on the experience of the restorer and, more importantly, is a technique that may affect the delicate layers of paint. The laser vibrometer may now be used for the non-invasive measurements of damage to these murals and paintings (Castellini *et al*. 1996 & 2000). The laser vibrometer technique requires the fresco painting to be acoustically stimulated. The vibrometer is then used to characterise any defects through the different vibrational behaviour of defective zones.

The laser vibrometer has recently found application as a novel technique for the detection and discrimination of artificial objects buried in the ground, with particular emphasis on land mine detection (Donskoy *et al*. 2002). At present, metal detectors and magnetometers are used for detecting metallic objects in the ground, but these cannot differentiate between land mines and metallic debris, which leads to many false alarms. Another problem with current methods is that many modern land mines are made of non-metallic materials, such as plastic or wood, with very few metal parts in them and, as such, are undetectable by metal detectors. A seismic (solid-borne sound waves) or acoustic (airborne sound waves) approach may be used to excite low frequency (less than 1kHz) vibrations of a buried mine. The surface vibration signature above the mine may then be remotely sensed using a laser vibrometer. This technique has been shown, in field and laboratory tests, to be able to successfully differentiate between land mines and tree roots, rocks and chunks of metal (Donskoy *et al*. 2002).

3.7.2 Applications in Industry

The list of industrial applications in which laser vibrometry has found use is vast and highly diverse, ranging between measuring the surface topography of magnetic disks (Bogy *et al*. 1986) and damage detection in large scale structures such as bridges (Khan *et al*. 2000). Laser vibrometry may be used for damage detection investigation since damage to a structure usually causes an increase in flexibility that may be detected as a change in the natural frequency of the object. There may also be localised regions of increased vibration displacement amplitude.

Wind turbine blades, such as those used in wind farms, are made of fibreglass due to the cost effectiveness of the material. However, with so many 'windmills' in close proximity to each other, aerodynamic interaction can occur, leading to unpredictable and excessive loads on the blades (Ghoshal *et al*. 2000). These blades may also be damaged by moisture absorption, fatigue, wind gusts and lightning strikes (Ghoshal *et al*. 2000). By using piezoceramic patches to initiate vibrations along the blade length, laser vibrometry can be used as a means of detecting damage to the blades.

3.7.3 Applications in Biology, Medicine and Dentistry

The tympanic frequency responses of the American bullfrog (*Rana catesbeiana*) have been investigated using laser vibrometry (Hetherington 1994) showing that there are clear sex-related differences in middle ear frequency responses between the sexes. The middle ear of adult males showed a peak in sensitivity at 200Hz that was not present in the female middle ear and it is thought that this enables male bullfrogs to recognise the mating calls of competing male bullfrogs.

Hearing is made possible when sound vibrations are detected by the ear and are then transmitted to the brain as electrical impulses. The ear is, therefore, a structure of the body that is highly dependent on vibrations and their accurate interpretation. Conduction hearing loss can occur for several reasons, including damage to the ossicles (the malleus, incus and stapes bones) either by trauma or disease. Since the eardrum and bones associated with the conduction mechanism of the ear are so small and sensitive, laser vibrometry has found unique application in many associated investigations (Stenfelt *et al*. 2002; Lord *et al*. 2001), including the measurement of stapes velocity in the design of a prototype middle ear hearing implant (Mills *et al*. 2001 a & b).

Published aspects of this thesis have shown that laser vibrometry is a suitable instrument for performing non-contacting investigations into the vibration characteristics of ultrasonic scaler tips and powered toothbrushes (Lea *et al*. 2002, 2003a&b, 2004a-c). These investigations have successfully studied the effect of water flow rate (Lea *et al*. 2002), generator power setting (Lea *et al*. 2003a) and load (Lea *et al*. 2003b) on scaler tip displacement amplitude. The oscillation frequencies and associated displacement amplitudes of powered toothbrush vibrations have also been examined (Lea *et al*. 2004c). Other research into the vibration characteristics of dental ultrasonic scalers, using laser vibrometry, has focussed more specifically on slimline inserts (Trenter *et al*. 2003). This research concluded that there is a high degree of variability between tips made by different manufacturers and even between tips made by the same manufacturer (Trenter *et al*. 2003). This work was in agreement with a previous study, which utilised the techniques of finite element analysis and laser vibrometry to model tip vibration (Trenter *et al*. 2002). It was demonstrated that tips of identical design produced significantly different vibration displacement amplitudes.

3.8 Infrared Thermography (Thermal Imaging)

Thermal imaging was first conceived of in 1800 by William Herschel. He discovered the presence of invisible heating rays, which are now known as infrared radiation (Ring 2000). Forty years later, John Herschel (William's son) made an image of solar heat by allowing this heat to disperse soot particles in an alcoholic suspension, in what is known as an evaporagraph (Ring 2000). Today, infrared thermography, (commonly known as 'thermal imaging') has found use in a wide range of applications.

Objects buried in the earth cause small surface temperature variations (less than 1ºC) because the buried object impedes the local thermal energy flow in the soil above it (Deans *et al*. 2001). These temperature variations on the ground can be measured using infrared thermography. This has lead to infrared thermography being used for the detection of land mines (Deans *et al*. 2001). Thermal imaging has also found use in a variety of medical and biological fields. Infrared imaging has been used to determine whether the begging of house sparrow nestlings can be detected as an observable change in body surface temperature (Ovadia *et al*. 2002). Depending upon pathogen type, plants can show either a resistance or susceptibility. It has been hypothesised that at points of infection, plants may display local temperature increases (Chaerle *et al*. 1999). High-resolution infrared cameras may be used to detect temperature increases at infection sites before necrotic lesions appear (Chaerle *et al*. 1999).

Thermography in cardiac surgery can be used to provide the surgeon with vital information such as coronary flow, coronary anatomy and myocardial perfusion and function (Gordon *et al*. 1998). Thermal imaging finds use in a wide variety of other medical applications because

of its ability to detect changes in localised skin blood flow, an example of which is given by the assessment of burns, where infrared thermography may be used to provide a useful estimate of burn depth (Liddington & Shakespeare 1996) and also in studying vascular reactions to smoking (Fushimi *et al*. 1998). Recent outbreaks of Severe Acute Respiratory Syndrome (SARS) lead to a requirement for a rapid screening process that would enable air travellers with an elevated body temperature to be detected. It was proposed that since SARS carriers experience high fever and, therefore, elevated body temperature, thermal imaging systems could be utilised to monitor passengers as they pass through airports (Seffrin 2003). However, factors such as environmental and equipment variables can affect the accuracy of data obtained and so this use of thermal imaging may be limited.

Published research from this thesis has recently shown that thermal imaging is a suitable tool for assessing the heat generated at the surface of a tooth, by ultrasonic scaling instruments, under various tip/tooth load conditions and for varying water flow rates (Lea *et al*. 2004d).

3.9 Cavitation

3.9.1 The Discovery of Cavitation

During early testing in 1894, the British torpedo-boat destroyer HMS Daring was suffering from inexplicably poor performance, with top speeds well below those predicted (Weitendorf 2001). Whilst investigating this problem, Sir John I. Thornycroft and Sydney W. Barnaby noticed a severe vibration from the destroyer's propeller and suggested that large bubbles or cavities, formed by the spinning propeller and imploded by water pressure, were the source of the vibration (Suslick 1989). With this, Thornycroft and Barnaby became the first to observe the phenomenon of cavitation, a name derived from the Latin word "cavus,-a,-um" (*Engl.*

"hollow") proposed by R.E. Froude (Weitendorf 2001). Thornycroft and Barnaby redesigned the propeller using much wider blades but as the Royal Navy built faster vessels the problem became increasingly significant (Suslick 1989). In 1917, the Royal Navy commissioned Lord Rayleigh to investigate the problem. Although he did not find a way to prevent the problem, he confirmed that the vibrations were due to the enormous turbulence, heat and pressure of imploding cavities (Suslick 1989) and derived useful equations to describe bubble growth and collapse.

3.9.2 Cavitation in Nature

It is perhaps interesting to note that, as with many of the phenomena that man discovers, nature not only already knows about cavitation but also understands and utilises it much more effectively than we do. The snapping shrimp (*Alpheus heterochaelis*) uses the shock wave produced following cavitation bubble collapse to stun or even kill its prey (Lohse *et al*. 2001). When the shrimp's claw snaps shut a high velocity jet of water is forced out. The pressure in the jet is reduced to below that of the vapour pressure of water. This reduced pressure enables air bubbles in the seawater to rapidly expand. As the water pressure then returns to its normal level the air bubbles implode, generating a shock wave. Snapping shrimp usually exist in large colonies and the background noise they create in many of the world's shallow oceans is intense enough to disturb the use of sonar for scientific and military applications (physicsweb 2000).

3.9.3 Cavitation in Dentistry

Ultrasonic scaling instruments, used in dentistry, operate at frequencies of between 25 and 30kHz (Laird & Walmsley 1991). The primary cleaning action of these instruments is

attributed to the vibratory motion of the scaler probe. However, another process that may aid in the removal of substances from tooth surfaces is the phenomenon of cavitation, which occurs in the cooling water as it flows over the insert probe (Laird & Walmsley 1991). Cavitational activity around dental ultrasonic instruments has previously been evaluated by two main methods. The first of these was by observing the effects of cavitation on both plaque removal and on the root surface itself (Walmsley *et al*. 1984, 1985, 1988 & 1990). This was performed by operating the scaling instruments both with and without the cooling water flow and observing any differences in the resulting tooth surface or in the amount of plaque removed from the tooth surface. The second method was by attempting to quantify the amount of cavitation around the instrument itself (Ahmad *et al*. 1987a & 1988, Lumley *et al*. 1988 and Walmsley *et al*. 1986b & 1991). This was done using techniques such as sonoluminescence, the Weissler reaction and Fricke's dosimeter, which are discussed in further detail in Chapter 4. More recently, the terephthalate dosimeter has been shown to be an effective method for determining whether cavitation occurs around dental ultrasonic scalers (Lea *et al*. 2005)

CHAPTER 4

MEASUREMENT TECHNIQUES

Assessment of Vibration

4.1 Introduction

There are many situations where analysis of a vibrating body may be performed using some form of contacting sensor such as an accelerometer. However, this method of vibration measurement is not suitable for bodies whose oscillation characteristics may be affected by the sensor itself. It is well documented that the vibration characteristics of scaler tips change when they are placed under load (Flemmig *et al*. 1998a&b). Therefore, the use of any form of surface contacting sensor for the assessment of scaler tip vibrations is highly unsuitable.

Previous assessment of the oscillation of these instruments was performed by directing a beam of light onto the tip of the scaler probe which, when reflected off a scratch on the surface, resulted in a pinpoint of light (Walmsley *et al*. 1986a&b). When the apparatus was operated this pinpoint of light became elongated into a thin bright line, the length of which indicated the excursion of the probe tip. However, this was a time-consuming procedure that did not allow detailed visualisation of the probe movement or accurate measurement of its displacement amplitude.

The use of laser vibrometers to analyse the vibrations of solid bodies has, in many situations, replaced the use of surface contacting sensors, due to its non-intrusive nature. The technique is particularly useful where surfaces may be very hot or easily damped. By employing this

technology, the vibration characteristics of dental scaler probes may be studied rapidly and with greater accuracy than previously possible.

4.2 Scanning Laser Vibrometer Optics

The principles behind the laser vibrometer have been discussed previously (Drain 1980; Pickering *et al*. 1986; Rothberg *et al*. 1989; Halliwell 1995; Ngoi *et al*. 2000). A typical scanning laser vibrometer (SLV) consists of a scanning head, which combines a laser, optics and integral video camera and a controller/workstation, where the measured data is decoded and manipulated. The optical system of a scanner head (Polytec OFV 056, Polytec GmbH, Polytec-Platz, Waldbronn, Germany) is shown schematically in Figure 4.1. The configuration of the scanner head is based on a modified Mach-Zehnder interferometer. The light source is a low power (<1mW), helium-neon (He-Ne) laser beam with a wavelength of 632.8nm and an initial frequency, designated f_0.

At the polarising beam splitter, BS1 (Figure 4.2), the randomly polarised laser beam is split into a reference and an object beam of approximately equal intensity. Both beams are linearly plane polarised, with their axes of polarisation orthogonal to each other i.e. vertical and horizontal polarisation axes (Figure 4.2). After BS1, the object beam passes through polarising beam splitter 2 (BS2), with no change in its polarisation state. BS2 is then followed by a quarter-wave plate ($\lambda/4$-plate) which is a device used for turning linearly polarised light into circularly polarised light and vice-versa.

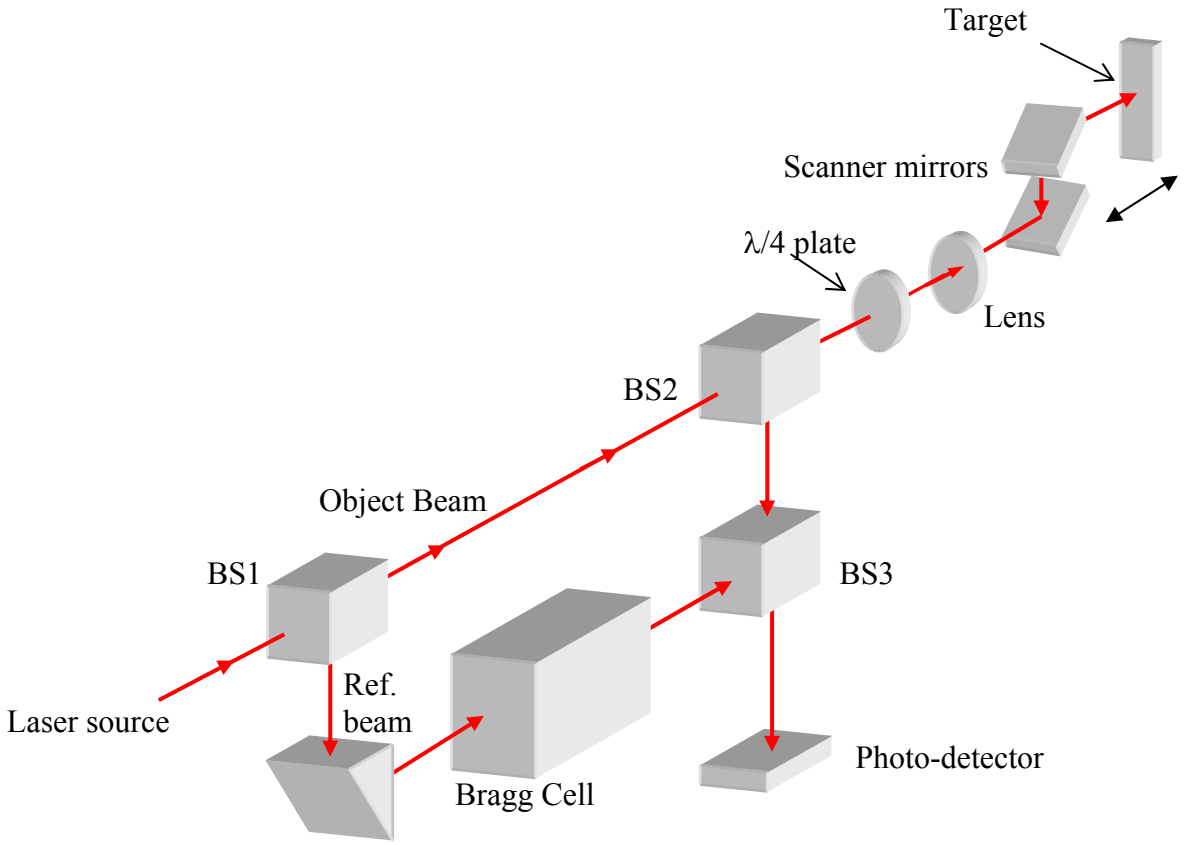


Figure 4.1 Optical configuration of a typical scanning laser vibrometer. At beam splitter BS1 the laser beam is split into a reference and object beam. After BS1, the object beam passes through beam splitter 2 (BS2). BS2 is then followed by a quarter-wave plate (λ/4-plate). The λ/4-plate turns the linearly polarised object beam into circularly polarised light, which is then focussed by a lens system onto the target, via the scanner mirrors. The beam is scattered from the target and collected within the scanner head. The λ/4-plate and BS2 direct the returning beam towards beam splitter 3 (BS3) where it is recombined with the reference beam. After BS3, the object beam and reference beams are heterodyned on the surface of the photo-detector.

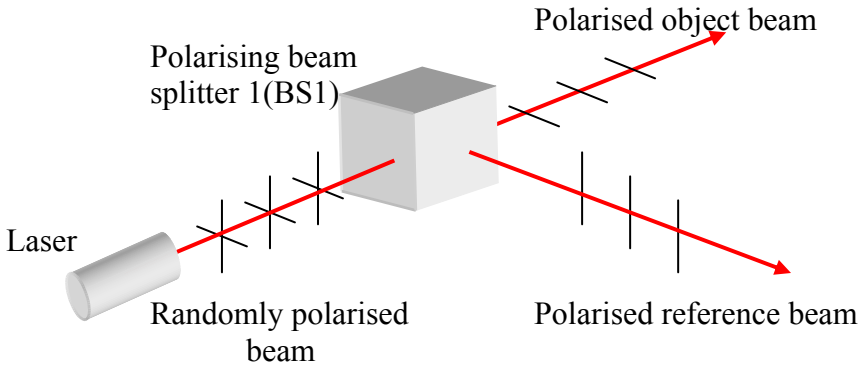


Figure 4.2 At the polarising beam splitter, BS1, the non-polarised laser beam is split into a reference and object beam of approximately equal intensity. Both beams are linearly plane polarised, with their axes of polarisation orthogonal to each other.

When properly aligned, the quarter wave plate turns the linearly polarised object beam into circularly polarised light (Figure 4.3a). The beam is then focussed by a lens system onto the target, via the scanner mirrors (Figure 4.1). These scanner mirrors differentiate the scanning laser vibrometer from a single point laser Doppler vibrometer. The mirrors may be controlled remotely from the workstation and enable the operator to scan the beam, horizontally and vertically, over the surface of the target object. During measurements, the oscillating target must be vibrating towards and away from the scanner head.

4.3 Measurement of Vibration Velocity

On being scattered by the target object, the laser beam is frequency shifted (due to the Doppler effect) by an amount, f_D from the initial frequency, f_0. The Doppler frequency shifted signal, discussed in Section 2.6, is designated as having frequency $f_0 \pm f_D$, which allows for the forward and backward motion of the target object, where

$$f_D = \frac{2u(t)}{\lambda} \qquad [4.1]$$

and u(t) is the vibration velocity of the specimen and λ the wavelength of the laser light. This leads to

$$u(t) = \frac{f_D \lambda}{2} \qquad [4.2]$$

If f_D is measured then the vibration velocity of the target can be determined. The associated computer software may then calculate the displacement amplitude of the target.

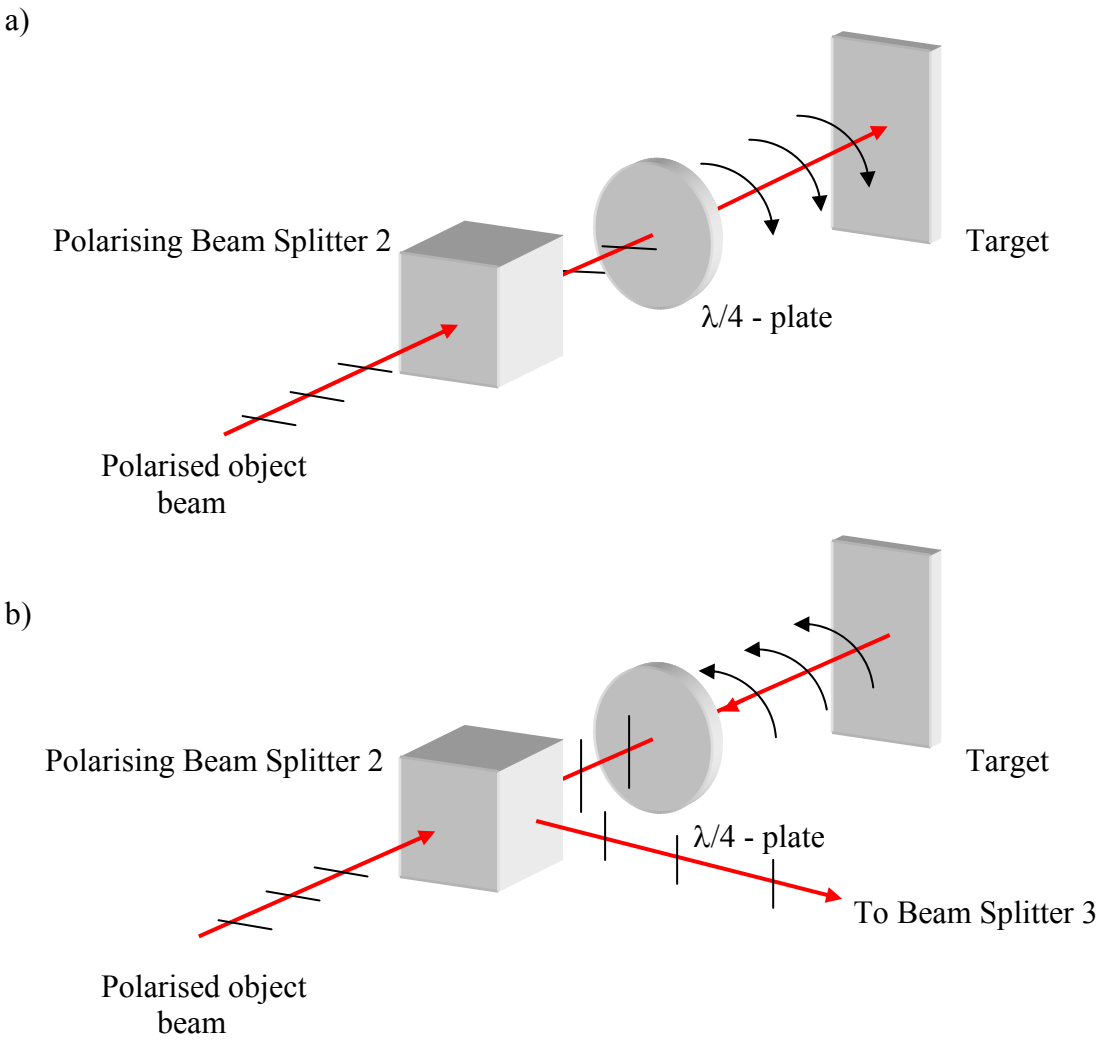


Figure 4.3 a) When properly aligned, the quarter wave plate turns linearly polarised light into circularly polarised light. b) The laser beam, scattered from the target object, is circularly polarised in the opposite direction to the original incoming beam. On re-entering the scanner head, the beam is linearly plane polarised by the quarter-wave plate, but in the plane orthogonal to the original outgoing object beam, due to the opposite polarisation of the outgoing and returning beams.

The laser beam, scattered from the target object, is circularly polarised in the opposite direction to the original incoming beam (Figure 4.3b). The returning beam follows the same path as the outgoing beam and is collected within the scanner head. On re-entering the scanner head, the beam is linearly plane polarised by the quarter-wave plate, but in the plane orthogonal to the original outgoing object beam (Figure 4.3b). This is due to the opposite polarisation (also referred to as opposite handedness) of the outgoing and returning beams. BS2 is polarisation sensitive and will only allow passage of light plane polarised in the same direction as the original object beam. BS2 and the λ/4-plate now act as an optical directional coupler and the returning beam is directed towards beam splitter 3 (BS3) where it is recombined with the reference beam. After BS3, the object beam and reference beams interfere (or are heterodyned) on the surface of the photo-detector.

The use of a λ/4-plate, in the scanner head configuration, improves the optical efficiency of the system. Without it, each of the beam splitters would require more laser power for the beam to make its outward and return journey. This increase in power would lead to the photo-detector being less sensitive to small velocity changes. A beat frequency in the current output of the photo-detector is produced, the frequency of which is determined by the difference in frequency between the object and reference beams. If the reference beam (frequency, f_0) and the object beam (frequency ($f_0 \pm f_D$)) interfere directly, a current output (I_{output}) proportional to f_D is produced, that is

$$I_{output} \propto \left| f_0 - (f_0 \pm f_D) \right| \qquad [4.3]$$

which is equivalent to

$$I_{output} \propto \left| f_D \right| \qquad [4.4]$$

4.4 The Bragg Cell

The present configuration, described by [4.4], gives a current output that is proportional to the magnitude of f_D but does not differentiate between the target surface moving toward or away from the camera. Directional discrimination is a fundamental problem with the heterodyning process used in laser Doppler velocity measurements.

To remove this ambiguity, the reference beam, after BS1, is passed through a Bragg cell or Acousto Optic Modulator (AOM). The operation principles of Bragg cells have been discussed previously (Drain 1980; Young 1986). Bragg cells use the diffraction of light by acoustic waves (of suitable wavelength) in a transparent medium, to frequency shift light (Figure 4.4). The acoustic waves are generated by a piezoelectric transducer (Figure 4.4), which is driven by a radio frequency (RF) signal. If the laser beam is incident at an angle θ to these wave fronts (Figure 4.4) and the reflections undergo constructive interference, then angle θ is known as the Bragg angle.

The Bragg condition for constructive interference between reflections from two surfaces, separated by a distance d in a medium, is given as

$$2d \sin \theta = n\lambda \qquad [4.5]$$

Substituting $d = \lambda_A$ (i.e the acoustic wavelength) and $n = 1$, the Bragg angle is given as

$$2\lambda_A \sin \theta = \lambda \qquad [4.6]$$

0

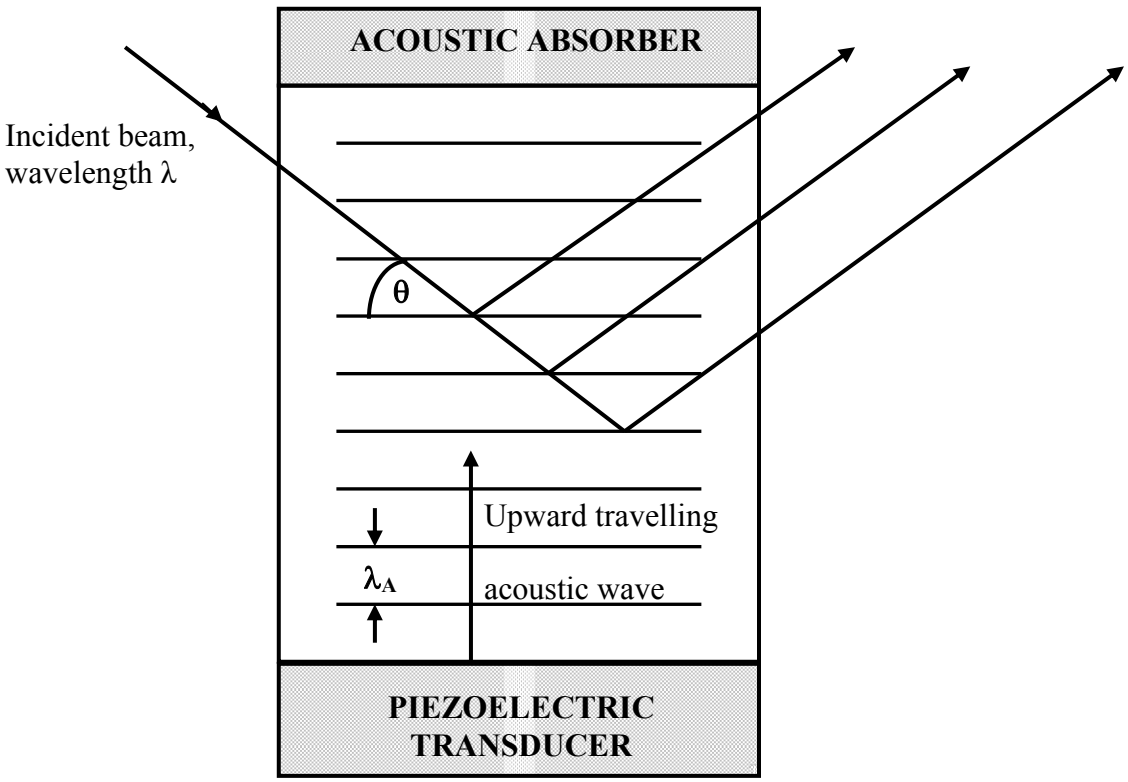


Figure 4.4. Problems with directional discrimination, in laser Doppler velocity measurements, are removed by passing the reference beam through a Bragg cell or Acousto Optic Modulator (AOM). These use the diffraction of light by acoustic waves (wavelength λ_A) in a transparent medium, to frequency shift the light.

where λ_A is the acoustic wavelength and λ the laser wavelength in the medium. The propagating sound wave causes the deflected light to be frequency shifted from the incident beam, by an amount equal to the sound frequency (Young 1986).

The addition of the Bragg cell in the reference arm of the optical system, therefore, shifts the reference beam frequency by a known amount, f_R, equal to the frequency of the acoustic waves within the Bragg cell. The reference beam now has a frequency of $f_0 + f_R$. When the reference beam (frequency, $f_0 + f_R$) and the reflected object beam (frequency $f_0 \pm f_D$) now interfere, a current output proportional to $f_R \pm f_D$ is obtained, given by subtracting the scattered object beam frequency from the reference beam frequency. That is,

$$I_{output} \propto \left| (f_0 + f_R) - (f_0 \pm f_D) \right| \qquad [4.7]$$

$$\text{i.e. } I_{output} \propto \left| f_R \pm f_D \right| \qquad [4.8]$$

Using f_R as the centre frequency, it is now possible to determine the direction of the surface motion of the target object.

From equation [4.6], it can be seen that the large differences in the acoustic and laser wavelengths leads to small diffraction angles and for this reason high acoustic frequencies of around 40MHz are used (i.e. f_R = 40MHz), to give as small an acoustic wavelength as possible.

Assessment of Heat Generation

4.5 Introduction

The primary cleaning mechanism of ultrasonic scaler systems is the mechanical chipping action of the scaler tip when it traverses the tooth surface. During dental ultrasonic scaling procedures, heat is generated due to friction between the tooth and the oscillating tip. To minimise this heating water is sprayed onto the site of instrumentation. Excessive heat production will occur if either the water flow rate over the tip is insufficient or an aerosol is produced. In the latter situation water is thrown off the scaler tip as a fine mist leading to inadequate tip cooling. If the resulting increase in temperature is large enough, damage to the tooth may occur.

4.6 Temperature Measurement

Temperature measurements in dental applications have generally been made by two methods: thermocouples or infrared (thermal) imaging. Several studies have used thermocouples to determine the temperature rises that occur (*in vitro*) whilst using high-speed dental instruments for cavity preparation (Walsh & Symmons 1972; Laur *et al*. 1990; Cavalcanti & Rode 2002), bone drilling (Iyer *et al*. 1997a&b), and post space preparation (Saunders & Saunders 1989).

Few studies have investigated heat generation caused by sonic and ultrasonic scaling instruments (Walmsley *et al*. 1986c; Kocher & Plagmann 1996; Nicoll & Peters 1998). In these investigations, temperature increases were measured within the teeth (*in vitro*) using thermocouples. Thermocouples rely upon a temperature rise in the absorbing element and this makes them less sensitive than photon detectors in thermal imaging systems (Webb 1988).

Thermal imaging has been shown to be a useful method for analysing patterns of temperature change to help locate areas of maximum heat production (McCullagh *et al*. 2000). Crandell and Hill (1966) first used thermal imaging for dental research purposes, as a diagnostic aid for periapical abscesses. Since then, thermal imaging technology has improved and found application in periodontology, for studying the thermodynamic behaviour of human gingiva (Mörmann *et al*. 1985, Barnett *et al*. 1989) and in several other dental disciplines (Biagioni *et al*. 1996, Hussey *et al*. 1997, McCullagh *et al*. 1997, Benington *et al*. 2002).

Thermal imaging has also been shown to be a suitable tool for assessing the heat generated at the surface of a tooth, by ultrasonic scaling instruments, under various tip/tooth load conditions and for varying water flow rates (Lea *et al*. 2004d).

4.7 Principles of Infrared Thermography (Thermal Imaging)

Friction between the oscillating scaler tip and the tooth surface causes an increase in temperature at the treatment site. This temperature rise excites the atoms within the tooth structure and the metallic tip. Those electrons in a lower energy orbital of an atom undergo a transition to a higher energy orbital. When the atom tries to return to its ground state it releases energy as a photon with a specific wavelength. Heat causes atoms to emit photons in the infrared region of the electromagnetic spectrum. It is possible to detect the infrared radiation emitted by an object using a phased array of detector elements. The energy carried by the photons may be converted into electrical signals, which are sent to a signal-processing unit from where an image is created, known as a thermogram. A colour-graduated scale can be used to conveniently indicate the intensity of the infrared emission (and hence the temperature) at the treatment site.

4.8 Imaging Systems

Thermal imaging systems are comprised of many complex components, each of which can affect the quality of the final image (Webb 1988). The optical system of the imaging system should be capable of transmitting and focusing the IR radiation. Silicon and germanium are commonly used for such optical components and lenses are often given antireflection coatings to raise their transmittance to as high as 95-97% (Webb 1988).

The performance of the detector in a thermal imaging system is usually specified in terms of temperature resolution and field of view (Webb 1988). The thermal imaging system used in this study was the Agema 900, which detects thermal IR radiation between wavelengths of 8 – 12μm. The system is cryogenically cooled and has a temperature range of –30°C to +1500°C with a sensitivity of 0.08°C at +30°C (EPSRC Engineering Instrument Pool, Brief Technical Guide 2002). Up to 25 frames per second may be captured (real time) using 10° or 20° field of view lenses. The Agema 900 also has a purpose built computer and operates the Erika thermal analysis software package (EPSRC Engineering Instrument Pool, Brief Technical Guide 2002).

Quantification of the thermal scene may be performed either by using a built in temperature reference source (if the system has one) that has been calibrated against a known standard or by placing an independent temperature reference in the field of view (Webb 1988). The Agema 900 used in this investigation had an internal reference that was calibrated using a radiation source, the accuracy of which was traceable to National Standards at the Swedish National Testing and Research Institute (Sweden).

4.9 Selection of scaler systems

As a scaler tip moves across the surface of a tooth, some of the tip's kinetic energy (KE) is converted into thermal energy, due to the frictional force between the scaler tip and the tooth. Since frictional force is independent of relative sliding speed (McMillan 1997), the speed of the scaler tip (determined by the generator power setting and the design of the tip) as it traverses the tooth surface will not, theoretically, affect the detected temperature rise.

However, scaler tips oscillate back and forth, with each oscillation converting KE into thermal energy. The more often the tip traverses the tooth surface per unit time, the more often the conversion of KE to thermal energy and therefore the greater the rise in temperature. Hence, the detected temperature rise will be affected by the frequency of the scaling tip system utilised. Therefore, when comparing ultrasonic generators made by different manufacturers they should operate at similar frequencies. This enables meaningful comparisons of the effects of load, generator power setting and water flow rate on the heat generated.

Variation in the magnitude of scaler tip vibration has previously been observed between different ultrasonic scaler systems. However, the scaler tip displacement amplitude should not contribute to the frictional force or the heat generated. A larger displacement amplitude will lead to the same temperature increase spread over a larger area.

Assessment of Cavitation Production

4.10 Introduction

The phenomenon of cavitation has been known about for over 100 years and may occur whenever a fluid is violently agitated or is subjected to an ultrasonic field. The effects of cavitation can be incredibly damaging, as in the case of cavitation occurring around propeller blades which may affect a ships performance by thrust breakdown, erosion, vibration and noise (Weitendorf 2001). Another area where cavitation may be damaging is when using ultrasound as a diagnostic / therapeutic tool in medicine. The use of ultrasound for imaging and extracorporeal shock-wave lithotripsy (the removal of kidney stones and gall stones) has increased greatly in recent years (Huber *et al*. 1994; Holland *et al*. 1996). However, there is still concern over the potential bioeffects, relating to the damage of organs and red blood cells, due to cavitation (Daniels *et al*. 1995, Holland *et al*. 1996 and Barnett *et al*. 1997).

Cavitation may also be harnessed as a useful phenomenon such as in the field of sonochemistry, which has been developed around this concept. A.L. Loomis first appreciated the unusual effects of intense sound waves travelling through a liquid, today known as sonochemistry, in 1927 (Suslick 1989). Today, ultrasound may be used to increase the reactivity of metal powders by more than 100, 000 times, can drive metal particles together at speeds so great that they melt at the point of collision and can even generate microscopic flames in cold liquids (Suslick 1989). These chemical effects of ultrasound arise from the physical processes of cavitation (Suslick 1989).

As with the field of sonochemistry, cavitation has potentially found useful application in dentistry, where the shock waves generated following bubble collapse may be used to aid the

removal of plaque and calculus from the surfaces of teeth (Walmsley *et al*. 1985 & 1988, Laird & Walmsley 1991). However, it is still uncertain whether cavitation occurs around dental ultrasonic instruments and several techniques have been utilised to detect it.

4.11 Cavitation Quantification used in Dentistry

Many methods exist for the quantification of cavitation including acoustic imaging, sonoluminescence and sub-harmonic generation (Price *et al*. 1997). Cavitation may also be quantified by monitoring its chemical effects. These include oxidation reactions such as in the Weissler reaction or Fricke's dosimeter and the detection of radical species (Price *et al*. 1997). Several of these methods have been employed in dentistry to assess the occurrence of cavitation around dental ultrasonic instruments.

4.11.1 Sonoluminescence

Cavitational activity around dental ultrasonic instruments has been evaluated by utilising the phenomenon of sonoluminescence (Ahmad *et al*. 1987a & 1988), which is the emission of light as a cavitation bubble implodes. This was performed using a sensitive photometric detection system in a light-tight environment. Any light generated through bubble implosion was detected by an image intensifier tube, amplified and delivered to a television video recorder which allowed the spatial and temporal characteristics of the emitted light to be studied (Ahmad *et al*. 1987a).

4.11.2 Weissler Reaction

The Weissler reaction involves monitoring the release of iodine (I_2) from potassium iodide (KI) in the presence of carbon tetrachloride (CCl_4), which is used to enhance iodine liberation

(Mason *et al*. 1989, Walmsley & Williams 1991). I_2 formation may occur via two routes (Nascentes *et al*. 2001), that is:

$$KI \rightarrow K^{\bullet} + I^{\bullet} \qquad \text{Scheme 1}$$

$$I^{\bullet} + I^{\bullet} \rightarrow I_2 \qquad \text{Scheme 2}$$

and

$$H_2O \rightarrow H^{\bullet} + {}^{\bullet}OH \qquad \text{Scheme 3}$$

$$HO^{\bullet} + {}^{\bullet}OH \rightarrow H_2O_2 \qquad \text{Scheme 4}$$

$$H_2O_2 + 2I^{-} + 2H^{+} \rightarrow I_2 + 2H_2O \qquad \text{Scheme 5}$$

The amount of cavitational activity is quantified by measuring the change in optical density of the sonicated sample at 350nm (which corresponds to the absorption spectrum of free iodine) using a spectrophotometer (Walmsley & Williams 1991). This may then be compared to an unsonicated control solution. By using a calibrated conversion curve relating iodine concentration to optical density, the change in optical density may be expressed as the concentration of iodine released in parts per million (ppm). This technique has been used to assess the occurrence of cavitation in ultrasonic baths (Walmsley & Williams 1991), around endosonic files (Lumley *et al*.1988) and around dental scalers (Mason *et al*. 1989).

4.11.3 Fricke's Dosimeter

Previous investigations into the occurrence of cavitation around dental ultrasonic scalers has also made use of the oxidation of ferrous (Fe^{2+}) to ferric (Fe^{3+}) ions in Fricke's dosimeter (Walmsley *et al*. 1984 & 1986b). Like ionising radiation, ultrasound in water is known to

cause the formation of OH radicals (Fang *et al*. 1996). It is these radicals, in part, which are responsible for the oxidation of Fe^{2+} to Fe^{3+} as given by;

$$Fe^{2+} + {}^{\bullet}OH \rightarrow Fe^{3+} + OH^{-} \qquad \text{Scheme 6}$$

As with the Weissler reaction, spectrophotometric analysis is used to record the change in optical density (compared to an unsonicated control sample) of the Fricke's solution, which occurs as Fe^{2+} ions are oxidised to Fe^{3+} ions. However, this oxidation is not OH radical specific (Fang *et al*. 1996) and may also be due to the H atom, HO_2 radical and H_2O_2 as given below;

$$Fe^{2+} + H^{\bullet} + H^{+} \rightarrow Fe^{3+} + H_2 \qquad \text{Scheme 7}$$

$$Fe^{2+} + HO_2{}^{\bullet} + H^{+} \rightarrow Fe^{3+} + H_2O_2 \qquad \text{Scheme 8}$$

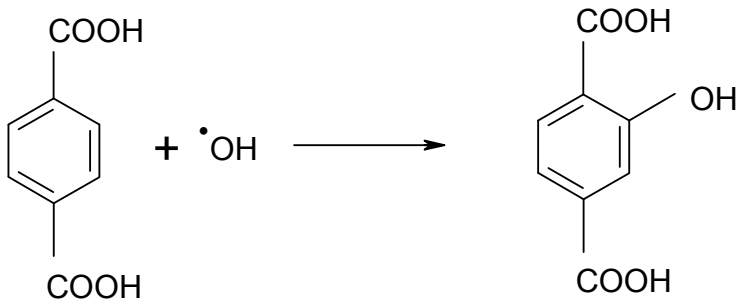
$$Fe^{2+} + H_2O_2 \rightarrow Fe^{3+} + OH^{-} + {}^{\bullet}OH \qquad \text{Scheme 9}$$

The Fricke dosimeter, therefore, does not measure OH radical production (by ultrasound) adequately and a system is required which will specifically measure the OH radical yield.

4.12 The Terephthalate Dosimeter

Both the Weissler reaction and Fricke's dosimeter are susceptible to all oxidising species in solution (Price *et al*. 1997). The terephthalate dosimeter is a system that measures OH radical yield specifically and disregards radicals such as $H^{\bullet}$, $HO_2{}^{\bullet}$ and also H_2O_2 (Fang *et al*. 1996).

The system uses an aqueous solution of terephthalic acid, which on reaction with hydroxyl radicals forms 2-hydroxyterephthalate (Price *et al*. 1997). The mechanism for this reaction is shown in Scheme 10. The hydroxyterephthalate product is fluorescent and is readily detectable using fluorescence spectroscopy where an excitation wavelength of 310nm causes the hydroxyterephthalate to fluoresce at 425nm (Digby *et al*. 1995; Price *et al*. 1997). The terephthalate dosimeter has been used in a range of studies (Price *et al*. 1997) and will be employed in this investigation to quantify the amount of cavitation occurring around dental ultrasonic instruments.



Scheme 10 Mechanism for the formation of 2-hydroxyterephthalate following the reaction of aqueous terephthalic acid with hydroxyl radicals.

CHAPTER 5

MATERIALS AND METHODS

The Scanning Laser Vibrometer

5.1 Introduction

The scanning laser vibrometer (SLV) uses sophisticated technology to enable vibration data to be acquired and analysed. However, there are several SLV acquisition settings that must be manually selected and adjusted to ensure that accurate and appropriate data are obtained.

As important as the internal acquisition settings of the SLV are external experimental factors such as arrangement of the target object (scaler tip, powered toothbrush, etc) relative to the SLV, generator power setting, water flow rate and loading of the tip, which may all affect the acquired data. A series of set procedures is therefore followed to ensure that measurements performed enable meaningful comparisons to be made between different operating conditions.

The research described here uses a SLV to investigate the vibration characteristics of ultrasonic scalers, including vibration frequency and displacement amplitude. The positions of nodes and antinodes were also determined. Once the scaler oscillation characteristics were better understood, factors such as water flow rate, generator power setting, load and tip wear on the magnitude of ultrasonic scaler tip displacement amplitude were investigated. The ability of the SLV to analyse powered toothbrush and endosonic K-file vibrations was also investigated.

5.2 Laser Vibrometer Instrumentation

5.2.1 Scanning Laser Vibrometer Specification

The SLV system (Figure 5.1), which is used throughout this research to measure the vibration of the oscillating ultrasonic scaler tips, is a PSV-300-F/S High Frequency Scanning Vibrometer System (Polytec GmbH, Polytec-Platz, Waldbronn, Germany). The SLV consists primarily of a controller and workstation (for data decoding and manipulation) and a scanning head, combining a laser and an integral video camera (vibrometer scanning head, OFV 056, Polytec GmbH, Polytec-Platz, Waldbronn, Germany). A low power (<1mW) eye-safe (class 2) Helium-Neon laser beam is contained within the scanner head along with the corresponding optics for data collection. An integral video camera provides a captured image for superposition of data. The scanner head may also be fitted with an OFV-056-C close-up module and magnifying lenses to allow objects of approximately 1mm^2 to be scanned.

The SLV achieves laser spot sizes of approximately 10-20µm and an angular scanning resolution of 0.01º, ensuring the high spatial resolution of the ultrasonic probe tips under investigation. Frequency response is from near DC to 1,000 kHz, covering all of the currently available ultrasonic devices and enabling viewing of higher order harmonic vibrations.

5.2.2 Defining a Scan Area – The Measurement Grid

The video camera within the scanner head is used to monitor the area under test and provide a captured image for subsequent vibration data analysis. The SLV is set to scan an area of the target object by creating a virtual measurement grid, which consists of a mesh of scan points superimposed on the video image of the object (Figure 5.2). As well as the grid being fully adjustable in shape, to enable any target shape to be analysed, the density of measurement

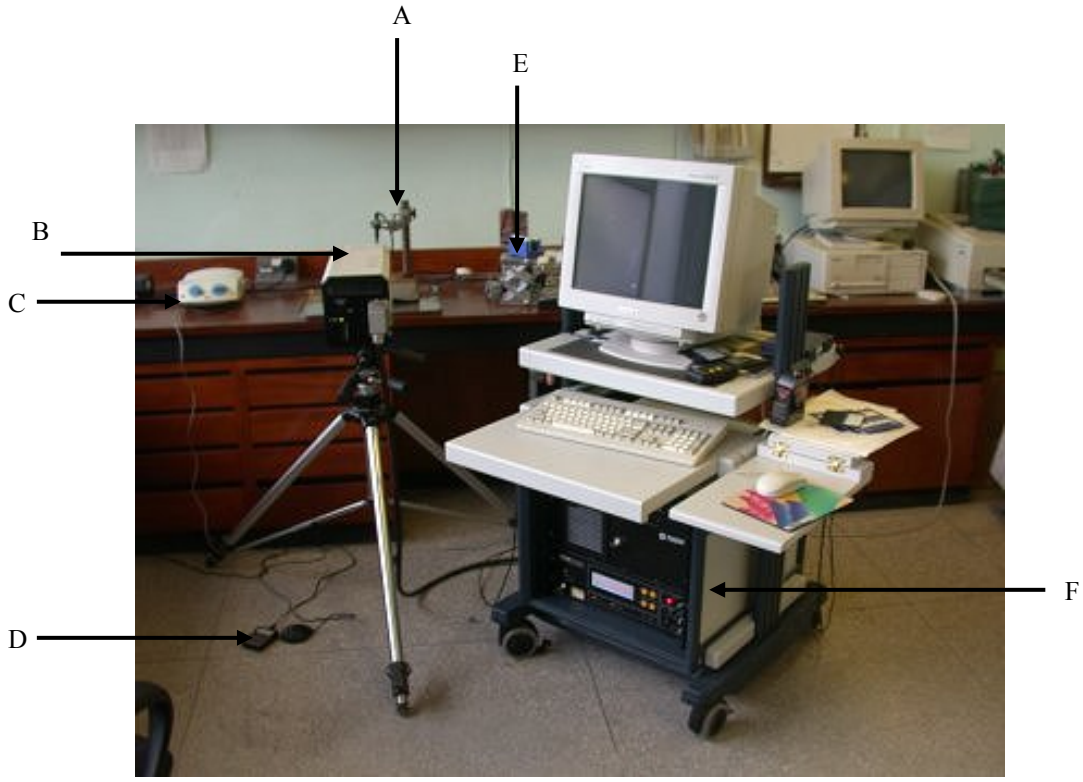


Figure 5.1 The scanning laser vibrometer system used throughout this investigation including; A: clamp and stand used for securing the ultrasonic scaler handpiece in position, B: the scanning laser vibrometer scanner head, which houses the laser and corresponding optics to enable data acquisition, C: Ultrasound generator used to drive the scaler, D: foot pedal used to control the handpiece, E: height-adjustable stand and F: vibrometer controller, used to store and manipulate data.

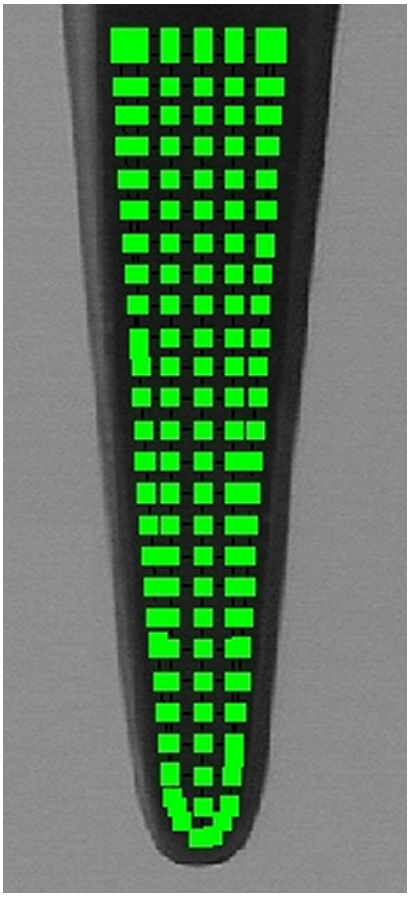


Figure 5.2 A measurement grid is superimposed over the video image of the target scaler tip. This guides the laser beam over the surface of the target during vibration analysis.

points within the grid may also be altered (up to 512 × 512 points). Fewer measurement points results in a faster scan time. However, this increase in scan speed is at the expense of the amount of vibration data. The vibrometer acquires data only from measurement points and, over any regions that are not covered by scan points the associated computer software interpolates the data, i.e. the computer will analyse data obtained from scan points nearest to the scan point-deficient regions and calculate an estimated value for the vibration data.

Measurement grids are made to cover the target's surface of interest as evenly as possible with a point density that minimises the amount of data interpolation required. However, dense measurement grids should be avoided to prevent excessively long scan times. Therefore, a balance has to be sought between the time available for the study and the spatial resolution of the data required. It is sometimes only necessary to observe the magnitude of vibration of the target object at a single point. In this situation, single point measurements may be performed at the region of interest, rather than using an entire grid.

5.2.3 Removing Parallax Error

Once a measurement grid (or point) has been superimposed over the target, it is essential that the laser beam be aligned such that, when a scan is initiated, the laser beam exactly follows every point in the measurement grid. If this is not so then the vibrometer may obtain vibration data from points on the target surface that exist in entirely different positions, or even from somewhere not on the target at all. This situation is avoided by aligning the laser scanning range with the video image's spatial extent. The laser beam from the scanner head can be manually moved over the surface of the target. The beam is moved to a position on the target and then the mouse cursor clicked over the centre of the laser dot. The beam is then moved to

several different areas on the target surface and the mouse cursor clicked over the centre of the laser dot each time. Once this has been completed, it is possible to drag the laser beam, using the mouse, over the surface of the target and observe it following each of the scan points exactly. If it does not follow each of the scan points precisely then the above procedure should be repeated to avoid inaccurate data acquisition.

5.2.4 The Reference Signal

The grid of measurement points guides the laser beam from the vibrometer over the target object. From each of these points the SLV acquires vibration data. Measurements at all points must be in phase with each other. That is, the target object must always be at the same stage in its vibration cycle when a measurement is performed. In order to accomplish this a reference signal is used. A trigger level is set, which controls the amount of signal required from the reference signal before a measurement is triggered and this ensures that the vibrating target is at the same stage of its vibration cycle when scans are performed. Throughout this work, two methods of reference signal generation were utilised.

5.2.4.1 Electromagnetic Induction

Dental ultrasonic instruments produce an Electro-Magnetic (EM) field. This may be detected using an electromagnetic induction coil, which consists of an iron core with a wire coil wrapped around it and the whole encased in an acrylic shell. The induction coil generates a reference signal using electromagnetic induction. If a conductor carries a time-dependent current and is near to a second conductor, the changing magnetic field of the first conductor can generate a current in the second conductor. Therefore, the changing magnetic field of the

scalers generates a current in the induction coil. This induced current can then be used as a reference signal to trigger readings.

5.2.4.2 Acoustic Reference

Most powered toothbrushes produce little or no EM field and so the induction coil cannot be used to trigger readings. Powered toothbrushes do, however, produce audible sound and so it is possible to trigger vibrometer measurements using a microphone (Sekaku Dynamic Microphone KUD-626, Sekaku Electron Industry, Taiwan) connected to a pre-amplifier.

5.2.5 Acquisition Settings

These settings are used to determine the frequency range over which scans are performed, the number of repeat measurements the SLV should perform at each measurement point and also the number of lines in the FFT calculation the system should perform (which determines the frequency resolution). Performing repeat measurements at the same data point improves the accuracy of the readings as well as helping to filter out random reflections from, for example, the cooling water flowing over the scaler tips, as noise. An increase in the number of lines in the FFT calculation increases the frequency resolution of the results. As well as affecting the resolution of the acquired data, these factors affect the time a scan requires and, as with the point density of the measurement grid, the level of resolution and detail required must be assessed against a reasonable time scale (i.e. approximately 30 seconds or less). These settings are user selected according to the target object under investigation and the resolution of the information required.

5.3 The Target Object

5.3.1 Identification of Vibration Orientation

Laser vibrometers perform measurements on vibrations towards and away from the scanner head, i.e. vibrations in the same plane as the laser beam. Any vibrations in the planes orthogonal to the laser beam direction (side-to-side or up and down vibrations) are not detected by the system since they cause no shift in the frequency of the laser beam. To measure these vibrations it is necessary to adjust the relative positions of the scanner head and target object such that the vibration of interest is toward and away from the camera.

To ensure that the scaler tip is fixed in position such that, if the apparatus is dismantled and then reassembled, all measurements may be repeated spirit levels were used. The stand upon which the scanner head of the SLV sits is fitted with two spirit levels that ensure the base is horizontal. Also a bull's-eye spirit level was located on top of the scanner head to allow any eccentricities from the perfectly horizontal position to be determined and corrected. Once the scanner head is properly adjusted it is important to ensure the scaler insert is properly aligned with it. To ensure the camera is orientated perpendicular to the surface of the target object the image of the target is observed on the computer monitor to ensure the image is in focus along all edges. A spirit level was also utilised to ensure that the front surface of the scaler tip was, when necessary, vertical and perpendicular to the SLV camera head.

5.3.2 Scaler Tip Water Flow Rate

During operation, ultrasonic scaler instruments are used with a continuous stream of water flowing through the scaler handpiece and over the length the tip. This is to prevent excessive

heating of the stack which drives the scaler tip and, clinically, to reduce the heat produced at the tip / tooth treatment site. During all investigations this constant stream of water must be present, to reproduce clinically realistic operating conditions. However, water flowing over the surface of a scaler tip may affect the amount of vibration. Therefore, to enable repeat measurements to be made and to allow comparisons between tips of different styles, the flow rate of this stream (i.e. the volume of water flowing over the tip per minute) must be known.

Prior to performing scans, the water flow rate over the surface of the tip was determined. A measuring cylinder, graduated in 1ml intervals, was placed under the tip of the clamped scaler insert. When the scaler tip is activated, the water flows through the handpiece, over the tip and into the measuring cylinder. Power was supplied to the instrument for one minute (measured with a stopwatch) and then discontinued. The volume of water in the measuring cylinder was recorded and the process repeated three times. This enabled the mean water flow rate to be expressed in millilitres per minute.

The water in the laboratory was provided via a pressurised water system that was fully adjustable. Water pressure was maintained between 30 and 35 pounds per square inch (2.1 - 2.5 bar). Each of the ultrasound generators used had a water flow control. The fine-tuning of the water flow rate over the tip was standardised using these generator controls.

5.3.3 Ultrasound Generator Power Dial Re-Calibration

Dental ultrasound generators have a power control dial, allowing the power delivered to the working end of the scaler to be varied. This, theoretically, increases or decreases the

displacement amplitude of the instrument tip. However, the scales on most ultrasound generator power controls do not allow accurate relocation of the control dial (Figure 5.3). An exception to this is the power control of the Mini Piezon generator (EMS), which has buttons to control the power setting rather than a dial and so it is therefore possible to accurately select a particular power setting (Figure 5.3). Much of this work required specific powers not only to be selected but also to be regularly reproduced. A 10-point graduated scale was constructed for each of the generators (except the Mini Piezon), which enabled the relocation of the generator power dials. When positioned over the original power output display the generator power setting could be varied in pre-determined increments and this allowed repeat measurements to be made at known power settings.

5.3.4 *In Vitro* Tooth Model

The vibration characteristics of dental scaler tips were analysed under unloaded conditions (i.e. freely oscillating in air) and also loaded conditions. Loaded measurements were made with the ultrasonic scaler contacting the tooth surface with a known load to reproduce the clinical situation when they are contacted against tooth surfaces. Extracted molars and premolar teeth were collected and fixed in formalin. Before use, teeth were washed in water and then partially embedded in resin (Orthoresin, Dentsply, Weybridge, Surrey) such that one root aspect was left exposed to allow instrumentation (Figure 5.4), as described by Flemmig *et al*. (1997, 1998a&b). To determine the load applied, the resin block containing the tooth, was fixed to a mount on a Model 31 (1000gm) tension / compression load cell (Sensotec, Columbus, Ohio, USA). The load cell was connected to an E725 Microprocessor Transducer Indicator / Controller. The load cell measured loads between –10.0N (tension) to +10.0N (compression) with an accuracy of 0.01N.



Figure 5.3 Ultrasound generators used throughout the course of this research including (clockwise from left); Cavitron SPS (30kHz magnetostrictive), Cavitron Select (25kHz magnetostrictive), Piezon Master 400 (30kHz piezoelectric) and Mini Piezon (30kHz piezoelectric).

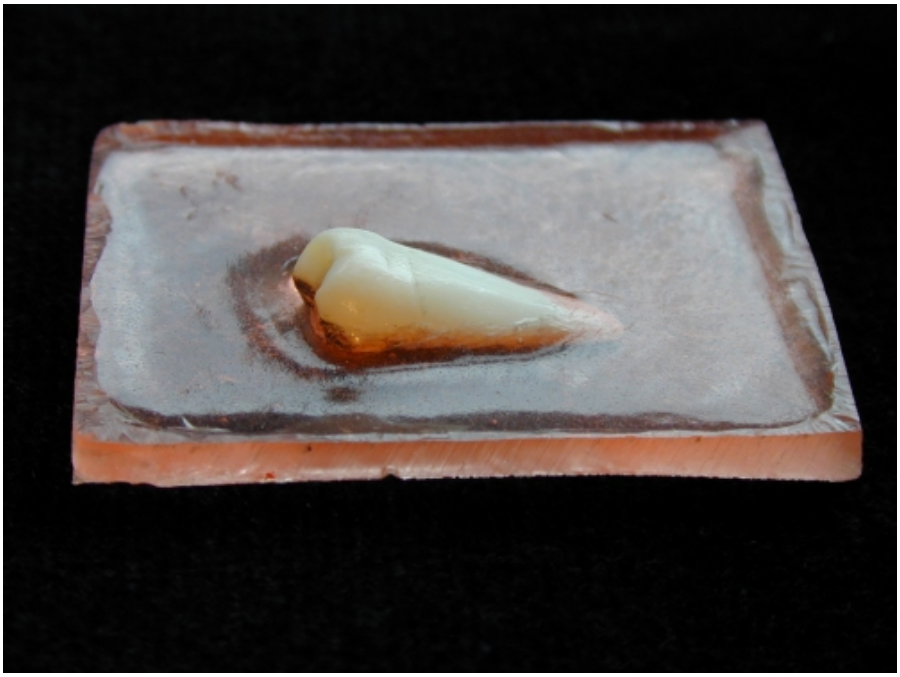


Figure 5.4 An extracted premolar tooth partially embedded in resin such that one root aspect was left exposed to allow instrumentation.

5.4 SLV Calibration

The SLV was calibrated against a VC10 Manfred Weber portable shaker (Germany) to determine the reproducibility of scans. The shaker has a known, fixed, displacement amplitude (10μm ± 3%) that is calibrated with PTB certified primary standard to ISO/IEC Guide 25/58 and En 45000 series. Using the SLV software a measurement point was superimposed on the front surface of the shaker and 50 repeat scans were performed, to determine the mean measured displacement amplitude.

5.5 Scaler Tip Vibration Characterisation

Scans were performed to assess the longitudinal vibration displacement amplitude of a variety of scaler tips whilst operated in air at various power settings, with cooling water flowing over them at a constant rate of 20mls/min. In turn, each tip was chosen and a virtual measurement grid, consisting of a mesh of scan points, was superimposed on the video image of the target. This grid was adjusted in size, shape and point density to guide the laser beam over the surface of the probe.

5.6 Water Flow Rate and Scaler Tip Vibration

The oscillation of five magnetostrictive, 30kHz, TFI-10 tips (Dentsply Preventive Care, York, PA, USA) was measured. All tips were new and previously unused and were driven by the same Cavitron SPS ultrasonic generator (Dentsply Preventive Care, York, PA, USA). The scaler handpiece and TFI-10 insert were fixed in place such that the anterior surface of the scaler tip was vertical and the scanner head was aligned perpendicular to the tip. A SLV frequency measurement range of 0-100kHz was selected to allow detection of the fundamental frequency of the scaler tip and higher order harmonics. A measurement grid was

superimposed over the anterior surface of the scaler tip and, at each data point in the measurement grid, four repeat measurements were taken and averaged. The SLV was set to perform a FFT using 800 data points, giving a frequency resolution of 125Hz.

Each tip was scanned at three different power settings including quarter, half and full power, which corresponded to power settings 3, 5 and 10 on the calibrated power scale. Water flow rates were selected in a similar manner to the power settings (quarter, half and full water flow rate settings respectively) and resulted in water flow rates of 18, 38 and 62 ml/min. Ten repeat scans were made at each power / water setting and the mean maximum displacement amplitude for each combination recorded (Table 6.1). Each scan lasted approximately 35 seconds with a 2-minute interval between scans.

5.7 Displacement Amplitude of Unloaded Ultrasonic Scaler Inserts

The four generators selected for this study (Figure 5.3) included the Cavitron SPS 30kHz generator (Dentsply, York, PA, USA), Cavitron Select 25kHz generator (Dentsply, York, PA, USA), Piezon Master 400 30kHz generator (Electro-Medical Systems, Switzerland) and Mini Piezon 30kHz generator (Electro-Medical Systems, Switzerland). The scaler tips utilised in this study (Figure 5.5) included the TFI-10 (with Cavitron SPS and Select), TFI-3 (with Cavitron SPS) and a P-style tip (with the Piezon Master 400 and Mini Piezon).

The basic geometric data of these tips are given in Table 5.1. One of the generators was selected and an insert placed within the scaler handpiece. The scaler was held in place via the use of a clamp, with the anterior face of the tip perpendicular to the camera. When attaching

the P-tips to the Mini Piezon / Piezon Master 400 handpiece an EMS flat spanner was used to tighten the tips firmly, as recommended by the manufacturer. The laser beam was aligned with the camera head and a virtual measurement point was created to guide the laser to a specific point on the surface of the vibrating target. Analysis of scaler tip oscillation characteristics shows that the maximum displacement amplitude for all tips occurs at the free, unconstrained end of the tip (Lea *et al*. 2002b) and so this is the point from which data were acquired. With the ultrasonic generator set to the first power graduation, scans were made over a frequency measurement range of 0 to 100kHz. The SLV was set to perform a FFT using 800 data points, giving a frequency resolution of 125Hz. Each scan lasted approximately 10 seconds, with an interval of 20 seconds between scans. The power of the generator was then increased, in successive increments, to the tenth power setting, which represented full power.

For each power setting 10 scans were performed and the mean maximum displacement of the scaler tip was recorded (Table 6.2). The insert was exchanged for another of the same type and the above measurement process repeated until all five tips had been scanned. The generator was then swapped for another type and the measurement procedure repeated. The displacement amplitude at the free end of each scaler tip was measured ten times, at each generator power setting. The mean maximum displacement amplitude at each power setting was then calculated (Table 6.2). To determine the reproducibility of the whole measurement process, the equipment was dismantled and, with the Mini Piezon, a tip was selected (Tip 3) and re-measured. The data were used to determine any statistical differences (using univariate analysis of variance) between like tips with the same generator. Significance values for all tip comparisons are summarised in Table 6.3.

	TFI-10 (25k)	TFI-10 (30k)	TFI-3	P-Tip
General description	Metal, sickle shaped probe: circular cross section (approx)	Metal, sickle shaped probe: circular cross section (approx)	Metal probe: flat, beavertail design	Metal probe: flat, beavertail design
Width (Max)/(Min) (mm)	1.6 / 0.5	1.5 / 0.5	2.9 / 1.4	2.1 / 0.7
Depth (Max)/(Min) (mm)	1.6 / 0.5	1.5 / 0.5	0.9 / 0.4	0.7 / 0.4
Probe length (mm)	22	22	19	25
Approximate probe angle of declination from main axis of scaler handpiece (degrees)	40°	40°	50°	60°

Table 5.1 Geometric data of tips used in this study including; TFI-10 (25k & 30k), TFI-3 and P-Tip.



Figure 5.5 Scaler tips used to investigate the effect of load on tip displacement amplitude including (from left to right); TFI-10 (25kHz), TFI-10 (30kHz), TFI-3 (30kHz) and P-tip (30kHz).

5.8 Load and Ultrasonic Scaler Tip Displacement Amplitude

The four generators selected for this study (Figure 5.3) were the same as those utilised in the unloaded investigation and included a Cavitron SPS 30kHz generator (Dentsply, York, PA, USA), Cavitron Select 25kHz generator (Dentsply, York, PA, USA), Piezon Master 400 30kHz generator (Electro-Medical Systems, Switzerland) and Mini Piezon 30kHz generator (Electro-Medical Systems, Switzerland). Like the ultrasonic generators, the scaler tips utilised in this study (Figure 5.5) were the same as those used in the unloaded investigation and included the TFI-10 (Cavitron SPS and Select), TFI-3 (Cavitron SPS) and P-style tip (Piezon Master 400 and Mini Piezon). Three scaling tips of each design were used, the basic geometric data of which are provided in Table 5.1.

One of the generators was chosen and an insert placed within the scaler handpiece. As before, when attaching the P-tips to the Mini Piezon handpiece an EMS flat spanner was used to tighten the tips firmly, as recommended by the manufacturer. The scaler was held in place via the use of a clamp, with the anterior face of the tip perpendicular to the camera. The scaler tip and tooth model were brought into contact with each other (Figure 5.6) and a load of 0.25N (25g) established. The tooth model used in this study is described in Section 5.3.4.

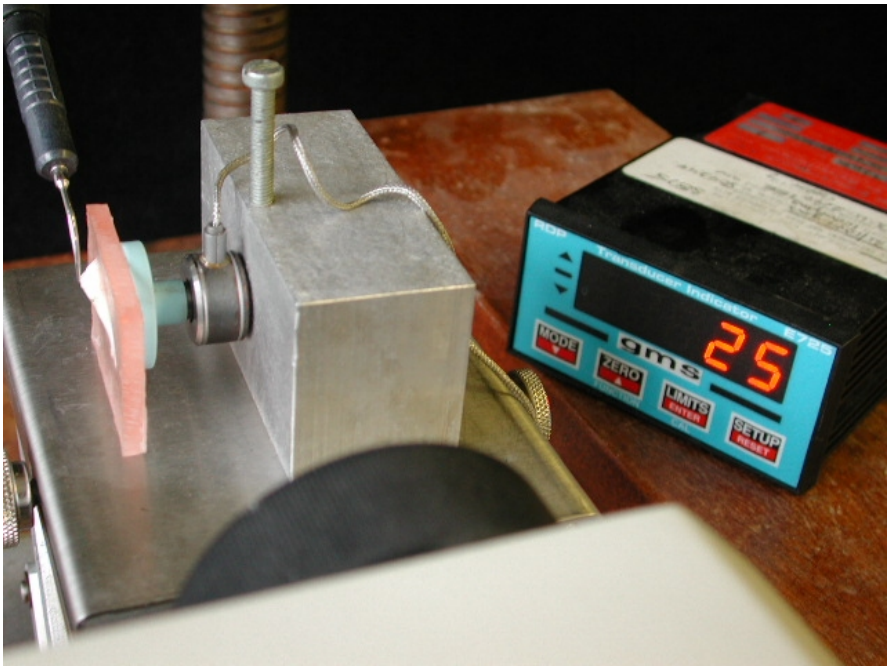


Figure 5.6 A TFI-10 scaler tip is brought into contact with a resin embedded tooth, which is attached to a mount connected to the load cell. The contact load was increased until a load of 0.25N (25g) was established.

The laser beam from the SLV was aligned with the camera head and a virtual measurement point was selected and superimposed over the video image of the free end of the vibrating scaler tip. The measurement point was used to guide the laser beam to the point on the tip from which we wished to obtain data (Figure 5.7). With the ultrasonic generator set to the first graduation on the superimposed power scale, 10 scans were made over a frequency measurement range of 0 to 100kHz. Each scan recorded and averaged 10 measurements and lasted approximately 5 seconds, with an interval of 15 seconds between scans. The power of the generator was then increased, in successive increments, to the tenth power setting, which represented full power. For each power setting 10 scans were performed and the mean maximum displacement of the scaler tip was recorded. Measurements were repeated at loads of 0.50N and then 1.00N. The measurements were repeated for all tip and generator combinations. The mean maximum displacement amplitude of each scaler tip was then calculated (Tables 6.4 & 6.5).

Throughout the investigation, water was allowed to flow over the length of each tip at a constant rate of 20mls/min. Using the acquired data it was possible for us to determine whether there was a linear increase in tip displacement amplitude with increasing power setting, if there were statistical differences in tip displacement amplitude between like tips with the same generator and whether load had a significant effect on tip vibration, for each specific insert.

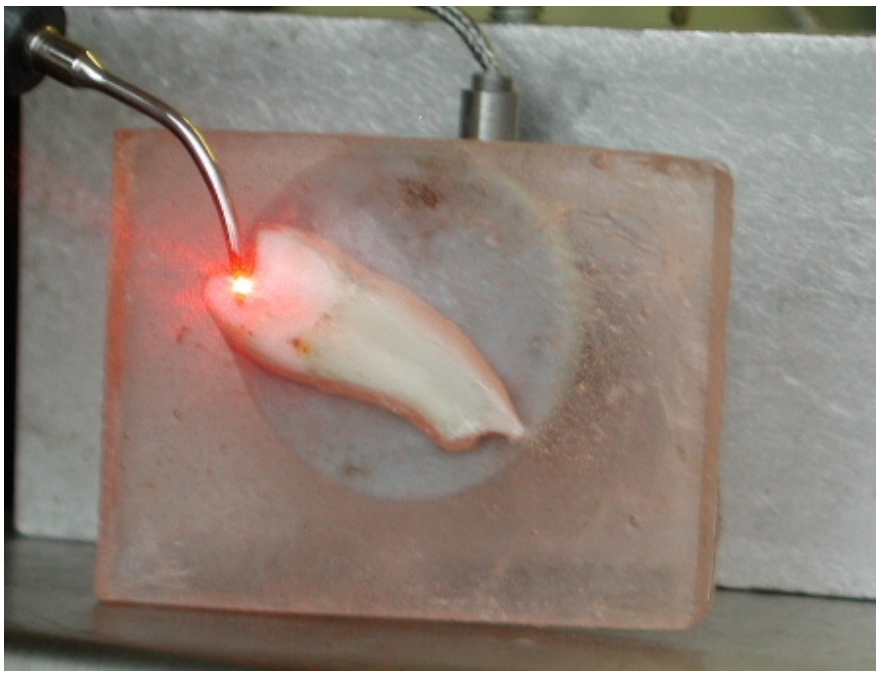


Figure 5.7 A measurement point, superimposed over the video image of the scaler tip, is used to guide the laser to the point on the tip from which data is to be obtained. Here the laser is aimed at what would be the free, unconstrained end of the tip (under unloaded circumstances).

5.9 Wear and Scaler Tip Displacement Amplitude

5.9.1 Unadjusted Scalers

The generator selected for this study was the Cavitron SPS 30kHz generator (Dentsply, York, PA, USA). Three designs of scaler tip (five tips of each design) were utilised in this study (Figure 5.8), including the FSI-100, FSI-1000 and FSI-SLI-10S (Slimline). All tips were new and previously unused.

The first FSI-100 insert was selected and placed within the scaler handpiece. The scaler and handpiece were held in place via the use of a clamp, with the anterior face of the scaler tip perpendicular to the SLV camera. A constant water flow rate of 20mls/min was established and used continuously throughout this investigation for all tips. A virtual measurement point was selected and superimposed over the video image of the unconstrained end of the vibrating scaler tip. Initially, measurements were performed with the scaler tip unloaded (Figure 5.9). With the ultrasonic generator set to half power, 10 scans were made over a frequency measurement range of 0 to 100kHz. Each scan recorded and averaged 10 measurements and lasted approximately 5 seconds, with an interval of 15 seconds between scans.



Figure 5.8 Tips utilised in this study including (from left to right); FSI-1000 and FSI-100 and FSI-SLI-10S ‘Slimline’.

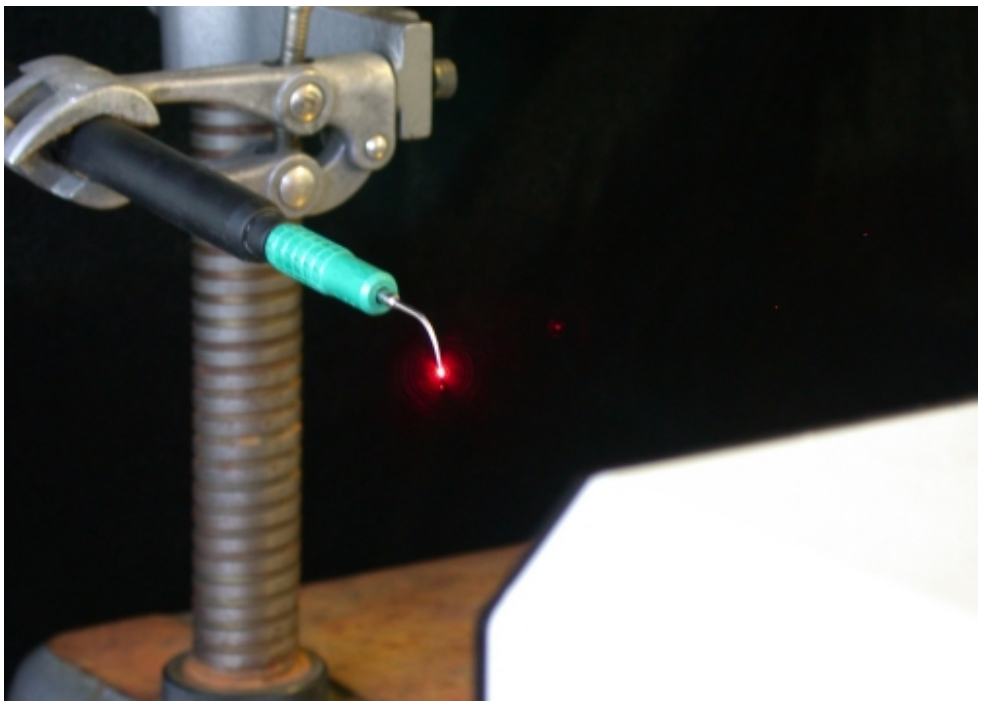


Figure 5.9 Orientation of unloaded FSI-SLI-10S scaler tip relative to SLV camera head. The anterior surface of the tip is perpendicular to the camera.

Once these scans were completed, the scaler tip was brought into contact with the resin-embedded tooth (Figure 5.10) until a load of 0.50N was established. Loads were measured using a load cell as described in Section 5.3.4. The laser beam was re-aligned and the above scans were then repeated. The contact load was then increased to 1.0N and again 10 scans were performed as described above. All data were collected and the mean tip displacement amplitude under unloaded and loaded conditions calculated (Table 6.6).

The whole procedure was then repeated for each of the five FSI-100 inserts and then for each of the five FSI-1000 inserts. Before performing scans for the five FSI-SLI-10S inserts, the SPS generator power setting was reduced to the maximum 'blue-zone' setting (approximately the 9 o'clock position on the dial) to more accurately represent the power levels used during proper clinical usage. All data were collected and the mean tip displacement amplitude under unloaded and loaded conditions calculated (Table 6.6).

5.9.2 Scaler tip grinding

Once the loaded and unloaded scans had been performed for all tips it was necessary to reduce the length of the tips to represent the effect of wear. Initially a length of 1mm was to be removed from the end of the tip. To do this accurately, a mark was made with a permanent marker pen on the tip length. A digital micrometer was then used to measure the distance between the bottom of this marker and the free end of the tip. A second mark, 1mm in length, was also made at the very end of the tip using the marker pen.

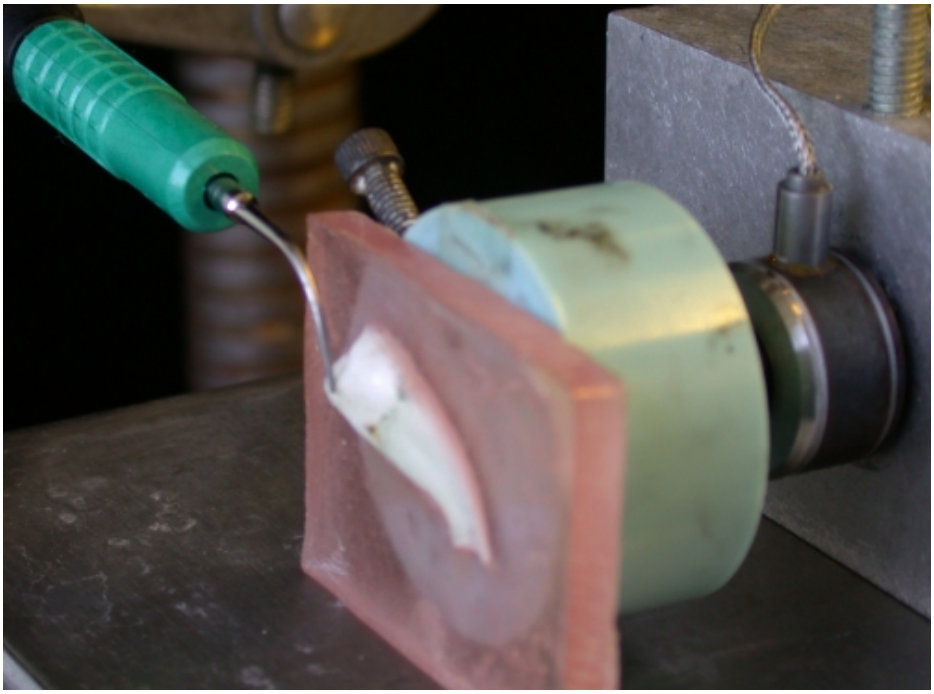


Figure 5.10 FSI-SLI-10S ‘Slimline’ scaler insert contacted against a resin embedded tooth. The resin block is fixed to the mount of a load cell to enable contact loads to be determined.

The tip was then held against a stone driven by a handpiece. The initial bulk removal of the tip was accomplished by holding the end of the tip against the side of the stone (Figure 5.11a). Once the majority of the marker at the end of the tip had been removed the tip was ground away more slowly using the top of the stone (Figure 5.11b). During this final stage of grinding, tip length was constantly monitored using the digital micrometer. By grinding the tip in this way it was also possible to round the edges of the tip (Figure 5.12), to more closely represent the effect of natural wear through usage. To ensure 1mm of tip length had been removed, the distance between the bottom of the marker and he new tip end was re-measured and compared with the original distance (Table 5.2). Once a tip length of 1mm had been removed, the process was repeated for the remaining tips.

Scans were then performed for the ground tips as described previously. Ten repeat measurements of tip displacement amplitude were performed under unloaded and loaded conditions and the mean displacement amplitudes calculated (Tables 6.7). The tip length was then reduced by a further 1mm (2mm total) as described above and scans performed to determine the mean tip displacement amplitude, under loaded and unloaded conditions (Tables 6.8). Using this data it was possible to determine if wear had a significant effect on scaler tip displacement amplitude and, therefore, on scaler tip efficiency.

The relative percentage decrease in scaler tip displacement amplitude, from the unadjusted scaler tip displacement amplitude, due to tip wear of 1mm and 2mm are provided for unloaded conditions (Table 6.9) and for tips under 0.5N load (Table 6.10) and 1.0N load (Table 6.11).

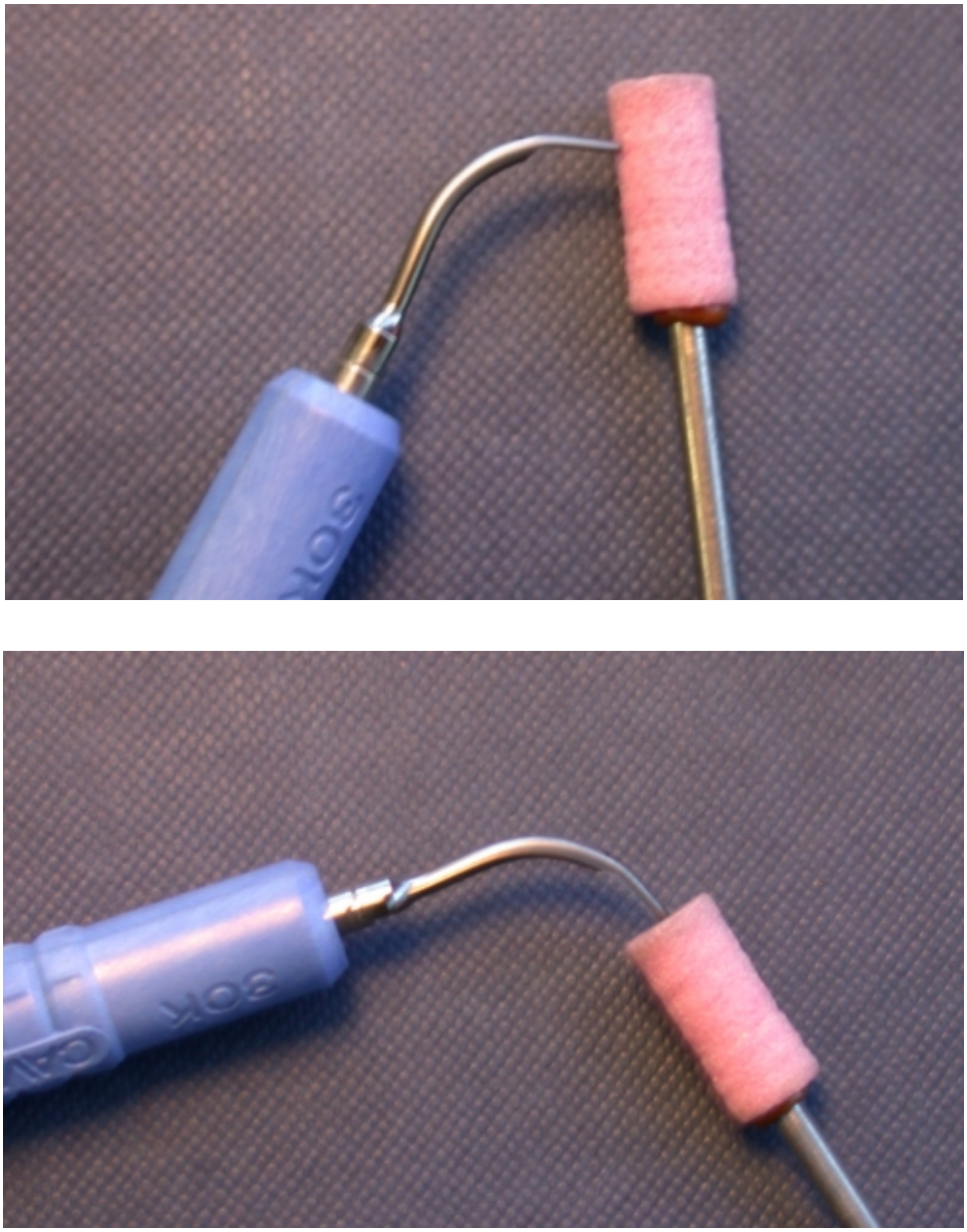


Figure 5.11 a) The bulk removal of the scaler tip length was performed by contacting the tip against the side of the grinding stone. b) Slower, more controlled, grinding was performed by contacting the tip against the top of the stone. This resulted in the tip more closely representing a natural worn effect.

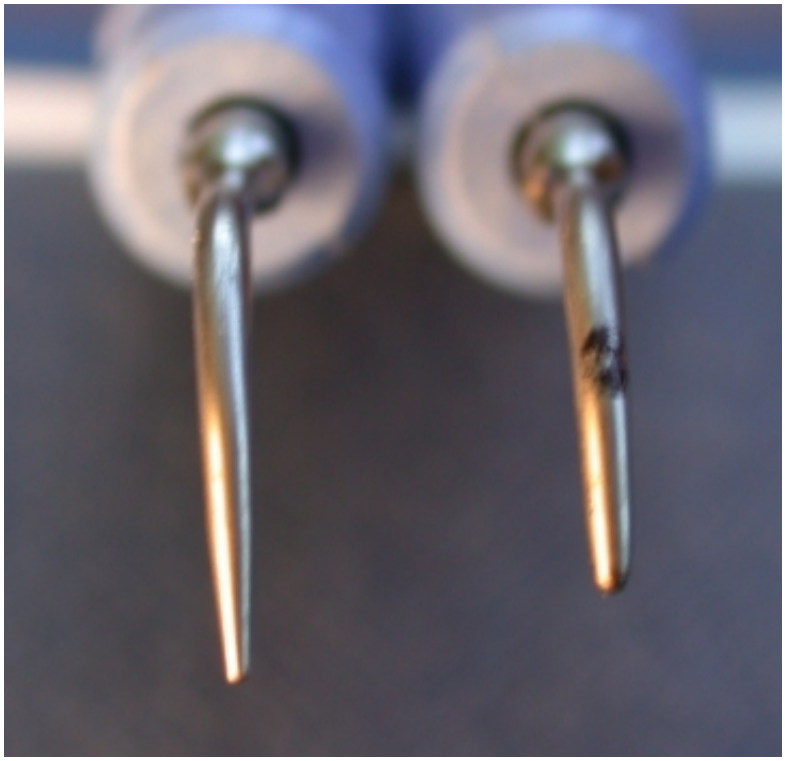


Figure 5.12 FSI-100 tip ground down by 2mm. The ground tip has a smooth, rounded tip, characteristic of tips worn down through normal usage.

5.10 Single-Scan Multi-Axial Assessment of Scaler Tip Vibrations

5.10.1 Theory

A schematic representation of the experimental set-up is shown in Figure 5.13. The laser beam follows two paths to the target scaler tip. The first is a direct path along line OT, which is used to acquire vibration data on the longitudinal vibration. Upon being scattered by the scaler tip, the laser returns along the same direct path. The second route to the scaler is via the mirror, which reflects the laser beam, enabling scans of the side of the instrument to be made. The laser follows line OM and is then reflected by the mirror along line MT. The returning laser beam follows the same path as the outgoing beam.

For the front and side scans to be in phase with each other the difference in the time the laser takes to travel to the scaler tip and back, via each path, must be as small as possible. The difference between the times required for the laser beam to traverse the two paths is calculated below.

Path OT

The distance between the SLV camera and the anterior surface of the scaler tip, OT, was set and measured to be 0.40m (40cm). The distance to the scaler tip and back, therefore, is double this distance, i.e. 0.80m. The time taken for the laser beam to travel this distance is obtained using the relationship;

$$\text{time} = \frac{\text{distance}}{\text{velocity}} \qquad [5.1]$$

where the distance is 2×OT (= 0.80m) and velocity is the velocity of light (≈ 3×10^8m/s). Using equation (1) the time, T_1, for the laser beam to travel to the scaler tip and back along path OT is 2.7×10^{-9} seconds or 2.7ns (nano seconds).

Path OMT

The distance between the SLV camera and the lateral surface of the scaler tip is the sum of the distance from the SLV to the mirror (OM) and the distance from the mirror to the scaler tip (MT), i.e. OM + MT. The distance MT (mirror to scaler tip) was measured and set to be 0.04m (4cm). The distance between the mirror and the SLV was determined using trigonometry. The two laser paths, OT and OMT, form a right-angled triangle (Figure 5.14), where OM is the hypotenuse. By Pythagoras' theorem,

$$OM^2 = OT^2 + MT^2 \qquad [5.2]$$

The paths OT and MT have been measured (0.40m and 0.04m respectively). Therefore the distance between the SLV and the mirror, OM, is 0.402m (0.40m to 2 decimal places). The distance OM + MT was therefore 0.44m and the distance from the SLV to the scaler tip and back (along the path OMT) is double this distance, i.e. 0.88m.

The time taken for the laser beam to travel this distance is again obtained using equation [5.1] and substituting for distance as 2×OMT (= 0.88m). The time, T_2, for the laser beam to travel to the scaler tip and back along path OMT, is 2.9×10^{-9} seconds or 2.9ns (nano seconds). This produces a difference in the time required to take a scan, via the two different routes, of approximately 0.2ns.

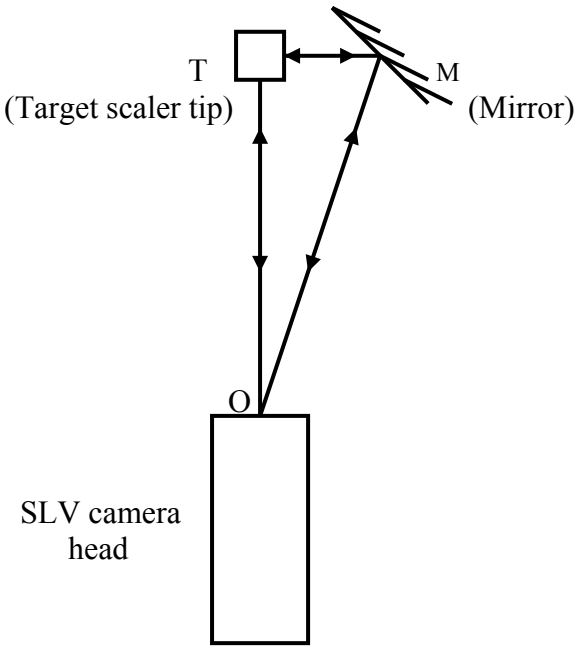


Figure 5.13 Schematic representation of the experimental set-up.

5.10.2 Method

A TFI-10 insert was used in conjunction with a Cavitron SPS 30kHz ultrasound generator (Dentsply Preventive Care, York, PA, USA). The TFI-10 insert was fixed in place such that its anterior surface was perpendicular to the camera of the SLV. A mirror was clamped vertically and positioned next to the scaler tip (Figure 5.14) such that the side aspect of the scaler tip could be viewed through the camera of the SLV. A measurement point was superimposed over each view of the free, unconstrained end of the tip (front and side view). Ten repeat scans were performed, using a medium generator power setting, at each point to determine the mean longitudinal and lateral scaler tip displacement amplitude. Water was allowed to flow over the surface of the scaler tip at a constant rate of 20ml/min.

A measurement grid, consisting of 8 measurement points, was created and superimposed over the front surface of the video image of the scaler tip. A second measurement grid was superimposed over the image reflected, from the mirror, of the side orientation of the tip. Both measurement grids consisted of the same number of measurement points, separated by equal distances, to enable longitudinal and lateral vibration data for the scaler tip to be acquired. The laser was scanned over both surfaces of the oscillating scaler tip, guided by the measurement grids and using a medium generator power setting. Water was allowed to flow over the surface of the tip at a rate of 20ml/min. Vibration displacement amplitude data over the length of the tip, from both orientations, was recorded.



Figure 5.14 A mirror clamped vertically next to the scaler tip may be orientated such that the side aspect of the tip may be viewed simultaneously with the front aspect. This enables vibration data to be obtained from multiple orientations during a single scan.

5.11 The Vibration Patterns of Powered Toothbrushes

This investigation comprised two parts. The first was to determine whether a microphone could be used to generate the reference signal to trigger SLV scans of powered toothbrushes. The second part was to utilise the microphone for this purpose to perform measurements on unloaded powered toothbrushes.

7.11.1 Microphone / Inductance Coil Comparisons

A Sonicare PS-1 powered toothbrush (Optiva Corporation, WA, USA) was fixed in place, using a clamp, with its side facing the SLV camera head (Figure 5.15). Unlike most powered toothbrushes, the Sonicare's vibrations are generated using magnetostriction, which produces a small EM field. As with ultrasonic instrumentation, it is possible to detect this field with a coil of wire and use this to generate the reference signal.

A measurement point was positioned over the tips of the group of bristles furthest from the toothbrush handle from where data were obtained (Figure 5.16). The reference coil was placed next to the toothbrush handle at a position where the EM field, generated by the toothbrush, could be detected. The displacement amplitude and frequency of oscillation of the Sonicare toothbrush bristles were then measured using the SLV. Fifty scans were performed, each lasting approximately 5 seconds. The toothbrush was re-charged in-situ (for 24 hours) and the reference coil was replaced with a microphone (Sekaku Dynamic Microphone KUD-626, Sekaku Electron Industry, Taiwan), connected to a pre-amplifier. Displacement amplitude measurements were repeated (50 readings), keeping the measurement point and all other acquisition settings constant.

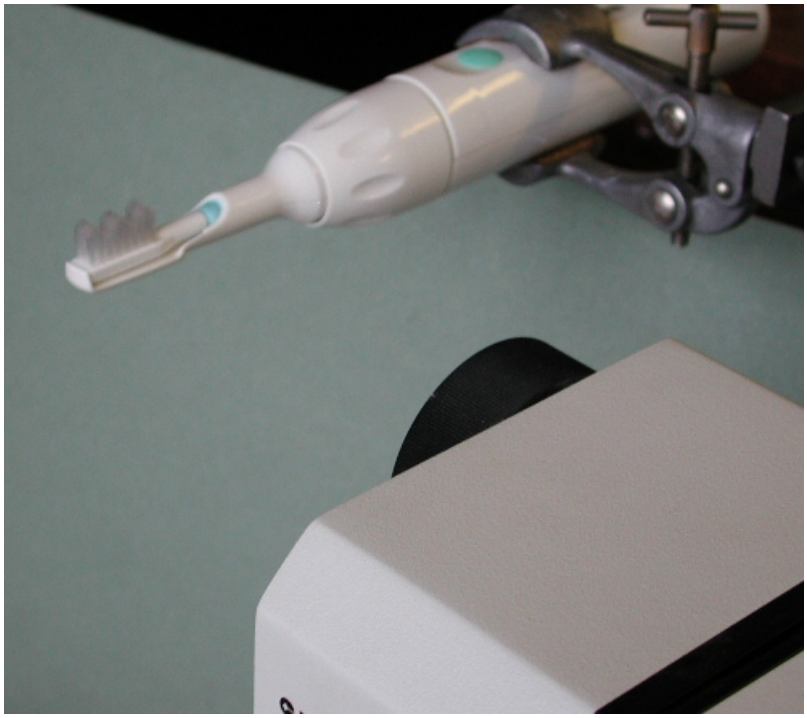


Figure 5.15 Orientation of Sonicare PS-1 powered toothbrush, relative to the SLV camera head.

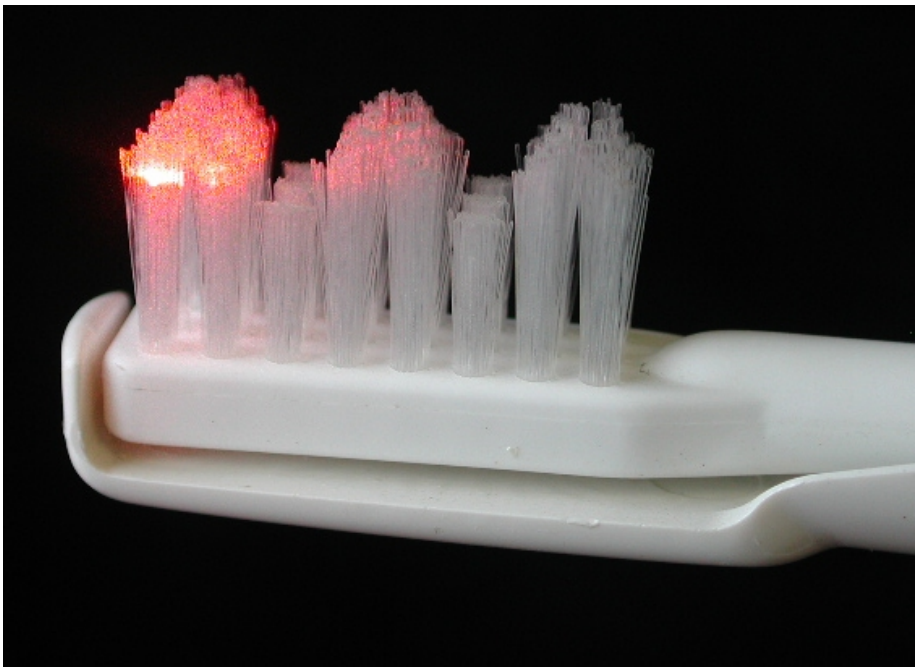


Figure 5.16 A measurement point was positioned over the tips of the group of bristles furthest from the toothbrush handle. The laser was then directed to this point from which data was acquired.

5.11.2 Toothbrush Area Scans

Area scans of the toothbrush head/bristles were performed for the Sonicare PS-1, Philips Sensiflex HX2520 (Groningen, Netherlands), Braun Plaque Remover D8 and Braun Oral-B 3D (Braun GmbH, Germany). In turn, each of the brushes was fixed in place, using a clamp, with the side of the toothbrush facing the camera of the SLV (Figure 5.16). Measurement grids were created, covering the head and bristles of each of the toothbrushes. The laser beam was then scanned across the surface of each brush, using the microphone as a reference signal to ensure all measurements were in phase with each other. For each toothbrush, 10 area scans were performed, enabling the relative motion of the toothbrush head and bristles to be observed, as well as the mean fundamental oscillation frequency and mean maximum displacement amplitudes to be determined (Table 6.12).

5.12 The Vibration Patterns of Endosonic K-Files

A Mini Piezon 30kHz generator (Electro-Medical Systems, Switzerland) was used in conjunction with a #15 K-file and #35 K-file (Dentsply). The #15 file was selected and connected to the generator handpiece. The handpiece was held in place via the use of a clamp, with the long axis of the file vertical and perpendicular to the SLV camera (Figure 5.17). A measurement grid was created and adjusted to cover the front surface of the file and comprised 35 measurement points, separated by a distance of approximately 0.6mm. With the ultrasound generator set to power setting one (minimum power), ten repeat scans were made of the oscillating file, using a frequency measurement range of 0 to 100kHz. The SLV was set to perform 10 repeat readings at each scan point. Scans lasted approximately 15 seconds, with an interval of 10 seconds between scans. The power of the generator was then increased, in successive increments, to the fifth power setting, which represented half power. Displacement

amplitude data at all scan points along the length of the file, for each generator power setting, were recorded and used to calculate the mean displacement amplitude at each scan point along the length of the file (Table 6.13).

The process was then repeated for the #35 file. Again, the displacement amplitude at each of the scan points along the length of the file, for each power setting, was recorded and used to calculate the mean displacement amplitude (Table 6.14). Throughout the investigation water was allowed to flow over the length of each file at a constant rate of 30mls/min.



Figure 5.17 Orientation of endosonic files, relative to the SLV camera head, used during this investigation. A #35 endosonic K-file is clamped in position such that it is vertical and perpendicular to the SLV camera head.

Thermal Imaging

5.13 Heat Generated during *In Vitro* Ultrasonic Instrumentation

The ultrasound generators selected for this study were the Cavitron SPS (Dentsply, York, PA, USA), 30kHz magnetostrictive generator and the Mini Piezon, 30kHz piezoelectric generator (Electro-Medical Systems, Switzerland). A TFI-3 style scaler insert (Dentsply, York, PA, USA) was used with the Cavitron SPS generator and with the Mini Piezon (Electro-Medical Systems, Switzerland) 30kHz piezoelectric generator a P-Tip (Electro-Medical Systems, Switzerland) was chosen (Figure 5.18). Water flow rates of 10, 20 and 40mls/min were measured and used throughout the course of the experiment.

One of the generators was selected and its corresponding insert placed within the scaler handpiece. The scaler was held in place, using a clamp, with the side of the tip and handpiece facing the thermal camera (Figure 5.19). The scaler tip was contacted against the surface of a tooth, which itself was fixed to a mount on a Model 31 (1000gm) load cell (Sensotec, Columbus, Ohio, USA) connected to an E725 Microprocessor Transducer Indicator/Controller. The load cell enabled contact loads of 0.25N, 0.50N and 1.00N to be used with an accuracy of ± 0.01N. For each of the loads, thermal ‘movies’ or image sequences were then taken, at a rate of 1 frame per second, over a period of 70 seconds. For the first 10 seconds, no power was supplied to the scaler handpiece. This enabled the ambient background temperature of the experimental set-up to be determined. For the following 60 seconds, power was supplied to the scaler handpiece, using a low, medium or high generator power setting (corresponding to power setting marks 2, 5 or 9 respectively).



Figure 5.18 Scaler tips used for thermal imaging investigation including; (left) P- tip used in conjunction with a Mini Piezon generator and (right) TFI-3 scaler insert used with the Cavitron SPS generator.

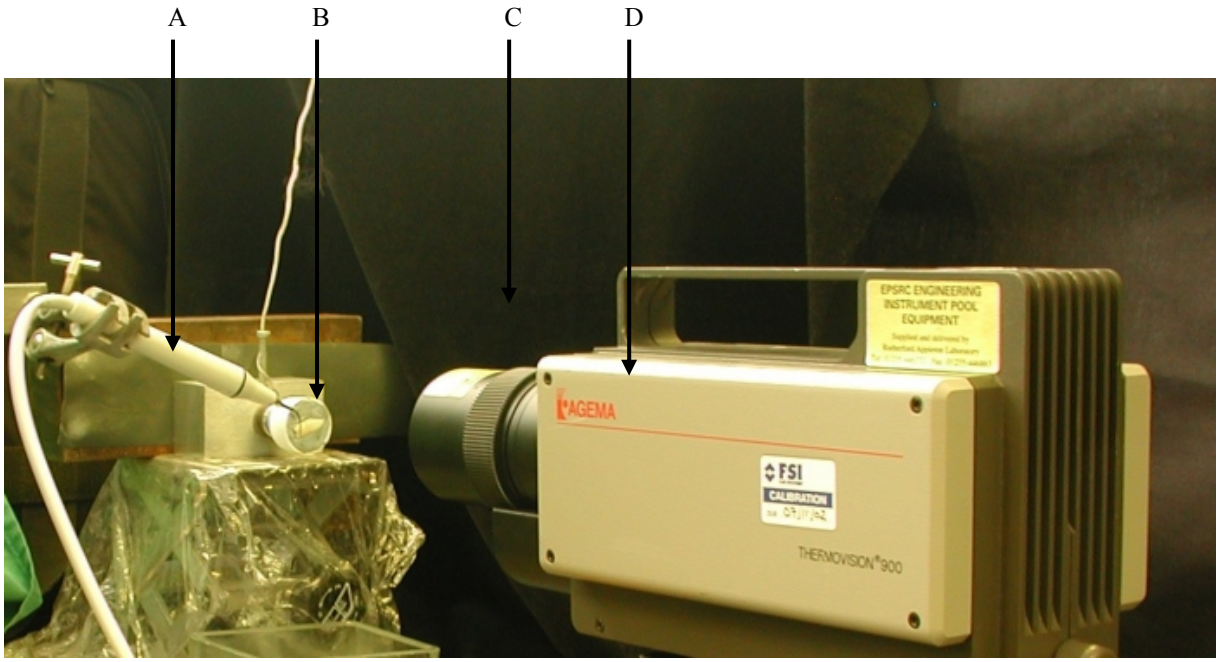


Figure 5.19 Experimental set-up of thermal imaging system and piezoelectric scaler tip including; A: Scaler and handpiece, B: tooth initially held in position using blue tack – during final experimentation this was replaced with the resin in vitro tooth model, the whole is situated upon the load cell, C: cloth used to help shield imaging area from external heat fluctuations and D; thermal imaging camera.

For each power and load combination, thermal sequences were obtained using water flow rates of 10, 20 and 40mls/min. After instrumentation, all power to the handpiece was stopped and the apparatus allowed time to cool. Thermal ‘movies’ were taken for all tip/tooth contact load, water flow rate and generator power-setting combinations. A measurement point was located on the images of the resulting thermal sequences, at the point where tip/tooth contact occurred. The sequences were reviewed frame by frame at the point of interest and the temperature variation as a function of time was recorded.

The Terephthalate Dosimeter

5.14 Cavitation around Ultrasonic Scalers

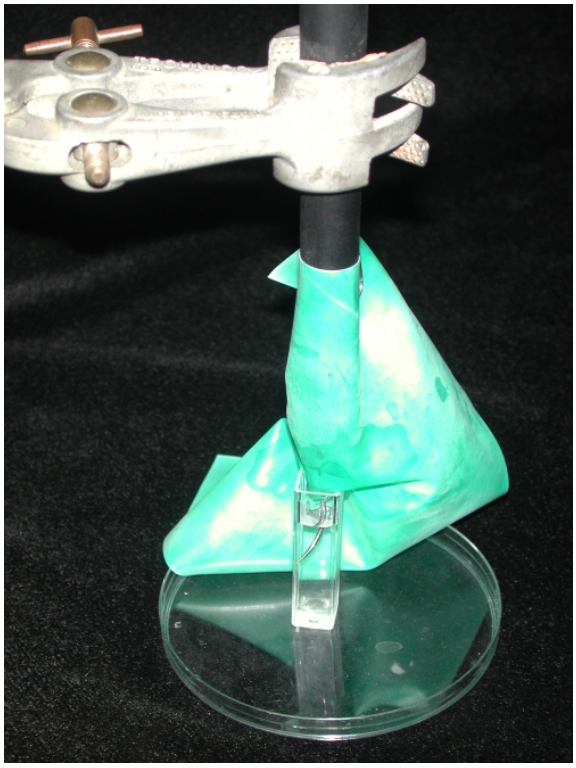
A solution of terephthalic acid (TA) was prepared by dissolving, with heating, 0.3323g (0.002mol) in 1dm^{-3} distilled water containing 25cm^{3} of pH 7.0 non-fluorescent buffer. Three different styles of tip (3 x TFI-10, 3 x TFI-3, 3 x TFI-1) were used in conjunction with a Cavitron SPS (Dentsply) ultrasonic generator (Figure 5.20). During normal use, water flows through the handpiece of the scaler and over the length of the tip. Water was still required throughout this investigation to regulate the handpiece temperature but could potentially interfere with the results (diluting the TA solution). Rubber dam was therefore placed over the tip so that the oscillations of the tips were unaffected but to ensure the water was kept away from the tip / cuvette (Figure 5.21).

The first tip was inserted into a cuvette containing 3.5mls of aqueous terephthalic acid solution. The tip was driven at a low generator power setting for 2 minutes and then the power to the tip was discontinued. The tip was removed from the cuvette and the cuvette of solution was then placed in a fluorescence spectrometer (Perkin Elmer 3000, Perkin Elmer, Beaconsfield, UK). The solution was excited at a wavelength of 325nm and the fluorescence emitted at wavelength 425nm, which is proportional to $^{\bullet}$OH radical concentration, recorded. The procedure was repeated 5 times to enable a mean $^{\bullet}$OH radical concentration to be calculated (Table 6.16). The sonication time was then increased from 2 to 5 minutes and 5 repeat measurements were performed as before. The power of the generator was then increased, successively, to medium and high power and 5 repeat measurements performed for 2 and 5 minutes sonication.



Figure 5.20 Scaler tips used during cavitation investigation including (from left to right); TFI-1, TFI-3 and TFI-10.

a)



b)

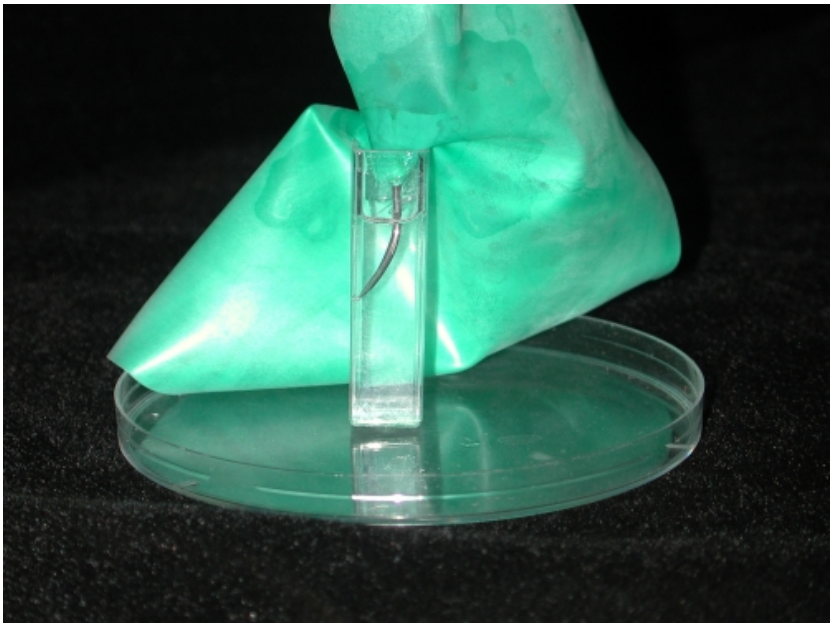


Figure 5.21 a) The scaler tip was fixed in position so that its tip was immersed in a cuvette containing terephthalic acid (TA) solution. b) Rubber dam was used to prevent water reaching the tip of the scaler and diluting the TA solution in the cuvette.

This process was repeated for all tip designs at low, medium and high generator power settings and at all sonication times. Measurements at each power / sonication time combination, for all tips, were repeated 5 times and a mean $^{\bullet}OH$ radical concentration calculated (Table 6.16).

Prior to all the measurements, each cuvette of unsonicated terephthalic acid solution was placed in the spectrometer to obtain a mean background reading of $^{\bullet}OH$ radical concentration.

5.15 Cavitation around Powered Toothbrushes

Five powered toothbrushes were used in this investigation (Figure 5.22) including; Sonicare Elite HX 7351/02 (Philips Oral Healthcare Inc, WA, USA), Sonicare PS-1 (Optiva Corporation, WA, USA), Philips Jordan Sensiflex HX2520 (Groningen, Netherlands), Braun Plaque Remover D8 (Braun GmbH, and Germany) and Braun Oral-B 3D excel (Braun GmbH, and Germany).

A toothbrush was inserted into a conical flask containing 50cm^3 of aqueous terephthalic acid (TA) solution, such that the head of the brush was completely submerged. The toothbrush was operated for 10 minutes and then removed. From the conical flask, 3.5cm^3 of solution was pipetted into a cuvette, which was placed in a fluorescence spectrometer (Perkin Elmer 3000, Perkin Elmer, Beaconsfield, UK) using an excitation wavelength of 325nm and monitoring the fluorescence emission at 425nm.

The solution was then replaced into the conical flask. The toothbrush was reinserted into the solution and the procedure was repeated for a further 10 minutes (20 minutes total). From the

conical flask, 3.5cm^3 of solution was again pipetted into the cuvette and placed in the fluorescence spectrometer to monitor the fluorescence emission at 425nm. The process was repeated for each of the toothbrushes.

The fluorescence detected is proportional to the concentration of [$^{\bullet}$OH] produced as a result of cavitation. Prior to each measurement, the spectrometer was zeroed using a cuvette of unsonicated TA solution.



Figure 5.22 Toothbrushes used throughout the cavitation investigation including (left - right): Sonicare Elite HX 7351/02, Sonicare PS-1, Philips Jordan Sensiflex HX2520, Braun Plaque Remover D8 and Braun Oral-B 3D excel.

CHAPTER 6

RESULTS

The Scanning Laser Vibrometer

6.1 SLV Presentation Mode

The SLV system measures vibration velocity, which it may use to calculate the vibration displacement amplitude. Vibration data are stored in the data manipulation system and, using the associated computer software, acquired data may be animated in several ways, described below.

6.1.1 Colour Map

Vibration data is superimposed over a captured video image of the target object (Figure 6.1). A colour-graded scale indicates the magnitude of the vibration velocity / displacement amplitude, as well as the direction of the motion relative to the scanner head. By superimposing data over the scaler probes' images the vibration displacement amplitude and velocity values at any position on the scaler tip can be rapidly evaluated. Thus the location of any node / antinode positions may be determined.

6.1.2 Colour Dots

This is a variation of the colour map display, which shows the data values obtained at the measurement points over which the scan was performed. Unlike the full colour map display facility no intermediate values, between measurement points, are calculated or displayed Figure 6.2a).

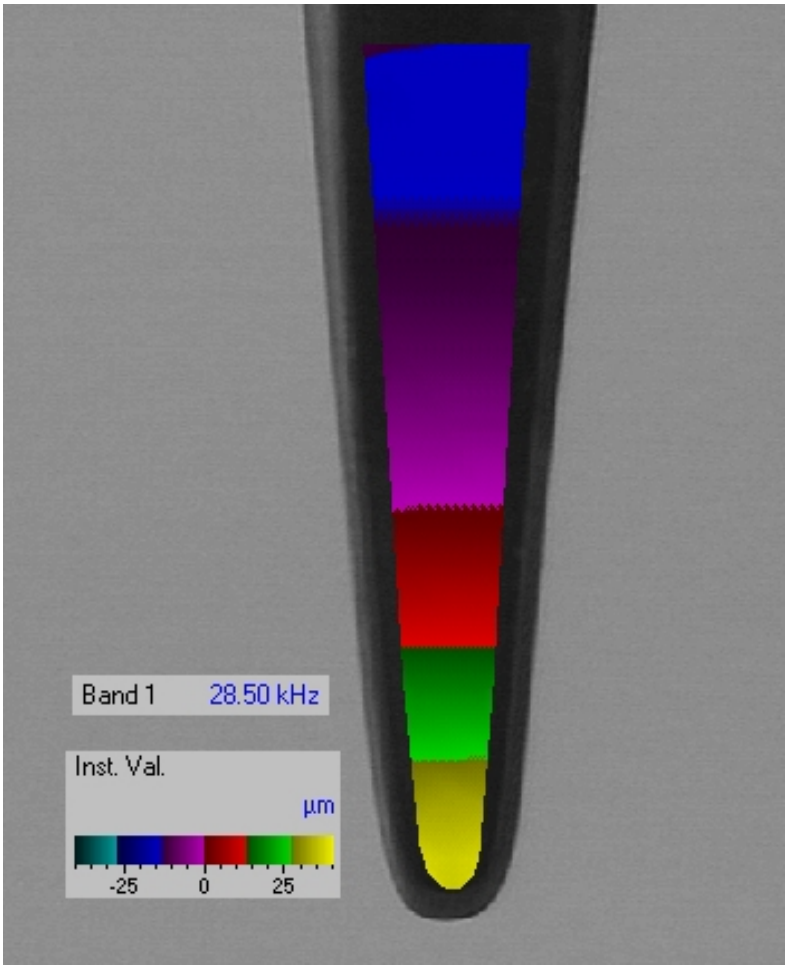
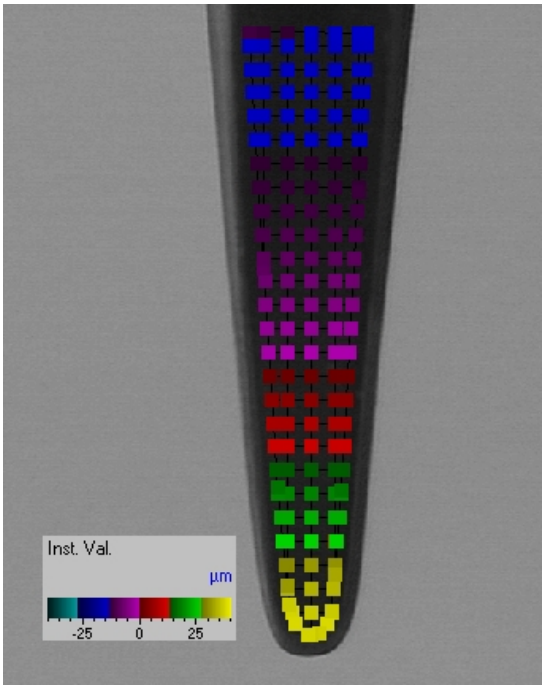
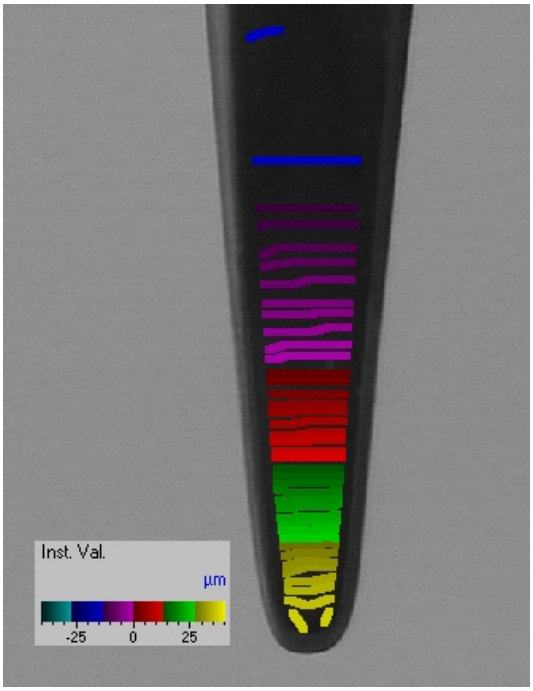


Figure 6.1 Colour map representation of a TFI-3 scaler tips vibration. Vibration data is superimposed over a captured video image of the scaler. A colour-graduated scale may be used to indicate the magnitude and direction of the vibration. A node is located at the red-pink boundary. Displacement amplitudes are given in micrometers.

a.



b.



c.

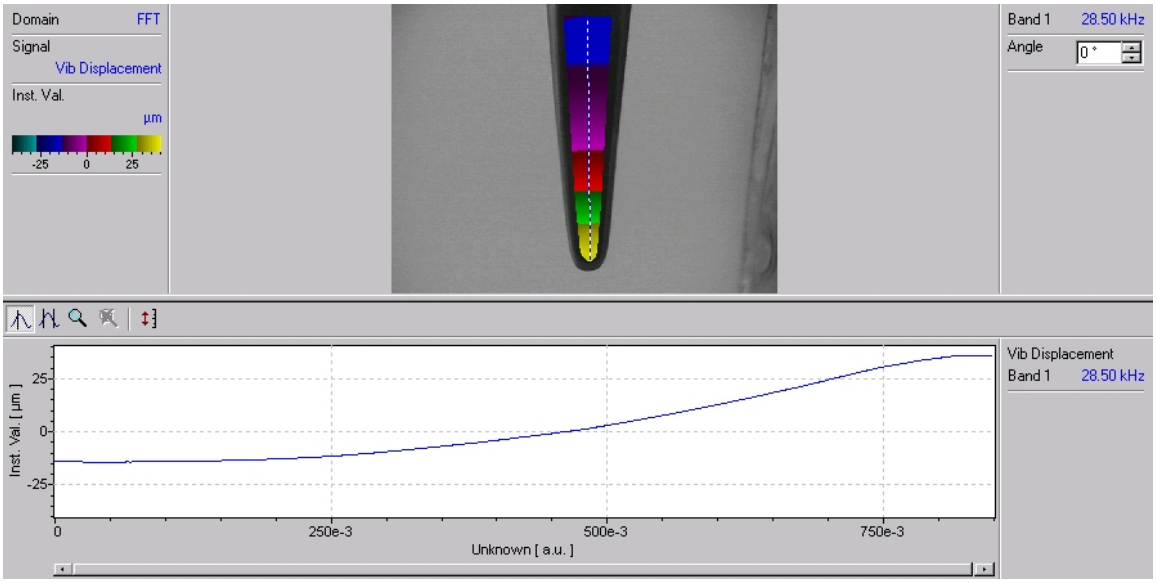


Figure 6.2 Methods of data visualisation include superimposing data over a captured video image of the target in the form of a) colour dots and b) isolines. c) A profile line may be drawn over the surface of the colour map to enable the profile of the vibration to be studied. Displacement amplitudes are given in micrometers.

6.1.3 Isolines

The isoline display facility is another variation of the colour map method of presenting vibration data. In the isoline display, lines connect measurement data of equal values (Figure 6.2b) in the same way as a weather map uses isobars to connect regions of equal atmospheric pressure and contour lines on a map represent equal points of height above sea level.

6.1.4 Profile Mode

Whilst displaying data in the colour map display mode, it is possible to superimpose a 'profile line' over a region of interest on the image. The SLV software sections the image along the length of this line. The vibration data may then be viewed in profile i.e. from the side of the vibration (Figure 6.2c).

6.1.5 3D-Mesh

Acquired data may be displayed as an animated 3D-mesh (Figure 6.3a-d). The same colour-graded scale, as utilised in the colour map display facility, is used to indicate the magnitude of the vibration velocity / displacement amplitude and to show the direction of the motion relative to the scanner head. However, unlike the previous display types, vibration data is allocated to the z-axis. The magnitude of this z-axis data alters with the phase of the oscillation (i.e. with time) and so leads to a flowing visual representation of the vibration at reduced frequency and magnified displacement amplitude. The manner in which the 3D-mesh is aligned with the physical scaler tip is demonstrated in Figure 8.4. Although no exact data values may be obtained from this type of display, the animation of a scaler tip, powered toothbrush or endosonic K-file oscillating with time allows initial interpretation of movement.

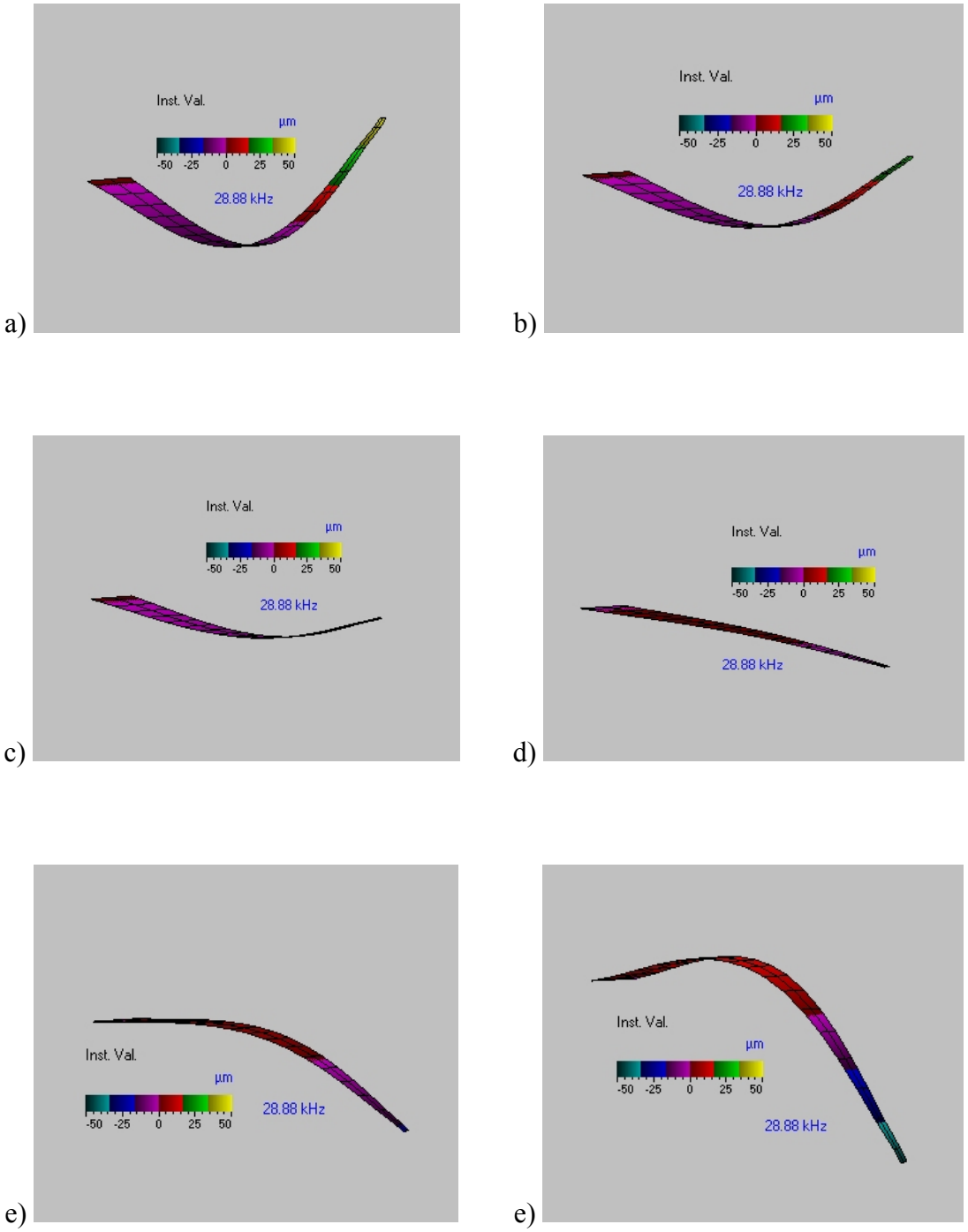


Figure 6.3 Stills from an animated 3D-mesh sequence representing the vibration data for an ultrasonic P-style tip as it moves through the different phases of its vibration. A colour-graduated scale indicates the magnitude of the vibration displacement amplitude.

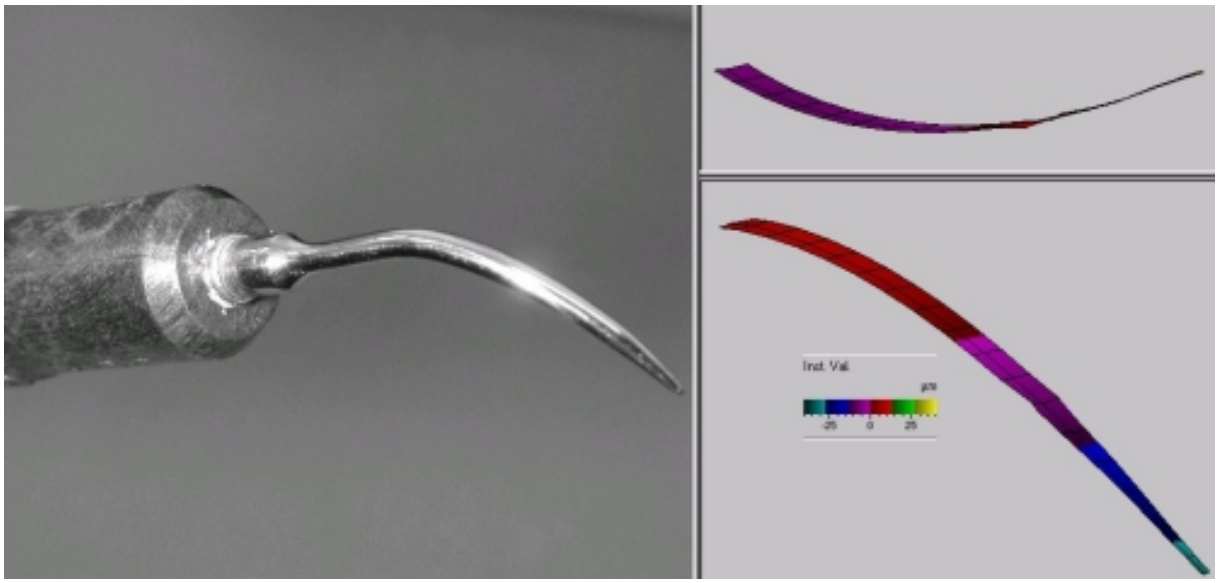


Figure 6.4 Orientation of 3D-mesh images relative to the front surface of scaler tip probe under investigation.

6.1.6 Summary

The most useful methods of analysing vibration data were found to be the colour map and 3D-mesh facilities. The 3D-mesh facility enables the motion of the target object vibration to be observed at reduced frequencies and velocities. The colour map facility enables more precise vibration data to be acquired and analysed.

6.2 SLV Calibration

The portable shaker is calibrated to produce vibrations with known displacement amplitude of 10μm ± 3%. Fifty point scans of the shaker produced a mean displacement amplitude (± 1 standard deviation) of 10.1μm ± 0.04μm thus demonstrating that the SLV produced highly reproducible and accurate results, within the nominal error range of the shaker.

6.3 Scaler Tip Vibration Characterisation

The SLV is able to analyse the vibrations of ultrasonic scaler insert probes. Comparisons of the vibration characteristics of different designs of insert probes, including a B-style and G-style tip used in conjunction with a piezoelectric system (Figure 6.5), and a TFI-10 insert and a TFI-3 insert in conjunction with a magnetostrictive system (Figure 6.5) are possible. The maximum displacement amplitude occurs at the free, unconstrained end of the tips and that this is independent of tip design. Tip evaluation also indicates those designs that produce the greatest displacement amplitude (for given power setting) and which, therefore, may theoretically be the most effective for removal of deposits in the clinical situation.

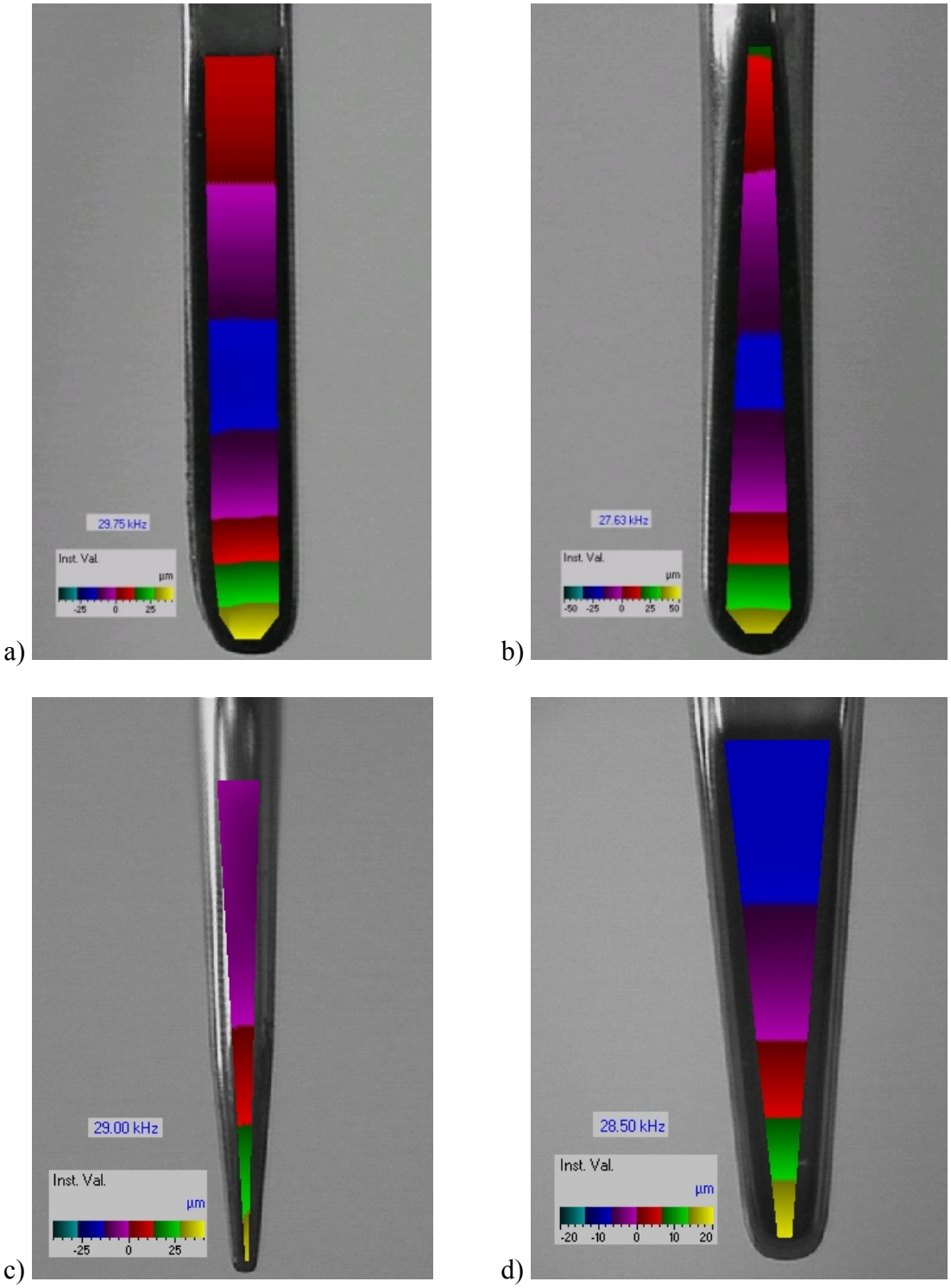


Figure 6.5 Colour map images of a) B-tip, b) G-tip, c) TFI-10 tip and d) TFI-3 tip. Analysis of various tip designs demonstrates that the maximum displacement amplitude occurs at the free, unconstrained end of the tips.

The fundamental frequency of scaler tip oscillation is determined through analysis of the frequency spectrum produced during SLV scans (Figure 6.6). The frequency range over which measurements are performed is selected during the initial set-up of the SLV and determines whether only the fundamental frequency of oscillation will be detected or the fundamental frequency and harmonics of that frequency. A set frequency range of 0 – 100kHz is usually selected.

6.4 Water Flow Rate and Scaler Tip Vibration

Scans were made of five TFI-10 scaler inserts under various generator power settings and for different water flow rates. The vibrometer detected the fundamental frequency of the scaler tip vibrations and the subsequent harmonics, within the frequency measurement range. A node was found to occur at approximately 4mm from the unconstrained end of the tip. Tips oscillated at fundamental frequencies (f_o) of 29.00kHz (Tips A, B, D and E) and 28.88kHz (Tip C) with higher harmonics at double ($2f_o$) and triple ($3f_o$) these frequencies, detected within our measurement range of 0-100kHz.

6.4.1 Oscillation of the Scaling Tip

The mean maximum displacement amplitudes for the five tips are shown in Table 6.1. The magnitude of the displacement amplitude of the scaling tips was affected by the water flow rate over the tip. Increasing the rate of flow of water over the tip surface, at a constant power setting, led to a general reduction in the displacement amplitude of the vibration of the tip (Table 6.1).

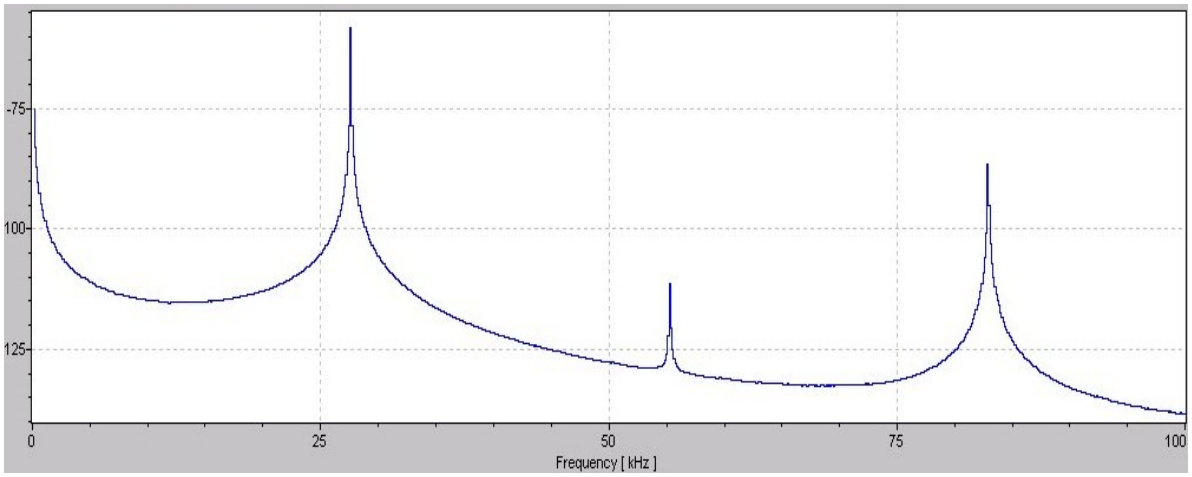


Figure 6.6 A typical frequency spectrum obtained during a laser vibrometer scan. The first peak, at approximately 28kHz, is the fundamental frequency of the oscillation. The following peaks are harmonics of the oscillation and occur at two times ($2f_o$) and three times ($3f_o$) the frequency of the fundamental (f_o). The y-axis gives displacement amplitude. This scale is logarithmic, so any difference in peak height corresponds to a large difference in vibration magnitude.

Tip	Water flow rate (ml/min)	Displacement amplitude (micrometres) at different generator power settings		
		Quarter Power	Half Power	Full Power
Tip A	18	22.2 ± 0.6	27.9 ± 1.0	26.8 ± 2.8
	38	19.9 ± 0.9	25.5 ± 1.1	17.2 ± 0.6
	62	16.7 ± 1.4	19.1 ± 2.0	18.5 ± 1.2
Tip B	18	20.9 ± 1.7	23.4 ± 1.1	30.4 ± 2.5
	38	19.0 ± 0.9	23.7 ± 1.8	18.0 ± 1.1
	62	10.6 ± 0.8	16.0 ± 1.6	18.2 ± 1.2
Tip C	18	14.2 ± 1.2	24.8 ± 0.7	25.9 ± 1.8
	38	10.8 ± 1.2	17.0 ± 0.8	24.8 ± 3.1
	62	8.2 ± 1.0	12.3 ± 1.3	22.6 ± 1.8
Tip D	18	20.6 ± 1.0	28.9 ± 0.4	27.0 ± 1.6
	38	20.9 ± 0.5	23.5 ± 0.9	26.1 ± 1.7
	62	13.0 ± 1.0	14.6 ± 1.0	30.2 ± 1.5
Tip E	18	20.3 ± 0.9	27.9 ± 1.2	23.2 ± 2.1
	38	19.8 ± 0.5	24.9 ± 1.4	17.9 ± 1.0
	62	14.4 ± 0.9	16.9 ± 1.5	19.6 ± 1.7

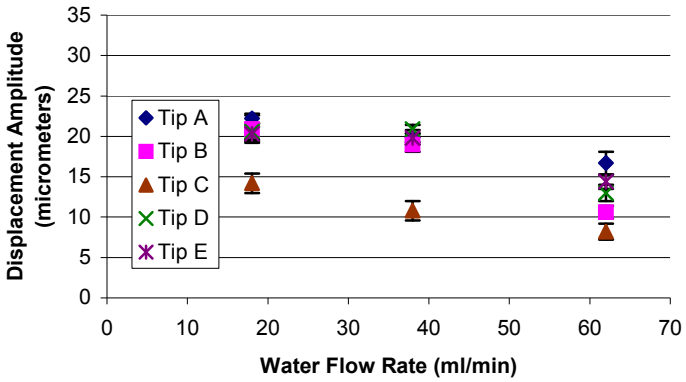
Table 6.1 The mean displacement amplitude (± 1 standard deviation), in micrometres, of the five scaling tips at different power control settings and water settings.

At the quarter power setting, an increase in the water flow rate led to a reduction in the mean displacement amplitude of the scaler tip (Figure 6.7a). This was similar for all five tips, although Tip C exhibited lower displacement amplitudes than the other four. At the half power setting, the mean displacement amplitudes of all the tips were greater than was observed for the quarter power setting. The tips were still influenced by the amount of water flowing over the working tip (Figure 6.7b), with increasing water flow rates causing a reduction in the measured displacement amplitude. Tip C again displayed smaller displacement amplitudes than the other four tips. At the full power setting and low / medium water flow rate, the displacement amplitude of the tips was similar to the half power setting. Increasing the water flow rate over the tip surface to the high setting (Figure 6.7c) led to a general increase in the observed displacement amplitude, with the exception of Tip C which showed a decrease. A univariate analysis of variance showed that both tip and power were significant variables ($p<0.0001$). Using multiple comparisons (Tukey) with the dependent variable being the displacement amplitude, all tips were significantly different ($p<0.0001$) for all power and water settings except for Tips B & E, which showed no differences ($p>0.1$).

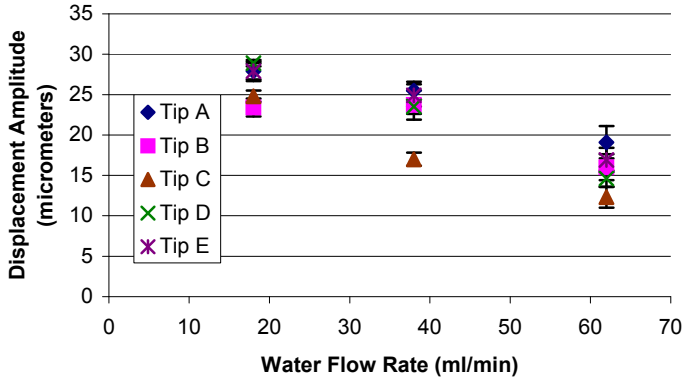
6.5 Displacement Amplitude of Unloaded Ultrasonic Scaler Inserts

6.5.1 Piezoelectric Generators

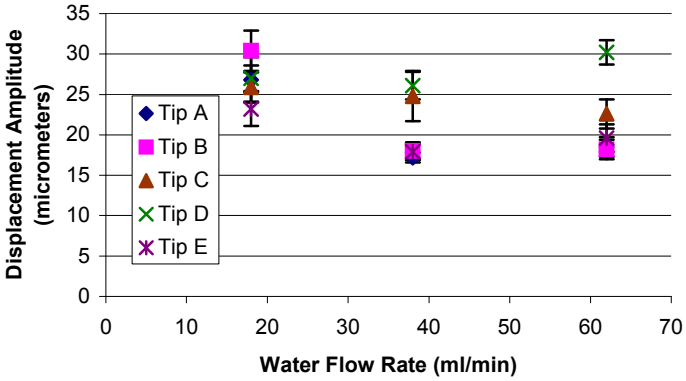
Displacement amplitude data for both piezoelectric generators show the Mini Piezon and Piezon Master 400 both produced an increase in displacement amplitude from power setting 1 to power setting 10 (Table 6.2). For the Mini Piezon generator the displacement amplitude at power setting 10 was found to be between 171% and 197% greater than the displacement amplitude at power setting 1. The Piezon Master 400 produced an increase in displacement amplitude from the first to the tenth power setting of between 45% and 110%.



a)



b)



c)

Figure 6.7 Graphs demonstrating the effect of water flow rate on scaler tip displacement amplitude at generator power settings corresponding to a) quarter power, b) half power and c) full power.

Tip		Power Setting										R^2	Percentage increase in displacement amplitude
		1	2	3	4	5	6	7	8	9	10		
Mini Piezon (P-Tip)	Tip 1	14.01 ± 1.48	21.65 ± 1.28	24.31 ± 1.52	29.15 ± 1.23	29.92 ± 1.03	33.17 ± 3.46	34.95 ± 4.68	34.44 ± 4.38	38.80 ± 3.39	38.00 ± 2.42	0.91	171%
	Tip 2	15.57 ± 1.87	20.04 ± 2.38	21.73 ± 1.75	25.50 ± 3.15	25.56 ± 2.57	27.29 ± 2.45	33.96 ± 2.45	36.08 ± 4.32	37.02 ± 1.77	42.91 ± 3.81	0.97	176%
	Tip 3	16.12 ± 0.12	19.02 ± 0.87	22.53 ± 0.33	25.89 ± 3.67	29.57 ± 2.13	32.71 ± 2.53	38.93 ± 2.93	39.05 ± 3.62	41.60 ± 3.74	44.03 ± 7.80	0.99	173%
	Tip 4	13.31 ± 2.13	18.45 ± 0.63	22.83 ± 0.54	24.03 ± 4.59	27.93 ± 2.51	24.50 ± 2.57	31.87 ± 2.57	33.83 ± 3.78	32.15 ± 6.61	38.84 ± 3.43	0.92	192%
	Tip 5	12.90 ± 1.44	14.82 ± 1.47	18.26 ± 1.61	22.80 ± 3.71	22.82 ± 3.46	27.07 ± 3.66	27.32 ± 2.95	34.01 ± 2.47	36.47 ± 6.68	38.31 ± 5.09	0.98	197%
	Tip 3#	16.68 ± 1.22	20.05 ± 0.98	23.42 ± 0.51	25.71 ± 2.97	31.45 ± 1.13	32.80 ± 1.87	38.23 ± 3.89	40.86 ± 3.22	41.86 ± 2.76	45.37 ± 1.73	0.99	172%
Piezon Master 400 (P-Tip)	Tip 1	17.11 ± 2.22	20.35 ± 2.55	20.65 ± 3.35	27.40 ± 4.10	25.27 ± 3.16	23.66 ± 1.65	28.13 ± 2.47	29.42 ± 3.83	25.82 ± 3.77	24.82 ± 3.46	0.52	45%
	Tip 2	17.06 ± 2.48	19.37 ± 1.23	21.53 ± 3.23	25.44 ± 2.34	31.37 ± 2.78	31.16 ± 3.78	32.04 ± 4.68	40.71 ± 0.89	35.55 ± 5.35	35.85 ± 5.29	0.87	110%
	Tip 3	16.02 ± 2.66	23.20 ± 3.07	21.73 ± 2.34	21.74 ± 1.95	22.75 ± 2.35	25.88 ± 4.20	28.77 ± 4.13	29.12 ± 4.05	25.37 ± 2.78	30.02 ± 0.84	0.75	87%
	Tip 4	17.50 ± 2.36	18.00 ± 1.96	19.21 ± 2.75	25.00 ± 3.55	24.20 ± 3.44	23.25 ± 2.18	30.60 ± 3.60	31.79 ± 3.82	29.27 ± 5.14	27.26 ± 4.95	0.76	56%
	Tip 5	16.51 ± 2.19	16.05 ± 3.49	21.13 ± 3.54	24.73 ± 3.74	26.29 ± 3.28	28.68 ± 2.42	27.48 ± 3.43	32.05 ± 4.88	31.04 ± 4.20	30.39 ± 3.75	0.87	84%
Cavitron SPS (TFI-10)	Tip 1	7.81 ± 0.51	10.28 ± 1.05	12.14 ± 0.97	15.82 ± 0.46	14.88 ± 1.74	15.77 ± 1.78	18.26 ± 2.07	24.17 ± 3.31	24.97 ± 3.42	24.79 ± 3.90	0.94	217%
	Tip 2	7.84 ± 0.81	11.98 ± 0.47	13.06 ± 1.37	12.73 ± 0.99	15.36 ± 1.38	17.91 ± 1.80	23.81 ± 0.45	24.79 ± 2.26	24.29 ± 4.44	25.50 ± 3.14	0.94	225%
	Tip 3	8.26 ± 0.94	11.23 ± 1.12	12.65 ± 0.66	13.48 ± 1.10	16.61 ± 0.68	16.79 ± 1.32	23.24 ± 1.92	23.99 ± 2.82	28.79 ± 2.77	25.79 ± 3.32	0.94	212%
	Tip 4	8.24 ± 0.69	10.68 ± 1.28	11.82 ± 0.95	14.20 ± 0.77	18.03 ± 0.92	22.09 ± 1.19	22.17 ± 1.97	25.95 ± 3.01	28.40 ± 2.99	29.70 ± 1.12	0.99	260%
	Tip 5	7.89 ± 1.13	11.78 ± 0.40	14.48 ± 0.34	17.23 ± 0.54	17.54 ± 1.28	21.73 ± 1.87	21.01 ± 1.74	23.17 ± 3.83	29.95 ± 1.27	26.34 ± 3.30	0.93	234%
Cavitron Select (TFI-10)	Tip 1	23.72 ± 0.30	24.29 ± 0.80	25.51 ± 0.60	25.93 ± 1.72	25.65 ± 3.19	28.20 ± 2.78	27.11 ± 4.11	29.28 ± 4.56	27.01 ± 4.72	31.28 ± 8.37	0.79	32%
	Tip 2	13.13 ± 1.44	16.67 ± 1.63	20.31 ± 1.17	26.62 ± 1.83	29.56 ± 0.77	28.58 ± 1.58	29.18 ± 2.95	23.86 ± 2.86	26.47 ± 3.03	26.89 ± 4.30	0.50	105%
	Tip 3	17.74 ± 0.42	16.86 ± 1.12	19.66 ± 0.77	29.44 ± 1.54	22.10 ± 2.28	24.88 ± 3.86	25.60 ± 7.55	23.79 ± 2.62	23.27 ± 2.32	23.99 ± 2.95	0.30	35%
	Tip 4	22.72 ± 1.12	24.29 ± 1.38	28.76 ± 0.61	34.93 ± 0.39	36.17 ± 0.43	29.80 ± 5.28	26.40 ± 1.39	32.02 ± 2.41	32.67 ± 2.17	33.77 ± 4.27	0.33	49%
	Tip 5	18.50 ± 0.36	18.27 ± 0.56	20.80 ± 0.25	23.71 ± 0.38	22.80 ± 0.49	23.18 ± 1.17	23.84 ± 1.41	21.81 ± 3.79	31.09 ± 3.18	31.95 ± 3.45	0.74	73%
Cavitron SPS (TFI-3)	Tip 1	5.50 ± 0.46	8.62 ± 0.72	10.33 ± 0.87	12.20 ± 1.06	14.09 ± 1.78	15.57 ± 1.60	19.57 ± 2.69	23.91 ± 3.65	27.72 ± 3.28	26.84 ± 3.32	0.97	388%
	Tip 2	9.32 ± 0.31	12.90 ± 0.60	14.57 ± 0.31	17.45 ± 0.67	17.38 ± 0.59	21.12 ± 0.88	19.83 ± 1.88	27.52 ± 4.19	31.95 ± 2.30	31.35 ± 3.62	0.94	236%
	Tip 3	10.51± 0.66	14.02 ± 0.26	16.16 ± 1.46	18.25 ± 0.99	19.95 ± 1.86	20.41 ± 2.99	23.91 ± 2.18	21.81 ± 4.29	21.64 ± 3.14	21.26 ± 3.79	0.76	102%
	Tip 4	9.49 ± 0.29	11.25 ± 0.83	12.80 ± 1.10	12.64 ± 1.13	14.14 ± 1.97	13.12 ± 1.67	14.26 ± 1.90	19.30 ± 2.62	24.31 ± 4.70	21.85 ± 4.59	0.82	130%
	Tip 5	9.01 ± 0.31	11.32 ± 0.13	13.58 ± 0.26	15.20 ± 0.60	14.59 ± 0.63	16.10 ± 2.11	18.12 ± 3.16	22.34 ± 4.74	26.56 ± 3.69	30.57 ± 4.27	0.91	239%

Table 6.2 Mean displacement amplitude (μm) of scaler tips at all power settings (± 1 standard deviation). Tip 3# indicates Tip 3 re-measured data.

Linear trend lines fitted to all tip data, produced R^2 values for the Mini Piezon of between 0.91 and 0.99 (Table 6.2). For the Piezon Master 400, R^2 values between 0.52 and 0.87 were obtained (Table 6.2). A univariate analysis of variance (General Linear Model) showed that, for both generators, tip and power were significant variables ($p<0.0001$). Using multiple post-hoc comparisons (Tukey test) with displacement amplitude as the dependent variable, all the P-tips used with the Mini Piezon were found to be significantly different ($p<0.04$) for all power settings (Table 6.3), except tips 1 and 3, which showed no differences ($p>0.1$). Tip 3 and its subsequent re-measure showed no significant differences ($p>0.4$). With the Piezon Master 400, tips 1, 3, 4 and 5 showed no differences at all power settings ($p>0.09$). Tip 2 was significantly different from all other tips ($p<0.0001$).

6.5.2 Magnetostrictive Generators

The displacement amplitude data, for both magnetostrictive generators, are shown in Table 6.2. Both generators (Cavitron SPS and Select) produced an increase in displacement amplitude from the first power setting to power setting 10. For the Cavitron SPS with TFI-10 tip, the displacement amplitude at generator power setting 10 was found to be between 212% and 260% greater than the displacement amplitude at the first power setting (Table 6.2). With the TFI-3 tip, the Cavitron SPS produced an increase in displacement amplitude, from the first to the tenth power setting of between 102% and 388%. The Cavitron Select, with TFI-10 tip, produced an increase of between 32% and 105% from power setting 1 to 10 (Table 6.2). Linear trend lines, fitted to all tip data, gave R^2 values of between 0.93 and 0.99 for the Cavitron SPS with TFI-10 tip (Table 6.2). R^2 values of between 0.76 and 0.97 (Table 6.2) were obtained for the Cavitron SPS with TFI-3 tip and for the Cavitron Select with TFI-10 tip, R^2 values of between 0.30 and 0.79 were produced (Table 6.2).

		Tip 1	Tip 2	Tip 3	Tip 4
Mini Piezon (P-Tip)	Tip 2	.043*	-	-	-
	Tip 3	.111	.000*	-	-
	Tip 4	.000*	.001*	.000*	-
	Tip 5	.000*	.001*	.000*	.038*
Piezon Master 400 (P-Tip)	Tip 2	.000*	-	-	-
	Tip 3	.994	.000*	-	-
	Tip 4	.950	.000*	.998	-
	Tip 5	.099	.000*	.243	.412
Cavitron SPS (TFI-10)	Tip 2	.023*	-	-	-
	Tip 3	.000*	.709	-	-
	Tip 4	.000*	.000*	.002*	-
	Tip 5	.000*	.000*	.002*	1.000
Cavitron Select (TFI-10)	Tip 2	.000*	-	-	-
	Tip 3	.000*	.006*	-	-
	Tip 4	.000*	.000*	.000*	-
	Tip 5	.000*	.689	.213	.000*
Cavitron SPS (TFI-3)	Tip 2	.000*	-	-	-
	Tip 3	.000*	.000*	-	-
	Tip 4	.009*	.000*	.000*	-
	Tip 5	.000*	.000*	.017*	.000*

Table 6.3 Significance values (General Linear Model) for multiple post-hoc comparisons (Tukey test) of tips. The dependent variable is displacement amplitude.

* indicates difference between tips is significant at .05 level.

A univariate analysis of variance (General Linear Model) showed that for all three generators, tip and power were significant variables ($p<0.0001$). Using multiple comparisons, (Tukey test), with displacement amplitude as the dependent variable, TFI-10 tips 2 and 3 showed no significant differences ($p>0.7$) when used with the Cavitron SPS (Table 6.3) but were significantly different from the other three tips ($p<0.003$). Likewise, tips 4 and 5 showed no significant differences ($p=1$) but were again significantly different from the other three tips ($p<0.003$). TFI-10 tip 1 was significantly different from all other tips at all power settings ($p<0.03$). With the Cavitron SPS used in conjunction with the TFI-3 tips, all tips were found to be significantly different ($p<0.02$) for all power settings. When the Cavitron Select was used with the TFI-10 tips, tips 1 and 4 were found to be significantly different from each other and all other tips ($p<0.0001$) for all power settings. Tips 2 and 5 showed no significant differences ($p>0.6$) and tips 3 and 5 showed no significant differences ($p>0.2$).

6.6 Load and Ultrasonic Scaler Tip Displacement Amplitude

For all generators, as power was increased from power setting 1 to power setting 10, an increase in scaler tip displacement amplitude was observed (Tables 6.4 & 6.5). Exceptions occurred for the Piezon Master 400 with P-tip 1 (0.25N load) and the Mini Piezon with P-tip 1 and 0.50N load (Table 6.4). These produced lower displacement amplitudes at power setting 10 than power setting 1. Linear trend lines, fitted to tip data for all generators, produced R^2 values which showed that the increase in tip displacement amplitude with power for the piezoelectric generators, was generally non–linear (Table 6.4). The magnetostrictive generators were found to produce more linear increases, especially the Cavitron SPS generator with the TFI-3 tips, which produced R^2 values of between 0.93 and 0.99 (Table 6.5).

Generator / Tip / Load		Power Setting 1	2	3	4	5	6	7	8	9	10	R^2 linear regression
Mini Piezon P-Tip / 0.25N	Tip 1	7.10 ± 1.11	7.14 ± 1.27	8.60 ± 0.49	11.85 ± 0.25	12.45 ± 0.35	12.91 ± 0.53	13.03 ± 0.44	11.96 ± 0.57	14.50 ± 1.46	13.61 ± 2.63	0.79
	Tip 2	10.54 ± 0.28	9.54 ± 0.50	10.71 ± 0.40	9.56 ± 0.34	9.15 ± 1.21	12.43 ± 1.84	16.66 ± 0.92	19.02 ± 0.39	18.48 ± 0.70	16.77 ± 1.57	0.72
	Tip 3	9.22 ± 0.88	11.23 ± 1.66	12.93 ± 0.58	14.13 ± 2.50	19.69 ± 0.48	22.16 ± 0.85	18.99 ± 1.68	18.75 ± 2.66	19.84 ± 1.21	26.82 ± 1.57	0.81
Mini Piezon P-Tip / 0.5N	Tip 1	7.45 ± 0.18	9.12 ± 0.27	8.51 ± 0.42	7.58 ± 0.44	9.93 ± 0.61	12.84 ± 1.11	14.18 ± 0.72	9.90 ± 1.00	8.04 ± 0.24	7.41 ± 0.38	0.03
	Tip 2	6.64 ± 1.38	11.58 ± 0.26	12.18 ± 0.34	9.97 ± 0.46	13.88 ± 0.98	13.62 ± 0.54	13.25 ± 0.56	16.11 ± 1.09	13.87 ± 0.58	19.60 ± 0.76	0.74
	Tip 3	8.04 ± 0.79	9.99 ± 0.61	12.51 ± 2.10	16.18 ± 0.61	19.44 ± 0.49	19.71 ± 0.71	22.73 ± 0.57	26.22 ± 0.77	33.11 ± 0.49	32.75 ± 1.20	0.97
Mini Piezon P-Tip / 1.0N	Tip 1	8.17 ± 0.17	9.48 ± 0.47	8.78 ± 0.33	7.78 ± 0.36	7.79 ± 0.32	11.27 ± 0.71	13.91 ± 0.35	16.29 ± 0.42	16.14 ± 0.61	16.24 ± 0.89	0.79
	Tip 2	9.08 ± 0.40	10.24 ± 0.28	8.94 ± 0.44	7.27 ± 0.29	9.43 ± 0.26	10.89 ± 0.54	12.24 ± 0.62	19.11 ± 0.51	19.72 ± 0.49	16.50 ± 1.47	0.67
	Tip 3	10.50 ± 0.86	12.42 ± 1.92	13.43 ± 0.99	16.54 ± 0.35	15.85 ± 0.79	20.99 ± 1.50	18.42 ± 0.77	23.50 ± 0.58	28.17 ± 4.24	24.32 ± 3.03	0.90
Piezon Master 400 P-Tip / 0.25N	Tip 1	13.35 ± 0.71	15.82 ± 1.91	16.88 ± 1.27	18.93 ± 0.69	21.25 ± 1.02	23.51 ± 0.92	22.25 ± 1.33	15.72 ± 1.41	15.59 ± 0.73	10.95 ± 0.88	0.01
	Tip 2	6.79 ± 0.35	7.55 ± 0.88	8.14 ± 0.53	11.00 ± 1.19	13.41 ± 0.98	15.46 ± 0.90	20.14 ± 0.22	17.32 ± 1.84	19.20 ± 1.32	21.57 ± 0.24	0.94
	Tip 3	8.75 ± 0.56	10.93 ± 0.44	12.00 ± 0.91	16.72 ± 1.14	18.96 ± 0.33	20.62 ± 1.30	22.00 ± 0.96	17.57 ± 1.50	24.07 ± 0.83	26.24 ± 0.30	0.87
Piezon Master 400 P-Tip / 0.5N	Tip 1	14.73 ± 0.87	18.43 ± 0.24	23.17 ± 1.23	28.43 ± 2.62	22.31 ± 0.75	26.92 ± 0.83	21.37 ± 1.66	29.16 ± 1.31	23.15 ± 1.94	20.67 ± 1.69	0.17
	Tip 2	12.07 ± 0.84	11.01 ± 1.11	14.00 ± 3.28	17.27 ± 0.46	20.99 ± 0.30	18.08 ± 2.08	20.74 ± 1.15	23.79 ± 0.95	21.67 ± 1.46	12.97 ± 1.40	0.32
	Tip 3	7.94 ± 0.83	9.62 ± 0.54	11.57 ± 0.94	13.88 ± 0.91	15.31 ± 1.44	16.82 ± 1.44	15.99 ± 2.50	11.63 ± 0.81	16.69 ± 1.34	14.39 ± 2.46	0.48
Piezon Master 400 P-Tip / 1.0N	Tip 1	12.75 ± 1.07	14.12 ± 1.38	19.63 ± 3.07	21.17 ± 3.51	27.55 ± 1.85	26.13 ± 3.22	34.54 ± 0.82	28.84 ± 4.38	28.19 ± 4.21	18.03 ± 1.75	0.36
	Tip 2	10.93 ± 0.76	14.52 ± 0.64	15.50 ± 0.73	19.32 ± 0.45	21.96 ± 0.59	20.56 ± 2.97	23.25 ± 1.43	25.11 ± 0.73	21.76 ± 1.16	13.32 ± 0.89	0.26
	Tip 3	7.32 ± 0.99	10.19 ± 1.08	13.04 ± 1.39	12.83 ± 2.16	13.56 ± 2.24	15.36 ± 1.06	20.89 ± 1.79	22.23 ± 1.42	21.29 ± 3.17	14.75 ± 1.41	0.65

Table 6.4 Mean displacement amplitude (μm) of all piezoelectric scalers at all power settings and loads (± 1 standard deviation).

Generator Tip / Load		Power Setting 1	2	3	4	5	6	7	8	9	10	R^2 linear regression
Select TFI-10 / 0.25N	Tip 1	16.84 ± 1.09	14.55 ± 2.19	17.18 ± 1.06	18.19 ± 1.20	18.00 ± 0.78	24.57 ± 0.96	26.31 ± 1.32	20.64 ± 1.09	21.58 ± 1.32	19.61 ± 2.16	0.39
	Tip 2	19.60 ± 0.84	17.89 ± 2.92	18.74 ± 2.03	19.77 ± 3.86	20.13 ± 3.59	27.03 ± 0.66	27.47 ± 1.54	28.17 ± 0.38	27.83 ± 1.11	26.48 ± 1.47	0.77
	Tip 3	12.30 ± 1.27	14.59 ± 1.03	16.43 ± 2.35	20.84 ± 1.67	27.34 ± 2.04	29.82 ± 0.62	30.69 ± 3.88	35.52 ± 1.25	36.55 ± 0.96	34.65 ± 1.63	0.94
Select TFI-10 / 0.5N	Tip 1	17.17 ± 0.22	17.71 ± 0.24	20.47 ± 0.53	20.92 ± 0.80	21.59 ± 1.15	22.62 ± 1.45	23.17 ± 1.34	24.78 ± 2.30	22.14 ± 0.92	21.15 ± 0.88	0.57
	Tip 2	17.58 ± 1.32	17.40 ± 2.45	19.18 ± 2.74	22.28 ± 1.66	21.25 ± 1.68	24.01 ± 1.24	22.93 ± 1.20	24.81 ± 1.16	25.46 ± 1.37	25.36 ± 1.72	0.90
	Tip 3	14.12 ± 3.59	10.23 ± 0.76	10.01 ± 1.27	12.50 ± 1.52	23.36 ± 1.17	25.86 ± 1.10	28.09 ± 1.74	29.80 ± 0.86	29.83 ± 0.73	29.73 ± 2.12	0.82
Select TFI-10 / 1.0N	Tip 1	12.60± 0.47	16.01 ± 0.23	17.58 ± 0.90	19.21 ± 0.65	19.56 ± 1.10	21.04 ± 0.84	21.91 ± 2.48	23.29 ± 0.81	22.65 ± 1.18	22.14 ± 0.76	0.86
	Tip 2	14.51 ± 0.85	14.01 ± 0.81	15.46 ± 2.00	14.79 ± 1.04	17.42 ± 3.32	24.06 ± 0.47	25.63 ± 0.91	26.16 ± 1.12	24.85 ± 1.66	25.56 ± 1.47	0.84
	Tip 3	10.21 ± 0.38	10.25 ± 0.45	13.33 ± 0.99	19.13 ± 0.90	20.42 ± 0.56	22.46 ± 0.62	24.13 ± 1.28	23.31 ± 2.14	23.65 ± 0.87	23.90 ± 1.59	0.84
SPS TFI-10 / 0.25N	Tip 1	4.61 ± 0.08	5.91 ± 0.54	7.09 ± 0.12	10.21 ± 0.48	9.86 ± 1.75	14.40 ± 0.64	14.58 ± 1.58	14.67 ± 0.57	19.19 ± 0.70	18.87 ± 0.66	0.96
	Tip 2	6.41 ± 0.15	8.99 ± 0.09	12.34 ± 0.20	11.36 ± 0.89	11.47 ± 0.69	10.79 ± 0.80	13.68 ± 0.71	17.05 ± 1.47	20.83 ± 0.28	21.34 ± 0.30	0.86
	Tip 3	5.21 ± 0.14	6.52 ± 0.67	8.54 ± 0.34	10.34 ± 0.98	14.78 ± 0.40	17.13 ± 0.15	15.13 ± 0.42	15.45 ± 0.62	19.25 ± 0.70	18.40 ± 0.96	0.89
SPS TFI-10 / 0.5N	Tip 1	6.09 ± 0.08	7.76 ± 0.39	7.76 ± 0.36	10.20 ± 0.20	9.99 ± 0.51	11.18 ± 0.93	11.44 ± 0.47	11.68 ± 0.44	21.63 ± 0.69	20.04 ± 1.24	0.78
	Tip 2	4.49 ± 0.11	6.52 ± 0.18	8.69 ± 0.08	9.86 ± 0.49	12.42 ± 0.14	14.70 ± 0.29	16.03 ± 0.41	15.41 ± 0.48	20.67 ± 0.42	21.23 ± 0.51	0.97
	Tip 3	4.90 ± 0.09	6.76 ± 0.12	7.46 ± 0.14	7.59 ± 0.89	11.11 ± 0.70	11.99 ± 1.57	12.45 ± 0.22	15.94 ± 0.44	20.41 ± 0.39	21.87 ± 0.36	0.94
SPS TFI-10 / 1.0N	Tip 1	5.02 ± 0.08	7.06 ± 0.11	8.75 ± 0.36	10.37 ± 0.24	11.12 ± 0.82	11.24 ± 0.58	11.75 ± 0.55	13.36 ± 0.62	17.53 ± 0.87	19.97 ± 0.50	0.92
	Tip 2	5.10 ± 0.18	6.37 ± 0.18	6.62 ± 0.17	8.45 ± 0.42	11.78 ± 0.43	13.04 ± 0.60	13.24 ± 1.26	14.98 ± 0.47	19.51 ± 0.46	20.42 ± 0.61	0.96
	Tip 3	4.33 ± 0.13	7.11 ± 0.10	8.55 ± 0.34	8.98 ± 0.21	8.57 ± 0.75	10.19 ± 0.60	13.53 ± 0.39	16.43 ± 0.48	20.30 ± 0.54	21.45 ± 0.29	0.92
SPS TFI-3 / 0.25N	Tip 1	8.30 ± 0.16	11.46 ± 0.20	13.88 ± 0.19	15.13 ± 0.18	16.00 ± 1.79	17.74 ± 0.69	18.58 ± 1.23	24.58 ± 0.70	25.76 ± 1.76	24.37 ± 2.51	0.95
	Tip 2	5.94 ± 0.41	7.91 ± 0.12	10.19 ± 0.69	13.14 ± 0.13	10.36 ± 1.68	13.39 ± 0.84	19.02 ± 0.66	22.65 ± 1.24	25.51 ± 1.37	28.11 ± 1.08	0.93
	Tip 3	5.09 ± 0.06	6.12 ± 0.10	8.56 ± 0.11	11.01 ± 0.13	12.05 ± 0.37	13.98 ± 1.13	16.42 ± 0.23	19.52 ± 0.66	24.00 ± 0.47	24.59 ± 0.46	0.98
SPS TFI-3 / 0.5N	Tip 1	7.40 ± 0.18	10.67 ± 0.09	13.85 ± 0.11	13.21 ± 0.45	14.29 ± 0.37	16.22 ± 0.44	21.54 ± 0.37	25.03 ± 1.62	25.96 ± 2.55	25.79 ± 3.17	0.94
	Tip 2	4.33 ± 0.19	5.39 ± 0.14	7.41 ± 0.14	10.33 ± 0.30	10.72 ± 0.50	12.28 ± 0.58	15.46 ± 1.33	21.33 ± 1.43	24.98 ± 0.91	25.68 ± 0.93	0.95
	Tip 3	4.20 ± 0.10	5.68 ± 0.14	8.28 ± 0.15	10.84 ± 0.08	12.38 ± 0.91	13.54 ± 0.29	15.53 ± 0.62	19.12 ± 0.59	21.75 ± 1.21	24.95 ± 0.83	0.99
SPS TFI-3 / 1.0N	Tip 1	6.00 ± 0.50	9.66 ± 0.09	11.61 ± 0.75	12.76 ± 1.51	14.84 ± 0.47	16.18 ± 0.39	18.61 ± 0.57	20.66 ± 0.85	21.14 ± 2.75	21.53 ± 4.15	0.97
	Tip 2	4.65 ± 0.13	5.43 ± 0.23	7.88 ± 0.12	10.96 ± 0.18	12.08 ± 0.87	10.94 ± 0.73	14.18 ± 1.11	18.55 ± 1.18	19.55 ± 1.41	22.57 ± 1.17	0.96
	Tip 3	3.89 ± 0.09	5.63 ± 0.10	8.28 ± 0.31	10.67 ± 0.07	10.97 ± 0.24	12.67 ± 0.50	13.90 ± 0.63	18.61 ± 1.05	22.33 ± 0.37	23.79 ± 0.68	0.96

Table 6.5 Mean displacement amplitude (μm) of all magnetostrictive scalers at all power settings and loads (± 1 standard deviation).

6.6.1 Statistical analysis

6.6.1.1 Piezoelectric generators

Variation between tips

A univariate analysis of variance (General Linear Model) showed that, for both generators, tip and power were significant variables ($p<0.0001$). Using multiple post-hoc comparisons (Tukey test) at a significance level of $p<0.05$ and with the dependent variable being the displacement amplitude, all P-tips used with the Mini Piezon were found to be significantly different ($p<0.0001$) for all power settings at each load. With the Piezon Master 400, all P-tips were found to be significantly different ($p<0.03$) for all power settings at each load.

Variation of individual tips due to load

Using multiple post-hoc comparisons (post-hoc Tukey test, General Linear Model) at a significance level of $p<0.05$ and with the dependent variable being the displacement amplitude, a significant difference was found between unloaded and loaded P-tips for both the Mini Piezon generator ($p<0.0001$) and the Piezon Master 400 generator ($p<0.002$) for all loads.

With the Mini Piezon generator, each tip was shown to produce a significantly different response with change in load ($p<0.03$) except P-tip 1, which showed no significant differences under loads of 0.25N and 1.0N ($p>0.74$) and P-tip 2 under loads of 0.25N and 0.50N ($p>0.83$). With the Piezon Master 400 generator, each tip was shown to produce a significantly different response with change in load ($p<0.0001$) except P-tip 1 with loads of 0.50N and 1.00N, which showed no significant differences ($p>0.85$).

6.6.1.2 Magnetostrictive generators

Variation between tips

As with the piezoelectric generators, a univariate analysis of variance (general linear model) showed that, for both generators, tip and power were significant variables ($p<0.0001$). Multiple post-hoc comparisons (Tukey test) at a significance level of $p<0.05$ for the Select (displacement amplitude being the dependent variable) showed that all tips were significantly different ($p< 0.01$) for each load at all power settings, except for tips 1 and 3 at 0.50N, which showed no significant differences ($p> 0.68$). With the SPS generator (TFI-10 tips), all tips were found to be significantly different ($p< 0.002$) for each load at all power settings, except for tips 2 and 3 under 1.00N load, which showed no significant differences ($p> 0.99$). When used with the TFI-3 inserts, multiple comparisons for the SPS showed that all the tips were significantly different ($p< 0.04$) at all power settings for each load, except for tips 2 and 3 at 0.50N, which showed no significant differences ($p>0.48$).

Variation of individual tips due to load

Using multiple post-hoc comparisons (Tukey test, general linear model, analysis of variance) at a significance level of $p<0.05$ and with the dependent variable being the displacement amplitude, a significant difference was generally found between unloaded and loaded tips for both the Select and SPS generators ($p<0.0001$) for all loads investigated. However, exceptions did occur for the Select with TFI-10 tip 2 with 0.25N and 0.50N loads, which showed no significant difference from the unloaded tip ($p>0.24$) and ($p>0.10$) respectively. The SPS with TFI-3 tip 2 with 0.25N load also showed no significant difference from the unloaded tip ($p>0.45$).

With the Select generator, each TFI-10 tip was shown to produce a significantly different response with change in load ($p<0.0001$) except tip 1, which showed no significant differences under loads of 0.25N and 1.0N ($p>0.91$). The TFI-10 tips with the SPS generator produced a significantly different response with change in load ($p<0.02$), except tip 1 with loads of 0.25N and 0.50N ($p>0.78$), 0.25N and 1.00N ($p>0.23$) and 0.50N and 1.00N ($p>0.78$). TFI-10 tip 3 also showed no significant differences between loads of 0.50N and 1.00N ($p>0.9$). Used in conjunction with the TFI-3 tips, each tip produced a significantly different response with change in load ($p<0.03$) except tip 1 with loads of 0.25N and 0.50N, which showed no significant differences ($p>0.88$). Tip 3 with loads of 0.25N and 0.50N also showed no significant differences ($p>0.05$).

6.7 Wear and Scaler Tip Displacement Amplitude

Scans were performed to determine the mean displacement amplitude of scaler tips under loaded and unloaded conditions. Tips were initially scanned in their new and unused state (Table 6.6). Data were then gathered for tip displacement amplitude following 1mm of wear (Table 6.7) and 2mm of wear (Table 6.8). The data were used to determine the percentage decrease in the mean maximum displacement amplitude, due to 'tip wear', for unloaded conditions (Table 6.9) and for tips contacted against tooth surfaces with loads of 0.50N (Table 6.10) and 1.0N (Table 6.11). The effect of tip length on the maximum displacement amplitude, for individual inserts under unloaded and loaded conditions, are presented graphically for the FSI-100 (Figure 6.8a-c), FSI-1000 (Figure 6.9a-c) and FSI-SLI-10S (Figure 6.10a-c). By combining the data for tips of the same type, the effect of tip length on the mean maximum displacement amplitude for inserts may also be shown graphically (Figure 6.11a-c).

	Mean Tip Displacement Amplitude (micrometres)		
Insert (Design / Number)	**Unloaded**	**0.5N Load**	**1.0N Load**
FSI-100			
Tip 1	21.93 ± 2.33	14.19 ± 1.02	14.37 ± 1.47
Tip 2	22.24 ± 1.55	18.19 ± 0.75	13.06 ± 1.73
Tip 3	10.37 ± 0.86	11.53 ± 1.65	11.31 ± 1.94
Tip 4	19.19 ± 2.72	11.30 ± 1.21	13.97 ± 1.69
Tip 5	20.20 ± 2.46	17.38 ± 2.38	14.48 ± 1.65
FSI-1000			
Tip 1	22.40 ± 2.25	16.10 ± 1.59	19.92 ± 0.79
Tip 2	22.22 ± 2.79	16.67 ± 1.54	14.21 ± 2.47
Tip 3	21.61 ± 2.97	17.72 ± 1.31	18.68 ± 2.52
Tip 4	21.58 ± 2.33	16.70 ± 1.79	14.07 ± 1.22
Tip 5	29.61 ± 2.85	17.88 ± 2.58	15.73 ± 1.88
FSI- SLI-10S			
Tip 1	12.57 ± 1.73	14.58 ± 1.55	10.97 ± 2.97
Tip 2	13.25 ± 1.98	9.51 ± 1.67	10.20 ± 0.93
Tip 3	14.23 ± 0.36	7.53 ± 0.95	6.27 ± 0.62
Tip 4	13.21 ± 1.64	11.64 ± 1.58	9.40 ± 0.54
Tip 5	11.51 ± 1.68	8.82 ± 0.84	8.98 ± 1.84

Table 6.6 Mean displacement amplitude data (measured in micrometres ± 1 standard deviation) for unadjusted FSI-100, FSI-1000 and FSI-SLI-10S scaler inserts under loaded and unloaded conditions.

	Mean Tip Displacement Amplitude (micrometres)		
Insert (Design / Number)	**Unloaded**	**0.5N Load**	**1.0N Load**
FSI-100			
Tip 1	8.38 ± 2.28	13.52 ± 1.74	11.56 ± 0.65
Tip 2	8.15 ± 1.81	10.71 ± 1.92	11.67 ± 1.30
Tip 3	9.96 ± 2.24	14.29 ± 1.72	15.02 ± 1.39
Tip 4	8.08 ± 2.98	13.17 ± 2.12	11.92 ± 1.28
Tip 5	11.42 ± 0.94	11.28 ± 2.03	11.29 ± 0.44
FSI-1000			
Tip 1	21.14 ± 1.80	14.99 ± 2.53	11.26 ± 1.31
Tip 2	17.10 ± 2.37	13.64 ± 2.38	15.01 ± 1.78
Tip 3	15.97 ± 3.02	8.11 ± 1.27	8.87 ± 2.08
Tip 4	21.36 ± 3.00	14.82 ± 1.78	17.45 ± 1.73
Tip 5	19.94 ± 1.04	15.37 ± 1.45	14.33 ± 1.10
FSI- SLI-10S			
Tip 1	9.63 ± 1.59	12.29 ± 2.33	6.57 ± 1.13
Tip 2	6.22 ± 0.63	6.37 ± 2.35	6.89 ± 0.32
Tip 3	6.96 ± 1.12	9.67 ± 2.26	11.20 ± 0.72
Tip 4	9.07 ± 0.78	8.27 ± 0.81	10.36 ± 1.13
Tip 5	7.30 ± 0.57	9.10 ± 1.34	6.50 ± 1.09

Table 6.7 Mean displacement amplitude data (measured in micrometres ± 1 standard deviation) for FSI-100, FSI-100 and FSI-SLI-10S scaler inserts with 1mm removed, under loaded and unloaded conditions.

	Mean Tip Displacement Amplitude (micrometres)		
Insert (Design / Number)	**Unloaded**	**0.5N Load**	**1.0N Load**
FSI-100			
Tip 1	13.78 ± 1.64	12.17 ± 1.24	8.91 ± 1.01
Tip 2	12.04 ± 2.51	8.24 ± 1.56	8.80 ± 0.64
Tip 3	9.41 ± 1.24	7.90 ± 1.06	7.26 ± 1.17
Tip 4	10.71 ± 2.61	10.75 ± 1.37	8.84 ± 1.57
Tip 5	8.69 ± 2.19	11.59 ± 3.98	13.10 ± 1.52
FSI-1000			
Tip 1	13.87 ± 1.88	12.77 ± 1.55	9.62 ± 0.95
Tip 2	14.48 ± 1.70	10.53 ± 1.75	10.13 ± 1.30
Tip 3	13.23 ± 1.75	12.62 ± 2.40	13.66 ± 0.48
Tip 4	13.02 ± 2.48	9.12 ± 0.99	12.02 ± 0.64
Tip 5	11.57 ± 2.54	10.34 ± 2.79	9.03 ± 1.05
FSI- SLI-10S			
Tip 1	5.98 ± 0.67	5.64 ± 0.92	5.98 ± 1.04
Tip 2	4.23 ± 0.46	4.19 ± 0.53	5.64 ± 0.94
Tip 3	5.98 ± 0.28	6.30 ± 0.93	5.39 ± 0.88
Tip 4	5.67 ± 0.86	5.16 ± 0.51	6.20 ± 0.98
Tip 5	5.58 ± 0.66	5.09 ± 0.62	5.06 ± 0.93

Table 6.8 Mean displacement amplitude data (measured in micrometres ± 1 standard deviation) for FSI-100, FSI-1000 and FSI-SLI-10S scaler inserts with 2mm removed, under loaded and unloaded conditions.

UNLOADED DATA				
Insert (Design / Number)	**Percentage decrease in tip displacement (1mm reduction)**	**Median decrease in tip displacement (1mm reduction)**	**Percentage decrease in tip displacement (2mm reduction)**	**Median decrease in tip displacement (2mm reduction)**
FSI-100 / 1	62%		37%	
FSI-100 / 2	63%		46%	
FSI-100 / 3	4%	58%	9%	44%
FSI-100 / 4	58%		44%	
FSI-100 / 5	43%		57%	
FSI-1000 / 1	6%		38%	
FSI-1000 / 2	23%		35%	
FSI-1000 / 3	26%	23%	39%	39%
FSI-1000 / 4	1%		40%	
FSI-1000 / 5	33%		61%	
FSI- SLI-10S / 1	23%		52%	
FSI- SLI-10S / 2	53%		68%	
FSI- SLI-10S / 3	51%	37%	58%	57%
FSI- SLI-10S / 4	31%		57%	
FSI- SLI-10S / 5	37%		52%	

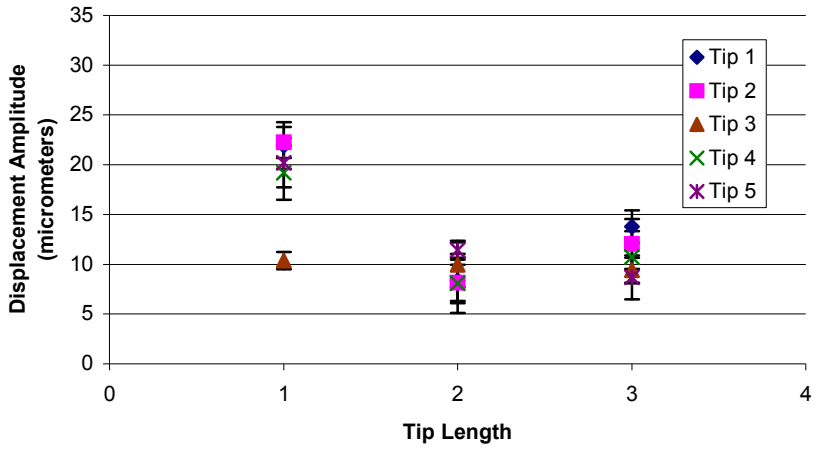
Table 6.9 The percentage decrease in the mean maximum tip displacement amplitude following a reduction in tip length of 1mm and 2mm for all tips under unloaded conditions. Also shown is the mean percentage decrease for each tip design.

LOADED DATA – 0.5N				
Insert (Design / Number)	**Percentage decrease in tip displacement (1mm reduction)**	**Median decrease in tip displacement (1mm reduction)**	**Percentage decrease in tip displacement (2mm reduction)**	**Median decrease in tip displacement (2mm reduction)**
FSI-100 / 1	5%		14%	
FSI-100 / 2	41%		55%	
FSI-100 / 3	-24%	5%	31%	31%
FSI-100 / 4	-17%		5%	
FSI-100 / 5	35%		33%	
FSI-1000 / 1	7%		21%	
FSI-1000 / 2	18%		37%	
FSI-1000 / 3	54%	14%	29%	37%
FSI-1000 / 4	11%		45%	
FSI-1000 / 5	14%		42%	
FSI- SLI-10S / 1	16%		61%	
FSI- SLI-10S / 2	33%		56%	
FSI- SLI-10S / 3	-28%	16%	16%	56%
FSI- SLI-10S / 4	29%		56%	
FSI- SLI-10S / 5	-3%		42%	

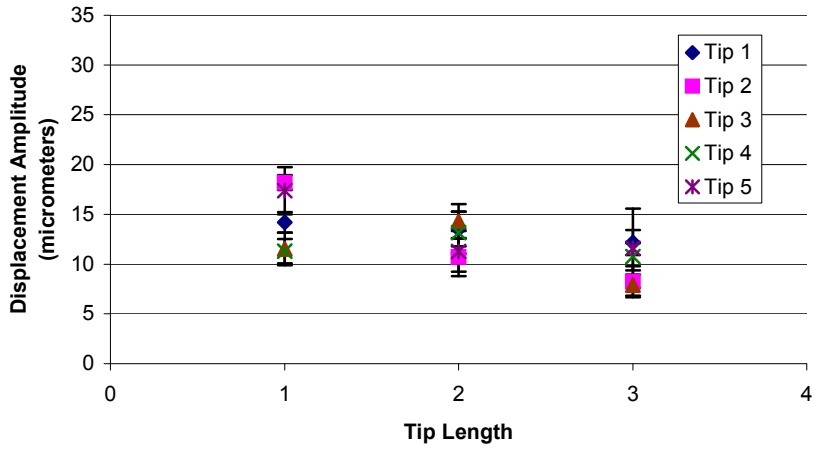
Table 6.10 The percentage decrease in the mean maximum tip displacement amplitude following a reduction in tip length of 1mm and 2mm for all tips under loaded conditions (0.5N). Also shown is the mean percentage decrease for each tip design. (Negative values indicate an increase in the mean maximum tip displacement amplitude).

LOADED DATA – 1.0N				
Insert (Design / Number)	**Percentage decrease in tip displacement (1mm reduction)**	**Median decrease in tip displacement (1mm reduction)**	**Percentage decrease in tip displacement (2mm reduction)**	**Median decrease in tip displacement (2mm reduction)**
FSI-100 / 1	20%	15%	38%	36%
FSI-100 / 2	11%		33%	
FSI-100 / 3	-33%		36%	
FSI-100 / 4	15%		37%	
FSI-100 / 5	22%		10%	
FSI-1000 / 1	43%	9%	52%	29%
FSI-1000 / 2	-6%		29%	
FSI-1000 / 3	53%		27%	
FSI-1000 / 4	-24%		15%	
FSI-1000 / 5	9%		43%	
FSI- SLI-10S / 1	40%	28%	45%	44%
FSI- SLI-10S / 2	32%		45%	
FSI- SLI-10S / 3	-79%		14%	
FSI- SLI-10S / 4	-10%		34%	
FSI- SLI-10S / 5	28%		44%	

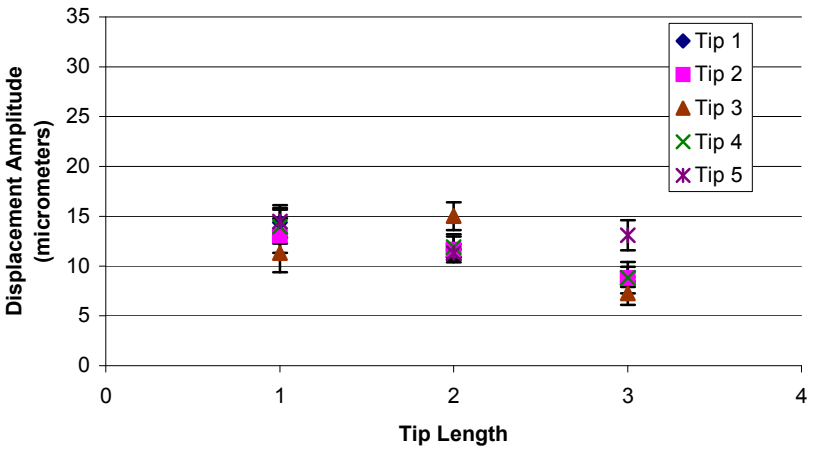
Table 6.11 The percentage decrease in the mean maximum tip displacement amplitude following a reduction in tip length of 1mm and 2mm for all tips under loaded conditions (1.0N). Also shown is the mean percentage decrease for each tip design. (Negative values indicate an increase in the mean maximum tip displacement amplitude).



a)

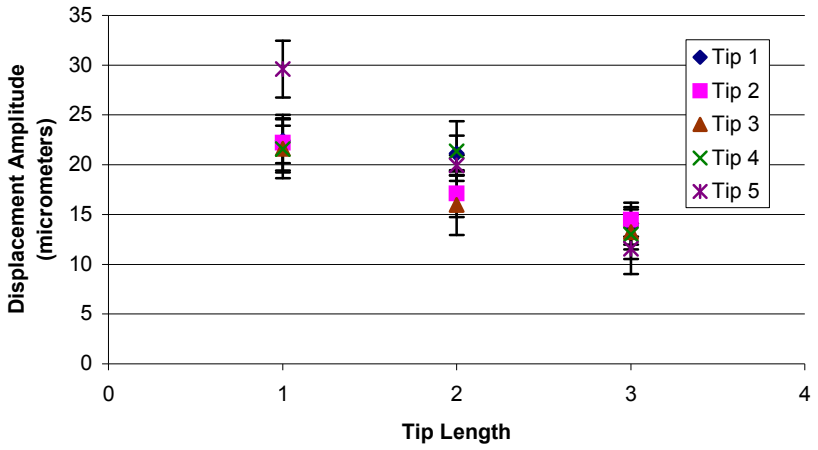


b)

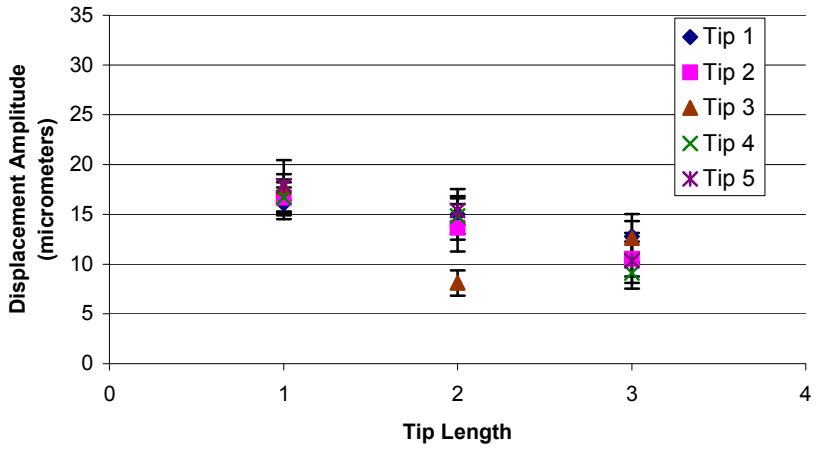


c)

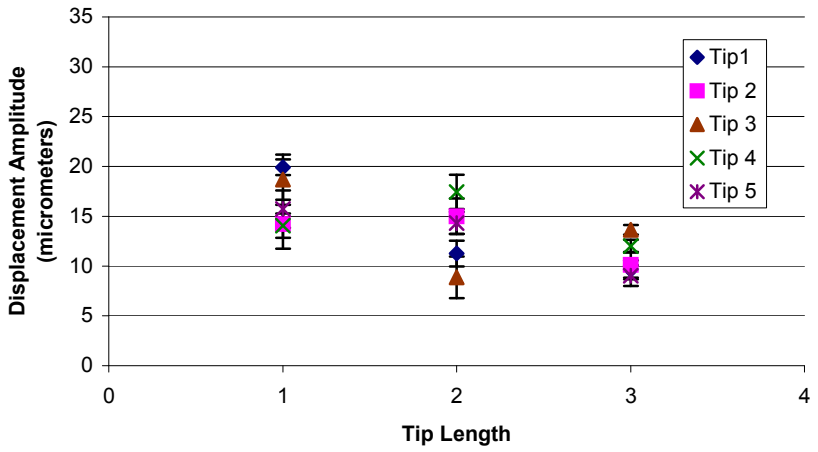
Figure 6.8 Displacement amplitude data for individual FSI-100 inserts under a) unloaded conditions b) 0.5N load and c) 1.0N load.



a)

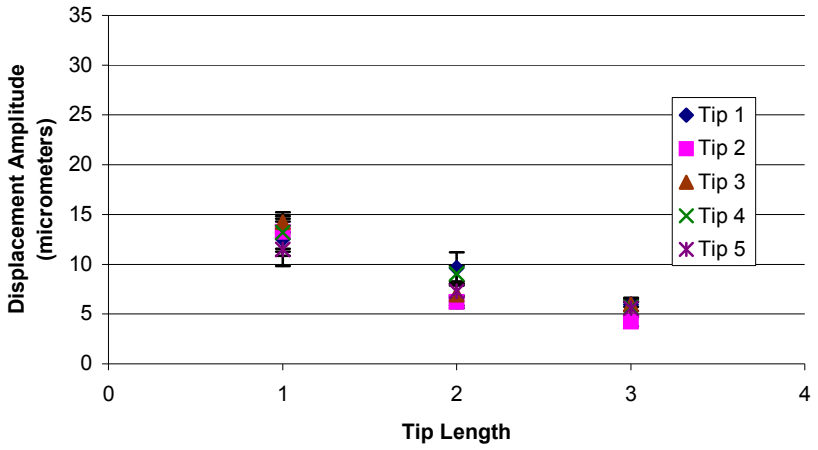


b)

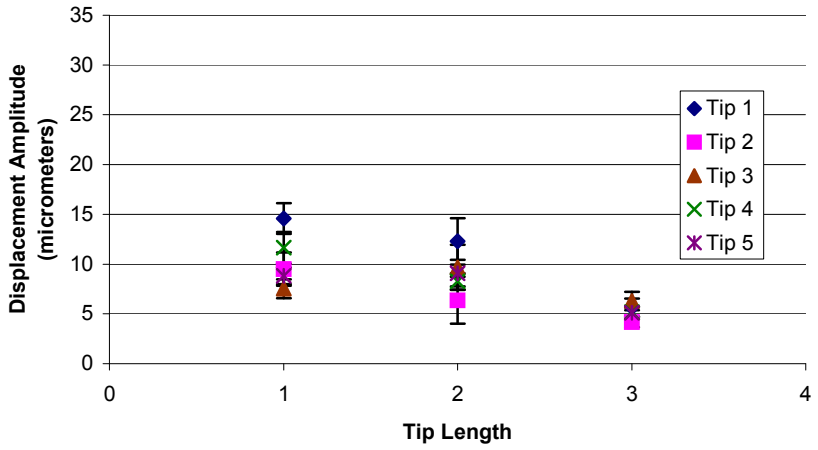


c)

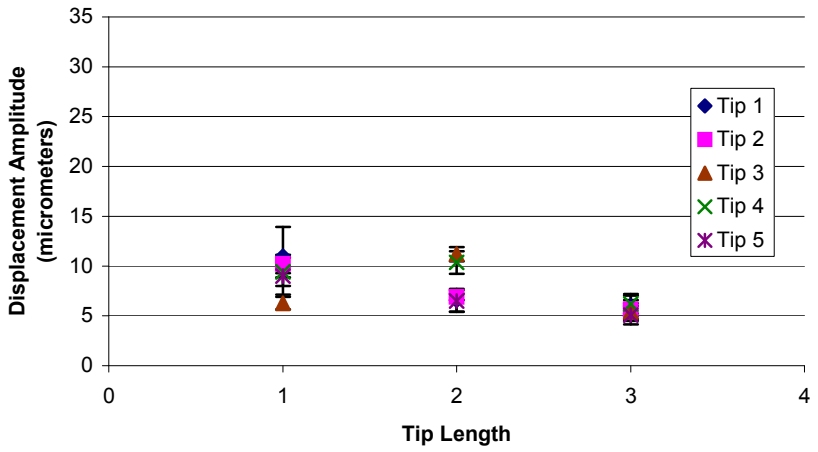
Figure 6.9 Displacement amplitude data for individual FSI-1000 inserts under a) unloaded conditions b) 0.5N load and c) 1.0N load.



a)



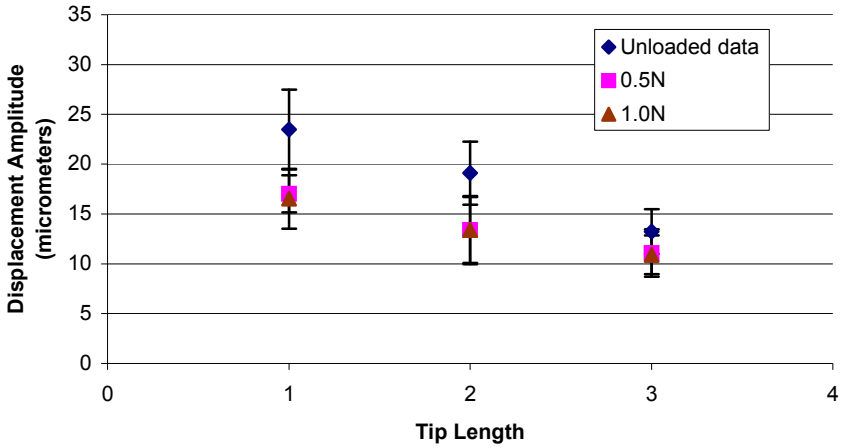
b)



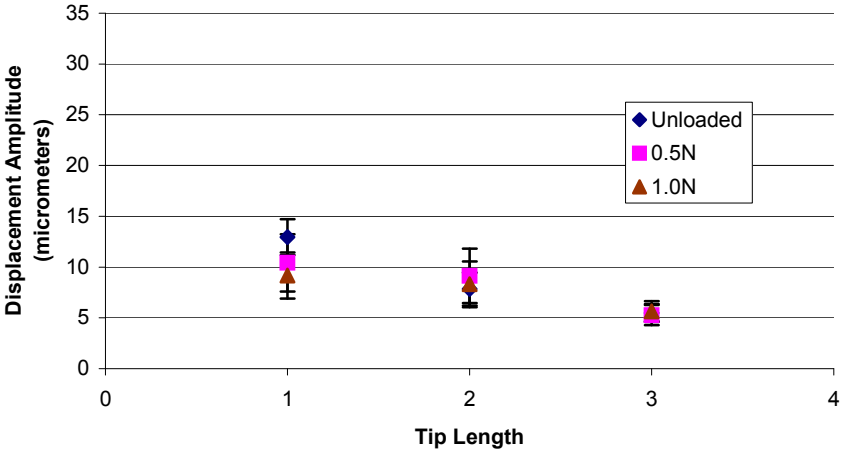
c)

Figure 6.10 Displacement amplitude data for individual FSI-SLI-10S inserts under a) unloaded conditions b) 0.5N load and c) 1.0N load.

a) **Error! Objects cannot be created from editing field codes.**



b)



c)

Figure 6.11 Combined displacement amplitude data for a) all FSI-100 inserts, b) all FSI-1000 inserts and c) all FSI-SLI-10S 'Slimline' inserts.

6.7.1 Statistical Analysis

Data were analysed using SPSS v10.0. The significance of variation in tip displacement amplitude, for different tip lengths under various load conditions, was tested using univariate analysis of variance (General Linear Model) and using multiple post-hoc comparisons (Tukey test) at a significance level of $p<0.05$, with displacement amplitude as the dependent variable. For all tips, load and length were found to be significant variables ($p<0.0001$).

6.7.1.1 FSI-100 Tips

General tip comparisons

For all load and tip length conditions, tip 3 was significantly different from all other tips ($p<0.0001$). There were no significant differences between tips 1 and 2 ($p>0.13$), tips 1 and 5 ($p>0.99$), tips 2 and 4 ($p>0.21$) and tips 2 and 5 ($p=0.07$). All other tips were significantly different to each other ($p<0.0001$).

Effect of tip length

1mm wear

Under unloaded conditions, a reduction in tip length of 1mm produced a significant difference in the vibration displacement amplitude, for all tips ($p<0.0001$) except tip 3 ($p>0.83$). Under a load of 0.5N, a reduction in tip length of 1mm produced a significant difference in the vibration displacement amplitude, for all tips ($p<0.04$) except tip 1 ($p>0.52$). Under a load of 1.0N, a reduction in tip length of 1mm produced a significant difference in the vibration displacement amplitude, for all tips ($p<0.02$) except tip 2 ($p>0.06$).

2mm wear

Under unloaded conditions, a reduction in tip length of 2mm produced a significant difference in the vibration displacement amplitude, for all tips ($p<0.0001$) except tip 3 ($p>0.36$). Under a load of 0.5N, a reduction in tip length of 2mm produced a significant difference in the vibration displacement amplitude, for all tips ($p<0.007$) except tip 4 ($p>0.72$). Under a load of

1.0N, a reduction in tip length of 2mm produced a significant difference in the vibration displacement amplitude, for all tips ($p<0.0001$) except tip 5 ($p>0.06$).

6.7.1.2 FSI-1000 Tips

General tip comparisons

For all load and tip length conditions there were no significant differences between tips 1 and 4 ($p>0.95$), tips 1 and 5 ($p>0.96$), tips 2 and 3 ($p>0.67$), tips 2 and 4 ($p=0.14$) and tips 4 and 5 ($p>0.64$). All other tips were significantly different to each other ($p<0.02$).

Effect of tip length

1mm wear

Under unloaded conditions, a reduction in tip length of 1mm produced a significant difference in the vibration displacement amplitude for tips 2, 3 and 5 ($p<0.0001$). No significant difference was observed for tip 1 ($p>0.34$) and tip 4 ($p>0.98$). Under a load of 0.5N, a reduction in tip length of 1mm produced a significant difference in the vibration displacement amplitude for tips 2, 3 and 4 ($p<0.04$). No significant difference was observed for tip 1 ($p>0.41$) and tip 5 ($p=0.06$). Under a load of 1.0N, a reduction in tip length of 1mm produced a significant difference in the vibration displacement amplitude for tips 1, 3 and 4 ($p<0.0001$). No significant difference was observed for tip 2 ($p>0.62$) and tip 5 ($p=0.08$).

2mm wear

Under unloaded conditions, a reduction in tip length of 2mm produced a significant difference in the vibration displacement amplitude, for all tips ($p<0.0001$). Under a load of 0.5N, a reduction in tip length of 2mm produced a significant difference in the vibration displacement amplitude, for all tips ($p<0.002$). Under a load of 1.0N, a reduction in tip length of 2mm

produced a significant difference in the vibration displacement amplitude, for all tips ($p<0.004$).

6.7.1.3 FSI-SLI-10S Tips

General tip comparisons

For all load and tip length conditions, all tips were significantly different to each other ($p<0.02$) except for tips 2 and 5 ($p>0.91$).

Effect of tip length

1mm wear

Under unloaded conditions, a reduction in tip length of 1mm produced a significant difference in the vibration displacement amplitude for all tips ($p<0.0001$). Under a load of 0.5N, a reduction in tip length of 1mm produced a significant difference in the vibration displacement amplitude for all tips ($p<0.02$) except tip 5 ($p>0.79$). Under a load of 1.0N, a reduction in tip length of 1mm produced a significant difference in the vibration displacement amplitude for all tips ($p<0.001$) except tip 4 ($p>0.06$).

2mm wear

Under unloaded conditions, a reduction in tip length of 2mm produced a significant difference in the vibration displacement amplitude, for all tips ($p<0.0001$). Under a load of 0.5N, a reduction in tip length of 2mm produced a significant difference in the vibration displacement amplitude, for all tips ($p<0.0001$) except tip 3 ($p>0.18$). Under a load of 1.0N, a reduction in

tip length of 2mm produced a significant difference in the vibration displacement amplitude, for all tips ($p<0.04$).

6.8 Single-Scan Multi-Axial Assessment of Scaler Tip Vibrations

Measurement points were positioned over the video images of the front and side aspects of the scaler tip and 10 repeat scans performed to enable the displacement amplitude of the longitudinal and lateral axes of vibration to be determined. The mean displacement amplitude for each axis was calculated and plotted as a function of phase angle, recorded by the SLV system (Figure 6.12). The data are plotted as a 2D graph with the x-axis representing the longitudinal displacement amplitude and the y-axis representing the lateral displacement amplitude.

Data were then obtained from scan points positioned along the length of the front and side aspect of the tip. For each scan point, the longitudinal and lateral displacement amplitudes were plotted as a function of phase angle (Figure 6.13). Since a greater amount of data was generated in this part of the investigation, the data were plotted using a 3D spreadsheet package to aid clarity.

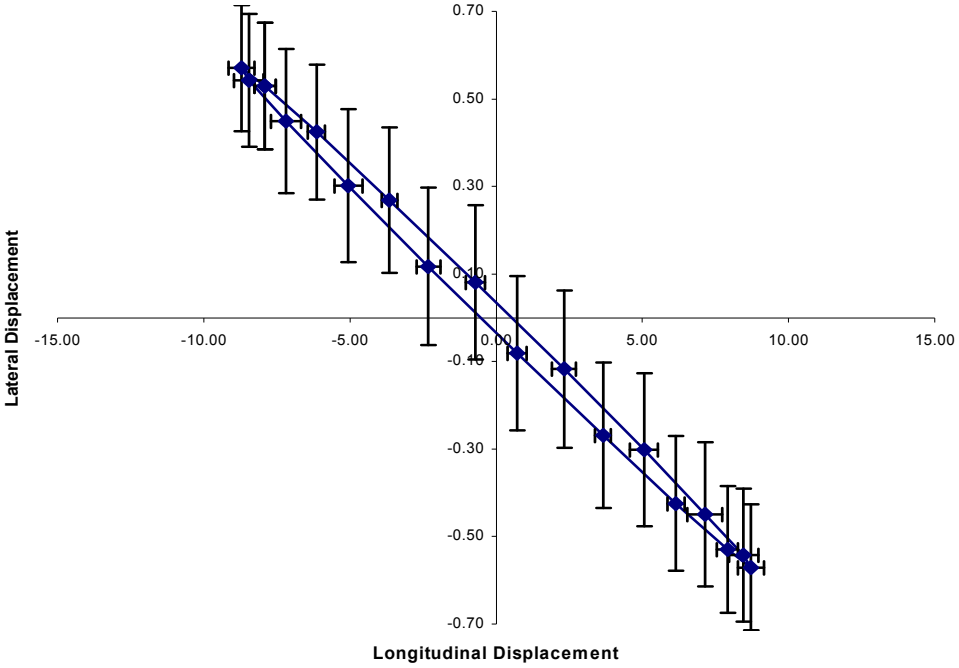


Figure 6.12 2-D graphical representation of the mean phase related longitudinal and lateral vibrations occurring at the unconstrained end of the tip. Displacement amplitudes are measured in micrometers.

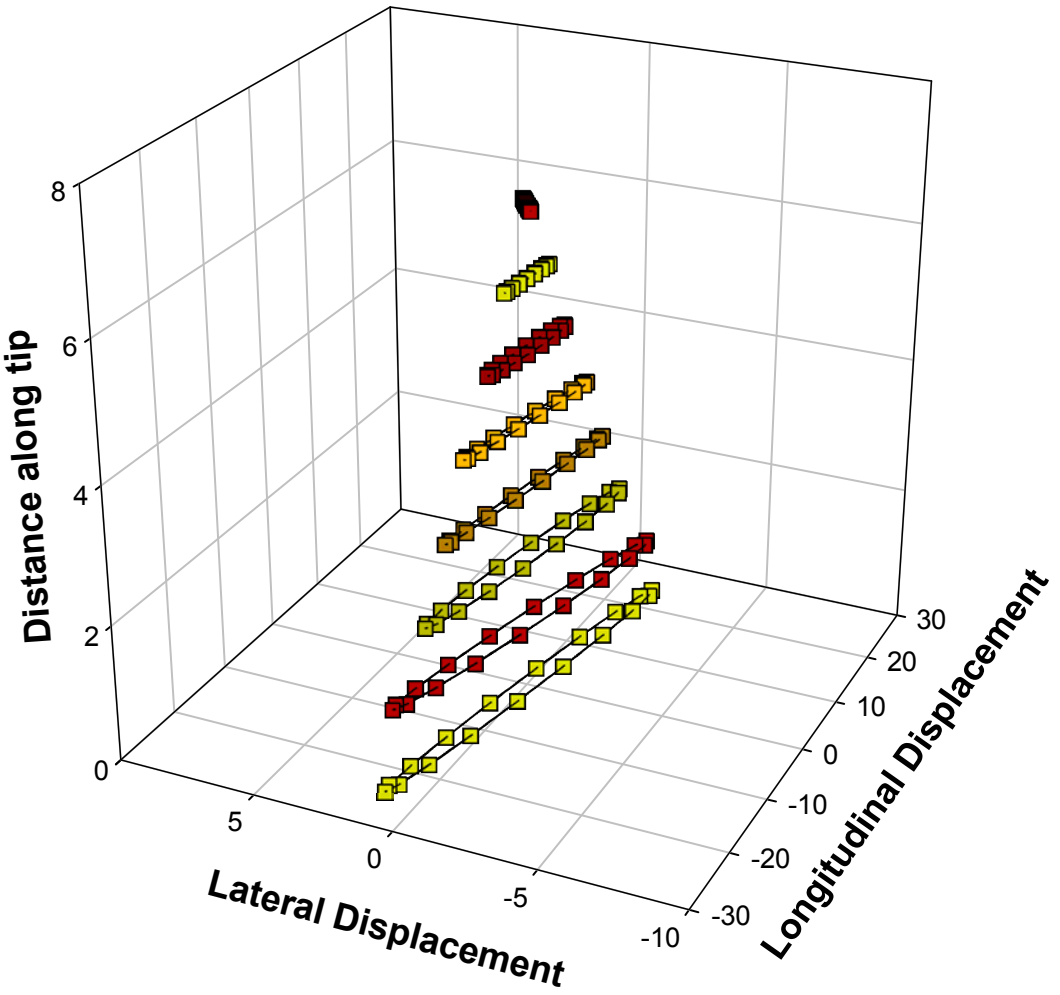


Figure 6.13 3-Dimensional representation recorded for scaler tip vibration pattern, which clearly depicts a small but definite elliptical motion of the instrument. Displacement amplitudes are measured in micrometers.

6.9 The Vibration Patterns of Powered Toothbrushes

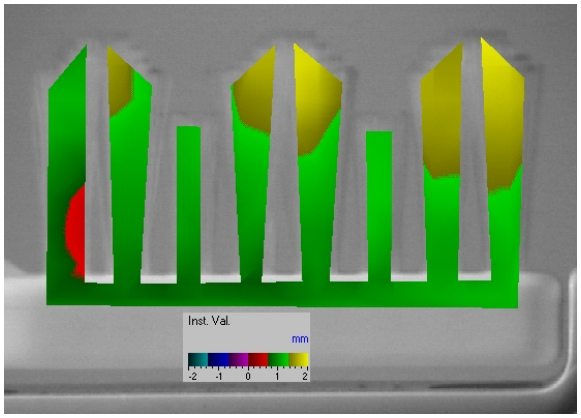
6.9.1 Microphone / Inductance Coil Comparison

Fifty SLV scans were performed, for each method of reference signal generation. This was to determine whether there was a significant difference in the measured displacement amplitudes of the toothbrush bristles, when using the two different types of reference signal. Using the coil as a reference signal, a mean displacement amplitude of 2.91 ± 0.06 mm at the bristle tips was obtained whilst with the microphone as a reference signal, the mean displacement amplitude was 2.91 ± 0.07 mm at the bristle tips. Data, analysed using t-test, showed there was no significant difference between displacement amplitude measurements performed using the two different methods of generating a reference signal ($p = 0.8$). For both reference signals, the fundamental frequency of oscillation of the Sonicare toothbrush was 262.5Hz.

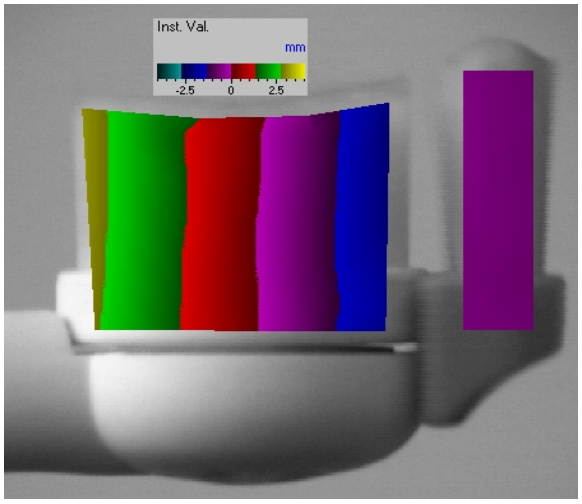
6.9.2 Toothbrush area scans

Area scans for the Sonicare, Philips Sensiflex HX2520, Braun 3D and Braun D8 were performed and the data displayed as colour maps (Figure 6.14) and as 3D-meshs (Figures 6.15 & 6.16). Colour map images obtained for the Braun D8 and Braun 3D were similar and so only a Braun D8 colour map image is shown. The colour map facility enables acquired data to be superimposed over a captured video image of the target object. A colour-graduated scale enables points of maximum/minimum vibration to be easily identified and readily located on the toothbrush area being assessed. The maximum displacement amplitudes (found at the longest bristle tips) and the fundamental frequencies of oscillation, for each of the toothbrushes, are shown in Table 6.12.

a)



b)



c)

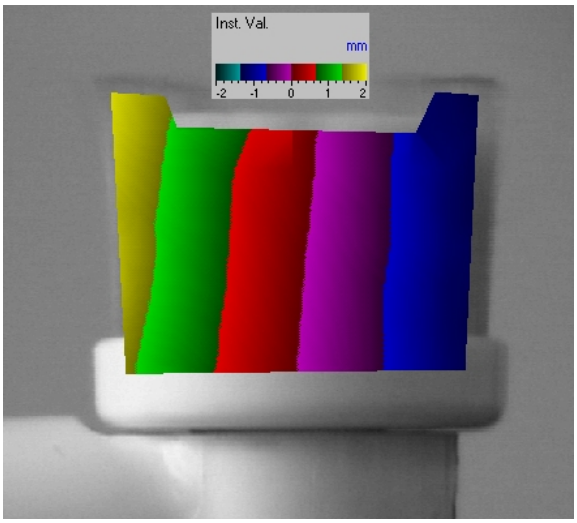


Figure 6.14 Colour map images of various powered toothbrushes, including a) Sonicare, b) Philips Sensiflex and c) Braun D8.

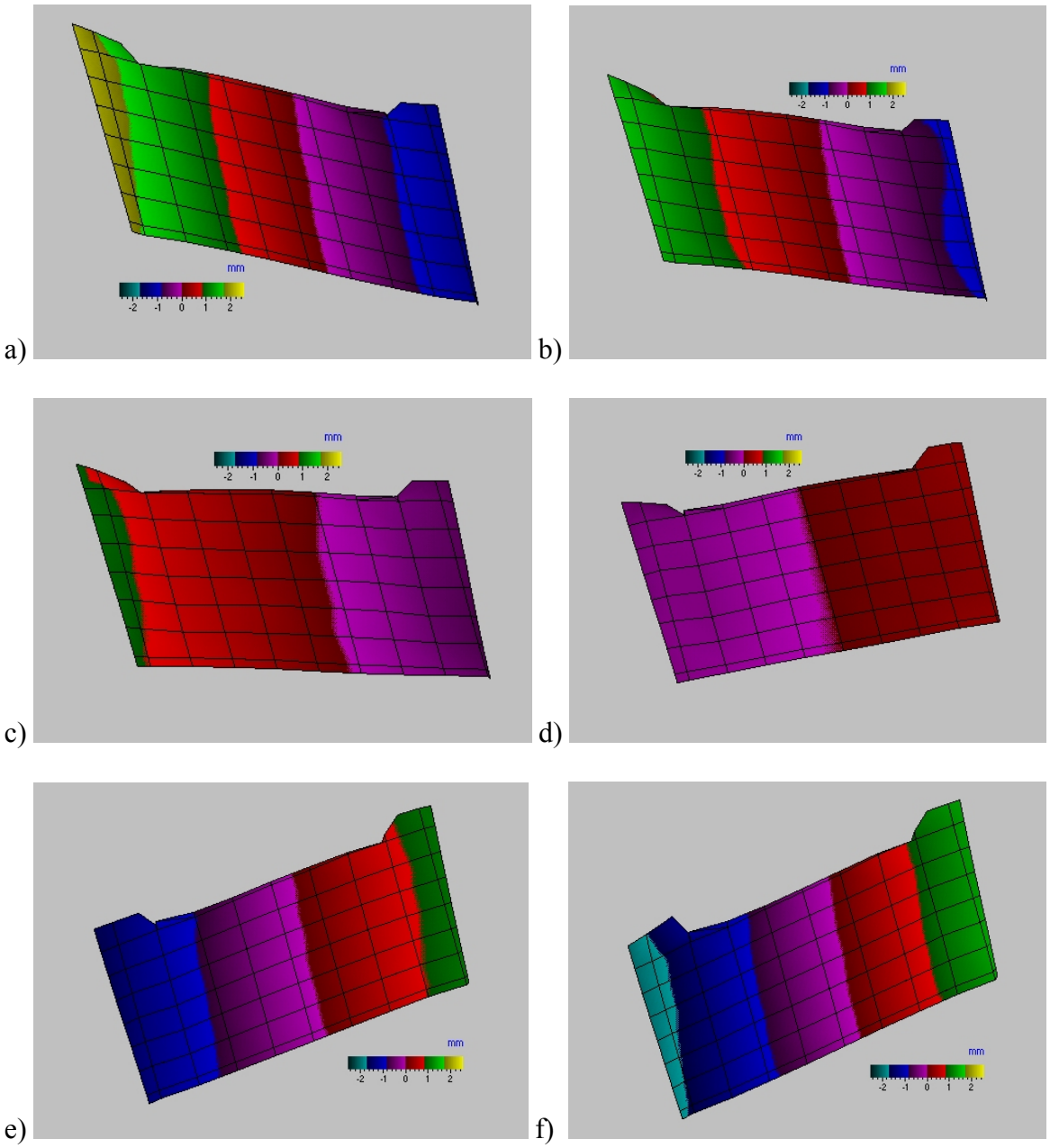


Figure 6.15 Stills from Braun 3D vibration data that has been animated as a 3D-mesh. These images demonstrate the typical counter-rotary motion of many powered toothbrushes, including the Braun D8 and Philips Sensiflex.

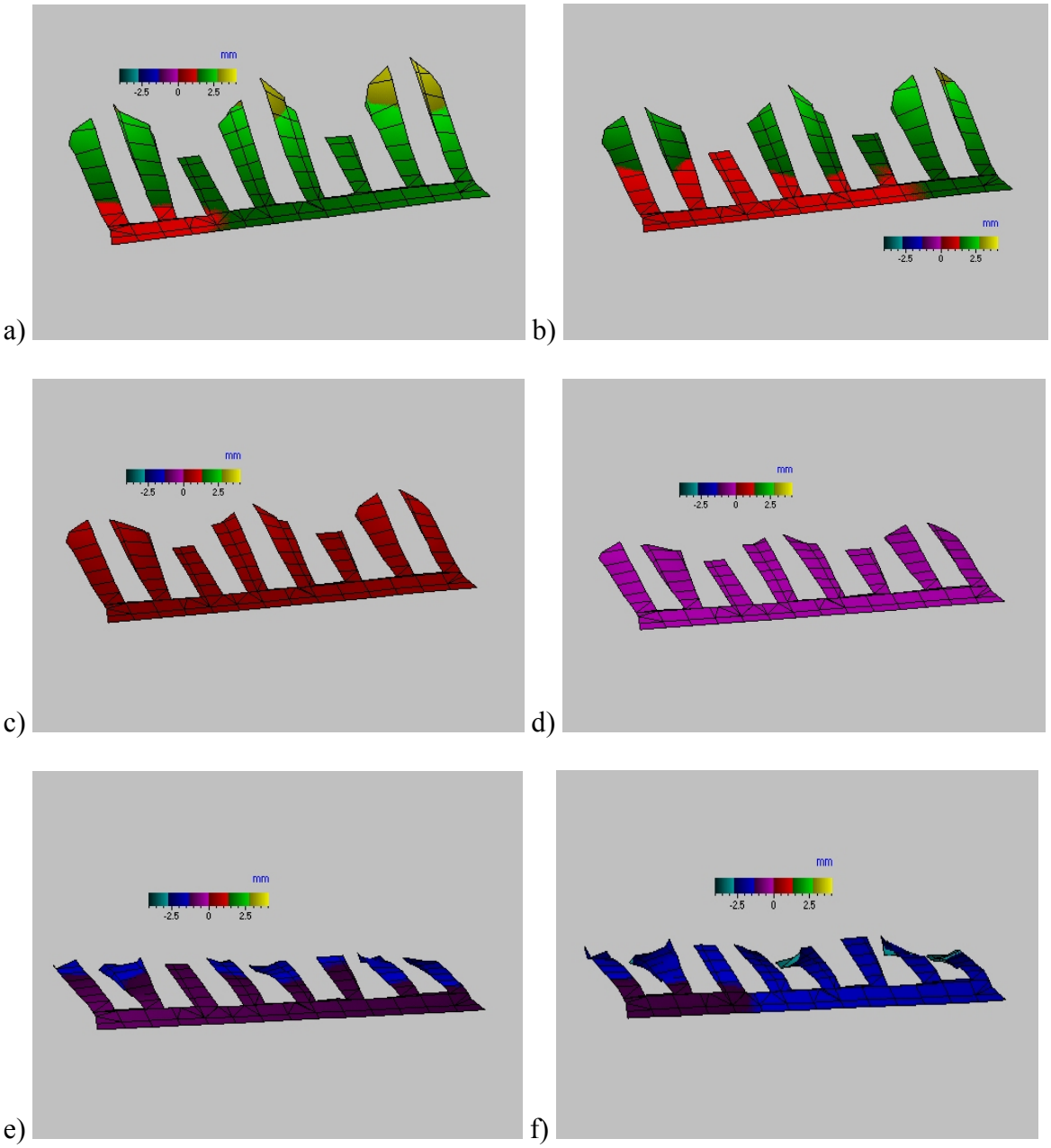


Figure 6.16 Stills from Sonicare vibration data that has been animated as a 3D-mesh. These images demonstrate the side-to-side motion of the powered toothbrush.

Powered toothbrush	Displacement Amplitude (at bristle tips) / mm	Fundamental oscillation frequency (Hz)
Sonicare	2.51 ± 0.18	262.5
Philips Sensiflex HX2520	2.60 ± 0.15	62.5
Braun 3D	2.14 ± 0.18	75.0
Braun D8	2.14 ± 0.21	62.5

Table 6.12 The fundamental frequency (Hz) and maximum displacement amplitude (± 1 standard deviation) of bristle tip vibration (mm) for some commonly available powered toothbrushes, assessed with the SLV.

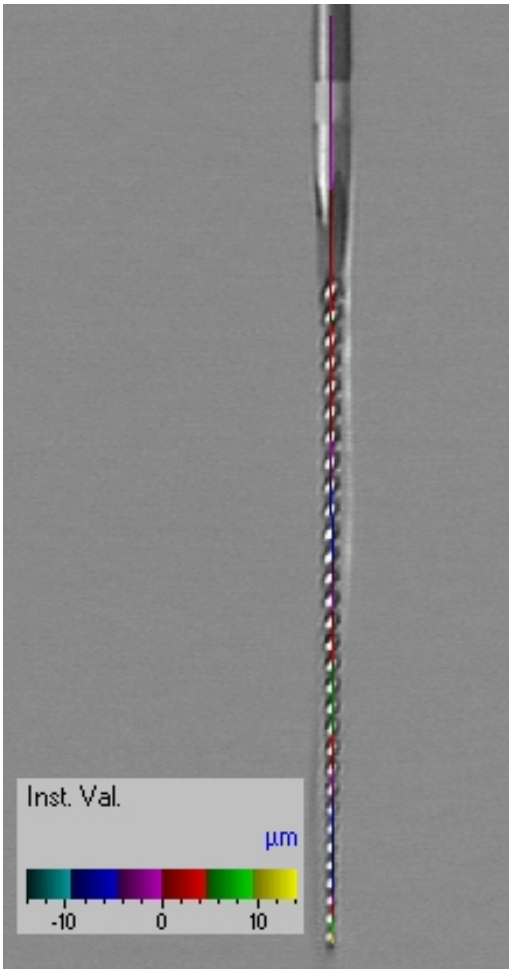
6.10 The Vibration Patterns of Endosonic K-Files

Vibration data of endosonic K-files may be displayed as both a colour map (Figure 6.17) or as a 3D-mesh (Figure 6.18). The fundamental vibration frequency for both the #15 file and #35 K-files, detected by the laser vibrometer, was found to be 27.50kHz. Displacement amplitude data for each file, at all power settings, was exported from the SLV software as an ASCII file, to Excel. This enabled the mean displacement amplitude at each measurement point along the length of the file, for all power settings, to be calculated and plotted as a function of position along the file (Figure 6.19). The maximum displacement amplitude for both files occurred at the free, unconstrained end of the file (Tables 6.13 & 6.14). For both files, the mean displacement amplitude at this point, for all generator power settings (Table 8.15), was plotted as a function of generator power setting (Figure 8.20).

6.10.1 Statistical Analysis

To determine whether generator power setting had a significant effect on the mean maximum file vibration displacement amplitude, data from the scan point located at the unconstrained end of the file were tested using univariate analysis of variance (General Linear Model). Multiple post-hoc comparisons (Tukey test) were used at a significance level of $p<0.05$, with the dependent variable being file displacement amplitude.

Analysis of vibration data from the unconstrained end of both files showed that, for the #15 file, power setting 5 was significantly different from all other power settings ($p<0.04$) except power setting 2 ($p>0.19$). No significant differences were observed between any of the other power settings ($p>0.13$). For the #35 file, all power settings were significantly different to each other ($p<0.0001$).

a) 

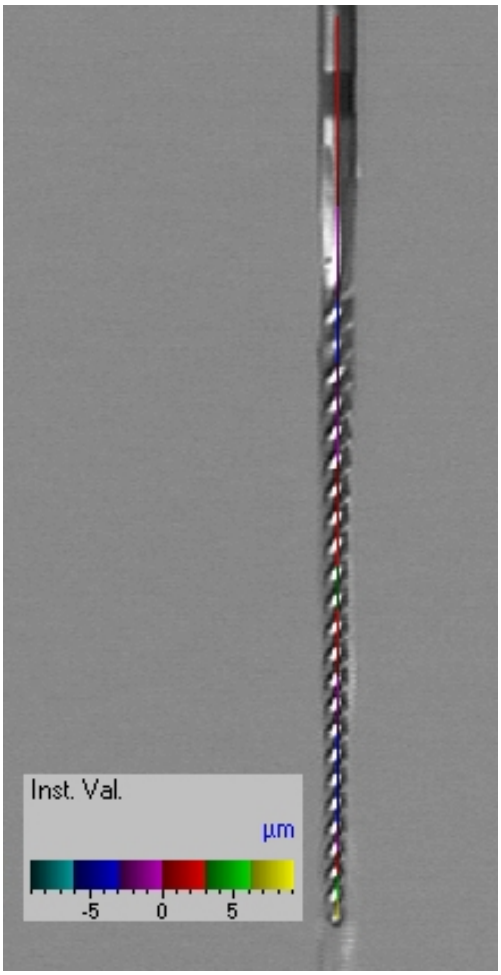
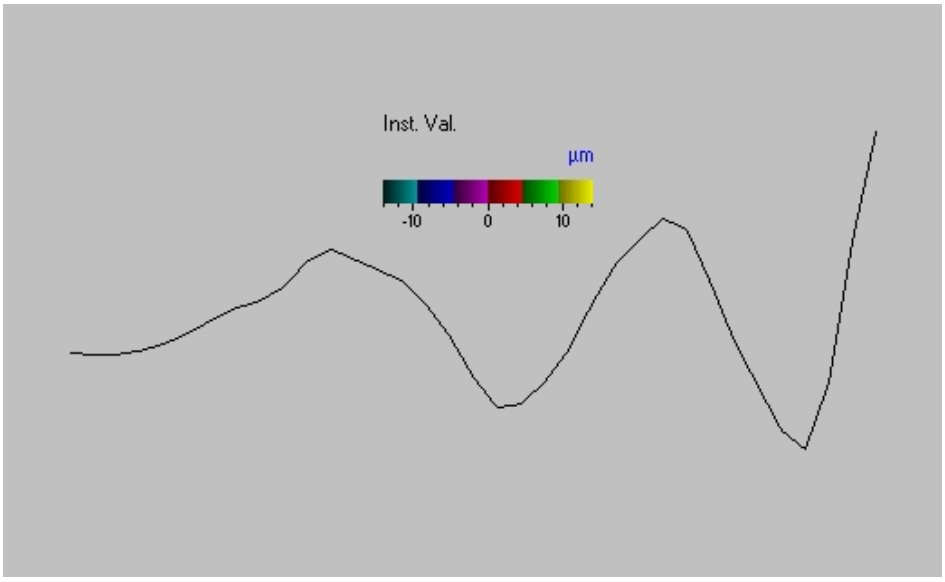
b) 

Figure 6.17 Colour map images of vibration data for a) #15 endosonic K-file and b) #35 endosonic K-file. Vibration data was acquired from the full length of each file.

a)



b)

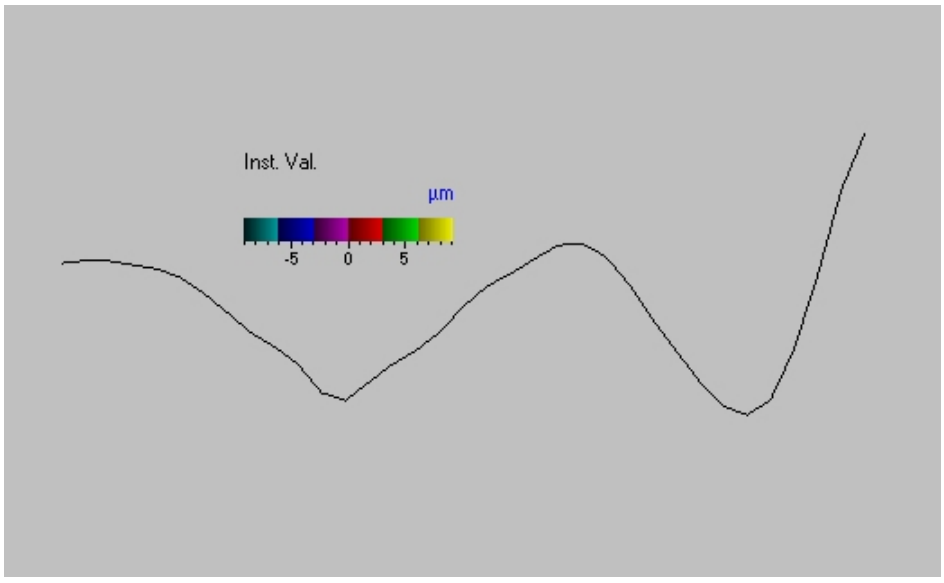


Figure 6.18 K-file vibration data displayed as a 3D-mesh for a) #15 K-file and b) #35 K-file. Analysis of data by this method demonstrates a distinct difference in the vibration characteristics between the two file sizes. The #15 K-file has 6 antinodes, whereas the thicker #35 K-file has 5.

	Displacement Amplitude (micrometers)				
Scan Point	**Power 1**	**Power 2**	**Power 3**	**Power 4**	**Power 5**
1	-2.43 ± 0.31	-2.07 ± 0.38	-2.01 ± 0.60	-2.51 ± 0.12	-2.17 ± 0.31
2	-2.53 ± 0.25	-2.14 ± 0.41	-2.06 ± 0.61	-2.53 ± 0.24	-2.22 ± 0.29
3	-2.53 ± 0.19	-2.13 ± 0.41	-2.10 ± 0.57	-2.43 ± 0.33	-2.19 ± 0.27
4	-2.28 ± 0.17	-1.93 ± 0.36	-2.01 ± 0.49	-2.21 ± 0.26	-1.97 ± 0.24
5	-1.80 ± 0.13	-1.53 ± 0.28	-1.63 ± 0.39	-1.81 ± 0.11	-1.53 ± 0.23
6	-1.12 ± 0.09	-0.95 ± 0.17	-0.99 ± 0.24	-1.13 ± 0.07	-0.91 ± 0.15
7	-0.26 ± 0.02	-0.22 ± 0.04	-0.23 ± 0.05	-0.25 ± 0.03	-0.16 ± 0.06
8	0.49 ± 0.06	0.44 ± 0.06	0.44 ± 0.11	0.51 ± 0.06	0.48 ± 0.06
9	0.97 ± 0.07	0.84 ± 0.11	0.88 ± 0.20	0.96 ± 0.09	0.83 ± 0.11
10	1.95 ± 0.05	1.65 ± 0.22	1.69 ± 0.43	1.83 ± 0.22	1.68 ± 0.27
11	3.65 ± 0.08	3.13 ± 0.41	3.05 ± 0.87	3.45 ± 0.48	3.31 ± 0.55
12	4.42 ± 0.11	3.76 ± 0.49	3.72 ± 1.04	4.25 ± 0.49	4.10 ± 0.69
13	3.67 ± 0.09	3.08 ± 0.43	3.09 ± 0.88	3.60 ± 0.30	3.37 ± 0.57
14	2.96 ± 0.13	2.50 ± 0.36	2.38 ± 0.76	2.90 ± 0.21	2.50 ± 0.47
15	2.29 ± 0.10	1.96 ± 0.27	1.83 ± 0.57	2.19 ± 0.21	1.80 ± 0.35
16	0.75 ± 0.03	0.64 ± 0.08	0.62 ± 0.18	0.66 ± 0.14	0.49 ± 0.13
17	-1.40 ± 0.08	-1.22 ± 0.20	-1.16 ± 0.45	-1.53 ± 0.14	-1.44 ± 0.18
18	-4.15 ± 0.15	-3.62 ± 0.54	-3.44 ± 1.14	-4.37 ± 0.20	-3.95 ± 0.53
19	-6.27 ± 0.12	-5.51 ± 0.73	-5.15 ± 1.57	-6.29 ± 0.45	-5.62 ± 0.95
20	-6.03 ± 0.12	-5.40 ± 0.67	-4.87 ± 1.53	-5.80 ± 0.73	-4.96 ± 0.98
21	-4.47 ± 0.12	-3.99 ± 0.50	-3.59 ± 1.21	-4.25 ± 0.62	-3.35 ± 0.73
22	-2.33 ± 0.06	-1.92 ± 0.27	-1.94 ± 0.61	-2.20 ± 0.25	-1.71 ± 0.40
23	0.98 ± 0.07	0.88 ± 0.09	0.57 ± 0.28	0.71 ± 0.30	0.56 ± 0.12
24	4.17 ± 0.36	3.33 ± 0.36	2.82 ± 0.98	3.00 ± 0.86	2.54 ± 0.31
25	5.99 ± 0.56	4.78 ± 0.52	4.38 ± 1.20	4.47 ± 1.04	3.85 ± 0.47
26	7.04 ± 0.37	5.76 ± 0.71	5.81 ± 1.40	5.94 ± 0.90	5.35 ± 0.82
27	6.05 ± 0.34	4.91 ± 0.67	5.09 ± 1.32	5.20 ± 0.74	5.09 ± 0.84
28	2.27 ± 0.22	1.76 ± 0.25	1.77 ± 0.54	1.82 ± 0.32	1.98 ± 0.37
29	-1.92 ± 0.09	-1.59 ± 0.23	-1.90 ± 0.43	-1.97 ± 0.11	-1.99 ± 0.24
30	-5.04 ± 0.29	-3.97 ± 0.66	-5.15 ± 1.17	-5.18 ± 0.50	-5.51 ± 0.77
31	-7.72 ± 0.37	-6.29 ± 1.11	-7.85 ± 1.82	-8.05 ± 0.62	-8.30 ± 1.25
32	-8.62 ± 0.37	-7.53 ± 1.26	-8.35 ± 2.03	-9.01 ± 0.82	-8.75 ± 1.42
33	-4.25 ± 0.21	-3.88 ± 0.63	-4.04 ± 0.99	-4.42 ± 0.62	-4.02 ± 0.75
34	5.36 ± 0.15	4.56 ± 0.63	4.84 ± 1.14	5.12 ± 0.45	4.16 ± 0.83
35	13.44 ± 0.38	11.50 ± 1.58	12.11 ± 2.79	12.63 ± 1.32	9.71 ± 2.05

Table 6.13 Mean displacement amplitude (± 1 standard deviation) along the length of a #15 K-file for various generator power settings. Scan point 1 is the point located nearest the file driver and point 35 is located at the free, unconstrained end of the file.

	Displacement Amplitude (micrometers)				
Scan Point	**Power 1**	**Power 2**	**Power 3**	**Power 4**	**Power 5**
1	1.04 ± 0.13	2.38 ± 0.19	4.15 ± 0.08	1.31 ± 0.23	3.25 ± 0.26
2	1.09 ± 0.10	2.47 ± 0.18	4.47 ± 0.07	1.43 ± 0.21	3.58 ± 0.30
3	1.10 ± 0.09	2.49 ± 0.16	4.52 ± 0.11	1.46 ± 0.17	3.56 ± 0.29
4	1.01 ± 0.10	2.36 ± 0.15	4.21 ± 0.15	1.33 ± 0.17	3.08 ± 0.21
5	0.87 ± 0.11	2.13 ± 0.14	3.95 ± 0.13	1.28 ± 0.22	2.68 ± 0.13
6	0.65 ± 0.11	1.65 ± 0.10	3.23 ± 0.08	1.08 ± 0.17	2.03 ± 0.16
7	0.39 ± 0.08	0.94 ± 0.06	1.90 ± 0.04	0.64 ± 0.10	0.97 ± 0.16
8	0.07 ± 0.04	0.10 ± 0.05	0.37 ± 0.01	0.17 ± 0.03	-0.13 ± 0.05
9	-0.33 ± 0.04	-0.82 ± 0.08	-1.22 ± 0.05	-0.27 ± 0.06	-1.19 ± 0.10
10	-0.64 ± 0.04	-1.56 ± 0.09	-2.79 ± 0.05	-0.80 ± 0.13	-2.26 ± 0.17
11	-0.98 ± 0.07	-2.37 ± 0.12	-4.63 ± 0.04	-1.51 ± 0.22	-3.52 ± 0.30
12	-1.36 ± 0.08	-3.42 ± 0.16	-6.62 ± 0.09	-2.07 ± 0.26	-4.98 ± 0.35
13	-1.36 ± 0.06	-3.61 ± 0.27	-7.15 ± 0.12	-1.95 ± 0.22	-5.46 ± 0.36
14	-1.11 ± 0.06	-2.86 ± 0.22	-5.73 ± 0.12	-1.28 ± 0.18	-4.33 ± 0.22
15	-0.86 ± 0.07	-2.15 ± 0.23	-4.22 ± 0.11	-0.92 ± 0.14	-2.89 ± 0.15
16	-0.57 ± 0.06	-1.51 ± 0.28	-3.17 ± 0.11	-0.87 ± 0.13	-1.87 ± 0.17
17	-0.25 ± 0.05	-0.66 ± 0.21	-1.52 ± 0.07	-0.50 ± 0.07	-0.71 ± 0.09
18	0.19 ± 0.04	0.44 ± 0.08	0.35 ± 0.03	0.11 ± 0.03	0.52 ± 0.07
19	0.57 ± 0.08	1.46 ± 0.14	1.81 ± 0.05	0.58 ± 0.09	1.56 ± 0.17
20	0.86 ± 0.22	2.27 ± 0.27	3.34 ± 0.12	0.85 ± 0.13	2.57 ± 0.29
21	1.05 ± 0.32	2.92 ± 0.29	5.40 ± 0.43	1.05 ± 0.18	3.42 ± 0.30
22	0.97 ± 0.21	3.26 ± 0.20	7.55 ± 0.75	1.28 ± 0.23	4.07 ± 0.33
23	0.90 ± 0.17	3.20 ± 0.17	7.95 ± 0.58	1.42 ± 0.22	4.33 ± 0.25
24	0.80 ± 0.18	2.57 ± 0.16	5.99 ± 0.21	1.26 ± 0.15	3.59 ± 0.29
25	0.44 ± 0.08	1.30 ± 0.09	2.99 ± 0.14	0.73 ± 0.08	1.80 ± 0.21
26	-0.06 ± 0.03	-0.17 ± 0.07	-0.02 ± 0.06	0.03 ± 0.04	-0.22 ± 0.11
27	-0.40 ± 0.11	-1.39 ± 0.24	-2.57 ± 0.21	-0.48 ± 0.08	-1.86 ± 0.12
28	-0.69 ± 0.28	-2.61 ± 0.39	-5.23 ± 0.31	-1.10 ± 0.15	-3.31 ± 0.13
29	-1.22 ± 0.42	-3.87 ± 0.43	-7.56 ± 0.42	-2.01 ± 0.21	-4.61 ± 0.45
30	-1.84 ± 0.30	-4.65 ± 0.43	-8.24 ± 0.36	-2.63 ± 0.37	-5.37 ± 0.65
31	-1.74 ± 0.14	-4.05 ± 0.29	-6.88 ± 0.18	-2.36 ± 0.42	-4.79 ± 0.54
32	-0.68 ± 0.10	-1.72 ± 0.12	-3.05 ± 0.12	-0.96 ± 0.19	-2.15 ± 0.20
33	0.71 ± 0.09	1.59 ± 0.16	3.11 ± 0.12	1.19 ± 0.17	2.10 ± 0.16
34	2.38 ± 0.20	5.52 ± 0.55	10.14 ± 0.18	3.59 ± 0.54	6.85 ± 0.50
35	3.65 ± 0.27	8.27 ± 0.95	14.55 ± 0.35	5.14 ± 0.86	9.86 ± 0.93

Table 6.14 Mean displacement amplitude (± 1 standard deviation) along the length of a #35 K-file for various generator power settings. Scan point 1 is the point located nearest the file driver and point 35 is located at the free, unconstrained end of the file.

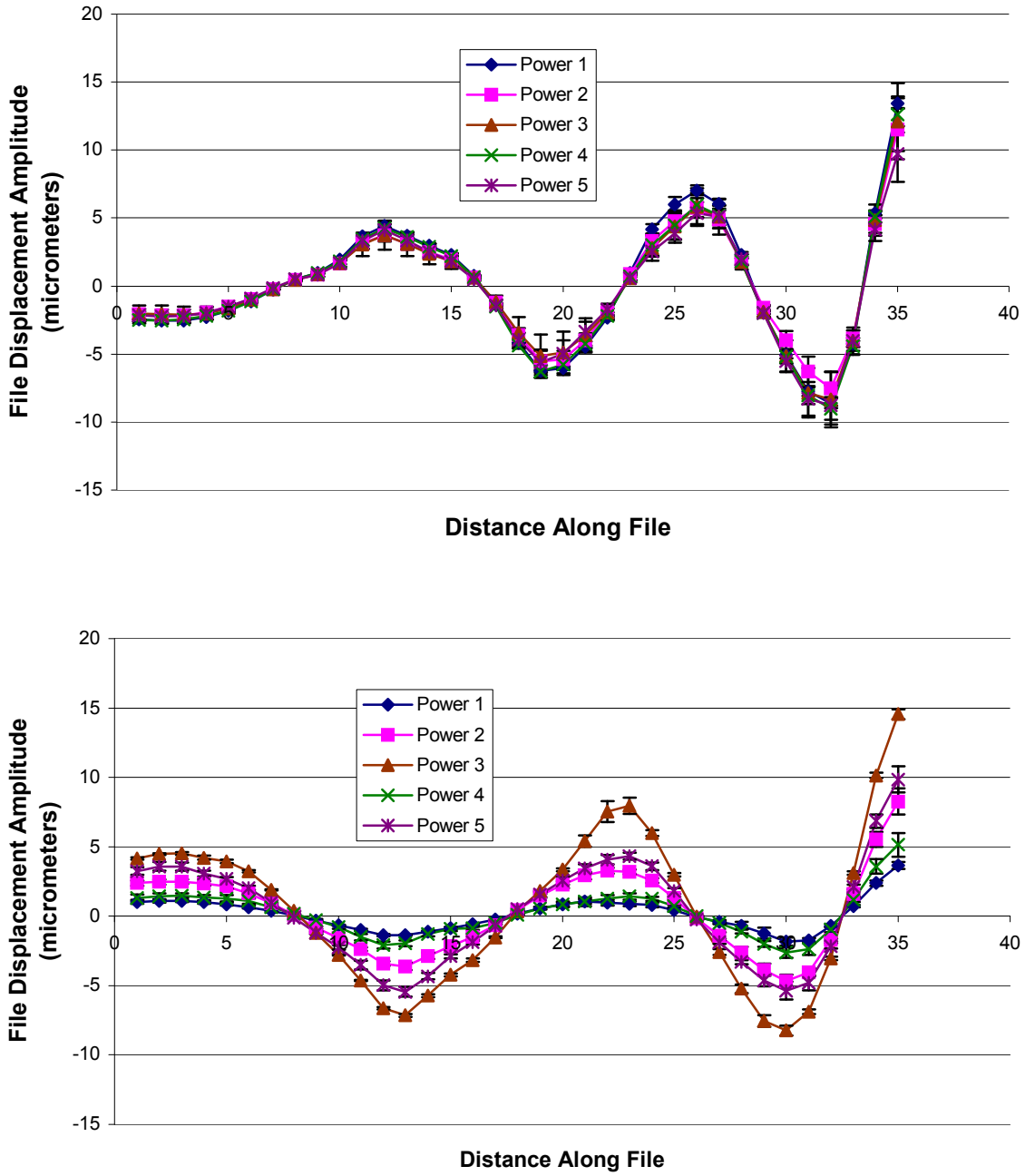


Figure 6.19 Mean file displacement amplitude as a function of position along the file length for a) #15 K-file and b) #35 K-file. Point 1 represents the position closest to the file driver and point 35 is at the free, unconstrained end of the file.

	Mean Maximum Displacement Amplitude (micrometers)				
	Power 1	**Power 2**	**Power 3**	**Power 4**	**Power 5**
#15 File	13.44 ± 0.38	11.50 ± 1.58	12.11 ± 2.79	12.63 ± 1.32	9.71 ± 2.05
#35 File	3.65 ± 0.27	8.27 ± 0.95	14.55 ± 0.35	5.14 ± 0.86	9.86 ± 0.93

Table 6.15 Mean maximum displacement amplitude (± 1 standard deviation) of the #15 and #35 K-file for generator power settings 1 to 5. Data obtained from the free, unconstrained end of the file is the mean of ten repeat readings.

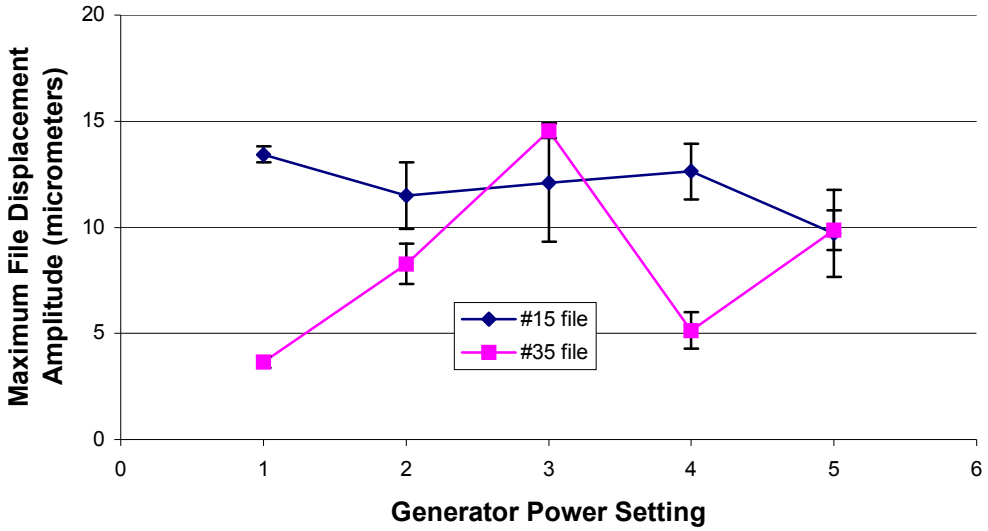


Figure 6.20 Mean maximum file displacement amplitude as a function of generator power setting for #15 and #35 K-file.

Thermal Imaging

6.11 Heat Generated during *In Vitro* Ultrasonic Instrumentation

Typical images obtained using the Agema 900 thermal imaging system, for both the magnetostrictive and piezoelectric scaling system, are shown in Figures 6.21 & 6.22 respectively. To obtain temperature data, measurement points were positioned along the length of the scaling instrument (Figure 6.23), including a point at the site of tip/tooth contact and the temperature recorded in successive 1-second intervals. Graphs of temperature increase with respect to time were created to observe the effects of generator power setting, water flow rate and tip/tooth contact load, on the heat generated during ultrasonic instrumentation of tooth surfaces (Figures 6.24 – 6.26).

With no power supplied by the generator (0 to 10 seconds) there is no scaler tip oscillation and so the recorded temperature is an indication of the ambient room temperature. For the following 60 seconds power was supplied and an increase in temperature was detected by the thermal imaging system for both generators, irrespective of instrumentation conditions. The mean background temperature (for each thermal sequence) was determined from the first 10 seconds of data. This value was then subtracted from all the data in that thermal sequence, enabling the increase in temperature, from room temperature, to be observed.

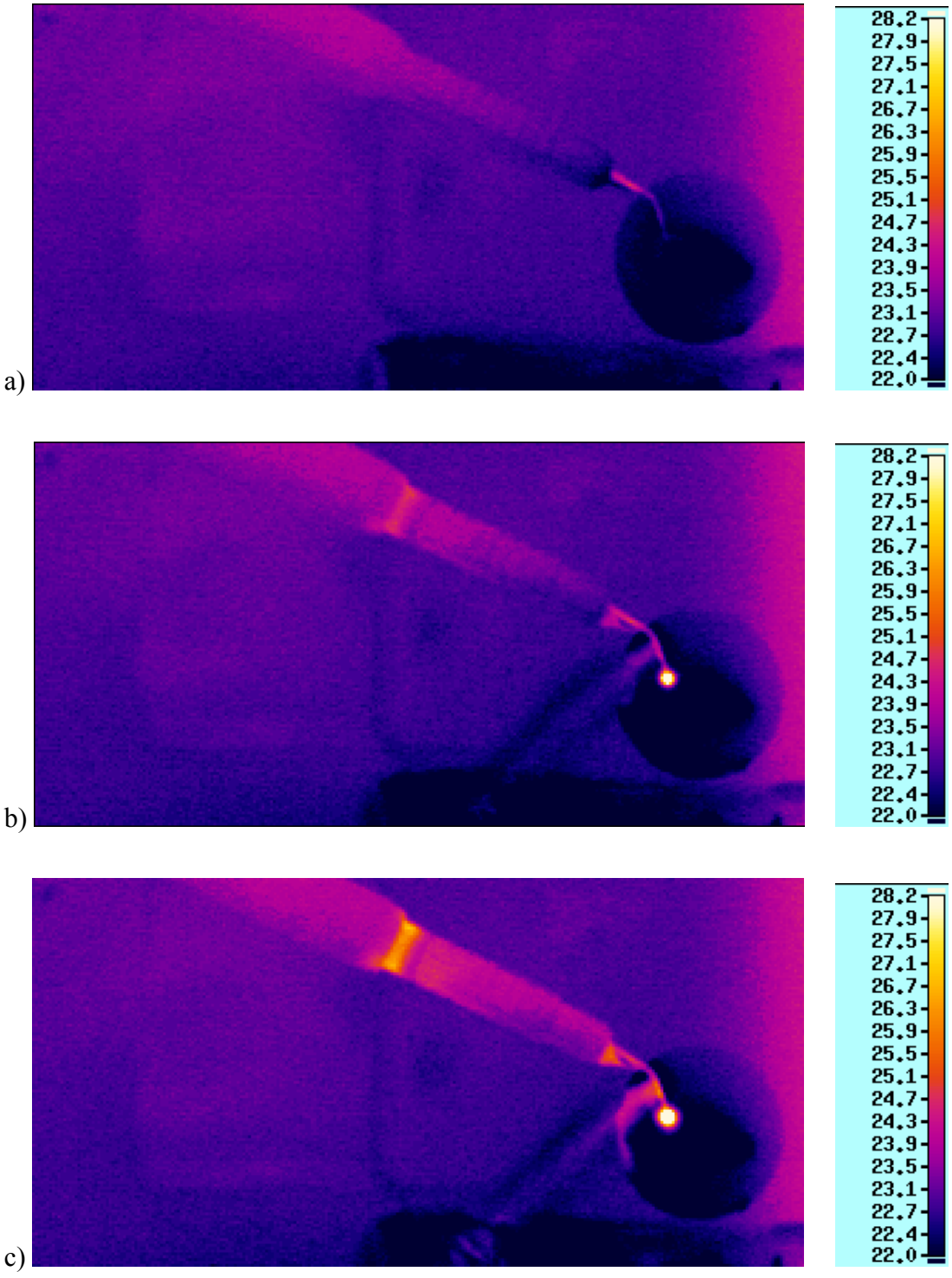


Figure 6.21 (a-c) Typical thermal images of a magnetostrictive scaler taken at a) 10 seconds (no power), b) 14 seconds and c) 17 seconds. The increase in temperature at the tip/tooth contact site may be clearly seen. The colour-graduated scale indicates image temperature.

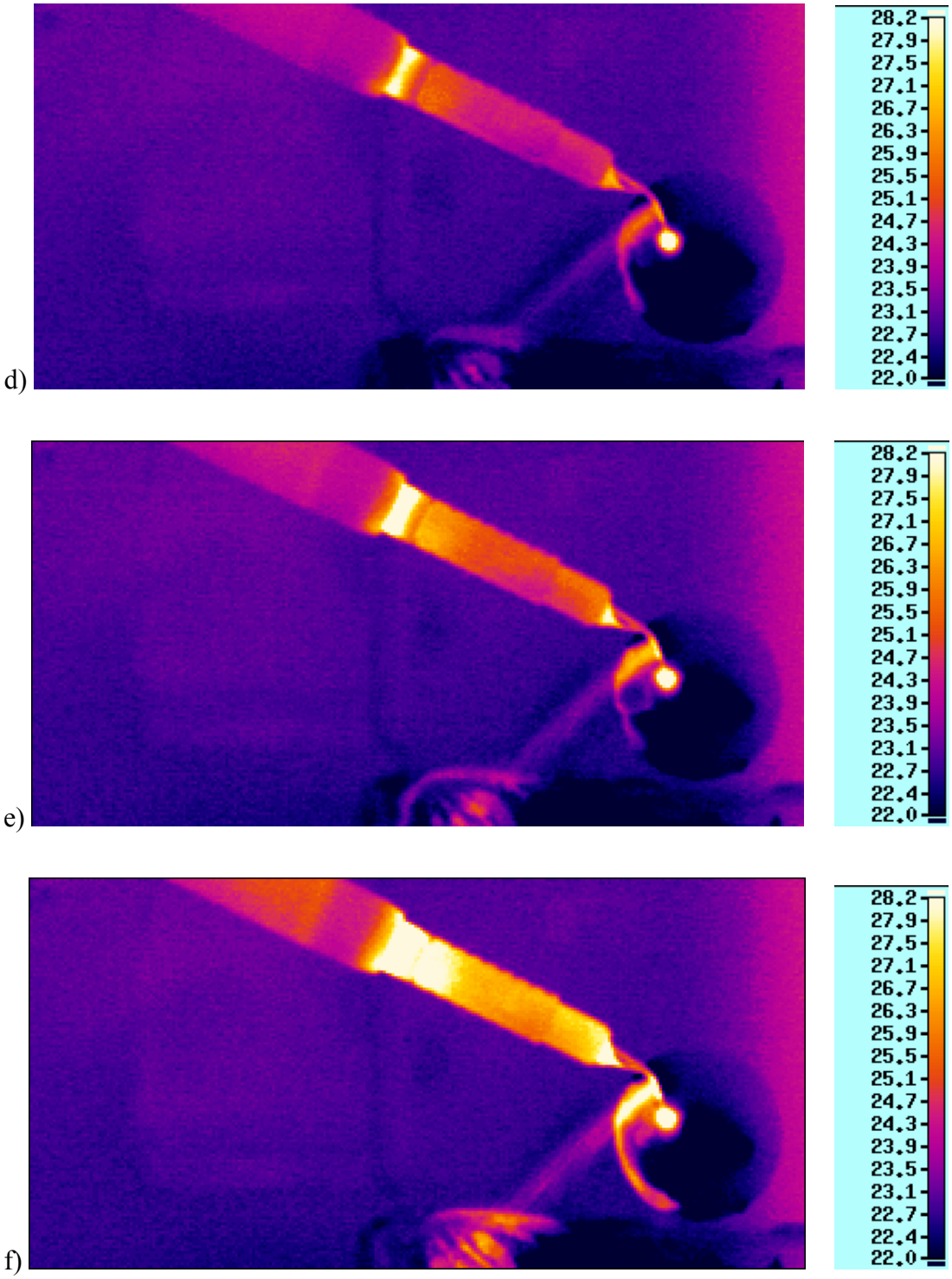


Figure 6.21 (d-f) Typical thermal images of a magnetostrictive scaler taken at d) 20 seconds, e) 23 seconds and f) 28 seconds. The increase in temperature at the tip/tooth contact site and scaler handpiece may be clearly seen. The colour-graduated scale indicates image temperature.

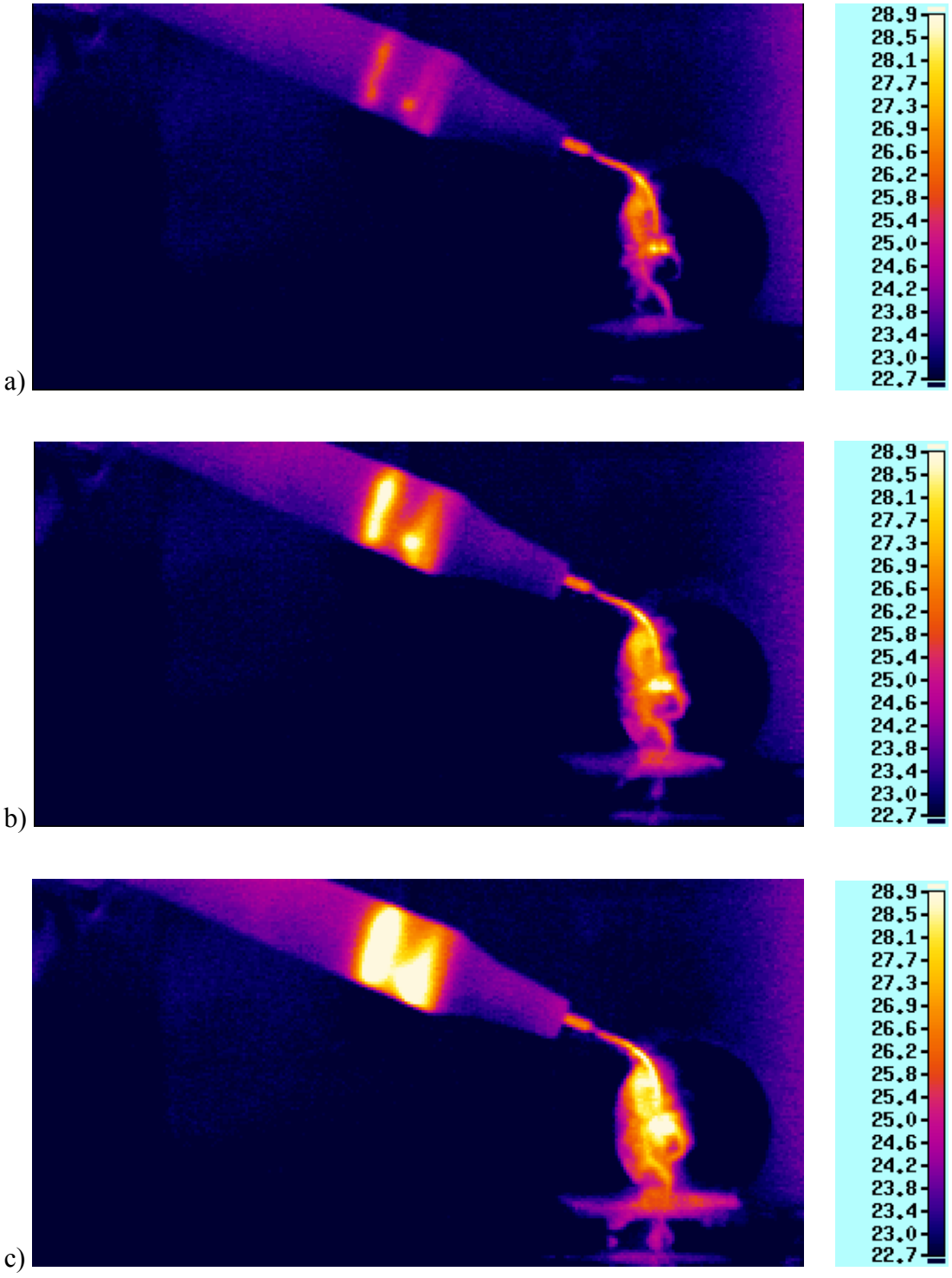


Figure 6.22 (a-c) Typical thermal images of a piezoelectric scaler taken at a) 17 seconds, b) 27 seconds and c) 37 seconds. The increase in temperature at the tip/tooth contact site and scaler handpiece may be clearly seen. The colour-graduated scale indicates image temperature.

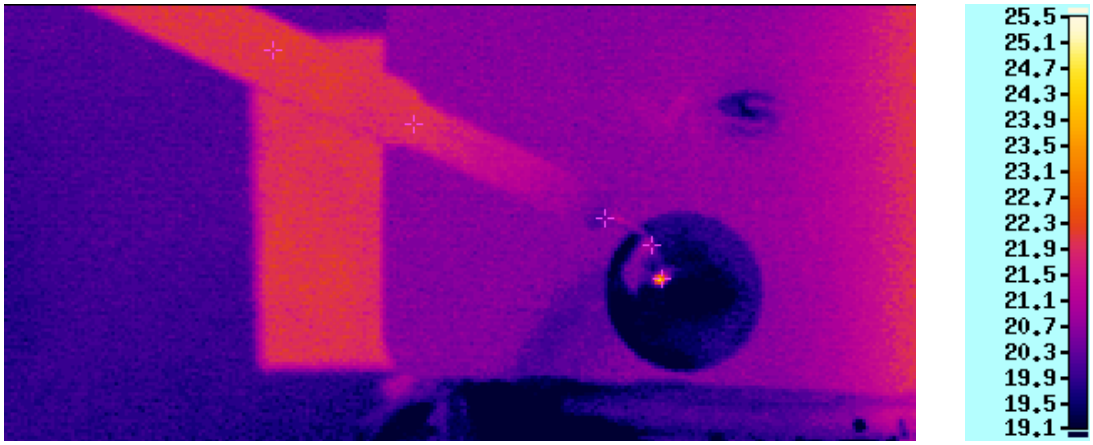


Figure 6.23 Measurement points are positioned along the length of the scaling instrument, including a point at the site of tip/tooth contact, to enable temperature variation to be recorded.

Data obtained for both scaler systems showed that an increase in load (for set water flow rate / generator power setting) and generator power setting (for set load / water flow rate) generally corresponded to an increase in detected temperature (Figures 6.28 & 6.29). It was also observed that an increase in water flow rate over the scaler tip (for set conditions of load / generator power setting) generally lead to a reduction in the maximum temperature attained (Figure 6.30) for both scaler systems.

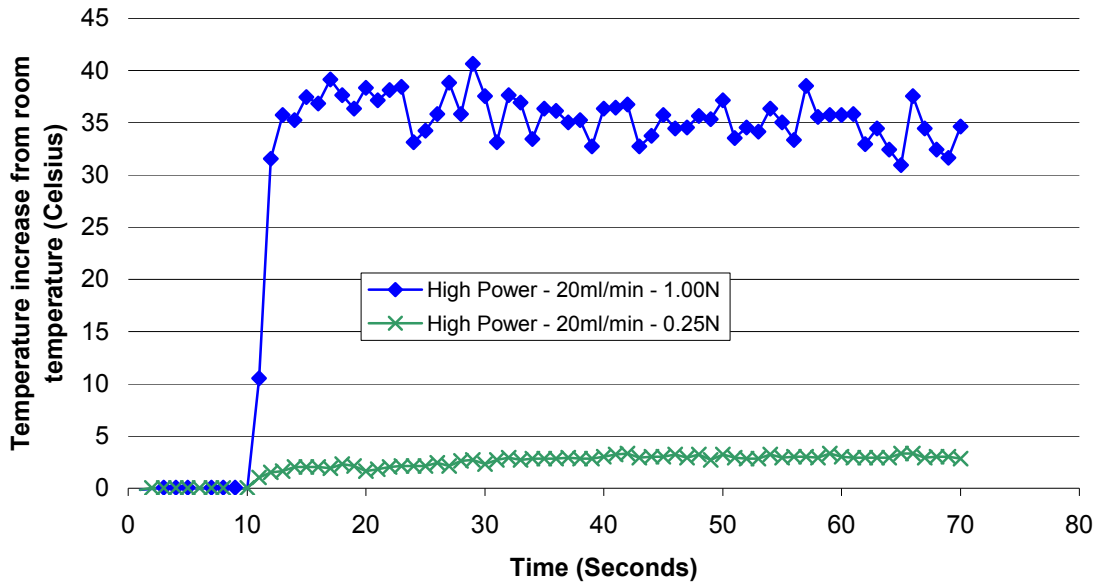


Figure 6.24 Graph of temperature variation with time for the Mini Piezon scaling system. Scaling conditions are constant water flow rate of 20ml/min, high generator power setting at tip / tooth contact loads of 0.25N and 1.00N.

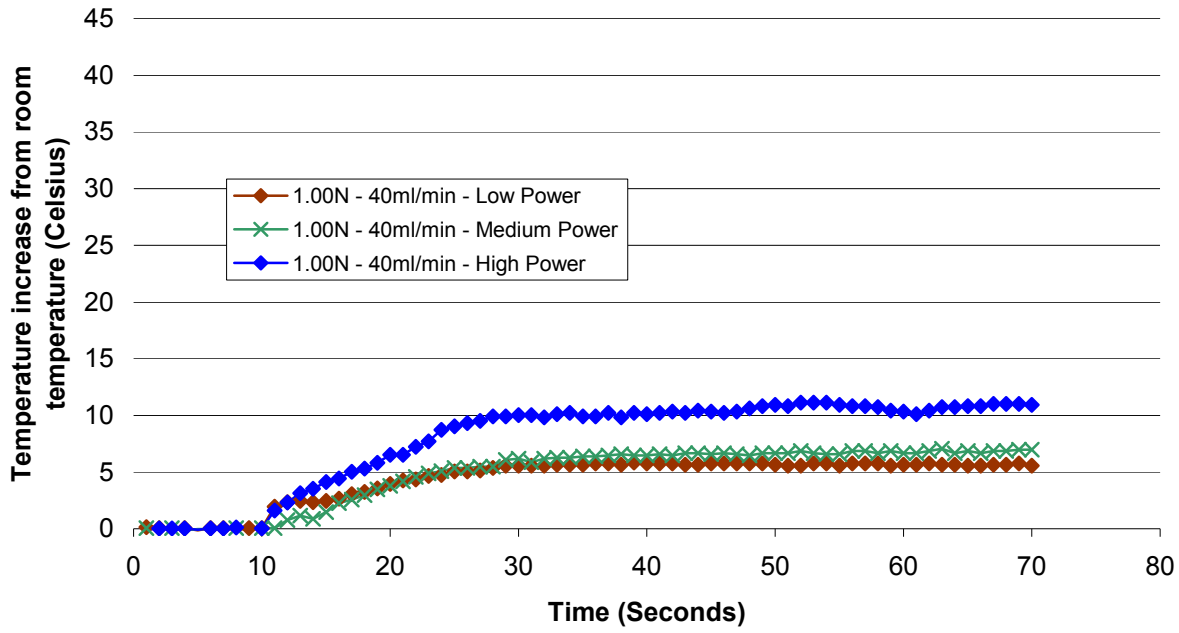
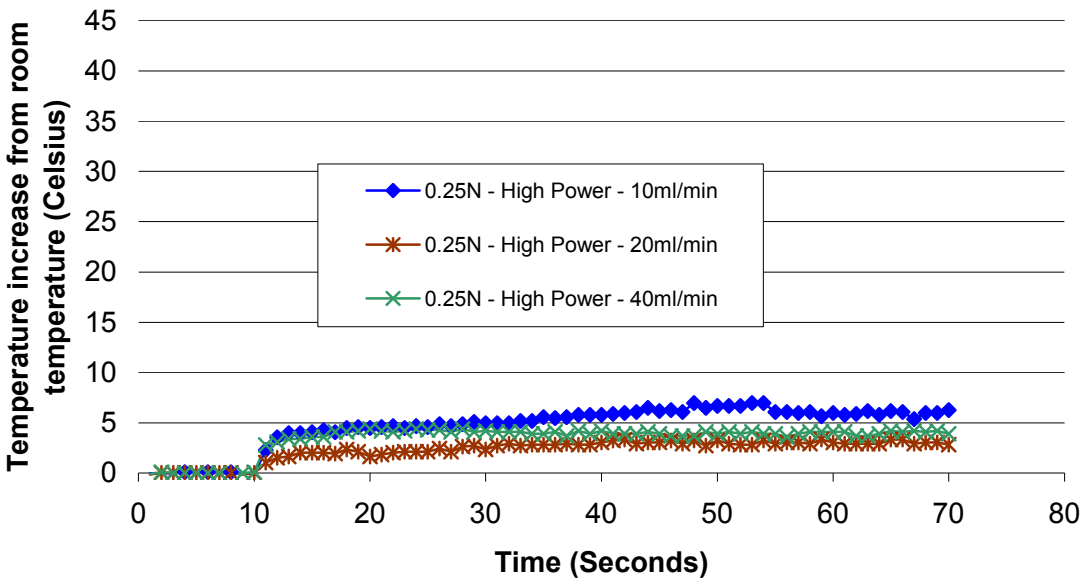
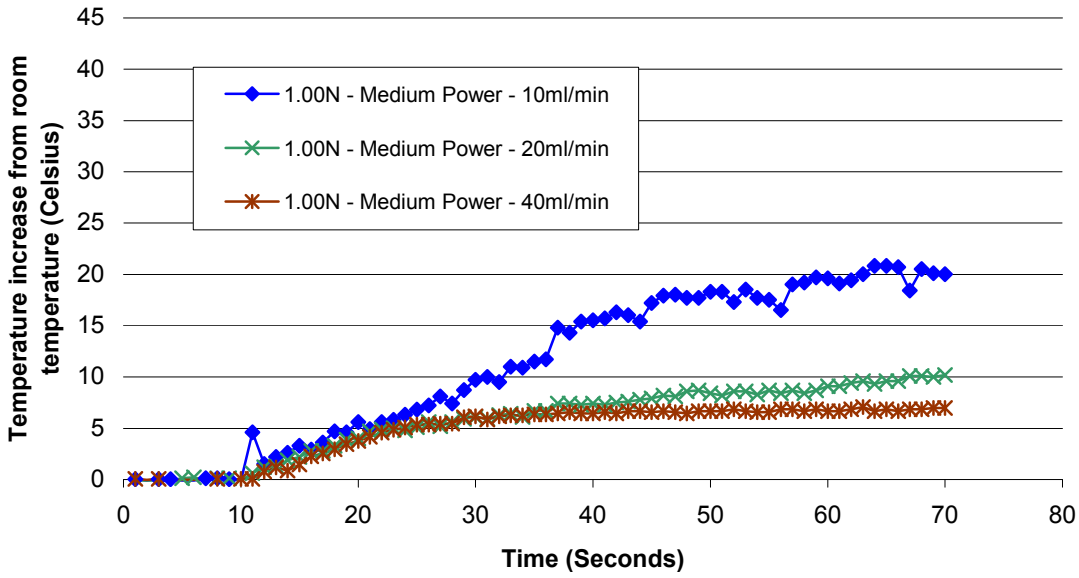


Figure 6.25 Graph of temperature variation with time for the SPS scaling system. Scaling conditions are constant water flow rate of 40ml/min, contact load of 1.00N and generator power settings of low, medium and high.



a)



b)

Figure 6.26 Graph of temperature variation with time for a) Mini Piezon scaling system. Scaling conditions are 0.25N load, high power and water flow rate of 10, 20 and 40ml/min. b) SPS scaling system. Scaling conditions are 1.00N load, medium power and water flow rates of 10, 20 and 40ml/min.

The Terephthalate Dosimeter

6.12 Cavitation around Ultrasonic Scalers

Prior to each measurement, the spectrometer was zeroed using a cuvette of unsonicated TA solution.

Any cavitation that might have been produced by the TFI-1 tips was below the limit of detection (< 10^{-8} Molar) at all powers. Likewise, any cavitation produced by the TFI-3 or TFI-10 scaler tips at low generator power setting (2 & 5 minutes) was also below the limit of detection (< 10^{-8} Molar). No cavitation was detected at medium power for the TFI-10 tips (2 & 5 minutes) except for tip 2, which showed very small $^{\bullet}OH$ radical concentrations (Table 6.16). All TFI-10 tips produced cavitation at the high power setting (Table 6.16). All TFI-3 tips produced cavitation at both medium and high power settings (Table 6.16).

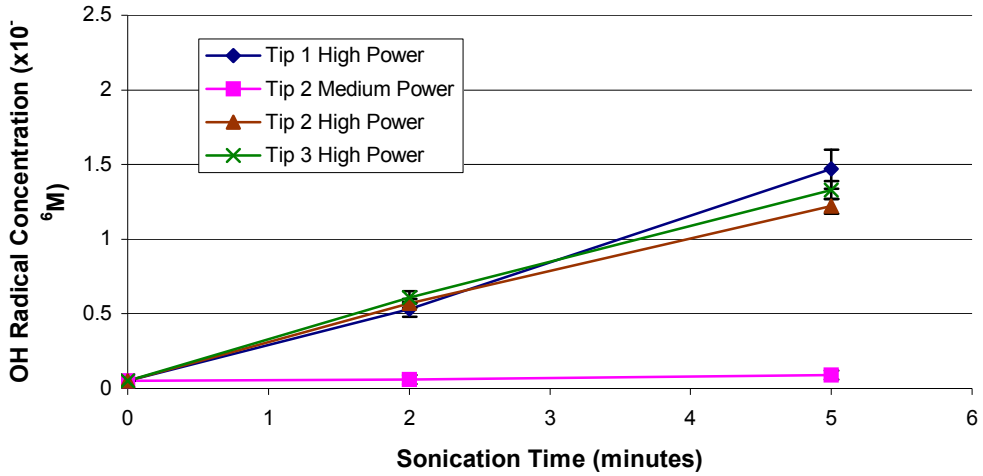
Graphs of [$^{\bullet}OH$] concentrations (x10^{-6} mol l^{-1}) as a function of sonication time were obtained for both the TFI-10 inserts (Figure 6.27a) and for the TFI-3 inserts (Figure 6.27b).

6.13 Cavitation around Powered Toothbrushes

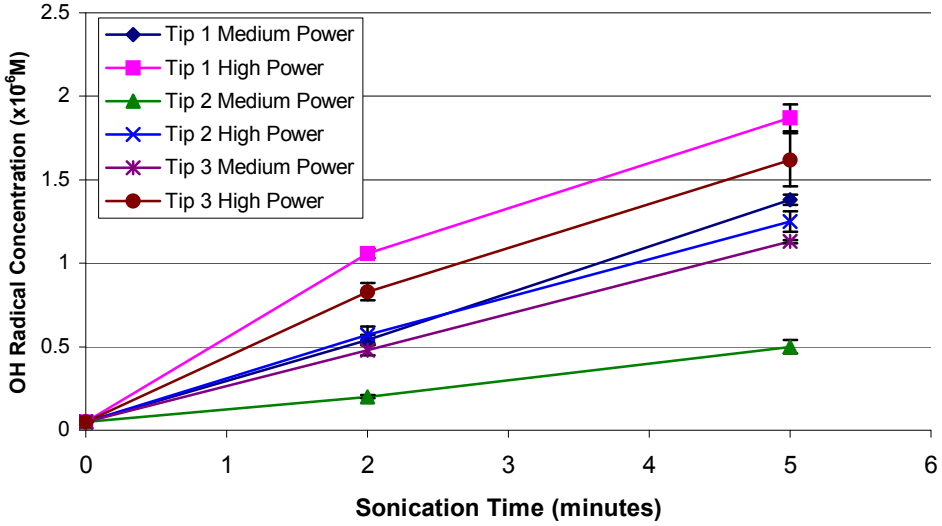
Any cavitation that might have been produced by the powered toothbrushes was below the limit of detection (< 10^{-8} Molar) for both 10 and 20 minutes of operation.

Tip design (# number) / generator power	[•OH] concentration (x10^{-6} mol l^{-1})		
	1 minute sonication	**2 minute sonication**	**5 minute sonication**
All **TFI-1** Tips / All Powers	NDC	NDC	NDC
All **TFI-10 / TFI-3** Tips / Low Power	NDC	NDC	NDC
TFI-10			
#1 Medium Power	NDC	NDC	NDC
#1 High Power	0.35 ± 0.01	0.53 ± 0.05	1.47 ± 0.13
#2 Medium Power	NDC	0.06 ± 0.03	0.09 ± 0.03
#2 High Power	0.34 ± 0.02	0.57 ± 0.03	1.22 ± 0.05
#3 Medium Power	NDC	NDC	NDC
#3 High Power	0.40 ± 0.03	0.61 ± 0.04	1.33 ± 0.06
TFI-3			
#1 Medium Power	0.30 ± 0.01	0.54 ± 0.03	1.38 ± 0.03
#1 High Power	0.47 ± 0.04	1.06 ± 0.03	1.87 ± 0.08
#2 Medium Power	0.12 ± 0.03	0.20 ± 0.01	0.50 ± 0.04
#2 High Power	0.30 ± 0.02	0.57 ± 0.05	1.25 ± 0.06
#3 Medium Power	0.26 ± 0.01	0.48 ± 0.03	1.13 ± 0.01
#3 High Power	0.54 ± 0.03	0.83 ± 0.05	1.62 ± 0.16

Table 6.16 [•OH] concentrations (x10^{-6} mol l^{-1}) obtained following sonication of terephthalic acid solution (± 1 standard deviation), for periods of 2 and 5 minutes, with TFI-1, TFI-10 and TFI-3 scaler tips. (NDC = no detectable cavitation).



a)



b)

Figure 6.27 Graphs of [$^{\bullet}$OH] concentrations (x10^{-6} mol l^{-1}) as a function of sonication time for a) the TFI-10 inserts and b) the TFI-3 inserts.

CHAPTER 7

DISCUSSION

7.1 Introduction

Since the first use of ultrasound in dentistry for drilling cavities in teeth (Catuna 1953), the ultrasonic scaling instrument has become established as the main application of ultrasound in dentistry. The basic methods of ultrasound generation have altered little over the last 50 years with research and development (mostly by manufacturers) being primarily in relation to insert design and the shape of the probes. In particular, slimmer probe tips have been introduced, which are designed to improve access to the tooth and root surfaces during scaling procedures.

Early work to assess the effectiveness of ultrasonic scalers, compared with routine hand scaling methods, was generally favourable towards the ultrasonic instrument (Johnson & Wilson 1957; Ewen, 1960; McCall & Szmyd 1960; Goldman 1961; Moskow & Bressman 1964; Sanderson 1966; Clark 1969). However some studies suggested that the ultrasonic scaler was less effective than hand planing and that it should only be used as an adjunct to curettage (Stende & Schaffer 1961; Suppipat 1974). More recent research (Torfason *et al*. 1979; Badersten *et al*. 1981; Drisko *et al*. 2000; Tunkel 2002) has suggested that ultrasonic scalers are not just suitable as an adjunct to hand instruments but that they should be used as a scaling technique in their own right.

As well as clinical *in vivo* investigations, there has been a large amount of research performed *in vitro* into the operational characteristics of dental scalers. These investigations assess the

effects of physical factors such as load, tip angulation and generator power setting on scaler tip oscillation characteristics (Walmsley *et al*. 1986a&b; Williams & Walmsley 1988; Lumley *et al*. 1993; Chapple *et al*. 1995, Flemmig *et al*. 1997 & 1998a&b, Busslinger 2001). However, the vibration characteristics of ultrasonic scalers are still not fully understood. The vibrations of scaler probes are difficult to analyse due to their high frequency vibrations and small associated displacement amplitudes. Previous assessment of the oscillation of these instruments was time-consuming and did not allow detailed visualisation or accurate measurement of the probe movement (Walmsley *et al*. 1986a&b). However, the acquired data gave an indication that there were potential problems with instrument variability.

This thesis has investigated the ultrasonic scaler from an *in vitro* perspective. The vibration characteristics of ultrasonic scalers have not been fully scientifically evaluated and various working parameters may have an influence on clinical outcomes. Clinicians should, therefore, be fully aware of the ultrasonic scaler vibration characteristics prior to commencing new research to enable the most meaningful data to be acquired. Although this research work has focussed primarily on the use of a scanning laser vibrometer to assess the oscillatory motion of the ultrasonic scaler tips, other parameters such as the amount of cavitation that occurs around the instrument and the thermal effects on the tooth surface were also investigated. Furthermore, the vibration characteristics of endosonic K-files and powered toothbrushes were assessed and a study into the presence or absence of cavitation around powered toothbrushes was also performed.

The Scanning Laser Vibrometer

7.2 Water Flow Rate and Scaler Tip Vibration

During normal clinical operation, ultrasonic scalers require a flow of water to be passed through the instrument. This flow of water serves two main purposes. The first is to cool the working instrument and is of particular importance for magnetostrictive devices which can heat up rapidly. The second is to regulate the heat generated at the point where the oscillating tip and the tooth surface are in frictional contact with each other. As well as these primary effects, the flowing water serves to produce useful secondary effects. Biophysical forces may be set up in the water as it flows over the working tip. The destructive forces of inertial cavitation may help to clean teeth by disrupting colonies of plaque and bacteria (Walmsley *et al*. 1988) and acoustic streaming may help to dislodge and transport removed tooth deposits from the treatment site. The effects of cavitation may also be enhanced by acoustic streaming, since streaming ensures there is a continuous supply of gaseous air surrounding the working tip, which is ideal for continued bubble formation and growth.

The first investigation was designed to evaluate the effect of water flow rate on the oscillation characteristics of dental ultrasonic scalers. The results showed the maximum displacement amplitude of the scaler tips vary with water flow rate and generator power setting. Water, flowing over the oscillating tip, was generally found to produce a damping effect, which corresponded to a reduction in the maximum measured displacement amplitude. Generator power settings used were denoted as ‘quarter’, ‘half’ and ‘full’ power and refer to a quarter, half and full turn of the power dial of the ultrasound generator respectively. Similarly, ‘quarter’, ‘half’ and ‘full’ water settings refer to a quarter, half and full turn of the water flow dial of the ultrasound generator and were measured as 18, 38 and 62ml/min respectively.

‘Quarter’ Generator Power

With the water flow rate set at the quarter dial setting (18ml/min) the water flows over the length of the tip, effectively covering the scaler (Figure 7.1). Increasing the water flow rate to ‘half’ and ‘full’ water settings means more water (per unit time) covers the tip. This reduces both the velocity and the displacement amplitude of the tip as it attempts to oscillate through a greater volume of the water (Figure 6.7a).

‘Half’ Generator Power

When the ultrasonic scaler is operated at the ‘half’ power setting and ‘quarter’ water flow rate an aerosol is produced (Figure 7.2). As the water flow rate is further increased the tip displacement decreases. Despite the production of aerosol, the majority of the water still flows over the length of the scaler tip (Figure 7.2) and, as before, an increase in the water flow reduces the displacement amplitude of the tip as it attempts to oscillate through a greater volume of the water (Figure 6.7b).

Full Generator Power

At full power settings with a ‘quarter’ water flow, an aerosol is produced but the water still flows over the tip. Increasing the water to half flow results in a decrease in scaler tip displacement amplitude for the reasons described previously. However, when full generator power is used in conjunction with full water flow an increase in the displacement amplitude of some scaler tips is observed (Figure 6.7c). This may be explained by closer inspection of the aerosol being thrown from the tip. At high power and high water flow rates the water leaves the body of the instrument as a water jet (Figure 7.3). This leaves the tip relatively free of water and it may oscillate with increased displacement amplitude.



Figure 7.1 At ‘quarter’ water settings (18ml/min) the water flows over the length of the tip, effectively covering the scaler tip and damping its vibrations. This was observed over the range of generator power settings used.



Figure 7.2 At ‘half’ water settings (38ml/min) aerosol is produced. However, the majority of the water flows over the length of the working instrument, covering the tip and damping its vibrations. This was observed irrespective of the generator power used.



Figure 7.3 When the scaler is operated at full power with full water flow (62ml/min), the water may be thrown from the body of the instrument as a jet. This leaves the tip free of water, which may then oscillate with increased displacement amplitude.

Previous work (Walmsley *et al*. 1986a) stated "…[water] flow was prevented from reaching the tip by a rubber disc… It is unlikely that such an arrangement will affect the oscillation of the descaling tip." However, here it has been demonstrated that the amount of water flowing over a tip whilst it is being operated can affect its displacement amplitude (Table 6.1). For the five tips investigated, it was generally observed that an increase in water flow rate from 18ml/min to 38ml/min and from 38ml/min to 62ml/min lead to a reduction in tip vibration displacement amplitude over the range of generator powers tested. However, at a given power setting, the decrease in displacement amplitude was not the same for all tips and in some cases an increase in vibration displacement amplitude was observed. Variability between tips of different designs driven by the same generator has been observed previously (Walmsley *et al*. 1986a&b; Williams & Walmsley 1988). However, this initial investigation has suggested that significant variability can also occur between tips of the same design and this will be investigated further.

7.3 Displacement Amplitude of Unloaded Ultrasonic Scaler Inserts

Having ascertained the effect the cooling water flow has on the magnitude of scaler tip vibrations it was necessary next to investigate the effect of generator power setting on scaler tip vibration displacement amplitude. Following the observation in the last investigation that the scaler tips did not all respond to varying water flow rates in the same manner the next stage was to determine whether tips of the same design would respond to varying generator power in the same manner or whether this variability would again be observed. Under normal clinical use, ultrasonic scaler tips are contacted against tooth and root surfaces and are, therefore, operated under load. However, to assess tip variability tips were operated under unloaded conditions (i.e. freely oscillating in air) since loading would add another variable.

By performing vibration measurements in air, variation in tip oscillation displacement amplitude could only be attributed to the tips or the generators themselves.

The generator / tip combinations used here were chosen for their universal use. This allowed us to compare the outputs of 25kHz and 30kHz magnetostrictive generators as well as the outputs of three 30kHz generators, when two machines are piezoelectric and the other magnetostrictive. The principle observation from this investigation was the high variability in tip vibration displacement amplitude. When used in conjunction with five scaler inserts of the same design, none of the generators statistically produced the same output for all tips (Table 6.2). The Piezon Master 400 (with P-Tip) was the closest to this with four of the tips demonstrating statistically similar responses to generator power. The Cavitron SPS with TFI-3 tip showed no similarities in oscillation between any of the tips.

A second observation is that tip displacement amplitude does not always increase in a linear manner with increasing generator power. Users of ultrasonic equipment assume that generators are standardised and are broadly similar in their operation characteristics. If tip displacement amplitude does not increase linearly with increasing power setting and the output between tips of the same style varied significantly, then this may raise problems for both the clinician and the researcher alike. Clinicians may find it difficult to familiarise themselves with a system because different power levels are required for different tips to achieve the same level of cleaning. Researchers who state the use of low, medium and high power settings will have potential inaccuracies introduced to their readings as there may be little or no difference (statistically) in tip displacement amplitude between, for example, low and medium power settings.

Some of the generator / tip combinations used in this study produced linearly increasing displacement amplitudes with increasing power setting. For example, correlation analysis of the Mini Piezon with P-Tips produced R^2 values of between 0.91 and 0.99 (Table 6.2) and the Cavitron SPS with TFI-10 tips produced R^2 values of between 0.93 and 0.99 (Table 6.2). However, some generator / tip combinations showed much less goodness of fit to a linear trend. The Cavitron Select used with TFI-10 tips produced R^2 values of between 0.30 and 0.79 (Table 6.2) and the Piezon Master 400 with P-Tips produced R^2 values of between 0.52 and 0.87 (Table 6.2).

This investigation provides an initial insight into the effects of generator power setting on scaler tip displacement amplitude. Scaler tip displacement amplitude can vary dramatically between not only generator type and tip design but can also vary significantly between tips of the same type used with the same generator. However, when used clinically scaler tips are contacted against tooth and root surfaces. It was demonstrated in the first investigation (Water Flow Rate and Scaler Tip Vibration) that even small loads, such as water flowing over the surface of the tip, could affect its vibration characteristics. Therefore, it is important to characterise the motion of the tips when in contact with a root surface under known loads.

7.4 Scaler Tip Performance under Various Load Conditions

The main observations from the initial investigations are that there can be significant variability in the oscillation characteristics of dental scalers and that, under unloaded circumstances, tip vibration displacement amplitude may not increase linearly with generator power setting. Having evaluated the effect of generator power setting on the vibration of unloaded scalers, it was important to assess the performance of ultrasonic scalers operating

under loaded conditions (i.e. a more clinically realistic circumstance) and determine the level of tip performance variability.

The generators and inserts selected for this investigation were the same as those used in the previous study (Displacement Amplitude of Unloaded Ultrasonic Scaler Inserts), which assessed the variability of tips in an unloaded environment. As with the previous investigation, the choice of generators made it possible to compare the outputs of 25kHz and 30kHz magnetostrictive units (Cavitron Select and SPS) as well as the outputs of three 30kHz generators (Mini Piezon, Piezon Master 400 and SPS). The application of different loads to the scaler inserts allowed us to determine if load had a significant effect on individual tip response and whether like-tips, operated by the same unit, would show similar outputs (for a given load). Furthermore, by using the same generator / tip combinations as in the unloaded study, we could compare our loaded tip measurements with the corresponding unloaded results.

This investigation showed that there is high variability associated with dental ultrasonic scaler inserts. For all tip data, R^2 values (Tables 6.4 & 6.5) indicated that the increase in displacement amplitude with increasing generator power was closest to linear for the larger, heavier tips. In particular the TFI-3 inserts, with the SPS generator, showed the most linear response to power of all the tips tested, with R^2 values ranging between 0.93 and 0.99 for all loads. Conversely, the tips that appeared to be the most affected by load were the lighter P-tips operated by both the Mini Piezon and the Piezon Master 400. Under conditions of no loading, the Mini Piezon produced a linear increase in tip displacement amplitude ($0.91<R^2<0.99$) with increased power setting and four of the five P-tips used with the Piezon

Master 400 demonstrated no significant differences. However, under load, R^2 values as low as 0.01 and 0.02 were observed for the P-tips with both generators (Table 6.4) and all of the P-tips were found to be significantly different to each other.

Variability in tip output with the different generators, with like-tips operated using the same generator and even individual tips operated under different loads, may cause problems for both clinicians and researchers. Studies on root substance removal using ultrasonic scalers, Flemmig *et al*. (1998a&b) concluded that defect depth / volume are strongly influenced by combinations of working parameters such as tip angulation, lateral force and instrument power setting. This project, however, has demonstrated that instrument power setting is often not a good indication as to how much a loaded insert tip is oscillating. The variation between tips may also explain the apparent disparity between investigations into root surface effects. Instrumentation with piezoelectric scalers has been shown to lead to both a rougher root surface than magnetostrictive instruments (Busslinger *et al*. 2001) and also to a smoother root surface than magnetostrictive instruments (Cross-Poline *et al*. 1995). However, neither of these studies standardised the operating conditions of the working instrument.

This investigation has advanced the understanding of ultrasonic scaler tip vibrations from the previous investigations. By performing measurements with the scaler tips under known loads, more clinically relevant data may be obtained. This study has shown that scaler tip displacement amplitude can vary significantly between generator type (piezoelectric or magnetostrictive), tips of different designs and even between tips of the same type used with the same generator. Individual tips, under different loading conditions, were also shown to

produce different outputs. Studying several generator units of the same type would make it possible to determine whether the generators used in this study were typical of their type.

7.5 The Effect of Wear on Scaler Tip Displacement Amplitude

During normal clinical usage, ultrasonic scaler tips may become worn and reduced in length. It is currently unknown what effect wear has on the magnitude of scaler tip vibrations when they oscillate in air and when they contact teeth under typical clinical loading forces. The primary cleaning mechanism of dental ultrasonic scalers is the mechanical chipping action of the scaler tip when contacted against the tooth surface. The magnitude of the tip vibration displacement amplitude could, therefore, be used as a convenient measure of the efficiency of the instrument (Walmsley *et al*. 1986a&b; Lea *et al*. 2003a&b). It is thought that a reduction in the length of a scaler insert tip, through wear, reduces the magnitude of the tip vibration, resulting in a potential reduction of scaling efficiency. Whether this is clinically significant has yet to be determined.

This work demonstrated that, for all styles of scaler tip investigated (FSI-100, FSI-1000 and FSI-SLI-10S), a reduction in the length of the tip significantly affected the vibration displacement amplitude of the instrument (Figures 6.8 - 6.10). This could potentially reduce the clinical efficacy of the instrument. Of the insert designs tested, the FSI-SLI-10S design showed the greatest degree of variability with all tips oscillating significantly differently to each other for all load and tip length conditions. Both the FSI-100 and FSI-1000 tips showed significant differences in oscillation between the inserts investigated. FSI-100 tip 3 performed differently to the other four FSI-100 tips, in air and under load, at its unadjusted length and when the tip was reduced in length by both 1 and 2mm. This confirms previous work that

showed differences in the oscillation of scaling tips both in the unloaded and loaded situation whether utilising the solid probe design (Lea *et al*. 2003a&b) or the thin design of scaling tip (Trenter *et al*. 2003).

7.6 Single-Scan Multi-Axial Assessment of Scaler Tip Vibrations

This thesis has concentrated primarily on the longitudinal displacement amplitude of the scaler instrument since this has been shown to be a useful indicator of clinical efficiency (Walmsley *et al*. 1986a&b). It was previously thought that ultrasonic scalers oscillated in a purely longitudinal manner. This was considered a difference from sonic scalers, which exhibited "a totally different vibratory action which is elliptical and which is particularly susceptible to lateral loading" (Walmsley *et al*. 1992). Elliptical motion had been noted when the scaler was used under operating conditions which included combinations of high displacement amplitude (high power) and without water cooling (Walmsley *et al*. 1986a&b). However, these conditions are not normally used during routine clinical operation since they can be damaging to both the patient and the scaling system.

This investigation was performed using a 'medium' generator power setting in conjunction with a constant water flow rate of 20ml/min. The results demonstrated quite clearly that ultrasonic scalers exhibit an elliptical path during their unloaded oscillation cycle. The manner in which ultrasonic scalers oscillate is important clinically since any lateral or side-to-side motion may contribute both to the cleaning effect of the instrument and also to the damage the instrument may potentially cause to the dental structures.

Initial results demonstrate that though the ultrasonic instrument oscillates with an elliptical motion, the lateral component is very small relative to the longitudinal vibration displacement amplitude. This work was performed under a single set of working parameters for an individual scaler tip / generator combination. More tips and generators need to be evaluated, under a greater range of operating conditions, before more conclusions may be drawn.

7.7 The Vibration Patterns of Powered Toothbrushes

The clinical effectiveness of powered toothbrushes compared to manual toothbrushes has been rigorously researched for over 40 years (Cross *et al*. 1962; Chilton *et al*. 1962; Hoover & Robinson 1962; Elliot 1963; Walsh & Glenwright 1984; Niemi *et al*. 1986; Niemi 1987; Baab & Johnson 1989; Killoy *et al*. 1989; Van der Weijden *et al*. 1993; Johnson & McInnes 1994; Grossman *et al*. 1996; Danser *et al*. 1998; Mantokoudis *et al*. 2001). Many initial studies concluded that powered toothbrushes have no additional benefits over manual toothbrushes. However, more recent research has suggested that powered toothbrushes may be superior to manual toothbrushes (Johnson & McInnes 1994; Walmsley 1997; Heasman & McCraken 1999; Heanu *et al*. 2003).

With so many powered toothbrushes now available it is inevitable that the question ‘which is the best powered toothbrush?’ should be asked. Comparisons of the relative cleaning efficacies of different makes and models of powered toothbrushes, each with their own modes of oscillation and vibration generation, is a keenly debated and much researched subject (Van der Weijden *et al*. 1993; Khambay & Walmsley 1995; Schemehorn & Henry 1996; Van der Weijden *et al*. 1996; Danser *et al*. 1998 & 2000; Scharma *et al*. 1998; Carter *et al*. 2001). Of the designs currently available, powered toothbrushes with counter-rotation actions appear to

achieve the most significant improvements in oral health when compared to manual and other powered toothbrushes (Van der Weijden *et al*. 1993a; Walmsley 1997; Scharma *et al*. 1998; Carter *et al*. 2001; Heanu *et al*. 2003).

Assessments of powered toothbrushes may be performed *in vitro* and *in vivo*. *In vitro* investigations assess the effects of variables such as contact load, duration of use and how brush head movements affect the removal of artificial deposits from tooth surfaces (Khambay & Walmsley 1995; Schemehorn & Henry 1996; Scharma *et al*. 1998; Danser *et al*. 2000; Carter *et al*. 2001). *In vivo* trials (Van der Weijden *et al*. 1993a&b; Johnson & McInnes 1994; Van der Weijden *et al*. 1996; Danser *et al*. 1998) are more difficult to evaluate fairly and non-subjectively, but are of value when considering the clinical cleaning efficacy of powered toothbrushes.

The cleaning mechanism of toothbrushes (powered or otherwise) relies upon the abrasive action of the toothbrush bristles when contacted against the tooth surface (Heasman & McCraken 1999). This is similar to the cleaning mechanism of ultrasonic scalers, which rely upon the mechanical chipping action of the instrument tip when contacted against the tooth surface. Ultrasonic scaler efficacy may be indicated by the magnitude of the displacement amplitude of the working tip of the instrument. It may therefore be argued that when investigating the efficacy of powered toothbrushes it is important to understand the mechanical motion of the toothbrush head and bristles, including the bristle vibration displacement amplitude and oscillation frequency. More detailed information about the vibration characteristics of different powered toothbrushes may aid the understanding of which toothbrush designs are the most effective at removal of plaque from teeth.

7.7.1 Interpretation of Data

Colour map images for the Philips Sensiflex HX2520 and Braun D8 / 3D (Figures 6.14b&c & 6.15) highlight the counter-rotary motion of these types of powered toothbrushes. The maximum displacement amplitude is observed for the bristles at the left and right edges of the toothbrush head, as viewed in the images (Figures 6.14b&c & 6.15). Colour map images for the Braun D8 and Braun 3D were very similar. Displacement amplitude data for both of these brushes were analysed using t-test. No significant difference in displacement amplitude was found between either of the toothbrushes ($p=0.5$). However, the measured fundamental frequency of the Braun 3D was greater than that of the Braun D8 (Table 6.12). The Sonicare toothbrush oscillates primarily from side to side and as such all bristles appear to move toward and away from the scanning head simultaneously (Figures 6.14a & 6.16). The maximum displacement amplitude is found to occur at the tips of the longest bristles, furthest from the toothbrush handle.

When analysing the colour map images for the Philips Sensiflex HX2520 and Braun D8 / 3D (Figures 6.14b&c & 6.15) there appears to be a nodal point (region of minimum vibration) down the centre of each of the images (shown as the red/lilac boundary). This would imply that there is no bristle motion at this point, but this is clearly not true. When analysing colour map images, it must be considered that the SLV measures vibration towards and away from the scanning head only. The bristles at point A (Figure 7.4) have a predominantly forward and backward motion relative to the camera and so this may be detected and measured. The bristles at B have side-to-side motion (relative to the camera head) and the camera does not, therefore, detect any movement. The bristles at A cannot be rotating without those at B also being in motion and this demonstrates the importance of the target's orientation relative to the

SLV when measuring the vibration characteristics of objects. This also explains why the 'pulse' motion of the Braun 3D is not observed, since from the orientation shown in Figure 6.15 the pulsation would be in the vertical plane and hence not detectable by the SLV. To measure these aspects of the toothbrush vibrations it is necessary to adjust the orientation of the scanning head relative to the brush and perform further scans.

This investigation into the vibration characteristics of powered toothbrushes was primarily to ascertain whether it was possible to perform such analysis using a SLV. It has been successfully demonstrated that it is possible to adapt the SLV to perform rapid and accurate analysis of powered toothbrush vibrations. This was accomplished by using the sound output of the toothbrush, detected and converted into an electrical signal by a microphone, to generate the reference signal. The magnitude and frequency of toothbrush oscillations from a single orientation and under unloaded conditions (i.e. vibrating in air) were quantified. Powered toothbrushes, especially those which oscillate with more complex actions, such as the Braun 3D, require scanning in different axes to give a more complete understanding of the overall motion. Scans should then be repeated to determine the effect of loading on the motion and vibration frequency of the toothbrush head and bristles. Evaluation of bristle motion, using the SLV, may potentially be used to aid the understanding of substance removal from tooth surfaces and allow the targeting of specific designs to improve efficacy.

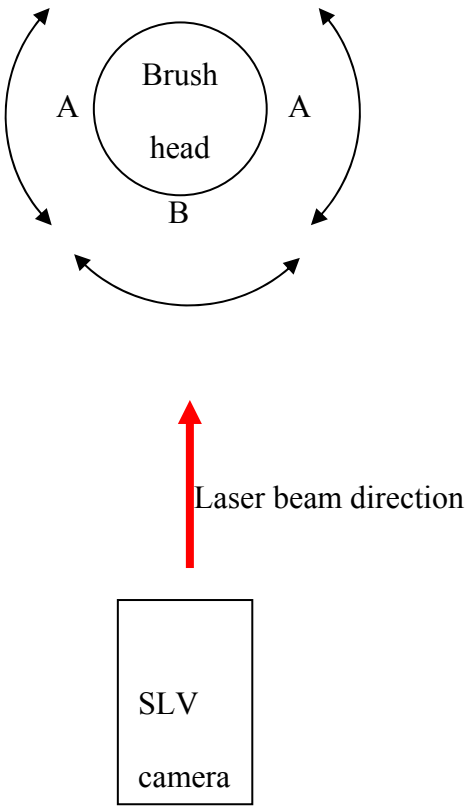


Figure 7.4 Representation of an end or side view scan of a powered toothbrush with a counter-rotation action. The SLV detects movements towards and away from the camera head. The bristles in the centre of the brush (point B) appear to have no movement whilst those bristles at point A appear to have the greatest amount of movement.

7.8 The Vibration Patterns of Endosonic K-Files

The first commercial machine designed specifically for ultrasonic root canal instrumentation was introduced by Martin (1976). Since then, the technique of endosonics has become an established part of root canal therapy (Lumley *et al*. 1991). Endosonic files are driven to oscillate at ultrasonic frequencies of up to 30kHz, by generators that utilise either magnetostriction or piezoelectricity. When operated, the files vibrate in a transverse manner, setting up a characteristic pattern of nodes and anti-nodes along the length of the file (Walmsley 1987; Walmsley & Williams 1989). When the file is moved vertically within the root canal, it is this transverse vibration that causes the filing of dentine.

The oscillation characteristics of endosonic K-files were previously assessed by shining a strong, directional light onto the length of a file. Points of light were reflected from the stationary file which, when operated, became elongated into lines, that could be measured and used to determine file excursion (Ahmad 1989; Walmsley & Williams 1989). However, this is a relatively crude and time-consuming procedure and does not allow precise characterisation of the file motion.

These preliminary scans have shown that it is possible, using laser vibrometry, to perform a detailed analysis of the oscillations of endosonic files, including their vibration frequency and displacement amplitude. Furthermore, it was also possible to determine the locations of nodes and anti-nodes along the length of the files and to observe file response to varying generator power (Figure 6.20). Animated sequences of the file oscillation can be produced, showing whole vibration cycles at greatly reduced velocities and frequencies. Stills of these sequences can then be used for further data analysis (Figure 6.18).

By exporting data from the SLV in the form of an ASCII file it was possible to plot the mean displacement amplitude, at each of the scan points, as a function of position on the file (Figure 6.19). The #35 file was shown to have fewer anti-nodes than the #15 file, as was expected due to the larger diameter of the #35 file.

The magnitude of vibration displacement amplitude at the unconstrained end of ultrasonic scaler tips has been used to indicate the efficacy of the instruments and to assess their response to increasing generator power setting (Walmsley *et al*. 1986b; Lea *et al*. 2003a&b). Similarly, the vibration characteristics of endosonic K-files have been assessed by measuring the magnitude of the vibration displacement amplitude at the unconstrained tip of the file (Ahmad *et al*. 1994).

This study demonstrated that the mean maximum displacement amplitude of file oscillation does not necessarily increase linearly with increasing generator power setting. The mean maximum displacement amplitude of the #15 file was found to be unaffected by increasing generator power setting (Figure 6.20) except for power setting 5, where a decrease in displacement amplitude was observed. The mean maximum displacement amplitude of the #35 file showed an initial increase in the mean maximum displacement amplitude from power setting 1 to 3 (Figure 6.20). However, a sharp drop in displacement amplitude was observed at power setting 4. The file displacement amplitude then increased at power setting 5.

The sharp decrease in displacement amplitude at power setting 4 for the #35 file may be explained by examining the frequency spectrum of the file oscillation at that power (Figure 7.5a) and comparing it to the spectra obtained at other generator powers (Figure 7.5b).

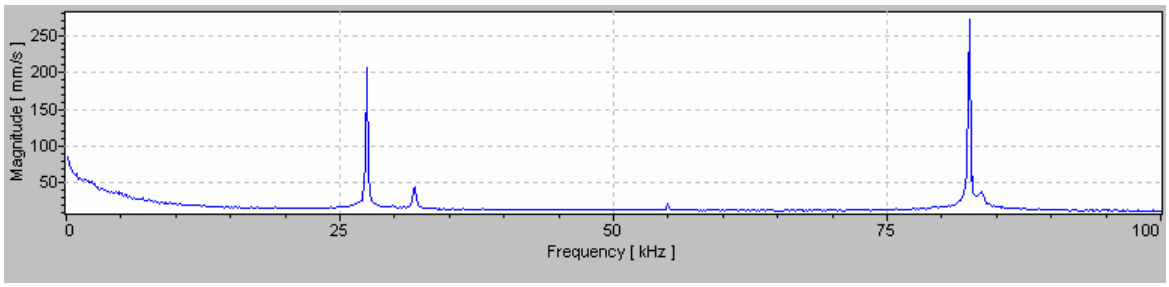
Generator power is used to drive the K-file at its fundamental frequency (27.50kHz). However, vibrations at other frequencies are also observed that correspond to multiples of the fundamental (known as harmonics). The displacement amplitudes of the file at these harmonic frequencies are usually very small (Figure 7.6a) and do not seem to contribute much to the overall vibration of the file. However, the magnitude of the harmonic vibration at 82.50kHz for the #35 file at power setting 4 (Figure 7.6b) is larger than the magnitude of those encountered at other generator power settings. Generator power, used to drive these harmonic oscillations could mean that there is less power available to drive the vibrations at the fundamental frequency, resulting in the observed decrease in the magnitude of the file displacement amplitude.

A biophysical effect associated with ultrasonic endosonic files is acoustic streaming. It has been suggested that the velocity of the acoustic streaming occurring around endosonic files is influenced by several factors such as the power setting of the generator, the size of the file and the position along the length of the file (Ahmad *et al*. 1987b). Streaming velocity, V_s, may be obtained, quantitatively, using:

$$V_s = \frac{\omega \varepsilon_0^2}{a} \qquad [7.1]$$

where ‘ω’ is the angular frequency or 2π times the oscillation frequency, ‘ε_0’ is the displacement amplitude of the file and ‘a’ is the radius of the file (Ahmad *et al*. 1987). Since displacement amplitude does not vary linearly with generator power setting, generator power cannot be used as a guide to the velocity of the associated streaming at different power settings.

a)



b)

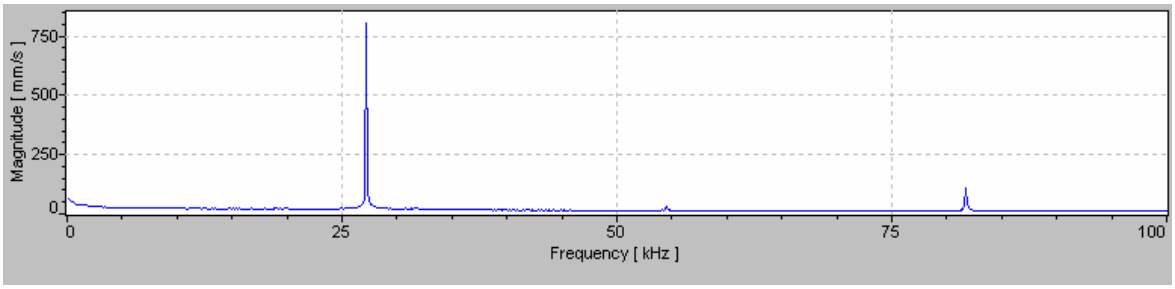
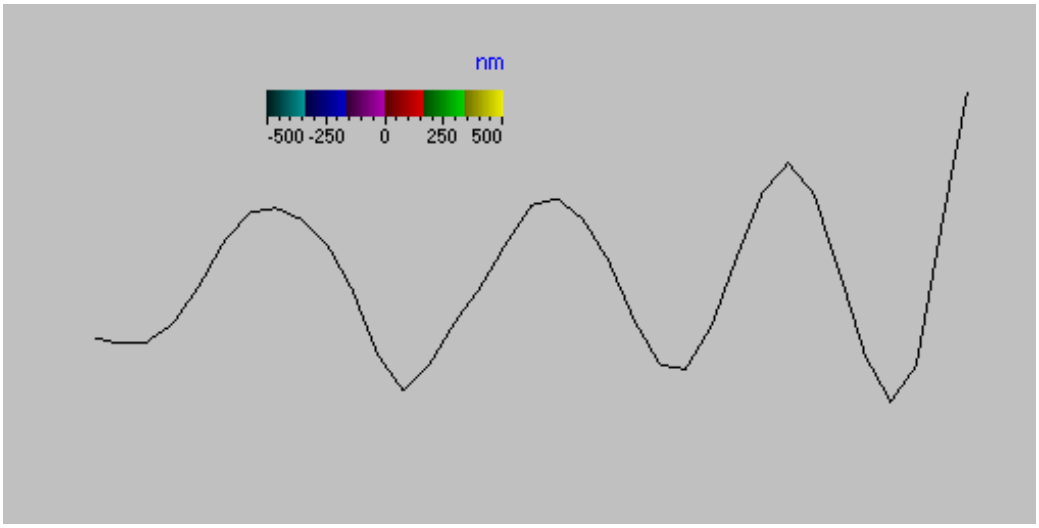


Figure 7.5 Frequency spectra obtained following a scan of #35 (unloaded) endosonic file a) at generator power setting 4 and b) at generator power setting 3. When operated at power setting 4, large peaks are obtained at the fundamental oscillation frequency of 27.50kHz and at the second harmonic (82.50kHz). The spectrum obtained at power setting 3 is more usual and consists of a single large peak at the fundamental oscillation frequency of 27.50kHz. The peak at 82.50kHz is small and contributes little to the overall motion of the file.

a)



b)

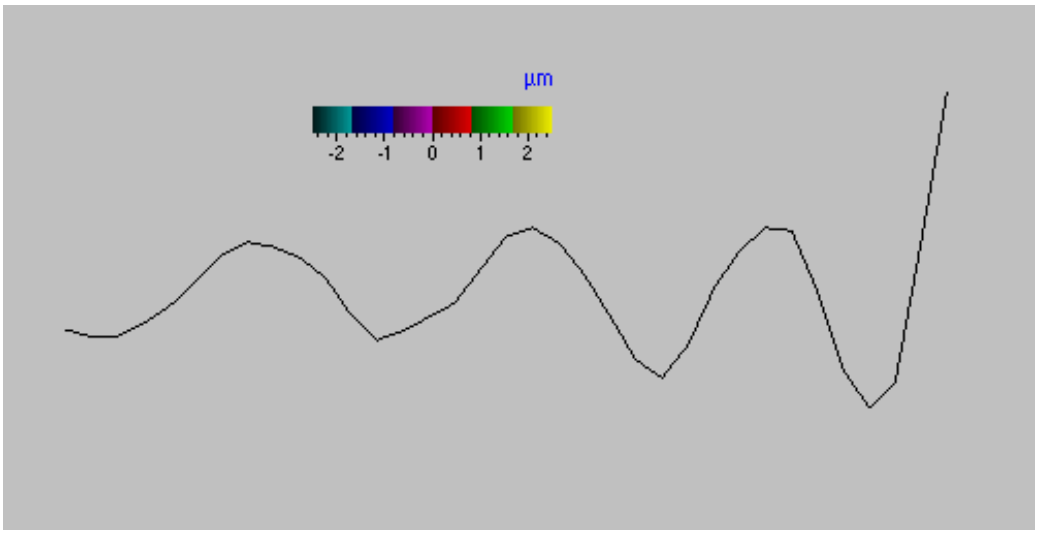


Figure 7.6 3D mesh representation of the second harmonic vibration data for a #35 file. a) At power setting 3 the maximum vibration displacement amplitude is no greater than 500 nanometers (0.5×10^{-6}m). b) At power setting 4 the maximum vibration displacement amplitude is 2.5 micrometers (2.5×10^{-6}m). The energy used to drive this harmonic is no longer available for driving the instrument at the fundamental frequency and results in a decrease in the overall file displacement amplitude.

Laser vibrometry enables the oscillation frequency and the displacement amplitude at any point along the length of the file to be determined. Therefore, by using the radius of the file along its length, the corresponding streaming velocity may be calculated accurately based on the laser vibrometer data. It has also been shown that the hydrodynamic shear stress may be expressed in terms of the kinematic viscosity of the fluid η, the oscillation frequency, ω, the displacement amplitude, ε_0, the radius of the file, a and the boundary layer thickness, δ, as given by;

$$\tau = \frac{\eta\omega\varepsilon_0^2}{a\delta} \qquad [7.2]$$

where τ is the hydrodynamic shear stress and ω is 2π times the file oscillation frequency. As with streaming velocity, accurate data for ε_0 and ω, obtained via laser vibrometry, would enable the generated shear stresses to be accurately calculated and their potential effect maximised.

It is unknown at present how the unloaded K-file vibration data will relate to the oscillation characteristics of the files when assessed under loaded or constrained conditions (i.e. more clinically realistic circumstances). An investigation to assess the vibration characteristics of unloaded ultrasonic scalers, using laser vibrometry, identified high variability in scaler tip performance, even between instruments of the same design (Lea *et al*. 2003a). It was also found that the application of various loads significantly affected the scalers' vibration characteristics (Lea *et al*. 2003b). By analogy, it seems reasonable to assume that any load or constraint placed on the K-files will lead to a diminution of its vibration displacement amplitude. The sharp drop in displacement amplitude observed with the #35 K-file at power setting 4 may not occur or, conversely, more such drops may become evident.

Thermal Imaging

7.9 Heat Generated during Ultrasonic Instrumentation

During normal operation, dental scaler tips have a continuous stream of water flowing over them. As well as potentially assisting in the cleaning process (through the generation of cavitation and acoustic streaming forces), this flow of water helps to regulate the heat generated at the tip / tooth interface. This is primarily achieved via the constant removal of the frictional heat through forced convection (Eastop & McConkey 1993). As the water flows over the surface of the tooth the heat generated, due to the friction between the scaler tip and the tooth, is conducted into the water and carried away by the bulk fluid movement.

An increase in water flow rate was generally shown to reduce the maximum heat generated at the tip/tooth contact point (Figure 6.26). An increase in generator power setting generally corresponds to an increase in scaler tip displacement amplitude (Lea *et al*. 2003a&b) and tip velocity. Frictional force depends only on the normal contact force and is independent of the relative sliding speed between the two surfaces. Therefore, any increase in tip velocity as it traverses the tip surface, due to an increase in generator power setting, should not affect the frictional force. However, the data obtained show that an increase in generator power setting often leads to an increase in heat generation (Figure 6.25). At lower power settings, scaler tip displacement amplitude is relatively small and the water flows down the length of the tip, to the treatment site, regulating heat generation as described previously. At higher power settings, the water tends to be dispersed as an aerosol before it reaches the working end of the tip (Lea *et al*. 2002b) and so provides little cooling. Since frictional force is directly proportional to the load perpendicular to the tooth surface (due to the contact of the moving

scaler tip), when greater tip contact loads are applied the frictional force will increase, causing an increase in the heat generated and detected. For both scaler systems an increase in contact load generally corresponded to an increase in heat generation and, at high power settings, caused large increases in the temperature measured (Figure 6.24). Data for the Mini Piezon show that the largest temperature increases (greater than 25°C) occurred when instrumentation conditions of high power with 0.50N load (10 and 20mls/min water flow rate) and 1.00N load (all water flow rates) were used. For all other operating conditions, the overall temperature increase at the tooth surface was less than 10°C. The data also show that a temperature increase of 25°C occurred for the SPS when instrumentation conditions of high power and 1.00N load were used with 10mls/min water flow rate. These data indicate that high generator power settings, in conjunction with low water flow rates and large loads, should be avoided to reduce the risk of large temperature increases.

7.9.1 Risk of tooth damage

It was not possible to determine the pulpal temperature rise using the thermal imaging system. However, enamel and dentine are poor thermal conductors and form an effective thermal barrier, which prevents large pulpal temperature rises (Walmsley *et al*. 1986c). This is due to the low thermal conductivity and thermal diffusivity of both enamel and dentine (Brown *et al*. 1970). Previous investigation into pulpal temperature rise (*in vitro*), due to heat generated during ultrasonic descaling procedures, reported a maximum pulpal temperature increase of approximately 8°C (Walmsley *et al*. 1986c). However, this investigation was performed under conditions of 14g (0.14N) load, medium generator power setting and with a water flow rate of 20mls/min. With greater loads of 0.50N and 1.00N, high generator power setting and water

flow rates of 10mls/min, as utilised in this investigation, it is likely that pulpal temperatures exceeding 8°C may be reached. It has been shown that pulp temperature increases of 5.5°C and 11°C caused 15% and 60% of healthy, Macaca rhesus monkey, dental pulps irreversible pulpitis, respectively (Zach & Cohen 1965) so the temperatures encountered in this study would pose a potentially serious threat to pulp vitality. However, the temperature rises observed here are not truly indicative of those observed *in vivo*. During clinical instrumentation, the scaler tip is moved constantly over the surface of the tooth and so this prevents spot heating from occurring. Blood flow through the pulp chamber and the diffusion of heat into the surrounding bone may also reduce the anticipated pulp temperature rise (Walmsley *et al*. 1986). Heat conduction relies on the presence of a temperature gradient, across a body, for heat energy to flow from the high temperature region to the low temperature region. Therefore, the heat energy at the tooth surface must be greater than body temperature (approximately 37°C) to be conducted to the pulp. Large temperature increases may not just be potentially damaging to dental pulp. Teeth subjected to sudden temperature increases, followed by temperature decreases, may be susceptible to crack development in their enamel (Brown *et al*. 1970). The largest temperature rises are observed for conditions of large load, high generator power and low water flow rates and these should be avoided to reduce the risk of pulpal damage and enamel cracking.

A possible source of error in this investigation is that the measurements were not performed in a temperature regulated room suggesting body heat and temperature fluctuations due to the time of day could affect acquired data. However, throughout the investigation the room temperature was determined to be between 20°C and 22°C. Fluctuations in temperature between measurements would therefore be minimal.

The Terephthalate Dosimeter

7.10 Cavitation around Ultrasonic Scalers

Cavitation, which potentially occurs in the cooling water as it flows over the insert probe, has long been thought to aid in the removal of substances from tooth surfaces (Walmsley *et al*. 1988 & 1990; Laird & Walmsley 1991). Cavitational activity around dental ultrasonic instruments may be evaluated by observing the effects of cavitation on both plaque removal and on the root surface (Walmsley *et al*. 1984, 1985, 1988 & 1990) and by attempting to quantify the amount of cavitation around the instrument itself using techniques such as sonoluminescence, the Weissler reaction and Fricke's dosimeter (Ahmad *et al*. 1987 & 1988, Lumley *et al*. 1988, Walmsley *et al*. 1986b & 1991, Mason *et al*. 1989).

This investigation has demonstrated that chemical reactions resulting from cavitational activity do occur around dental ultrasonic scaler tips under certain operating conditions and is in agreement with previous work (Mason *et al*. 1989). Tip shape and generator power setting were both shown to have an effect on radical production. The geometry of the scaler tips affects the magnitude of their vibration displacement amplitude. The TFI-10 and TFI-3 style scaler tips have greater vibration displacement amplitudes, at a given power setting, than the TFI-1 scaler tip and this is reflected in the results obtained in this study. The TFI-10 style tips produced cavitation (that could be detected) at the high generator power setting and the TFI-3 style tips produced cavitation at both medium and high generator powers. The TFI-1 tips produced no detectable cavitation at any generator power setting.

Sonication time was also shown to affect cavitation production (Figure 6.27). For the TFI-10 and TFI-3 tips, [$^{\bullet}$OH] production increased with time. Regression analysis of the data showed that this increase was linear, with R^2 values of between 0.97 and 1. However, although hydroxyl radical production increased with increasing sonication time the rate of radical production was approximately the same for each sonication period.

Variation in the amount of cavitation detected was also shown to occur between tips of the same style. The amount of cavitation produced / detected around TFI-3 tip 2 was less than that detected around the other two tips and statistical analysis demonstrated that in fact all three tips behaved significantly different to each other. TFI-10 tip 2 produced cavitation at the medium power setting, whereas tips 1 and 3 did not.

This variation in the amount of cavitation produced / detected, between tips of the same design (for given generator power setting / sonication time), is likely to be due to the variation in the vibration displacement amplitude of the tips that has been shown to occur (Lea *et al*. 2002a, 2003a&b). Differences in the amount of cavitation generated between tips of different styles may be due to the differences in the surface areas of the tip surfaces transmitting the ultrasound into the terepthalic acid solution. Following experimentation, the TFI-3 scaler tips were observed to have regions of increased wear on their surfaces (Figure 7.7). It is thought that these regions correspond to positions on the scaler tip of high cavitational activity and this warrants further investigation.

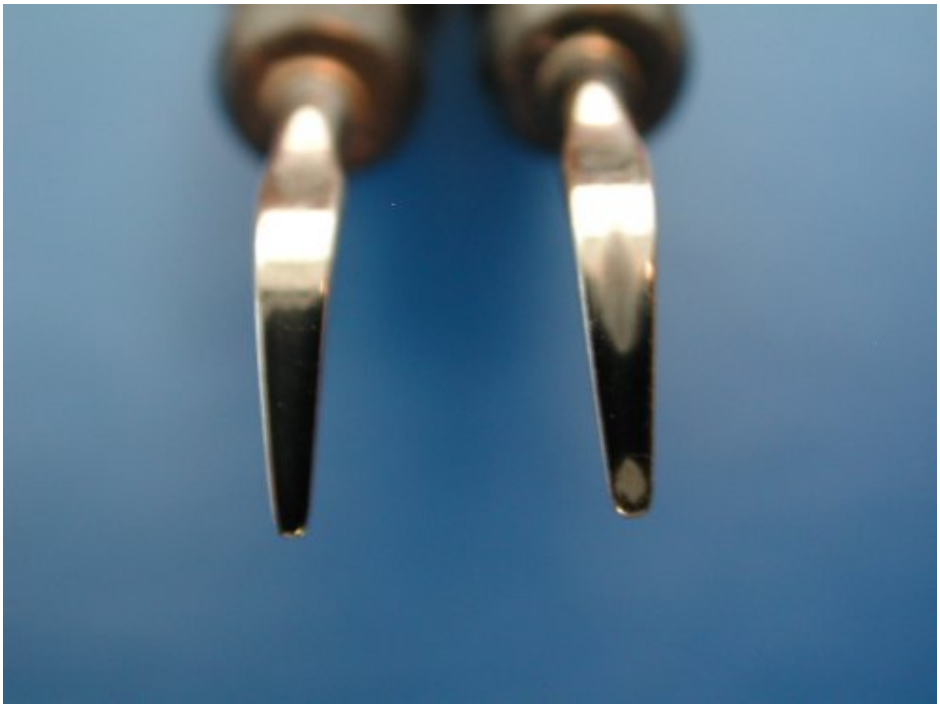


Figure 7.7 An unused TFI-3 scaler tip (left) and a TFI-3 scaler tip following sonication (right). Following instrumentation, TFI-3 scaler tips were observed to have regions of increased wear on their surfaces. These regions may correspond to positions on the scaler tip of high cavitational activity.

7.11 Cavitation around Powered Toothbrushes

Powered toothbrushes have vibration frequencies of up to 262.5Hz (Lea *et al*. 2004c). Although the destructive properties of cavitation are normally observed at ultrasonic frequencies, some researchers claim cavitational activity occurs around sonic toothbrushes (Engel *et al*. 1993; O'Beirne *et al*. 1996). Others have maintained a more sceptical view about the contribution of cavitation to the cleaning process (Khambay and Walmsley 1995; Walmsley 1997).

Blanco *et al*. (1997) suggested that the high frequency bristle motion of sonic toothbrushes, in a fluid environment, generates an alternating pressure field producing, what is referred to less specifically as 'dynamic fluid activity' and 'acoustic effect'. Such phrases are used by toothbrush manufacturers in their advertising literature (Sonicare Elite web site 2003; Oral B web site 2003). However, the terephthalate dosimeter has demonstrated that chemical reactions resulting from cavitational activity do not occur to any significant extent around the commercially available powered toothbrushes investigated here. To ensure the system was working correctly measurements were performed on a TFI-3 ultrasonic scaler insert, around which cavitational activity was readily detected. Operating the toothbrushes for periods up to 20 minutes resulted in no radical activity being detected.

7.12 Impact of the Current Work on Previous Research

Studies into the clinical use of the ultrasonic scaler commonly assess both the clinical efficacy of the instrument and the damage the instrument may potentially cause to dental structures. Such investigations have been performed since the introduction of the ultrasonic scaler in the

1950's and our understanding of this instrument since this time has generally built upon these original investigations.

Using laser vibrometry, the vibration characteristics of ultrasonic scalers and the effects of factors such as water flow rate, generator power setting and load have been assessed. Water flow rate and load have both been shown to have a significant effect on the longitudinal vibration displacement amplitude of an ultrasonic scaler, whereas generator power setting has been shown to have a more variable effect which is dependent on the type and style of instrument used. This new knowledge demonstrates quite clearly that attempts to compare ultrasonic instruments to hand or other ultrasonic instruments must specify quite clearly the exact operating conditions under which the scaler is being used. If one views the presently available literature with this in mind it becomes apparent that, from the start, there has been inadequate standardisation amongst investigators who assess these instruments.

McCall & Szmyd (1960) were amongst the first to clinically evaluate the ultrasonic scaling technique using a range of conventional and ultrasonic instruments and 240 military subjects from Randolph and Lackland Air Force Base dental clinics. However, apart from the legend to 'Figure 2' in their article which tells us which scaler tips are utilised in the investigation (P-7, P-1, P4-R, P4-L, P-3), we are told nothing further about how the instrument is utilised. Details regarding generator power setting, whether or not water was flowing over the working tip or even which generator was utilised for driving the instruments are simply not included.

This lack of detail regarding the operating conditions of ultrasonic scalers is not unusual. Goldman (1961), compared healing following ultrasonic and hand instrumentation and stated,

"For the ultrasonic method, a blunt or small scaler was used for debridement, whereas a larger straight tip was used for scaling." No information regarding the operating conditions of the instrument was provided. Similarly, Stende & Schaffer (1961) state that in their investigation two sets of ultrasonic instruments are utilised, including "Ultrasonic (regular) # P-2L, P-2R, P-4L, P-4R, P-3 / Ultrasonic (similar to McCall) # P-10, P-11L, P-11R." However, as with the research of McCall & Szmyd (1960) they do not discuss how the instrument is utilised.

Moskow & Bressman (1964) improve the reporting of ultrasonic scaler investigations by describing in more detail the operating parameters of the ultrasonic technique. In their work they wrote "…half the number of teeth to be extracted on any patient were scaled with ultrasonic instruments (no. P-7, P-41, P-4r, P-9). In these instances, the power control knob was set on high and the instrument tuned to its optimum efficiency. A free flow of water was used during the operation." However, this does not explain what is meant by a generator power that is described as 'set on high' or whether the flow of water over the various tips was the same in each case. Nor does this work inform us under what load scaling procedures are performed. The work contained within this thesis has demonstrated that 'high power' under various loads and with various designs of tips may correspond to a wide spectrum of displacement amplitudes (Lea *et al*. 2003b). Water flow rate too has been shown to significantly affect the vibrations of dental ultrasonic scalers (Lea *et al*. 2002b). This makes it difficult to perform a meaningful analysis of the results produced in this investigation.

Although the work of Moskow & Bressman (1964) appeared to signify the start of more accurate recording of the instrumentation parameters it was, unfortunately, not so. Jones *et al*. (1972) describe the ultrasonic instruments used in their investigation as, "…(Cavitron 660 and

700 with the use of tips P10, P11-R, P11-L only)" and Donze *et al*. (1973) mention only that they utilise a Cavitron unit. In neither article are any other details given regarding the instrumentation conditions. Pameijer *et al*. (1972) described their instrumentation conditions as, "One third of this [smooth, polished dentin] surface area was treated with hand instruments, one third ultrasonically and one third served as a control… A pressure simulating the clinical procedure was applied and each part was subject to twenty strokes. The direction of the strokes was approximately perpendicular to the direction of polishing." We are further told that the ultrasonic instrument is "A Cavitron Unit with a new P 10 tip." However, we are not informed of key operating conditions such as whether water was utilised, what loads the tips were placed under or what generator power setting(s) is/are used. Work by Wilkinson & Maybury (1973) reported, "…two teeth were debrided with an ultrasonic instrument using Cavitron tips P11L and P11R with tuning, water supply and medium power setting as recommended by the manufacturer…" Once again, there is no specific information regarding the operating conditions of the instrument.

By the late 1970's, standardisation of instrumentation conditions had still not been achieved. D'Silva *et al*. (1979) described their ultrasonic instrumentation conditions as, "A Cavitron unit with a new P10 insert… used with medium power setting with 12 strokes brushed lightly over the tooth surface." Torfason *et al*. (1979) introduce a new level of instrumentation variability in their work comparing hand and ultrasonic instrumentation. The four operators used in the investigation are given a Cavitron Model 600 unit, in conjunction with three Cavitron P-10 tips. However, we are then informed, "The setting of the power, tuning and water irrigation was adjusted to the preference of each operator." Within this report we are not

told what these preferences are and, again, this means that meaningful data evaluation is difficult to make.

During the 1980's the importance of reporting the exact ultrasonic instrumentation conditions was realised. Work by Walmsley *et al*. (1984, 1986a-c, 1988, 1990) demonstrate accurate recording of all ultrasonic operating parameters including descriptions of the exact tips and generators used, the load under which the instruments were used and the volume of water flowing over the working tip. Another step forward was the assignment of 'low', 'medium' or 'high' generator power settings based on the vibration displacement amplitude of the oscillating tip, rather than simply on the position of the power control knob. This produced greater standardisation of ultrasonic instrumentation, allowing data to be obtained that would enable fair and meaningful comparisons to be made. It was through this standardisation of instrumentation that the variability in vibration characteristics of dental ultrasonic scalers was first clearly demonstrated (Walmsley *et al*. 1986a&b).

Despite the importance of stating the exact operating conditions of ultrasonic scalers being demonstrated, many subsequent researchers failed to report accurate details or to perform their research in a properly standardised manner. When investigating the 'effects of curet and ultrasonics on root surfaces', Cross-Poline *et al*. (1995) stated that for ultrasonic instrumentation "only the high power setting was used throughout the experiment." In their work we are told nothing of the loads or volume of cooling water (if any) used during instrumentation.

When evaluating the working parameters of magnetostrictive and piezoelectric ultrasonic systems, Flemmig *et al*. (1998a&b) consistently refer to generator power settings of 'low', 'medium' and 'high' without measuring the displacement amplitudes of the tips at these settings. Although they measure accurately the loads, instrumentation times and tip / tooth angulations, they describe the amount of cooling water used as "…operated according to the manufacturer's instructions under profuse water irrigation; i.e. medium setting, for cooling of the tip." By failing to standardise the amount of water flowing over each of the instruments and using the phrases 'low, medium and high power', almost no meaningful comparison can be made between these different styles of instrument. One of the conclusions of both studies is that, of all the operating parameters investigated, generator power setting appeared to play a minor role in affecting defect depth and volume. The investigations in this thesis may help to explain these findings since it has been shown that, for piezoelectric and certain magnetostrictive scaling instruments under loads of 0.25N, 0.5N and 1.0N (25g, 50g and 100g) there is generally no linear increase in scaler tip vibration displacement amplitude with increasing generator power setting. If generator power setting has no predictable effect on the oscillation of the scaler tip, it is unlikely to have a large contribution to the production of defect depth and volume which are themselves affected by the oscillations of the scaler instrument. For example, consider the data acquired from the load investigations (Section 6.6) for the Piezon Master 400 generator used in conjunction with P-tip 1 under 0.5N load and with constant water flow rate of 20ml/min. Relate the 'low', 'medium' and 'high' generator power settings used by Flemmig *et al*. (1998a&b) to power settings 2, 5 and 10 in this thesis. The tip vibration displacement amplitudes measured in this thesis are; power setting 2: 18.43 ± 0.24μm, power setting 5: 22.31 ± 0.75μm and power setting 10: 20.67 ± 1.69μm. There is a maximum difference of only 3.9μm between vibration displacement amplitudes at all three

power settings and the 'medium' power setting (setting 5) has greater mean maximum displacement amplitude than that observed at the 'high' power setting (setting 10). It is also worth noting that both the piezoelectric and magnetostrictive systems were evaluated using a single tip per system only and it is, therefore, impossible to ascertain whether the results obtained in these studies are an accurate reflection of instruments of their type. The work of Schmidlin *et al*. (2001), to assess tooth substance loss resulting from mechanical, sonic and ultrasonic root instrumentation, compared a magnetostrictive ultrasonic scaling system to hand and sonic instruments. The operating conditions for the sonic and ultrasonic instruments are described as "…done at application pressure of 40g…, at high power settings, for 120s…" There is a slight discrepancy with this statement in the Discussion section where it is stated "…forces between 20-40g were chosen for the power-driven instruments in this study." This use of 'high power settings' again prevents meaningful comparisons between the power-driven instruments.

Work by Busslinger *et al*. (2001), to compare (*in vitro*) magnetostrictive and piezoelectric ultrasonic systems, is in some places quite vague. For example, although they measure the instrumentation loads accurately, it is not until approximately half way through the Discussion section that we are informed that a 'medium' power setting was utilised throughout the investigation. Furthermore, we are told, "The instrumentations with the ultrasonic devices were carried out under water-cooling, where the Cavitron device had internal cooling, and the piezoelectric ultrasonic inserts had to be cooled with an external water source from a 3-in-1 spray from a dental unit." There is no information regarding water flow rates utilised and whether they were the same for each instrument. Unusually, compared to the other researchers discussed here, Busslinger *et al.* (2001) acknowledged that the use of

a ‘medium’ power setting means “there was no way of knowing if the two electric devices delivered similar power at the same settings. In this way the power of the piezoelectric device could have been higher than that of the magnetostrictive device causing more root damage which was interpreted as a higher Ra [average tooth surface roughness] value.” The data obtained in the loading investigation (Section 6.6) demonstrate that at power settings 5 and 6 (i.e. approximately medium power), the mean displacement amplitude of the three P-tips with the Piezon Master 400 piezoelectric device was 21.0μm (power setting 5) and 20.7μm (power setting 6). The mean vibration displacement amplitudes of the TFI-10 and TFI-3 tips in conjunction with the Cavitron SPS generator were; TFI-10 tip: 10.5μm (power setting 5) and 11.5μm (power setting 6) and TFI-3 tip: 12.6μm (power setting 5) and 13.3μm (power setting 6). This demonstrates that the vibration displacement amplitudes of the piezoelectric device is higher than the vibration displacement amplitudes for the magnetostrictive devices. As a consequence, the suggestion of Busslinger *et al*. (2001) that the greater root damage occurred with the piezoelectric device may be explained using the data within this thesis. The piezoelectric device produces greater displacement amplitude at the medium power settings and therefore, theoretically, may provide a greater ‘chipping’ action than the magnetostrictive system. It is worth noting, however, that the mean displacement amplitudes of the three P-tips with the Mini Piezon piezoelectric device (from the loading project) are 11.0μm (power setting 5) and 14.4μm (power setting 6). If we compare the magnetostrictive data, above, with these values we see there is little difference and now we may not be able to explain the findings of Busslinger *et al*. (2001) using the differences in displacement amplitude. This situation demonstrates how important it is to standardise measurements using vibration displacement amplitude rather than generator power setting which can have, for certain systems, little bearing on how the working tip is operating.

CHAPTER 8

CONCLUSIONS

8.1 The Scanning Laser Vibrometer

8.1.1 Specific Conclusions

Water flow rate and scaler tip vibration

Water flow rate was shown to affect the magnitude of scaler tip vibration displacement amplitude. Water flow was found to cause varying responses in scaler tip displacement amplitude, despite tips of the same design being utilised throughout the investigation.

Displacement Amplitude of Unloaded and Loaded Ultrasonic scalers

These studies demonstrated further that tip displacement amplitude can vary significantly between generator type (piezoelectric or magnetostrictive), tips of different designs and even between tips of the same type used with the same generator. Individual tips, under different loading conditions, were also shown to produce different outputs. Studying several generator units of the same type would indicate whether the generators used in this study were typical. Research of this type may enable the control and production of dental ultrasonic inserts with a more standardised and better-understood performance, providing operators with greater control during both research and clinical procedures.

Wear and Scaler Tip Displacement Amplitude

There is a theoretical link between clinical scaling efficiency and the magnitude of the scaler tip's vibration displacement amplitude. The wear investigation demonstrated that tip wear reduces the magnitude of the oscillation of ultrasonic scaling tips and so, therefore, may

potentially reduce the efficiency of the scaling system. Clinicians should be aware that the performance of their scaling instruments might be limited by physical wear of the tips.

The Vibration Patterns of Endosonic K-Files

Laser vibrometry was used to analyse the vibration patterns of unloaded ultrasonic files, to evaluate the effect of generator power setting variation on individual files and to observe the differences in oscillation characteristics between different sized files. The positions of nodes and antinodes along the length of the files were also determined. Future work will investigate the effects of loading and constraint on file vibration to more closely simulate the clinical situation. A larger number of files and generators require investigation to ensure that those studied here were typical of their type. This work could lead to the introduction of better designed instruments for clinical use. Such instruments would not only produce more efficient oscillations for root canal filing but the effectiveness of the associated biophysical streaming forces which enhance debridement and irrigation, may be maximised.

8.1.2 General Conclusions

The scanning laser vibrometer has allowed us to study, in detail, many of the vibrational characteristics of dental ultrasonic scaler tips. Information such as vibration velocity and frequency of oscillation (fundamental frequency and higher order harmonics) may be measured and displayed rapidly. From the velocity data, the displacement amplitude of the scaler tips may be calculated. The ability to superimpose data over a video image of the target object allows the observation of nodes and anti-nodes along the length of the probe surface. The 3D mesh display facility enables the motion of the probe to be viewed at much reduced velocities, making the visualisation of probe motion much easier to understand and study.

This research has highlighted the high variability in vibration displacement amplitude between tips of different designs and even tips of the same design. Such variability was demonstrated through different tip responses to varying water flow rates, varying generator power settings and varying scaler tip / tooth contact loads. This vibration displacement amplitude variability was also suggested as the reason for the observed differences in the amount of cavitation produced around tips of the same design.

Increasing our understanding of the motion of the probes under various operating conditions will allow us to better understand how ultrasonic scalers work and may ultimately lead to aiding the design of more effective instruments for clinical use.

8.2 Thermal Imaging

Due to the non-invasive nature of the thermal imaging system, which relies only on the emission of thermal infrared radiation to operate, it may be of interest to repeat the investigation *in vivo*. This would facilitate the monitoring of temperature rise, on the external surface of the tooth, during ultrasonic instrumentation under standard clinical conditions. Heat generation is minimised by using light loads in conjunction with low/medium generator power settings and water flow rates of at least 20mls/min. Care must be taken to ensure adequate water is present at the site of instrumentation to prevent patient discomfort due to excessive heating.

8.3 The Terephthalate Dosimeter

Cavitation around Ultrasonic Scalers

This investigation demonstrated that under certain operational conditions cavitation occurs around dental ultrasonic scalers. The terephthalate dosimeter method was effective in measuring hydroxyl radical concentration produced due to cavitation from scaler tips. Increased cavitational activity occurred at higher power settings and with increased operating time. The TFI-3 tip working at high power resulted in the most cavitational activity. The dimensions of the tip and the generator power setting are both important factors that affect the production of cavitation.

Cavitation around Powered Toothbrushes

Using the terephthalate dosimeter, it was demonstrated that chemical reactions resulting from cavitational activity do not occur to any significant extent around the commercially available powered toothbrushes investigated. To ensure the system was working correctly measurements were performed on a TFI-3 ultrasonic scaler insert, around which cavitational activity was readily detected. Operating the toothbrushes for periods up to 20 minutes resulted in no radical activity being detected.

CHAPTER 9

FURTHER WORK

Scanning Laser Vibrometer

9.1 Design of New Scaler Instruments for Clinical Use

The research contained in this thesis indicates that the vibration of ultrasonic scaler tips is highly variable, even between tips of like styles and that for certain scaler tip designs vibration displacement amplitude does not increase linearly with increasing generator power. These factors can make it difficult for clinicians to familiarise themselves with a particular design of instrument and for the researcher to standardise their investigations without physically measuring the scaler tip displacement amplitudes.

A natural progression of this work is to design a new ultrasonic scaler that has a more consistent performance. Laser vibrometry may be used to measure the vibration displacement amplitude of the scaler tips and, by breaking open the instrument handpiece, it may be possible to measure the vibration characteristics of the piezoelectric crystal / magnetostrictive stack used to drive the instruments. This would help to determine whether the variability occurs at the point where the ultrasound is generated or if it is related to the manner in which the scaler tip is connected to the crystal / stack.

9.2 Further Evaluation of Endosonic K-Files using SLV

Work has been performed, using the SLV, to assess the vibration characteristics of unloaded ultrasonic K-files (Lea *et al*. 2004b). In the initial investigation only one generator was assessed with two different sized, unloaded, K-files. When used clinically, K-files may be constrained by the walls of the root canal. To advance our understanding of these instruments their vibration characteristics should now be assessed whilst either loaded or constrained.

9.3 SLV to Correlate Tip Vibration with Cavitation Production

It has been demonstrated that cavitation occurs around ultrasonic scaling instruments (Lea *et al*. 2005). This work indicated that different styles of instrument tip and even different tips of the same style produced different hydroxyl radical concentrations (corresponding to greater or lesser cavitation production). In the discussion of these results, it was suggested that the reason for these observations was due primarily to the variation in tip vibration displacement amplitude, which has also been observed between different styles of instrument tip as well as tips of the same style (Lea *et al*. 2003a & b). Further work should be performed, with unused tips, to determine whether or not there is any correlation between scaler tip displacement amplitude and cavitation production. Since cavitation investigations are performed with the instrument tip operating within a cuvette of TA solution, SLV vibration displacement amplitude measurements should similarly be performed with the working tip immersed in a cuvette of solution (possibly water).

Thermal Imaging

9.4 Thermal Imaging of Scaling Procedures *In Vivo*

The thermal imaging investigation described within this thesis (Section 5.13 and Lea *et al*. 2004b) was performed *in vitro* using experimental conditions that could have been more clinically realistic. Since thermal imaging systems do not emit radiation but only detect emitted thermal radiation it may be possible to repeat the investigation using two different methods.

Method 1

Instead of the scaler tip being fixed in position and generating a localised hot spot during instrumentation, it may be possible for an operator to manoeuvre the tip of the instrument over the surface of the tooth. The load cell to which the tooth is attached is connected to a data logger which outputs load values, in quarter second intervals, throughout the course of the experiment to an Excel spreadsheet. Using this data it would be possible to estimate the mean load applied during the data acquisition period.

Method 2

Thermal imaging systems detect emitted thermal radiation and as such it may be possible to repeat the investigation on clinic. The clinician could practice their technique on an *in vitro* tooth model to gauge the typical load used. A thermal imaging system could then be used during a scaling session to estimate the heat generated in the clinical situation.

The Terephthalate Dosimeter

9.5 Terephthalate Dosimeter to Assess Cavitation around Loaded Scalers

The initial investigation to determine whether or not cavitation occurs around ultrasonic scaling instruments (Lea *et al*. 2005), was performed with the instruments operating under unloaded conditions (insofar as the tips were not contacted against the surface of a tooth, although they were in contact with the TA solution, which would have affected their vibration patterns). Although 'unloaded' measurements may provide a useful indication as to how the instruments perform, it is more clinically relevant to perform measurements with the scaler tips under load, i.e. in contact with tooth or root surfaces. Therefore, cavitation measurements (or more specifically hydroxyl radical concentration measurements) should be performed with the scaler tip contacted against a tooth surface during sonication.

9.6 Does Cavitation Occur in the Flowing Water Supply?

The method described in the terephthalate dosimeter investigation (Section 5.14 and Lea *et al*. 2004e & 2005) and the suggested continuation work described in 9.5 above, use cuvettes that contain a predetermined quantity (2.5mls) of TA solution. Clinically, the cooling water flows over the length of the tip, from within the handpiece, and over the treatment site, from which it removes heat and aids in the removal of debris. This water does not normally accumulate in large pools, but rather flows in a continuous stream away from the treatment site. The experimental methodology should therefore be adapted to be more clinically realistic.

The cooling water supply was provided via a sealed tub fitted with a plunger and a water escape hose connected to the back of the ultrasound generator. The pressurised tub should now be filled with TA solution rather than water. This would then pass through the ultrasound generator and instrument handpiece and over the instrument tip. Terephthalic acid is only weakly acidic and so there should be no damage to the internal mechanisms of the instruments. The TA solution that flows over the working tip should be collected in a vessel that enables fluid volume to be accurately measured. Sonication should proceed until the desired volume of TA solution has been obtained. The flow rate used should be selected such that the production of aerosol is minimised to prevent damage to skin or clothing and to maximise the quantity of TA solution collected.

9.7 Is Tip Surface Wear Due to Cavitation?

It was interesting to note in the original investigation that areas of wear had occurred on the surface of the scaler tip following sonication in the TA solution (Figure 7.4). Further investigation to ascertain whether or not it was cavitation that caused this increased wear should be performed.

REFERENCES

Ahmad M, Pitt Ford TR & Crum LA. Ultrasonic debridement of root canals: an insight into the mechanisms involved. Journal of Endodontics, 1987a; **13**: 93-101.

Ahmad M, Pitt Ford TR & Crum LA. Ultrasonic debridement of root canals: acoustic streaming and its possible role. Journal of Endodontics, 1987b; **13**: 490-499.

Ahmad M, Pitt Ford TR & Crum LA. Ultrasonic debridement of root canals: acoustic cavitation and its relevance. Journal of Endodontics, 1988; **14**: 486-493.

Ahmad M. An analysis of breakage of ultrasonic files during root canal instrumentation. Endodontics and Dental Traumatology, 1989; **5**: 78-82.

Ahmad M, Pitt Ford TR, Crum LA & Wilson RF. Effectiveness of ultrasonic files in the disruption of root canal bacteria. Oral Surgery, Oral Medicine and Oral Pathology, 1990; **70**: 328-332.

Ahmad M, Roy A & Kamarudin AG. Variations in the power output of the Piezon-Master 400 ultrasonic endodontic unit. International Endodontic Journal, 1994; **27**: 26-31.

Baab DA & Johnson RH. The effect of a new electric toothbrush on supragingival plaque and gingivitis. Journal of Periodontology, 1989; **60**: 336-341.

Badersten A, Nilveus R & Egelberg J. Effect of non-surgical periodontal therapy. 1. Moderately advanced periodontitis. Journal of Clinical Periodontology, 1981; **8**: 57-72.

Barnett ML, Gilman RM, Charles CH & Bartels LL. Computer based thermal imaging of human gingiva: preliminary investigation. Journal of Periodontology, 1989; **60**: 628-633.

Barnett SB, Rott H-D, ter Haar GR, Ziskin MC & Maeda K. The sensitivity of biological tissue to ultrasound. Ultrasound in Medicine & Biology, 1997; **23**: 805-812.

Benington IC, Biagioni PA, Briggs J, Sheridan S & Lamey P-J. Thermal changes observed at implant sites during internal and external irrigation. Clinical Oral Implants Research, 2002; **13**: 293-297.

Biagioni PA, Longmore RB, McGimpsey JG & Lamey P-J. Infrared thermography. Its role in dental research with particular reference to craniomandibular disorders. Dentomaxillofacial Radiology, 1996; **25**: 119-124.

Blanco VL, Cobb CM, Williams KB & Manch-Citron JN. In vitro effect of the Sensonic toothbrush on Treponema denticola. Journal of Clinical Periodontology, 1997; **24**: 318-323.

Bogy DB, Bouchard G, Chang WR & Talke FE. Use of the laser Doppler vibrometer to measure the surface topography of magnetic disks. Wear, 1986; **107**: 227-244.

Brand RW & Isselhard DE. Anatomy of Orofacial Structures. 6th Edition. 1998; Missouri, USA. Mosby. ISBN: 0-8151-1000-6.

Brown WS, Dewey WA & Jacobs HR. Thermal properties of teeth. Journal of Dental Research, 1970; **49**: 752-755.

Burman LR, Alderman NE & Ewen SJ. Clinical application of ultrasonic vibrations for supragingival calculus and stain removal. Journal of Dental Medicine, 1958; **13**: 156-161.

Busslinger A, Lampe K, Beuchat M & Lehmann B. A comparitive in vitro study of a magnetostrictive and a piezoelectric ultrasonic scaling instrument. Journal of Clinical Periodontology, 2001; **28**: 642-649.

Carter K, Landini G & Walmsley AD. Plaque removal characteristics of electric toothbrushes using an in vitro plaque model. Journal of Clinical Periodontology, 2001; **28**: 1045-1049.

Castellini P, Paone N & Tomasini EP. The laser Doppler vibrometer as an instrument for nonintrusive diagnostic of works of art: application to fresco paintings. Optics and Lasers in Engineering, 1996; **25**: 227-246.

Castellini P, Esposito E, Paone N & Tomasini EP. Non-invasive measurements of damage of frescoes paintings and icon by laser scanning vibrometer: experimental results on artificial samples and real works of art. Measurement, 2000; **28**: 33-45.

Catuna MC. Sonic energy. A possible dental application. Preliminary report of an ultrasonic cutting method. Annals of Dentistry, 1953; **12**: 256-260.

Cavalcanti BN & Rode SM. High-speed cavity preparation techniques with different water flows. Journal of Prosthetic Dentistry, 2002; **87**: 158-161.

Chaerle L, Van Caeneghem W, Messens E, Lambers H, Van Montagu M & Van Der Straeten D. Presymptomatic visualization of plant-virus interactions by thermography. Nature Biotechnology, 1999; **17**: 813-816.

Chapple ILC, Walmsley AD, Saxby MS & Moscrop H. Effect of instrument power setting during ultrasonic scaling upon treatment outcome. Journal of Periodontology, 1995; **66**: 756-60.

Chapple ILC & Gilbert AD. Understanding periodontal diseases: assessment and diagnostic procedures in practice. 2002; Quintessence Publishing Co. Ltd, London. ISBN: 1-85097-053-X.

Chiew SYT, Wilson M, Davies EH & Kieser JB. Assessment of ultrasonic debridement of calculus-associated periodontally-involved root surfaces by the limulus amoebocyte lysate assay: an in vitro study. Journal of Clinical Periodontology, 1991; **18**: 240-244.

Chilton NW, DiDi0 A & Rothner JT. Comparison of the clinical effectiveness of an electric and standard toothbrush in normal individuals. Journal of the American Dental Association, 1962; **64**: 777-782.

Clark SM. The ultrasonic dental unit: a guide for the clinical application of ultrasonics in dentistry and in dental hygiene. Journal of Periodontology, 1969; **40**: 621-629.

Collins WJN, Walsh TF & Figures KH. A handbook for dental hygienists. 4th Edition. 2000; Reed Educational and Professional Publishing Ltd, Oxford, UK. ISBN: 0-7236-1740-6.

Crandell CE & Hill RP. Thermography in dentistry: A pilot study. Oral Surgery, Oral Medicine & Oral Pathology, 1966; **21**: 316-320.

Cross WG, Forrest JO & Wade AB. A comparative study of tooth cleansing using conventional and electrically operated toothbrushes. British Dental Journal, 1962; **113**: 19-22.

Cross-Poline GN, Stach DJ & Newman SM. Effects of curet and ultrasonics on root surfaces. American Journal of Dentistry, 1995; **8**: 131-133

Daniels S, Kodama T & Price DJ. Damage to red blood cells induced by acoustic cavitation. Ultrasound in Medicine & Biology, 1995; **21**: 105-111.

Danser MM, Timmerman MF, Ijzerman Y, Van der Velden U, Warren PR & Van der Weijden GA. A comparison of electric toothbrushes in their potential to cause gingival abrasion of oral soft tissues. American Journal of Dentistry, 1998; **11**: S35-S39.

Danser MM, Driesen GM, Timmerman MF, Van der Velden U & Van der Weijden GA. A laboratory and clinical investigation comparing 2 oscillating/rotating electric toothbrushes. Journal of Clinical Periodontology, 2000; **27**: 277-283.

Deans J, Schmithals G & Carter LJ. An analysis of a thermal imaging method for landmine detection using microwave heating. Journal of Applied Geophysics, 2001; **47**: 123-133.

Debus J, Spoo J, Jenne J, Huber P & Peschke P. Sonochemically induced radicals generated by pulsed high-energy ultrasound in vitro and in vivo. Ultrasound in Medicine & Biology, 1999; **25**: 301-306.

Dhinojwala A, Lenore C & Granick S. Critique of the friction coefficient concept for wet (lubricated) sliding. Langmuir, 1996; **12**: 4537-4542.

Digby M, Duck FA, Lenz EJ & Price GJ. Technical note: Measurement of collapse cavitation in ultrasound fields. The British Journal of Radiology, 1995; **68**: 1244-1248.

Donze Y, Kruger J, Ketterl W & Rateitschak KH. Treatment of gingivitis with Cavitron or hand instruments: a comparative study. Helvetica Odontologica Acta, 1973; **17**: 31-37.

Donskoy D, Ekimov A, Sedunov N & Tsionskiy M. Nonlinear seismo-acoustic land mine detection and discrimination. Journal of the Acoustical Society of America, 2002; **111**: 2705-2714.

Drain LE. The laser Doppler technique. 1980; John Wiley & Sons Ltd., Norwich, Great Britain. ISBN: 0-471-27627-8.

Drisko CH. Root instrumentation: power driven versus manual scalers, which one? The Dental Clinics of North America, 1998; **42**: 229-244.

Drisko CL & the Research, Science and Therapy Committee of the American Academy of Periodontology. Sonic and ultrasonic scalers in periodontics. Journal of Periodontology, 2000; **71**: 1792-1801.

D'Silva IV, Nayak RP, Cherian KM & Mulky MJ. An evaluation of the root topography following periodontal instrumentation – a scanning electron microscope study. Journal of Periodontology, 1979; **50**: 283-290.

Duck FA, Baker AC & Starrit HC. Ultrasound in medicine. 1998; Institute of Physics Publishing; Bristol and Philadelphia. ISBN: 0-7503-0593-2.

Eastop TD & McConkey A. Applied Thermodynamics for Engineering Technologists. 5th Edition 1993; pp. 599-610 Harlow: Longman Scientific & Technical.

Eisberg R & Resnick R. Quantum physics of atoms, molecules, solids, nuclei and particles. 2nd Edition. 1985; John Wiley & Sons, New York. ISBN: 0-471-87373-X.

Elliot JR. A comparison of the effectiveness of a standard and electric toothbrush. Journal of Periodontology, 1963; **34**: 375-379.

Elmer F-J. Nonlinear dynamics of dry friction. Journal of Physics A: Mathematical and General, 1997; **30**: 6057-6063.

Engel D, Nessly M, Morton T & Martin R. Safety testing of a new electronic toothbrush. Journal of Periodontology, 1993; **64**: 941-946.

EPSRC Engineering Instrument Pool, Brief Technical Guide (Version 2.7 of 17/4/2002). Available at www.eip.rl.ac.uk/loanpool.htm (Accessed: 25/5/02).

Evans D, Reid J, Strang R & Stirrups D. A comparison of laser Doppler flowmetry with other methods of assessing the vitality of traumatised anterior teeth. Endodontics and Dental Traumatology, 1999; **15**: 284-290.

Ewen SJ. Ultrasound and periodontics. Journal of Periodontology 1960; **31**, 101-106.

Ewen SJ. The ultrasonic wound – some microscopic observations. Journal of Periodontology, 1961; **32**: 315-321.

Fang X, Mark G & von Sonntag C. OH radical formation by ultrasound in aqueous solutions Part 1: the chemistry underlying the terephthalate dosimeter. Ultrasonics Sonochemistry, 1996; **3**: 57-63.

Flemmig TF, Petersilka GF, Mehl A, Rüdiger S, Hickel R & Klaiber B. Working parameters of a sonic scaler influencing root substance removal in vitro. Clinical Oral Investigations, 1997; **1**: 55-60.

Flemmig TF, Petersilka GF, Mehl A, Hickel R & Klaiber B. The effect of working parameters on root substance removal using a piezoelectric ultrasonic scaler in vitro. Journal of Clinical Periodontology, 1998a; **25**: 158-163.

Flemmig TF, Petersilka GJ, Mehl A, Hickel R & Klaiber B. Working parameters of a magnetostrictive ultrasonic scaler influencing root substance removal in vitro. Journal of Periodontology, 1998b; **69**: 547-53.

Frame JW. Removal of oral oft tissue pathology with the CO_2 laser. Journal of Oral Maxillofacial Radiology, 1985; **43**: 850-855.

Fricke-Begemann T, Gülker G, Hinsch KD & Joost H. Mural inspection by vibration measurements with TV-holography. Optics and Lasers in Engineering, 2000; **32**: 537-548.

Fushimi H, Kubo M, Inoue T, Yamada Y, Matsuyama Y & Kameyama M. Peripheral vascular reactions to smoking – profound vasoconstriction by atherosclerosis. Diabetes Research and Clinical Practice, 1998; **42**: 29-34.

Gankerseer EJ & Walmsley AD. Preliminary investigation into the performance of a sonic scaler. Journal of Periodontology, 1987; 58: 780-784.

Garrett JS. Root planing: a perspective. Journal of Periodontology, 1977; **48**: 553-557.

Gazelius B, Olgart L & Edwall B. Restored vitality in luxated teeth assessed by laser Doppler flowmeter. Endodontics and Dental Traumatology, 1988; **4**: 265-268.

Gellin RG, Miller MC, Javed T, Engler WO & Mishkin DJ. The effectiveness of the Titan-S sonic scaler versus curettes in the removal of subgingival calculus. Journal of Periodontology, 1986; **57**: 672-680.

Ghoshal A, Sundaresan MJ, Schulz MJ & Pai PF. Structural health monitoring techniques for wind turbine blades. Journal of Wind Engineering, 2000; **85**: 309-324.

Goldman HM. Histologic assay of healing following ultrasonic curettage versus hand instrument curettage. Oral Surgery, Oral Medicine and Oral Pathology, 1961; **14**: 925-928.

Gordon N, Rispler S, Sideman S, Shofty R & Beyar R. Thermographic imaging in the beating heart: a method for coronary flow estimation based on a heat transfer model. Medical Engineering & Physics, 1998; **20**: 443-451.

Grossman E, Cronin M, Dembling W & Proskin H. A comparative clinical study of extrinsic tooth stain removal with two electric toothbrushes (Braun D7 and D9) and a manual brush. American Journal of Dentistry, 1996; **9** (Special Issue): S26-S29.

Halliwell NA. The Laser Torsional Vibrometer: A Step Forward in Rotating Machinery Diagnostics. Journal of Sound and Vibration, 1995; **190**: 399-418.

Hansen LS & Nielson AG. Comparison of tissue response to rotary and ultrasonic dental cutting procedures. Journal of the American Dental Association, 1956; **52**: 131-137.

Heanue M, Deacon SA, Deery C, Robinson PG, Walmsley AD, Worthington HV & Shaw WC. Manual versus powered toothbrushing for oral health (Cochrane Review). 2003; In: The Cochrane Library, Issue 1. Oxford: Update Software.

Heasman PA & McCracken GI. Powered toothbrushes: a review of clinical trials. Journal of Clinical Periodontology, 1999; **26**: 407-420.

Hetherington TE. Sexual differences in the tympanic frequency responses of the American bullfrog (Rena catesbeiana). Journal of the Acoustical Society of America, 1994; **96**: 1186-1188.

Holland CK, Deng CX, Apfel RE, Alderman JL, Fernandez LA & Taylor KJW. Direct evidence of cavitation in vivo from diagnostic ultrasound. Ultrasound in Medicine & Biology, 1996; **22**: 917-925.

Hoover DR & Robinson HBG. Effect of automatic and hand toothbrushing on gingivitis. Journal of the American Dental Association, 1962; **65**: 361-367.

Huber P, Debus J, Peschke P, Hahn EW & Lorenz WJ. In vivo detection of ultrasonically induced cavitation by a fibre-optic technique. Ultrasound in Medicine & Biology, 1994; **20**: 811-825.

Hussey DL, Biagioni PA, McCullagh JJP & Lamey P-J. Thermographic assessment of heat generated on the root surface during post space preparation. International Endodontic Journal, 1997; **30**: 187-190.

Hutson AM, Mickleburgh SP & Racey PA. Microchiropteran bats: global status survey and conservation action plan. IUCN/SSC Chiropteran Specialist Group. 2001; IUCN, Gland, Switzerland & Cambridge, UK. ISBN: 2-8317-0595-9.

Iyer S, Weiss C & Mehta A. Effects of drill speed on heat production and the rate and quality of bone formation in dental implant osteomies. Part 1: Relationship between drill speed and heat production. The International Journal of Prosthodontics, 1997a; **10**: 411-414.

Iyer S, Weiss C & Mehta A. Effects of drill speed on heat production and the rate and quality of bone formation in dental implant osteomies. Part 2: Relationship between drill speed and healing. The International Journal of Prosthodontics, 1997b; **10**: 536-540.

Jamieson V. Sound waves deliver a faster pint. Physics World, 2001; **14**: 21.

Jeffrey IWM, Lawrenson B, Saunders EM & Longbottom C. Dentinal temperature transients caused by exposure to CO_2 laser irradiation and possible pulpal damage. Journal of Dentistry, 1990; **18**: 31-36.

Jenkins FA & White HE. Fundamentals of optics. 4th Edition. 1981; McGraw-Hill Book Company, Singapore. ISBN: 0-07-032330-5.

Johnson WN & Wilson JR. The application of the ultrasonic dental unit to scaling procedures. Journal of Periodontology, 1957; **28**: 264-271.

Johnson BD & McInnes C. Clinical evaluation of the efficacy and safety of a new sonic toothbrush. Journal of Periodontology, 1994; **65**: 692-697.

Jones SJ, Lozdan J & Boyde A. Tooth surfaces treated in situ with periodontal instruments. Scanning electron microscopic studies. British Dental Journal, 1972; **132**: 57-64.

Khambay BS & Walmsley AD. An in vitro evaluation of electric toothbrushes. Quintessence International, 1995; **26**: 841-848.

Khambay BS & Walmsley AD. Acoustic micrstreaming: detection and measurement around ultrasonic scalers. Journal of Periodontology, 1999; **70**: 626-631.

Khambay BS & Walmsley AD. Investigations into the use of an ultrasonic chisel to cut bone. Part 1: forces applied by clinicians. Journal of Dentistry, 2000a; **28**: 31-37.

Khambay BS & Walmsley AD. Investigations into the use of an ultrasonic chisel to cut bone. Part 2: cutting ability. Journal of Dentistry, 2000b; **28**: 39-44.

Khan AZ, Stanbridge AB & Ewins DJ. Detecting damage in vibrating structures with a scanning LDV. Optics and Lasers in Engineering, 2000; **32**: 583-592.

Killoy WJ, Love JW, Love J, Fedi PF & Tira DE. The effectiveness of a counter-rotary action powered toothbrush and conventional toothbrush on plaque removal and gingival bleeding. Journal of Periodontology, 1989; **60**: 473-477.

Knapp MJ & Bernier JL. The response of oral tissues to ultrasound. Journal of the American Dental Association, 1959; **58**: 50-61.

Kocher T & Plagmann H-C. Heat propagation in dentin during instrumentation with different sonic scaler tips. Quintessence International, 1996; **27**: 259-264.

Kocher T & Plagmann HC. The diamond-coated sonic scaler tip. Part 1: oscillation pattern of different sonic scaler inserts. International Journal of Periodontics & Restorative Dentistry, 1997a; **17**: 393-399.

Kocher T & Plagmann HC. The diamond-coated sonic scaler tip. Part 2: Loss of substance and alteration of root surface texture after different scaling modalities. International Journal of Periodontics & Restorative Dentistry, 1997b; **17**: 485-493.

Kocher T, Fanghanel J, Sawaf H & Litz R. Substance loss caused by scaling with different sonic scaler inserts – an in vitro study. Journal of Clinical Periodontology, 2001; **28**: 9-15.

Laird WRE & Walmsley AD. Ultrasound in dentistry. Part 1 – biophysical interactions. Journal of Dentistry, 1991; **19**: 14-17.

Laur HC, Kraft E, Rothlauf W & Zwingers T. Effects of the temperature of cooling water during high-speed and ultrahigh-speed tooth preparation. Journal of Prosthetic Dentistry, 1990; **63**: 407-414.

Laurell L & Pettersson B. Periodontal healing after treatment with either the Titan-S sonic scaler or hand instruments. Swedish Dental Journal, 1988; **12**: 187-192.

Laurell L. Periodontal healing after scaling and root planning with the Kavo Sonicflex and Titan-S sonic scalers. Swedish Dental Journal, 1990; **14**: 171-177.

Lea SC & Walmsley AD. Technology, ultrasonics and dentistry. Dental Update, 2002a; **29**: 390-395.

Lea SC Landini G & Walmsley AD. Vibration characteristics of ultrasonic scalers assessed with scanning laser vibrometry. Journal of Dentistry, 2002b; **30**: 147-151.

Lea SC, Landini G & Walmsley AD. The displacement amplitude of ultrasonic scaler inserts. Journal of Clinical Periodontology, 2003a; **30**: 505-510.

Lea SC, Landini G & Walmsley AD. Ultrasonic scaler tip performance under various load conditions. Journal of Clinical Periodontology, 2003b; **30**: 876-881.

Lea SC, Landini G & Walmsley AD. Assessing the vibrations of dental ultrasonic scalers. Journal of Sound and Vibration, 2004a; **271**: 1113-1120.

Lea SC, Walmsley AD, Lumley PJ & Landini G. A new insight into the oscillation characteristics of endosonic files used in dentistry. Physics in Medicine & Biology, 2004b; **49**: 2095-2102.

Lea SC, Landini G & Walmsley AD. A novel method for the evaluation of powered toothbrush oscillation characteristics. American Journal of Dentistry, 2004c; **17**: 307-309.

Lea SC, Landini G & Walmsley AD. Thermal imaging of ultrasonic scaler tips during tooth instrumentation. Journal of Clinical Periodontology, 2004d; **31**: 370-375.

Lea SC, Price GJ & Walmsley AD. Does cavitation occur around powered toothbrushes? Journal of Clinical Periodontology, 2004e; **31**: 77-78.

Lea SC, Price GJ & Walmsley AD. A study to determine whether cavitation occurs around dental ultrasonic scaling instruments. Ultrasonics Sonochemistry, 2005; **12**: 233-236.

Leighton TG. The acoustic bubble. 1994; Academic Press, London, UK. ISBN: 0-12-441920-8.

Liddington MI & Shakespeare PG. Timing of the thermographic assessment of burns. Burns, 1996; **22**: 26-28.

Loe H, Theilade E & Borglum Jensen S. Experimental gingivitus in man. Journal of Periodontology, 1965; **36**: 177-187.

Lohse D, Schmitz B & Versluis M. Snapping shrimp making flashing bubbles. Nature, 2001; **413**: 477-478.

Loos B, Kiger R, & Egelberg J. An evaluation of basic periodontal therapy using sonic and ultrasonic scalers. Journal of Clinical Periodontology, 1987; **14**: 29-33.

Lord RM, Abel EW, Wang Z & Mills RP. Effects of draining cochlear fluids on stapes displacement in human middle-ear models. Journal of the Acoustical Society of America, 2001; **110**: 3132-3139.

Lumley PJ, Walmsley AD & Laird WRE. An investigation into cavitational activity occurring in endosonic instrumentation. Journal of Dentistry, 1988; **16**: 120-122.

Lumley PJ, Walmsley AD & Laird WRE. Streaming patterns produced around endosonic files. International Endodontic Journal, 1991; **24**: 290-297.

Lumley PJ, Walmsley AD, Harrington E & Marquis PM. Variations in stroke rate and loading using hand sonic or ultrasonic instrumentation. Endodontics and Dental Traumatology, 1993; **9**: 153-156.

Mallernee RE. The effect of ultrasonic energy on the periodontal membrane, alveolar bone, and gingivae. Journal of Prosthetic Dentistry, 1958; **8**: 147-152.

Mantokoudis D, Joss A, Christensen MM, Meng HX, Suvan JE & Lang NP. Comparison of the clinical effects and gingival abrasion aspects of manual and electric toothbrushes. Journal of Clinical Periodontology**,** 2001; **28**: 65-72.

Martin H. Ultrasonic disinfection of the root canal. Oral Surgery, Oral Medicine and Oral Pathology, 1976; **42**: 92-99.

Mason TJ, Lorimer JP & Cuthbert T. Power ultrasound in dentistry – radical production. Ultrasonics International 89 Conference Proceedings: 1989; 1279-1282.

Mason TJ. (Ed) Chemistry with Ultrasound. 1990; Elsevier Science Publishers Ltd, Essex, England. ISBN 1-85166-422-X.

McCall Jr CM & Szmyd L. Clinical evaluation of ultrasonic hand scaling. Journal of the American Dental Association, 1960; **61**: 559-564.

McComb K, Reby D, Baker L, Moss C & Sayialel S. Long-distance communication of acoustic cues to social identity in African elephants. Animal Behaviour, 2003; **65**: 317-329.

McCullagh JJP, Biagioni PA, Lamey P-J & Hussey DL. Thermographic assessment of root canal obturation using thermomechanical compaction International Endodontic Journal, 1997; **30**: 191-195.

McCullagh JJP, Setchell DJ, Gulabivala K, Hussey DL, Biagioni PA, Lamey P-J & Bailey G. A comparison of thermocouple and infrared thermographic analysis of temperature rise on the root surface during the continuous wave of condensation technique International Endodontic Journal, 2000; **33**: 326-332.

McMillan AJ. A non-linear friction model for self-excited vibrations. Journal of Sound and Vibration, 1997; **205**: 323-335.

Mesaros SV & Trope M. Revascularization of traumatized teeth assessed by laser Doppler flowmetry: case report. Endodontics and Dental Traumatology, 1997; **13**: 24-30.

Mills RP, Wang ZG, Abel EW, Phil M & Eng C. In vitro study of a multi-layer piezoelectric crystal attic hearing implant. Journal of Laryngology and Otology, 2001a; **115**: 359-362.

Mills RP, Abel EW & Lord R. In vitro evaluation of a malleus head to stapes bead 'incus replica' prosthesis. Journal of Laryngology and Otology, 2001b; **115**: 97-100.

Monroe R. The deep end of sound. A Scripps scientist listens for the inaudible. Explorations, 2002; **9**: (Accessed: 14/03/04). Available online at: http://sio.ucsd.edu/explorations/back/exp_pdfs/Volume_9_n2/The_Deep_End_Of_Sound_V9n2.pdf

Mörmann WH, Bösiger P, Grau P & Scaroni F. The thermodynamic behaviour of labial gingiva in patients with destructive periodontal disease. Journal of Clinical Periodontology, 1985; **12**: 477-493.

Moskow BS & Bressman E. Cemental response to ultrasonic and hand instrumentation. Journal of the American Dental Association, 1964; **68**: 698-703.

Nascentes CC, Korn M, Sousa CS & Arruda AZ. Use of ultrasonic baths for analytical applications: a new approach for optimisation conditions. Journal of the Brazilian Chemical Society, 2001; **12**: 57-63.

Ngoi BKA, Venkatakrishnan K & Bo Tan. Laser scanning heterodyne-interferometer for micro-components. Optics Communications, 2000; **173**: 291-301.

Nicoll BK & Peters RJ. Heat generation during ultrasonic instrumentation of dentin as affected by different irrigation methods. Journal of Periodontology, 1998; **69**: 884-888.

Nielson AG, Richards JR & Wolcott RB. Ultrasonic dental cutting instrument: I. Journal of the American Dental Association, 1955; **50**: 392-399.

Niemi M-L, Ainamo J & Etemadzadeh H. Gingival abrasion and plaque removal with manual versus electric toothbrushing. Journal of Clinical Periodontology, 1986; **13**: 709-713.

Niemi M-L. Gingival abrasion and plaque removal after toothbrushing with an electric and a manual toothbrush. Acta Odontologica Scandinavica, 1987; **45**: 367-370.

O'Beirne G, Johnson RH, Persson GR & Spektor MD. Efficacy of a sonic toothbrush on inflammation and probing depth in adult periodontitis. Journal of Periodontology, 1996; **67**: 900-908.

Oman CR & Applebaum E. Ultrasonic cavity preparation. Preliminary report. New York Dental Journal, 1954; **20**: 256-260.

Oman CR & Applebaum E. Ultrasonic cavity preparation. II. Progress report. Journal of American Dental Association, 1955; **50**: 414-417.

Oral B web site. Accessed (16/07/03) via http://www.oralb.com/pdfs/B8_d15.pdf

[Research performed by Guerrero DM. *et al*. Effect of a powered toothbrush on in vitro bacterial plaque. Journal of Dental Research, 1999; **78**: 414.]

Ovadia O, Pinshow B & Lotem A. Thermal imaging of house sparrow nestlings: the effect of begging behaviour and nestling rank. The Condor, 2002; **104**: 837-842.

Pameijer CH, Stallard RE & Hiep N. Surface characteristics of teeth following periodontal instrumentation: a scanning electron microscope study. Journal of Periodontology, 1972; **43**: 628-633.

Physicsweb. The bubble bursts for shrimps. 2000; Accessed (31/01/2003) via http://physicsweb.org/article/news/4/9/13/1.

Pick RM, Pecaro BC & Silberman CJ. The laser gingivectomy: the use of the CO_2 laser for the removal of phenytoin hyperplasia. Journal of Periodontology, 1985; **56**: 492-496.

Pickering CJD & Halliwell NA. The Laser Vibrometer: A Portable Instrument. Journal of Sound and Vibration, 1986; **107**: 471-485.

Pitt Roche HA. Demonstration at the annual meeting: the ultrasonic drill. British Dental Journal, 1954; **97**: 96-98.

Postle HH. Ultrasonic cavity preparation. Journal of Prosthetic Dentistry. 1958; **8**: 153-160.

Price GJ, Duck FA, Digby M, Holland W & Berryman T. Measurement of radical production as a result of cavitation in medical ultrasound fields. Ultrasonics Sonochemistry, 1997; **4**: 165-171.

Raichel DR. The science and applications of acoustics. 2000; Springer-Verlag, New York.

Richman RJ. The use of ultrasonics in root canal therapy and root resection. The Journal of Dental Medicine, 1957; **12**: 12-18.

Ring EFJ. The discovery of infrared radiation in 1800. Imaging Science Journal, 2000; **48**: 1-8.

Roebuck EM, Evans DJP, Stirrups D & Strang R. The effect of wavelength, bandwidth and probe design on assessing the vitality of anterior teeth with laser Doppler flowmetry. International Journal of Paediatric Dentistry, 2000; **10**: 213-220.

Roed-Peterson B. The potential use of CO_2-laser gingivectomy for phenytoin-induced gingival hyperplasia in mentally retarded patients. Journal of Clinical Periodontology, 1993; **20**: 729-731.

Rothberg SJ, Baker JR & Halliwell NA. Laser Vibrometry: Pseudo-Vibrations. Journal of Sound and Vibration, 1989; **135**: 516-522.

Rozell N. Listening to the heartbeat of the world. Alaska Science Forum, Article #1454. 1999; Available online at: http://www.gi.alaska.edu/ScienceForum/ASF14/1454.html (Accessed: 14/03/04).

Samaranayake LP. Essential microbiology for dentistry. 1998; Churchill Livingstone, Edinbugh. ISBN: 0-443-04989-0.

Sanderson AD. Gingival Curettage by hand and ultrasonic instruments: a histologic comparison. Journal of Periodontology, 1966; **37**: 279-290.

Saunders FM & Saunders WP. The heat generated on the external root surface during post space preparation. International Endodontic Journal, 1989; **22**: 169-173.

Sharma NC, Galustians J, Qaqish J & Cugini M. A comparison of two electric toothbrushes with respect to plaque removal and subject preference. American Journal of Dentistry, 1998; **11**: S29-S33.

Schemehorn BR & Henry GM. A laboratory investigation of stain removal from enamel surface: comparative efficacy of three electric toothbrushes. American Journal of Dentistry, 1996; **9** (Special Issue): S21-S24.

Schlageter L, Rateitschak-Plüss EM & Schwarz J-P. Root surface smoothness or roughness following open debridement: an in vivo study. Journal of Clinical Periodontology, 1996; **23**: 460-464.

Schmidlin PR, Beuchat M, Busslinger A, Lehmann B & Lutz F. Tooth substance loss resulting from mechanical, sonic and ultrasonic root instrumentation assessed by liquid scintillation. Journal of Clinical Periodontology, 2001; **28**: 1058-1066.

Scott JH & Symons NBB. Introduction to dental anatomy. 7th Edition. 1974; Churchill Livingstone, Edinburgh and London. ISBN: 0-443-01125-7.

Scruby CB & Drain LE. Laser ultrasonics: techniques and applications. 1990; Adam Hilger, Bristol. ISBN: 0-7503-0050-7.

Seffrin RJ. Thermal imaging for detecting potential SARS infection. 2003; Available via http://metrology.org.sg/presentation/Thermal%20imaging%20for%20detecting%20potential%20SARS%20infection.pdf. (Accessed:16/07/2003)

Smart GJ, Wilson M, Davies EH & Kieser JB. The assessment of ultrasonic root surface debridement by determination of residual endotoxin levels. Journal of Clinical Periodontology, 1990; **17**: 174-178.

Sonicare web site. (Accessed: 16/07/2003) via http://sonicare.com/elite/clinical.asp

Stern RH & Sognnaes RF. Laser beam effect on dental hard tissues. Journal of Dental Research, 1964; **43**: 873.

Street EV. A critical evaluation of ultrasonics in dentistry. Journal of Prosthetic Dentistry, 1959; **8**: 132-141.

Stende G & Schaffer EM. A comparison of ultrasonic and hand scaling. Journal of Periodontology, 1961; **32**: 312-314.

Stenfelt S, Hato N & Goode RL. Factors contributing to bone conduction: the middle ear. Journal of the Acoustical Society of America, 2002; **111**: 947-959.

Suppipat N. Ultrasonics in periodontics. Journal of Clinical Periodontology, 1974; **1**: 206-213.

Suslick KS. The chemical effects of ultrasound. Scientific American, 1989; February: 80-86.

Tascher PJ & Ewen SJ. An ultrasonic method for root scalings – Preliminary report. New York State Dental Journal, 1957; **23**: 266-269.

Ten Cate AR. Oral histology: development, structure and function. 3rd Edition. 1989; The C.V. Mosby Company, Missouri. ISBN: 0-8016-4902-1.

Torfason T, Kiger R, Selvig KA & Egelbery J. Clinical improvement of gingival condtions following ultrasonic versus hand instrumentation of periodontal pockets. Journal of Clinical Periodontology, 1979; **6**: 165-176.

Trenter SC, Walmsley AD, Landini G & Shippen JM. Assessment of the ultrasonic dental scaler insert. Medical Engineering & Physics, 2002; **24**: 139-144.

Trenter SC & Walmsley AD. Ultrasonic dental scaler: associated hazards. Journal of Clinical Periodontology, 2003; **30**: 95-101.

Trenter SC, Landini G & Walmsley AD. Effect of loading on the vibration characteristics of thin magnetostrictive ultrasonic scaler inserts. Journal of Periodontology, 2003; **74**: 1308-1315.

Tuffun JR & Carruth JAS. The carbon dioxide surgical laser. British Dental Journal, 1980; **149**: 255-258.

Tunkel J, Heinecke A & Flemmig TF. A systematic review of efficacy of machine-driven and manual subgingival debridement in the treatment of chronic periodontitis. Journal of Clinical Periodontology, 2002; **29**: 72-81.

Tylman SD. Ultrasonic techniques for crown and bridge retainers. Journal of Prosthetic Dentistry, 1958; **8**: 167-269.

Vaezy S, Martin R, Mourad P & Crum L. Hemostasis using high intensity focused ultrasound. European Journal of Ultrasound, 1999; **9**: 79-87.

Vaezy S, Martin RW & Crum LA. Acoustic surgery. Physics World, 2001; **14**: 35-39.

Van der Weijden GA, Danser MM, Nijboer A, Timmerman MF & Van der Velden U. The plaque removing efficacy of an oscillating/rotating toothbrush. Journal of Clinical Periodontology, 1993a; **20**: 273-278.

Van der Weijden GA, Timmerman MF, Nijboer A, Lie MA & Van der Velden U. A comparative study of electric toothbrushes for the effectiveness of plaque removal in relation to tooth brushing duration. Timerstudy. Journal of Clinical Periodontology, 1993b; **20**: 476-481.

Van der Weijden GA, Timmerman MF, Snoek IM, Reijerse E & Van der Velden U. Toothbrushing duration and plaque removing efficacy of electric toothbrushes. American Journal of Dentistry, 1996; **9** (Special Issue): S31-S36.

Wade G. Human uses of ultrasound: ancient and modern. Ultrasonics, 2000; **38**: 1-5.

Watson ADM, Pitt Ford TR & McDonald F. Blood flow changes in the dental pulp during limited exercise measured by laser Doppler flowmetry. International Endodontic Journal, 1992; **25**: 82-87.

Walmsley AD, Laird WRE & Williams AR. A model system to demonstrate the role of cavitational activity in ultrasonic scaling. Journal of Dental Research, 1984; **63**: 1162-1165.

Walmsley AD, Laird WRE & Williams AR. Gas bubble fragmentation in an ultrasonic field. Ultrasonics, 1985; **23**: 170-172.

Walmsley AD, Laird WRE & Williams AR. Inherent variability of the performance of the ultrasonic descaler. Journal of Dentistry, 1986a; **14**: 121-126.

Walmsley AD, Laird WRE & Williams AR. Displacement amplitude as a measure of the acoustic output of ultrasonic scalers. Dental Materials, 1986b; **2**: 97-100.

Walmsley AD, Williams AR & Laird WRE. Acoustic absorption within human teeth during ultrasonic descaling. Journal of Dentistry, 1986c; **14**: 2-6.

Walmsley AD. Ultrasound and root canal treatment: the need for scientific evaluation. International Endodontic Journal, 1987; **20**: 105-111.

Walmsley AD, Hickson FS, Laird WRE & Williams AR. Investigation into patients hearing following ultrasonic scaling. British Dental Journal, 1987; **162**: 221-224.

Walmsley AD, Laird WRE & Williams AR. Dental plaque removal by cavitational activity during ultrasonic scaling. Journal of Clinical Periodontology, 1988; **15**: 539-543.

Walmsley AD & Williams AR. Effects of constraint on the oscillatory pattern of endosonic files. Journal of Endodontics, 1989; **15**: 189-194.

Walmsley AD, Walsh TF, Laird WRE & Williams AR. Effects of cavitational activity on the root surface of teeth during ultrasonic scaling. Journal of Clinical Periodontology, 1990; **17**: 306-312.

Walmsley AD & Williams AR. Measurement of cavitational activity within ultrasonic baths. Journal of Dentistry, 1991; **19**: 62-66.

Walmsley AD, Laird WRE & Lumley PJ. Ultrasound in dentistry. Part 2 – periodontology and endodontics. Journal of Dentistry, 1992; **20**: 11-17.

Walmsley AD. The electric toothbrush: a review. British Dental Journal, 1997; **182**: 209-218.

Walmsley AD, Lumley PJ, Johnson WT & Walton RE. Breakage of ultrasonic root-end preparation tips. Journal of Endodontics, 1996; **22**: 287-289.

Walmsley AD, Lumley PJ, Blunt L & Spence D. Surface integrity of composite inlays following ultrasonic vibration. American Journal of Dentistry, 1997; **10**: 102-106.

Walsh JP & Symmons HF. A comparison of the heat production and mechanical efficiency of diamond instruments, stones and burs at 3,000 and 60,000rpm. New Zealand Dental Journal, 1972; **68**: 58-64.

Walsh TF & Glenwright HD. Relative effectiveness of a rotary and conventional toothbrush in plaque removal. Community Dentistry and Oral Epidemiology, 1984; **12**: 160-164.

Waplington M, Lumley PJ, Walmsley AD & Blunt L. Cutting ability of an ultrasonic retrograde cavity preparation instrument. Endodontics & Dental Traumatology, 1995; **11**: 177-180.

Webb S. The Physics of Medical Imaging. 1988; IOP Publishing Ltd, Bristol, England. ISBN 0-85274-349-1.

Weitendorf EA. On the history of propeller cavitation and cavitation tunnels. 2001; Presented at CAV 2001: Fourth International Symposium on Cavitation, California Institute of Technology, USA. Accessed (31/01/2003) at http://resolver.library.caltech.edu/cav2001:sessionB9.001.

Wilkinson RF & Maybury JE. Scanning electron microscopy of the root surface following instrumentation. Journal of Periodontology, 1973; **44**: 559-563.

Williams AR. Ultrasound: biological effects and potential hazards. 1986; Academic Press. ISBN: 0-12-756960-X.

Williams AR & Walmsley AD. Exposimetry of low-frequency ultrasonic dental devices. IEEE Transactions on Ultrasonics, Ferroelectrics and Frequency Control, 1988; **35**: 264-269.

Wilson JR. The use of ultrasonics in periodontal treatment. Journal of Prosthetic Dentistry, 1958; **8**: 161-166.

Yeh Y & Cummins HZ. Localized fluid flow measurements with a He-Ne laser spectrometer. Applied Physics Letters, 1964; **4**: 176-178.

Young M. Optics and lasers including fibers and optical waveguides. 3rd Revised Edition. 1986; Springer-Verlag, Berlin, Germany. ISBN: 0-387-16127-9.

Zach L. Ultrasonic cavity preparation: effect on the immature dentition. Journal of Prosthetic Dentistry, 1958; **8**: 139-146.

Zach L & Cohen G. Pulp response to externally applied heat. Oral Surgery, Oral Medicine & Oral Pathology, 1965; **19**: 515-530.

Zander HA. Effects of ultrasonic cavity preparation upon the pulp. Journal of Prosthetic Dentistry, 1958; **8**: 137-138.

Zinner DD. Recent ultrasonic dental studies including periodontia without the use of an abrasive. Journal of Dental Research, 1955; **34**: 748-749.

Appendices

Appendix 1. Published Papers

Appendix 2. Published Abstracts

Appendix 3. EPSRC Individual Grant Review

These appendices are not available in the web copy of this thesis